Bioprocess development for polyhydroxybutyrate (PHB) production from waste carob pods and its application in food packaging: A biorefinery approach

A Thesis

Submitted in partial fulfilment of the requirements for the award of the degree of

DOCTOR OF PHILOSOPHY

by

ARUL MANIKANDAN N

DEPARTMENT OF CHEMICAL ENGINEERING
INDIAN INSTITUTE OF TECHNOLOGY GUWAHATI
GUWAHATI - 781039, ASSAM, INDIA

July 2020

For of him, and through him, and to him, are all things: to whom be glory forever. Amen.

Dedicated to my sweet heavenly father

INDIAN INSTITUTE OF TECHNOLOGY GUWAHATI

DEPARTMENT OF CHEMICAL ENGINEERING

DECLARATION

I, hereby declare that the content embodied in this thesis entitled "**Bioprocess development for polyhydroxybutyrate (PHB) production from waste carob pods and its application in food packaging: A biorefinery approach**" is the result of investigations carried out by me at the Department of Chemical Engineering and Department of Biosciences and Bioengineering, Indian Institute of Technology Guwahati, Guwahati, India, under the supervision of **Prof. G. Pugazhenthi** and **Prof. Kannan Pakshirajan.**

In keeping with the general practice of reporting scientific observations, due acknowledgements have been made wherever the work described is based on the findings of other investigators.

Date: **Arul Manikandan N**

Place: IIT Guwahati

INDIAN INSTITUTE OF TECHNOLOGY GUWAHATI

DEPARTMENT OF CHEMICAL ENGINEERING

CERTIFICATE

It is certified that the work described in this thesis entitled **"Bioprocess development for polyhydroxybutyrate (PHB) production from waste carob pods and its application in food packaging: A biorefinery approach"** by **Arul Manikandan N** for the award of degree of Doctor of Philosophy is an authentic record of the results obtained from the research work carried out under our supervision in the Department of Chemical Engineering and Department of Biosciences and Bioengineering, Indian Institute of Technology Guwahati, India, and this work has not been submitted either in whole or in part elsewhere for a degree.

Date:
Place: IIT Guwahati

(Signature of Thesis Supervisor)
Prof. G. Pugazhenthi
Professor
Department of Chemical Engineering
Indian Institute of Technology Guwahati
Guwahati-781039, Assam, India

Date:
Place: IIT Guwahati

(Signature of Thesis Supervisor)
Prof. Kannan Pakshirajan
Professor
Department of Biosciences & Bioengineering
Indian Institute of Technology Guwahati
Guwahati-781039, Assam, India

ACKNOWLEDGEMENTS

First of all, I would like to thank my Lord Jesus, for choosing only the best and offering it to me right from my birth. Yes, he has chosen for me the best parents to bring me into the world and Pastors after his own heart to lead me. At every stage of my life, he has selected only the best and offered it to me. Even when it was his plan that I should carry out my PhD degree, he has chosen not only the finest supervisors but also the most excellent combination of supervisors too. Yes, I am always thankful to my God and will be continually grateful to him for bringing Prof. Kannan Pakshirajan sir and Prof. G. Pugazhenthi sir into my life. I personally would like to be thankful to my parents, except in the last few months for the past many years they have given me full liberty to pursue my career. I am so grateful to Prof. Kannan Pakshirajan sir for giving me an opportunity for the past five years to grow with him. I still remember how I came after completing my Bachelor degree and joined under him of being ignorant about many things. But it was his constant perseverance to involve me in all sort of work whereby I have learnt many things right from the beginning and grown under his guidance. More than sirs professional life; it was his personal way of handling diverse matters touched me a lot and moulded me to a certain extent. When I was lagging in the research work, he had done his best in all possible way to bring me out of the lag state for which I am so grateful to him. Similarly, I am so thankful to Prof. G. Pugazhenthi sir too for providing me with an excellent opportunity to carry out my research work under his guidance. Rather than merely saying a chance, I should say he has come out of the realm of being a supervisor and provided me with the freedom to approach him not only on the research work but on other aspects too. I am so thankful to Prof. G. Pugazhenthi sir for his help extended throughout my research career.

I am so thankful to my doctoral committee members: Dr Prasanna Venkatesh sir, Dr Prabhu Vairakannu sir and Dr Senthilkumar Sivaprakasam sir for their precious suggestions. When I look at my thesis, it

was their sculpting and etching working that gave a finishing touch to my work. I am thankful to Mr M Dhana Singh, Mr S Baneesh, Mr P Premsagar, Mr SRR Tadi and Mr M Mohan Kumar for their assistance in performing cytotoxicity assay, CFD analysis, Gel electrophoresis test and membrane separation experiments. I would like to acknowledge the facility extended by Central Instrumentation Facility, Department of Biosciences and Bioengineering, Department of Chemical Engineering and Centre for excellence – sustainable polymers at IIT Guwahati to carry out various characterization using different High-end equipment. I am thankful to the Department of Chemical Engineering and Student Affairs section at IIT Guwahati for the financial assistance provided to attend various conference inside and outside India.

I am so thankful to Pastors, Co-believers, well-wishers inside and outside the campus for their constant support through their precious counselling and prayers. I would like to thank Mr Arun Sakthivel, right from my Bachelor's degree he was continuing with me in affording various help in sundry times. I am grateful to all my former and current lab mates; they all were so kind in extending their helping hands and comforting words. When I have joined initially in IITG, it was their support which made me feel as if I am not out of my home. I used to call them in the local language as my elder brother and elder sister. Indeed they also have behaved with me in the same way. Since the list of names would be exhaustive, and it would be difficult for me to mention all names here, I would like to thank all my labmates both in Prof. Kannan Pakshirajan sir and Prof. G. Pugazhenthi sir research group. I also take this opportunity to thank all the non-teaching staff and teaching assistants who helped in different instrumentations. As in the beginning, even in the last, I would like to thank my God for bringing all these precious people into my life.

July 2020 *Arul Manikadan N*

IIT Guwahati

Abstract

The depletion of fossil resources and increasing threat to the accumulation of non-biodegradable polymers in the environment has necessitated recent research toward suitable alternative polymer with outstanding performance. In this context, polyhydroxybutyrate (PHB) is a biodegradable, sustainable and environmentally friendly polymer that is produced entirely from microorganisms, and it shares properties similar to those of the fossil fuel-based polymers. However, the cost incurred for PHB production is considerably higher than that of petroleum-based polymers, which limits its commercialization. Recently, PHB production has gained considerable attention due to utilization of waste biomass refused from domestic and agri-food industries as a cheap raw material source. In this context, carob pods which are rich in cellulose, hemicellulose and lignin and refused from the locust bean gum industry amounts to an annual production of around 400,000 tons and can serve as an excellent inexpensive carbon source for PHB production. Therefore, this study adopted a novel closed-loop biorefinery approach for utilizing waste carob pods as the feed material.

After an initial washing, carob pods were treated with methanol to recover lignin. In the next step, sugars present in the delignified carob pods were extracted using water. *Ralstonia eutropha* and *Bacillus megaterium* were then grown on carob extract under optimized conditions of 10 C/N ratio, 10% (v/v) inoculum size, 40 g/L sugar concentration and no added adjunct in the medium, as concluded from the results of Taguchi experimental design. *R. eutropha* outperformed *B. megaterium* in terms of its capability to grow at a maximum initial sugar concentration of 40 g/L with a maximum PHB production of 12.2 g/L. Finally, the concentrated lignin from the previous step was diluted with different proportions of chloroform to extract PHB from the bacterial biomass. The PHB yield and purity obtained were more than 90% using either *R. eutropha* or *B. megaterium*.

In order to scale up the PHB production, a novel annular bioreactor (ABR) with a wide gap was used for the cultivation of *Ralstonia eutropha*, which produces PHB as an intracellular

product. Hydrodynamic studies demonstrated the uniform distribution of fluid in the ABR due to the Taylor and Couette flow in the bioreactor. The effect of different agitation and sparging rates on biomass growth and PHB production by the bacterium was studied using the ABR, which revealed a maximum PHB production of 14.89 g/L at 500 rpm and 0.8 vvm. The value obtained was nearly 1.4 times higher than that obtained using a conventional stirred tank bioreactor (STBR). Furthermore, performances of the bioreactors were compared by operating the reactors under fed-batch mode. At the end of 90 h of operation, the highest PHB volumetric productivity observed with the ABR (0.74 g/L·h) is 1.6 times the PHB volumetric productivity (0.46 g/L·h) obtained using the STBR.

For an efficient separation of polyhydroxybutyrate (PHB) containing *Ralstonia eutropha* cells from the culture broth, performance of a novel ceramic-based tubular membrane module was investigated. The number of ceramic membranes in the module was raised from 1 to 4 and its biomass separation efficiency was assessed by measuring the broth flux, biomass and PHB recovery as a function of applied pressure (49 kPa - 196 kPa). The present ceramic membrane was found to be highly efficient (99.9%) in recovering the PHB intact cells from the culture broth. A maximum initial water flux of 444 $L/m^2 \cdot h$ and a permeate broth flux of 52 $L/m^2 \cdot h$ were observed at the maximum applied pressure (196 kPa) with four membranes assembly. Thus, the recovery of both biomass and PHB were enhanced by increasing the number of membranes in the membrane assembly. Furthermore, an increase in the number of membranes resulted in a drastic reduction of the filtration resistance.

The potential of PHB produced in this study was successfully tested for food packaging applications, and for which PHB based nanocomposite films with varying concentration (0-1.3 wt%) of graphene nanoplatelets (Gr-NPs) were synthesized by a simple solution casting method. The prepared nanocomposites were characterized for their morphology, mechanical, thermal, barrier, cytotoxicity and biodegradable properties. Gr-NPs concentration of 0.7 wt%

was found to be optimum and an increase in the concentration caused agglomeration. In comparison with pristine PHB, PHB/Gr-NPs nanocomposite with an optimum Gr-NPs concentration of 0.7 wt% was found to be superior in terms of high melting point (10^{o}C), thermal stability (10^{o}C) and tensile strength (2 times). In addition, the nanocomposite resulted in 3 and 2 times reduction in oxygen and water vapour permeability, respectively, along with a negligible cytotoxic effect on the packing material. Thus, a four-fold increase in shelf-life of moisture and oxygen-sensitive food items like potato chips and milk product was achieved using the packaging material prepared with PHB/Gr-NPs nanocomposite.

Finally, techno-economic analyses of PHB production process under different existing and proposed scenarios were performed and compared based on pay-out period and turnover accumulated at the end of 7th year of a PHB plant operation. The use of carob pod extract as the alternative feedstock to pure sugars in the production process reduced the pay-out period from 12.6 to 6.8 years. Moreover, switching onto ABR instead of the conventional STBR decreased the pay-out period from 6.8 to 4.8 years and increased the turnover from 0.06 to 1.35 billion USD. Finally, solid-liquid separation using the aforementioned ceramic membranes instead of centrifugation resulted in a similar pay-out period of 4.8 years with enhanced turnover of about 1.4 billion USD. Consequently, a significant decrease in the cost of the sugar feedstock along with an improved PHB titre in ABR and incorporation of low-cost ceramic membrane based separation of PHB rich biomass resulted in a highly cost-effective and green approach for PHB production. Thus, the closed-loop zero-waste discharge biorefinery model developed in this study based on novel waste lignocellulosic feedstock, annular bioreactor design and operation, ceramic membrane-based biomass separation and food packaging application of PHB nanocomposites demonstrated that the bioprocess is economical, sustainable and environmentally safe with potential industrial application.

Contents

List of Figures

List of Tables

Abbreviation		
ABR	:	annular bioreactor
ABS	:	acrylonitrile butadiene styrene
AFEX	:	ammonia fibre expansion
AFM	:	atomic force microscopy
Ag	:	silver
$Al_2(Si_2O_5)_2(OH)_2$	:	pyrophyllite
$Al_2Si_2O_5(OH)_4$	:	kaolin
ALR	:	airlift reactor
ARA	:	arachidonic acid
ATR	:	attenuated total reflectance
$BaSO_4$	:	barium Sulphate
BLBR	:	bubble column bioreactor
C/N	:	Carbon to Nitrogen
C_4H_8O	:	tetrahydrofuran
$CaCl_2$	:	calcium chloride
$CaCO_3$	:	calcium carbonate
$CDCl_3$	:	deuterated chloroform
CFD	:	computational fluid dynamics
CFV	:	cross-flow velocity
CH_4	:	methane
$CHCl_3$	:	Chloroform
CNC	:	cellulose nanocrystal
$CO(NH_2)_2$	:	urea
CO_2	:	carbon dioxide
CO_2	:	carbon dioxide
CSL	:	corn-steep liquor
DMEM	:	Dulbecco's modified Eagle's medium
DNA	:	deoxyribo nucleic acid

DO	:	dissolve oxygen
DSC	:	differential Scanning Calorimetry
DTG	:	differential thermo gravimetric analysis
ELALR	:	external loop airlift reactors
FACS	:	flow cytometry analysis
FBS	:	fetal bovine serum
FDA	:	fluorescein diacetate
FESEM	:	field emission scanning electron microscopy
$FeSO_4 \cdot 7H_2O$	:	ferrous sulphate heptahydrate
FETEM	:	field emission transmission electron microscopy
FTIR	:	fourier transform infrared spectroscopy
GAE	:	gallic acid equivalents
GHG	:	greenhouse gasses
GPC	:	gel Permeation Chromatography
GRAS	:	generally regarded as safe
Gr-NPs	:	graphene nanoplatelets
Gr-NPs	:	graphene Nanoplatelets
H_3BO_3	:	boric acid
HCl	:	hydrochloric acid
HDPE	:	high density polyethylene
HMF	:	hydroxymethylfurfural
HPLC	:	high-Performance Liquid Chromatography
H_sSO_4	:	sulphuric acid
ILALR	:	inner loop airlift reactor
KCl	:	potassium chloride
KH_2PO_4	:	pottasium dihydrogen phosphate
kPa	:	kilo Pascal
LAQ	:	long alkyl chain quaternary
LDPE	:	low density polyethylene
LPM	:	litre per minute

MetHb	:	methemoglobin
$MgSO_4 \cdot 7H_2O$	:	magnesium sulphate heptahydrate
MSM	:	mineral salt medium
MTCC	:	microbial type culture collection
MTT	:	3-(4,5-dimethylthiazol-2-yl)-2,5-diphenyltetrazolium bromide
N_2O	:	nitrous oxide
Na_2HPO_4	:	di-sodium hydrogen phosphate
$(Na, Ca)(AlSiO_8)$	:	feldspar
$(NH_4)_6Mo_7O_{24} \cdot 4H_2O$	:	ammonium molybdate tetrahydrate
NaOCl	:	sodium hypochlorite
NaOH	:	sodium hydroxide
NH_4Cl	:	ammonium chloride
NMR	:	nuclear magnetic resonance
NOM	:	natural organic matter
OD	:	optical density
OP	:	oxygen permeability
OTR	:	oxygen transmission rate
PBS	:	polybutylene succinate
PE	:	polyethene
PEG	:	polyethylene glycol
PET	:	polyethene terephthalate
PGA	:	polyglycolic acid
PHA	:	polyhydroxyalkanoates
PHB	:	polyhydroxybutyrate
PHBV	:	Polyhydroxybutyrate valerate
PI	:	Propidium Iodide
PLA	:	Polylactic acid
PP	:	polypropylene
PS	:	Polystyrene
PS	:	polystyrene

PVA	:	polyvinyl alcohol
RI	:	refractive Index
S/N	:	signal to noise
SCBG	:	spent coffee bean grounds
SD	:	standard deviation
SDS- PAGE	:	sodium dodecyl sulfate-polyacrylamide gel electrophoresis
SiO_2	:	quartz
$3SiO_2Al_2O_3$	:	ball clay
STBR	:	stirred tank bioreactor
TCBR	:	Taylor and Couette bioreactor
TGA	:	thermogravimetric analysis
TMS	:	tetramethylsilane
TOC	:	total organic carbon
TPE	:	thermoplastic elastomer
TPPB	:	two-phase partitioning bioreactors
UV	:	ultra violet
WVP	:	water vapour permeability
WVTR	:	water vapour transmission rate
XRD	:	x-ray diffraction
ZnO	:	zinc oxide
$ZnSO_4 \cdot 7H_2O$	:	zinc sulphate heptahydrate

Notations

A	:	cross-sectional area of the sample (m^2)
a	:	Specific air-liquid interfacial surface area
A	:	outer surface area of the membrane (m^2)
$^{\circ}C$	:	Degree Celsius
C_*	:	Saturated dissolved oxygen concentration (mg/L)
C_c	:	cake concentration
C_{ib}	:	initial biomass concentration (g/L)
C_{iP}	:	initial PHB concentration (g/L)
C_{pb}	:	permeate biomass concentration (g/L)
C_{pP}	:	permeate PHB concentration (g/L)
C_t	:	Dissolved oxygen concentration at a given time (s)
d	:	thickness of the film (mm)
F_{max}	:	Maximum force needed to pull the sample apart (kN)
g/L	:	Gram per litre
J_b	:	broth flux ($L/m^2 \cdot h$)
J_w	:	water flux ($L/m^2 \cdot h$)
k_L	:	mass transfer coefficient
k_{O_2}	:	Oxidation rate constant
k_La	:	Volumetric mass transfer coefficient
L	:	Litre
L	:	Original length of the sample (mm)
M_b	:	Bacterial biomass weighed gravimetrically (mg)
M_g	:	Mass of PHB as quantified by gravimetric analysis (mg)
M_s	:	Mass of PHB as quantified by spectrophotometer (mg)
M_w	:	polymer molecular weight (g/mol)
N	:	Normality
Θ	:	Shelf life (days)
$O_{2\ (max)}$	:	maximum concentration of oxygen (mg/L)
P	:	Probability

PhaA	:	β-ketothiolase
PhaB	:	acetoacetyl-coA reductase
PhaC	:	PHA synthase
P_{PHB}	:	Percentage of PHB content in PHB rich bacterial biomass
P_{purity}	:	Percentage purity of PHB (%)
p_{O_2}	:	partial pressure of oxygen
Q_b	:	permeate broth flowrate (L/h)
Q_w	:	permeate water flowrate (L/h)
R_F	:	filtration resistance (m^{-1})
R_M	:	membrane resistance (m^{-1})
rpm	:	Rotation per minute
R_T	:	total resistance (m^{-1})
t	:	arbitrary time
t	:	filtration time (h)
T_g	:	Glass transition temperature (˚C)
T_m	:	Melting temperature (˚C)
T_{max}	:	Maximum degradation temperature (˚C)
T_{strain}	:	Tensile strain
T_{stress}	:	Tensile strength (MPa)
UV – Vis	:	Ultraviolet – Visible
vvm	:	Vessel volume per minute
W_i	:	Initial weight of the polymeric film (mg)
W_t	:	Weight of the polymeric film at a respective time interval (mg)
Y	:	PHB concentration (g/L)
Y_{yield}	:	Percentage yield of PHB (%)
ΔL	:	Extended length of the sample at the time of rupture (mm)
ΔP	:	applied pressure (Pa)
η_b	:	viscosity of broth (Pa s)
η_w	:	viscosity of water (Pa s)
$	:	United States dollar

Chapter 1

Introduction

1.1 Introduction

Our continued reliance on non-renewable energy sources originates from the widespread use and utilization of crude petroleum-based products, which, along with the dwindling petroleum assets, has led to ecological and political concerns. Evidently, the emission of greenhouse gasses (GHG) (carbon dioxide (CO_2), methane (CH_4) and nitrous oxide (N_2O)), from massive utilization of non-renewable energy sources and human practices has resulted in global warming and climate change (Liguori and Faraco, 2016). The world's necessary source of energy for vehicle use and generation of chemicals is crude oil. While vehicle use keeps on extending in the US and Europe, development in the rising economies of India and China is expected to increase vehicle use even more significantly (Mittal et al., 2016). Chemicals production is significantly dependent on fossil assets. A large proportion of the present-day commodities are derived from crude oil refineries, out of which 4% of crude oil is overall utilized for plastic production (Cherubini, 2010). Furthermore, the use of plastics concomitantly increases with its accumulation in the environment every year, and it is predicted to reach 33 billion tons in the year 2050 (Goh et al., 2016). More specifically, in the year 2014, 40% of the entire plastic source was used just for packaging applications (Bomrungnok et al., 2019). Keeping in mind the end goal to reduce the continuous reliance on petroleum and reduce environmental effects due to plastic accumulation, alternative feedstocks other than crude oil sources are essential. It is progressively recognized around the globe that biomass is an alternative to the conventional feedstock for modern commodities, including chemicals and polymer (Kajaste, 2014). At national, provincial and worldwide levels, there is a huge drive for utilization of biomass in biorefinery for creation of bioenergy, biofuels and biochemicals. Even though power and heat can be generated by various sustainable options like wind, sun, ocean, etc., chemicals and polymers can be derived only by utilizing biomass as the initial feedstock, as it

contributes the main C-rich material source accessible on the earth, other than fossils (Brar et al., 2017). Furthermore, biomass is a sustainable alternative to fossil assets for the production of transportation fuels and chemicals. (Fig. 1.1).

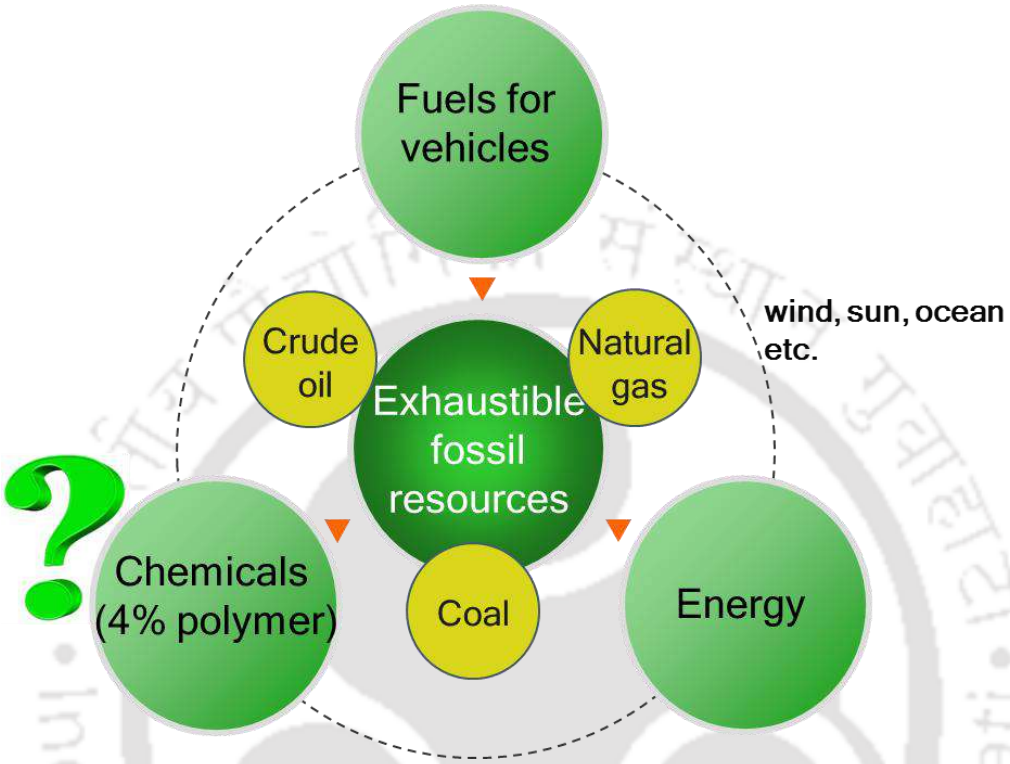

Fig. 1.1. Fuels, energy and chemical dependency on exhaustible fossil resources

The use of plastics concomitantly increases with its accumulation in the environment every year and it is predicted to reach 33 billion tons in the year 2050 (Goh et al., 2016). Many efforts are being made to reduce the dependency of the conventional petroleum-based polymer, so as to avoid its environmental impact (Goh et al., 2016; Li et al., 2019; Xu et al., 2020). In this context, the use of biopolymers with properties derived to meet the standards of food packaging materials is considered as the best solution (Goh et al., 2016; Li et al., 2019). Biopolymers including starch, chitosan, cellulose and few other multipurpose polymers such as polylactic acid (PLA), polyglycolic acid (PGA), polybutylene succinate (PBS), polyhydroxybutyrate (PHB) are well studied for their biocompatible, biodegradable and ecofriendly nature (Xu et al., 2020). In particular, the

fully biodegradable, non-toxic and highly crystalline nature of the bacterial polyhydroxybutyrate makes it more attractive and is at the forefront of the contemporary research (Acevedo et al., 2018; Xu et al., 2020). Unlike the petroleum-based plastics like high density polyethylene (HDPE), low density polyethylene (LDPE) and Polystyrene (PS), PHB is completely produced from sustainable biomass resources. Secondly, the PHB properties are similar to that of the conventional petroleum-based polymers such as polypropylene (PP), polystyrene (PS), polyethene (PE) and polyethene terephthalate (PET) (Serafim et al., 2004). Therefore the present research focuses primarily on the production of polyhydroxybutyrate.

1.2. Polyhydroxybutyrate (PHB)

1.2.1. Properties of PHB

PHB application is expanding with support from purchasers of plastic thermoformed objects as it is seen as a sustainable and biodegradable plastic product obtained from non-petroleum based raw materials. Moreover, PHB is exceedingly crystalline because of its stereo consistency. PHB is water-insoluble and moderately impervious to hydrolytic degradation. In comparison with oil-based polymers (e.g. polypropylene), PHB has low oxygen permeability and excellent thermoplastic properties (Snell, 2009). However, the oxygen permeability was higher than the permissible limit (1 $cm^3 \cdot mm/m^2 \cdot d^2 \cdot atm$) framed for food packaging application (Xu et al., 2020). Further, mechanical properties such as Young's modulus and elasticity were also considerably poor (Table 1.1). The densities of crystalline and amorphous PHB are 1.26 and 1.18 g/cm^3, respectively. The molecular weight of PHB obtained from wild type microbial strains is often in the range of 10-3,000 kDa with a polydispersity index of around 2. PHB is optically pure and piezoelectric, which aids in the initiation of osteogenesis. PHB is exceptionally brittle and solid material. Increasing the molecular weight of PHBs enhances their physical properties.

Table 1.1. Physical properties of PHB in comparison with those of biopolymer (PLA) and other conventional polymers

S. No.	Polymer	Young's Modulus (GPa)	Tensile strength (MPa)	Elongation at Break (%)	*T_m (°C)	*T_g (°C)
1	PHB	3.5-4	40	3-8	172–180	5-9
2	Isotactic polypropylene	1.0-1.7	29.3-38.6	500-900	170–176	-10
3	Polylactic acid	4	80	6	160	60
4	HDPE	0.4-1.0	17.9-33.1	12-700	112-132	-80
5	LDPE	0.05-0.1	15.2-78.6	150-600	88-130	-36
6	PS	3.0-3.1	50	3-4	80-110	21
7	Nylon-6,6	2.8	83	60	265	50
8	Polyethylene-terepthalate	2.2	56	7300	262	3400

* T_m - Melting temperature; T_g - Glass transition temperature

Polylactic acid (PLA) is also biodegradable and not synthesized from petroleum derivatives. However, PLA has a low mechanical strength when used at an elevated temperature. At a high temperature around 60 °C, an article formed from PLA loses its ability to withstand twisting forces, which are often observed during the handling of packaging materials. Thus the PLA products may not be suitable for their use in temperate regions (Arrieta et al., 2015). PHB is a distinctive part of various life forms in a different environment and exists as both high and low molecular weight compounds. High molecular

weight PHB (>60,000 Da) is direct polyester that accumulates in a wide variety of Gram-positive and Gram-negative microorganisms. In some Archaea, PHB is accumulated as an intracellular granular stockpiling material, when the organisms are exposed to harsh conditions (for example, under nutrient starvation) (Patnaik, 2006; Valentino et al., 2015). The stored polymeric granules are used for biomass growth when the condition becomes favourable. Low sub-atomic weight PHB (< 15,000 Da) is essentially made out of the monomer 3-hydroxybutyrate, a characteristic ketone body found in human blood. Low atomic weight PHBs have been found in a wide variety of prokaryotes and eukaryotes, including humans, and are accepted to be a constituent of each living cell (Rodríguez-Contreras et al., 2016; Valentino et al., 2015). High sub-atomic weight PHBs have invoked a great enthusiasm from the industry, since chemically these are polyesters and, from physical properties viewpoint, these are thermoplastics that can be dissolved in solvents and cast to form long-lasting structures. Therefore, these materials are often referred to as PHB bioplastics. They are biodegradable in all bio-active environments and can be produced from various industrial refuses/wastes. Microorganisms responsible for PHB production are found in a range of environment. However, they can be mainly isolated from root nodules as they lead a symbiotic relationship with nitrogen-fixing organisms found in the root nodules.

Biocompatibility of PHB bioplastics in living creatures has been established in sheep, swine, and chicken (Lizarraga-Valderrama et al., 2016). Different areas in which PHB bioplastics can be used include restorative applications in the human body where the material is implanted or used as a strong carbon substrate or as a support for aquaculture de-nitrification forms. Studies with the monomers of 3-hydroxybutyrate have recommended for their nutraceutical and other therapeutic applications (Borowitzka, 2013; Snell, 2009). In wild type microorganisms, PHB bioplastics are produced intracellularly as

well-defined granules by various pathways that have been widely reported in the literature. This research focuses on the production of PHB as a large volume, value-added product in a closed-loop biorefinery set up.

1.2.2. Applications of PHB

With excellent physical properties of PHB, it finds an extensive array of end-use applications, which include blend formed materials from golf tees to hardware lodgings; films for diapers, packaging and agriculture; thermoforming for holders and espresso mug tops; strands for monofilament; non-wovens for use in everything from soundproofing in vehicles to non-woven articles for wipes or diapers; froth for both packaging and foodservice wear; and coatings for paper for packaging and pharmaceutical products (Fig. 1.2).

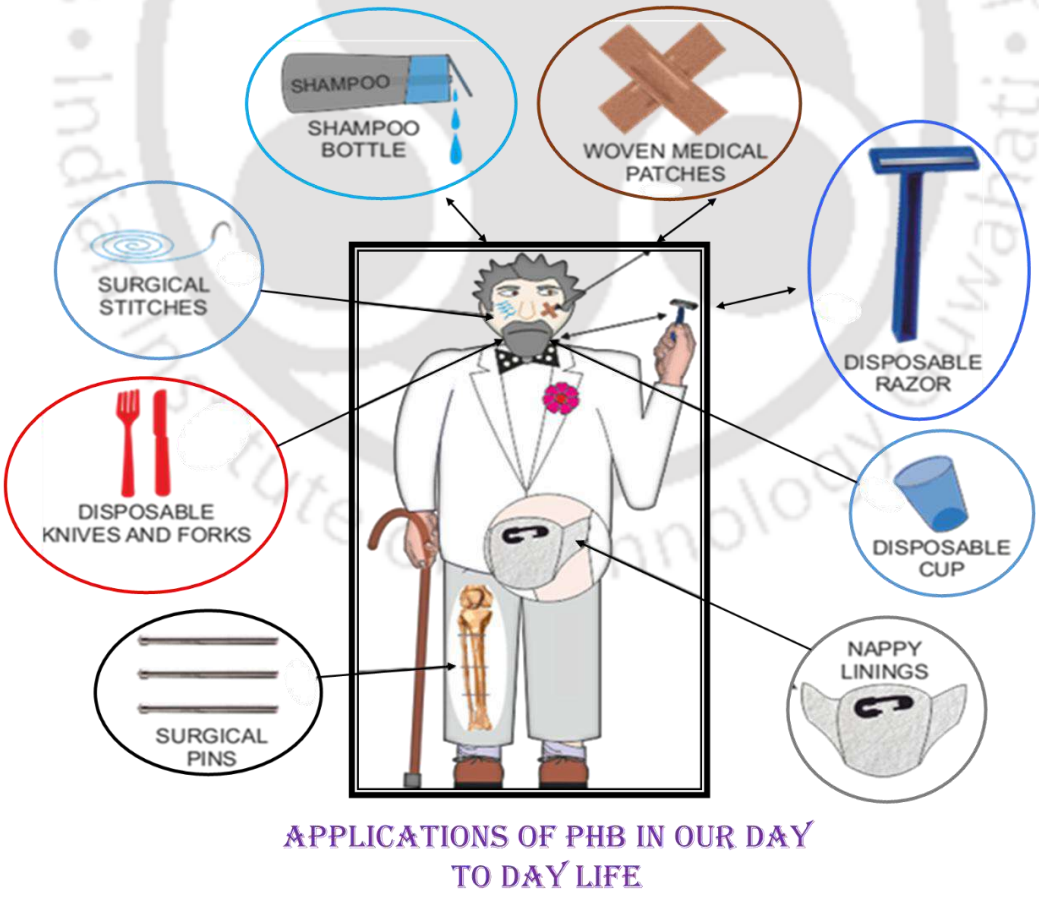

Fig. 1.2. Various applications of PHB

The properties and uses of PHB bioplastics can also be improved by mixing PHB with other biobased/biodegradable materials and oil resins. Hence, PHB bioplastics can replace a critical extent of the oil-based polymers used worldwide. In any case, little is thought about the use of PHB for food packaging applications. One of the difficulties confronted by the food packaging industry is on its endeavours to create biodegradable and tough packaging film with excellent barrier properties. The natural-based packaging material must remain stable without any change in mechanical or potentially obstruction properties and must work appropriately without damage until disposal. Natural conditions prompting biodegradation must be abstained from the damage of the food item, though streamlined conditions for biodegradation must emerge in after the discarding (Savenkova et al., 2000).

Further, before using biodegradable material for essential food packaging, the safety must be analyzed. Biodegradability of PHB is another important feature that it offers completely new applications. For example, agricultural films, which are used as a sunscreen on the plants, degrade toward the end of utilization and don't require to be gathered again (Arrieta et al., 2015; Costa et al., 2013). Of the billions of pounds of petroleum-based plastics created each year, packaging materials utilize around 33%, which unavoidably gets piled up in landfills. Therefore, finding appropriate biobased, sustainable, biodegradable choices for packaging material have got enormous market potential.

PHB based bioplastics are currently produced by the process of microbial fermentation utilizing a two-stage cultivation process. The primary stage includes fermentation, which produces PHB intracellularly by utilizing sugars such as fructose, glucose, xylose, etc. as the carbon source. In order to keep the PHB production cost low, cheaply available raw materials, such as hydrolysate of lignocellulosic materials, starchy feedstocks, were often examined (Kajaste, 2014; Naranjo et al., 2014). Following the fermentation stage, PHB rich bacterial cells are collected and the product (PHB polymer)

is isolated and recovered from the microbial cells by utilizing either a polymer dissolvable extraction procedure or an aqueous procedure in which the non-PHB part of the microbial cell is processed, either synthetically or enzymatically, leading to the separation of PHB polymer. The significant cost associated with the PHB production is majorly due to the high capital cost involved in establishing of efficient aerobic fermentation facilities as well as the huge cost involved in the purchase of sugar feedstock for production and organic solvents for polymer extraction. Hence, there is a need to evaluate cheaper PHB production methods utilizing suitable industrial waste/refuse as a potent source for biomass production and PHB extraction.

1.2.3. PHB production pathway

The monomeric group of the polyhydroxyalkanoates (PHA) based polymer depends upon the type of sugar source present in the culture broth. For instance, polyhydroxybutyrate synthesis in *Cupriavidus necator* or *Ralstonia eutropha* takes place as follows: two acetyl-coA generated from the tricarboxylic acid (TCA) cycle is condensed to form acetoacetyl-coA and this condensation reaction occurs in the presence of enzyme, β-ketothiolase (PhaA). After that, acetoacetyl-coA is reduced to 3-hydroxybutyrylcoA by the action of acetoacetyl-coA reductase enzyme (PhaB). Finally, 3-hydroxybutyrylcoA is polymerized to form polyhydroxybutyrate by the esterification process that takes place in the presence of PHA synthase enzyme (PhaC) (Anjum et al., 2016). This PHB is then reserved as inclusion material in bacterial cells (Fig. 1.3).

1.3. Refused biomass sources

Biomass and biomass derived from plant materials have been identified as the single most alternative to petroleum-based raw materials for polymer production. These materials are produced from CO_2 in the atmospheric air, water from the soil with the help of chlorophyll

and sunlight through the process, photosynthesis. Accordingly, biomass has been considered to be the main practical source of natural carbon in the earth and the ideal proportionate to oil for the generation of energies and fine chemicals with net-zero carbon emission (Kajaste, 2014; Naranjo et al., 2014).

In this context, lignocellulosic biomass, which is the most abundant resource on the earth, is of high volume. Many reports have demonstrated that lignocellulosic biomass holds massive potential for sustainable and large scale production of chemicals and fuels. Also, it is an inexhaustible feedstock available throughout the world (Pradhan et al., 2017; Saratale et al., 2019). The use of lignocellulosic can further diminish CO_2 emission and environmental contamination. In this way, it is a promising alternative to conventional petroleum feedstock, for the production of biofuels, biomolecules and biomaterials. Lignocellulosic feedstocks are more interesting compared to other biomass varieties as these are a non-consumable segment of a plant and, consequently, it doesn't compete with the food supplies (Arul Manikandan et al., 2019). Also, forestry, farming and agro modern lignocellulosic wastes are gathered every year in huge amounts; their disposal causes serious environmental concerns. Therefore, it could be beneficial to use such lignocellulosic biomass for the production of various value-added products (Brar et al., 2017). From a financial perspective, lignocellulosic biomass can be produced rapidly and more cheaply than the other agronomically critical biofuel feedstocks, for example, corn starch, soybean and sugarcane. Also, these feedstocks are less expensive than crude oil.

However, the advancement of lignocellulosic biomass conversion to fine chemicals and polymers remains a great challenge. Table 1.2 presents literature on biomass production and PHB accumulation by different microorganisms using industrial waste as feedstock, which reveals that the recent research is focused on value addition of such waste resources using suitable microorganisms. During the process of deriving key feedstock

components from the raw agricultural plants, a vast amount of residues was refused from these industries.

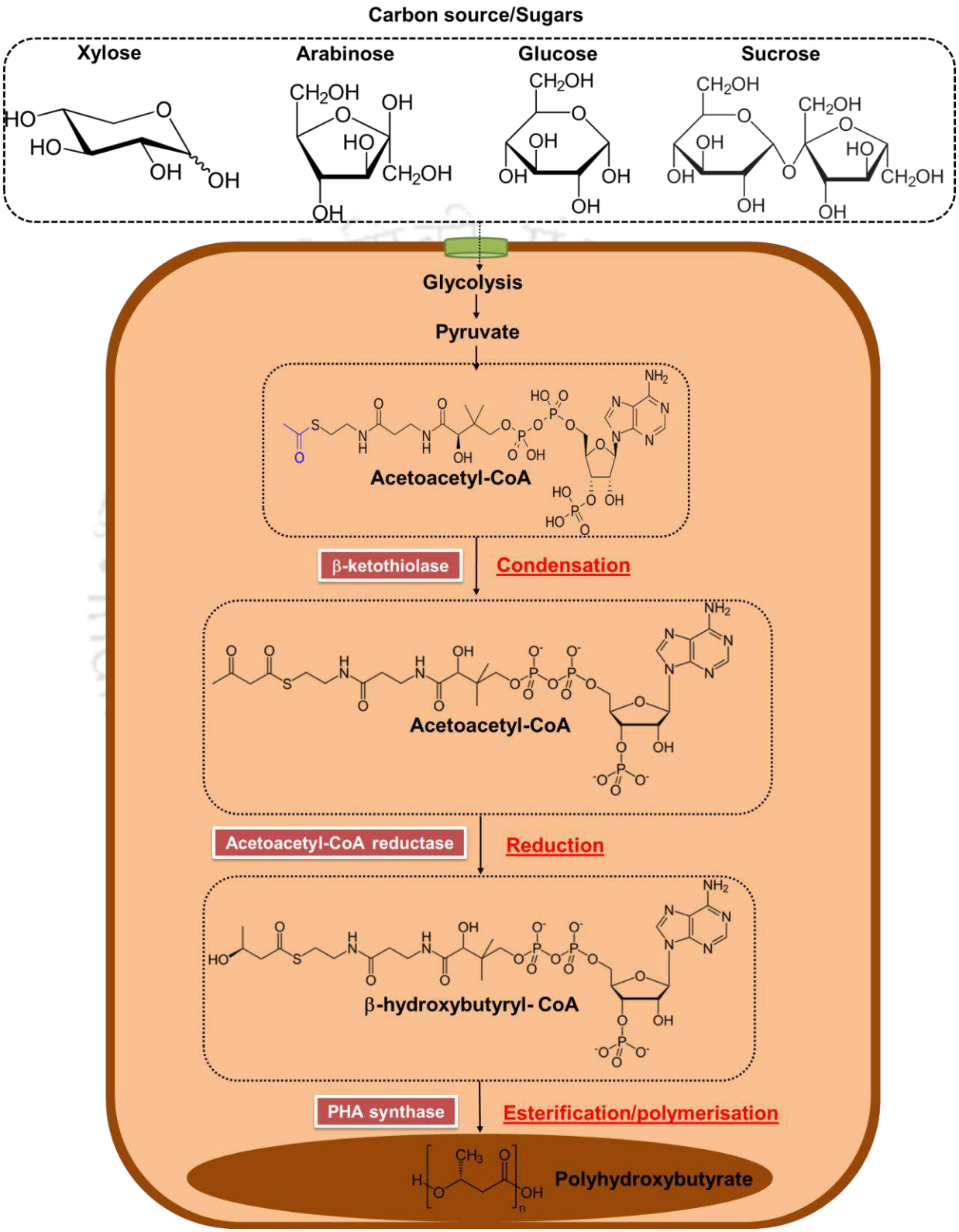

Fig. 1.3. Metabolic pathway for PHB production

Table 1.2. PHB production by different microorganism using industrial refuse as cheap feedstock

Biomass	Producer strain	Industrial source	Biomass (g/ L)	PHB (g/L)	References
Bagasse hydrolysate	*Ralstonia eutropha*	Sugar mill	11.1	6.3	(Yu and Stahl, 2008)
Xylose	*Burkholderia sacchari*	Grassland	5.5	3.2	(Lopes et al., 2011)
Coir pith	*Azotobacter beijerinickii*	Coir industry	5.0	2.4	(Sathesh Prabu and Murugesan,
Xylose	*Burkholderia sacchari*	Grassland	5.3	2.7	(Lopes et al., 2011)
Wood hydrolysate	*Burkholderia cepacia*	Sawmill	16.9	8.7	(Pan et al., 2012)
Hyacinth hydrolysate	*Ralstonia eutropha*	Municipal refuse	12	7.0	(Radhika and Murugesan, 2012)
Grass biomass	*Pseudomonas sp.*	Grassland	0.9	0.3	(Davis et al., 2013)
Rice straw hydrolysate	*Bacillus firmus*	Agro-industries	1.9	1.7	(Sindhu et al., 2013)
Softwood hydrolysate	*Sphingobium scionense*	Sawmill	1.23	0.4	(Bowers et al., 2014)

Spent coffee hydrolysate	*Burkholderia cepacia*	Instant coffee manufacture	5.5	3.1	(Obruca et al., 2014)
Sunflower husk	*Ralstonia eutropha*	Agro industry	13.13	8.82	(Saratale and Oh, 2015)
Soybean straw			12.12	7.54	
Wood straw			11.42	6.79	
Rice paddy straw			15.50	10.9	
Fructose	*Cupriavidus necator*	Beverage industry	9.58	7.3	(Guzman Lagunes and Winterburn, 2016)
Date seed	*Cupriavidus necator*	Food industry	6.3	4.6	(Yousuf and Winterburn, 2016)
Parthenium	Pentose	*Ralstonia eutropha*	2.93	0.24	(Pradhan et al., 2017)
	Hexose		3.35	0.60	
Hyacinth	Pentose		3.70	0.30	
	Hexose		4.44	0.96	

Even though some of these refused sources were used as a cattle feed and in some cases with fewer processing, they were returned to the land as organic fertilizers. Much of these refused sources were disposed of as municipal, agro-industrial, and grassland wastes. Therefore, utilizing such waste feedstock for PHB production stands to be unique and an attractive topic of recent research. Since lignocellulosic material is a complex mixture of three polymers, viz. lignin, cellulose and hemicellulose, it needs to be fractionated. The inhibitory portion (lignin) and the sugars (cellulose and hemicellulose) require for growth

of microorganism. After fractionation, the cellulose and hemicellulose-containing portion are generally hydrolyzed using acid or enzyme to extract the sugars, which can be used as a ready source for PHB production in the presence of other mineral salts (Fig. 1.4).

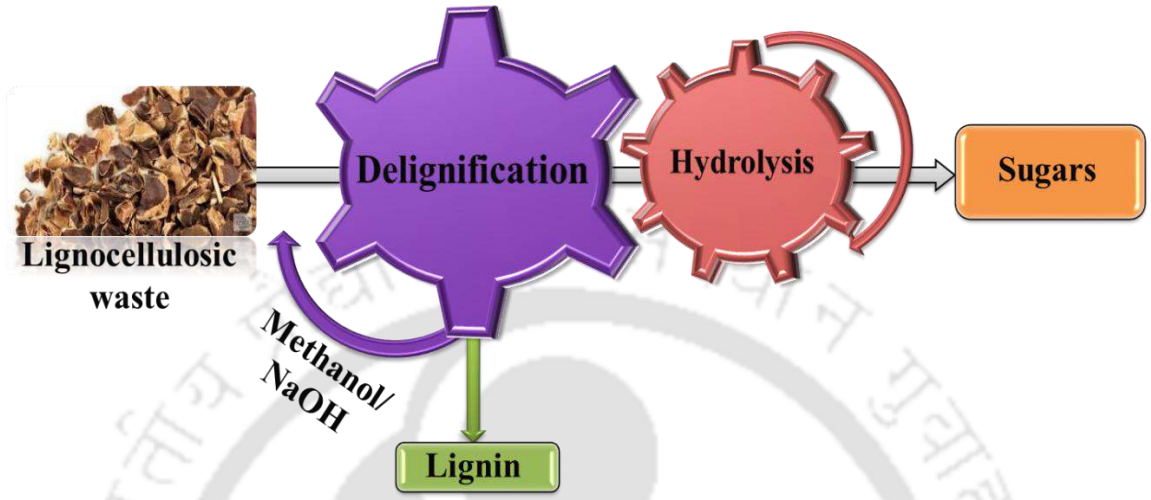

Fig. 1.4. Fractionation and hydrolysis of lignocellulosic waste for the extraction of sugars

1.3.1. Bagasse

Bagasse is a refused source from the sugar industry. Wherein sugarcanes are mainly processed for the production of sugar juice and the latter for the production of fine sugars and molasses. Though bagasse is used as a fuel for boilers, many occasions, it is found to be less noticed and refused from the industry due to its lower fuel efficiency. Bagasse is fibrous in nature, and many studies have reported the utilization of bagasse hydrolysate as a promising feedstock for PHB production. For instance, Silva et al. (2004) used *Burkholderia sp.*, a bacterial strain for the production of PHB from the bagasse hydrolysate. In the particular study, the bagasse hydrolysate was processed by a three-fold pretreatment technique to enhance its fermentability and consecutively for PHB production. As a first step, the hydrolysate was concentrated to increase the sugar concentration and, thereafter, it is treated with lime to bring the hydrolysate to neutral pH; as a final step, the hydrolysate is treated with activated charcoal for the removal of growth inhibitors. Using the processed

hydrolysate, among the different organisms, *Burkholderia sp.* yielded a maximum biomass concentration of 4.4 g/L and PHB concentration of 2.7 g/L (Silva et al., 2004).

In a study conducted by Yu and Stahl, (2008), *Ralstonia eutropha* grown on dilute acid pre-treated bagasse yielded a biomass and PHB concentration of 11.1 g/L and 6.3 g/L, respectively. In another study carried out by Gowda and Shivakumar (2014), growth of *Bacillus thuringiensis* on sugarcane bagasse hydrolysate resulted in the biomass and PHB concentration of 10.6 g/L and 4.2 g/L, respectively. In a prudent study carried out by Munoz and Riley, (2008), the authors used cellulosic fibre obtained from a tequila manufacturing industry and cultured *Saccharophagus degradans* without hydrolyzing the fibres but in the presence of minimal salt in the medium. The organism was able to degrade cellulose and directly utilize the sugars thereof for polyhydroxyalkanoate (PHA) production. This study is unique and interesting due to the fact that the upstream strategy involved no hydrolysis step for the fibres, which reduces the overall cost drastically. However, PHA yield obtained in the study could not be ascertained, and no progress seems to be made further following this strategy.

1.3.2. Spent coffee bean grounds

Next to bagasse, spent coffee bean grounds were observed to be the next promising feedstock for PHB production. For the past two century, coffee beans have gained commercial interest as it is one of the most widely used beverages around the world. As of the statistics in 2010, it was reported that there were more than 8 million tons of coffee beans produced worldwide annually. In the process of coffee drink preparation, the solid residues are rejected from instant coffee manufacturers, and these are commonly regarded as spent coffee bean grounds (SCBG) (Al-Battashi et al., 2019). This SCBG comprises around 15% of oil, which can be extracted and used as a carbon source for PHB producing organisms, more specifically for *Cupriavidus necator* (Cruz et al., 2014; Obruca et al.,

2014). Even after the extracting oil from SCBG, the residue comprises primarily of hemicelluloses and cellulose, which can be further hydrolyzed to acquire sugars. The sugars can be used for the production of PHB by using *Burkholderia cepacia.* It was reported that hexoses, i.e. galactose and mannose were the major sugars in the hydrolysate and these hexoses were found to be more favourable than the pentose sugars for PHB production. Furthermore, levulinic acid produced due to partial degradation of hexose during the acid pretreatment step gave rise to PHA production as it is considered a good precursor for the production of the copolymer, poly- 3-hydroxy-butyrate-valerate (Obruca et al., 2014).

1.3.3. Coir Pith

From the coir industry, majority of coconut fibres are refused as coir pith, and, in many cases, due to their recalcitrant nature and high lignin content, it is considered a waste material. It is observed that on an average, the coir pith takes a decade to degrade, which gives severe environmental threat and creates a further problem in solid waste management (Al-Battashi et al., 2019). Sathesh Prabu and Murugesan, (2010) used this solid waste for PHB production by using *Azotobacter beijerinickii* by a multi-step pretreatment procedure, wherein the coir pith was first delignified, and the cellulose fibres in it were treated with cellulase enzyme for the extraction of reducing sugars. Finally, these sugars were fed to *A. beijerinickii* that resulted in a maximum PHB titre value of 2.4 g/L (Sathesh Prabu and Murugesan, 2010).

1.3.4. Rice straw

Rice straw obtained from the vegetative part of paddy during its harvest is well-known as a cattle feed. However, in most cases, a large quantity of it is burnt or ploughed, which leads to air/land pollution. Sindhu et al. (2013) utilized rice straw hydrolysate for PHB production by *Bacillus firmus*. The rice straw hydrolysate in the study was obtained by acid pretreatment, and the hydrolysate was reported to certain sugars and other sugar

products such as acetic acid, furfuraldehyde, formic acid and hydroxymethylfurfural (HMF). The authors cultured the organisms without removing the inhibitors, which lead to low biomass and PHB titre value of 1.9 g/L and 1.7 g/L, respectively. However, very high PHB content of about 89 % was observed. This study suggests that though the inhibitors reduced the biomass growth and PHB production, the PHB content was induced in the presence of these inhibitors (Sindhu et al., 2013).

1.3.5. Empty oil palm fruit bunches

In Southeast Asia, significantly high production of oil palm of about 15 million tonnes and even more is noticed annually. Oil palm is considered an industrial crop and is used as the feedstock for palm oil industries. Following the extraction of palm oil, the empty oil palm fruit bunches are refused from the industries (Obruca et al., 2014). These oil palm empty fruit bunch were reported to comprise of cellulose, hemicellulose, lignin and ash content of 50.4 %, 21.9 % 10 % and 17.7 %, respectively. Zhang et al. (2013) in their study, utilized this empty fruit bunches and hydrolyzed it first with chemical pretreatment. After that, the authors used a cocktail of cellulase enzyme for the synthesis of reducing sugars. The reducing sugars in the hydrolysate in the presence of tryptone were identified to be a suitable source for the growth of *Bacillus megaterium* and PHB production. A maximum PHB content of 51.6 %, PHB concentration of 12.48 g/L and a PHB productivity of about 0.260 g/L·h was achieved (Zhang et al., 2013).

1.2.6. Wheat straw

During wheat processing, wheat straw and wheat bran are refused as residues, which can serve as a potential feedstock for PHB production. In the year 2012-2013, about 660 million tonnes of wheat were produced worldwide, and of which about 15-20 % was wheat straw (Obruca et al., 2014). The primary producers of wheat are Asia, Europe and North America, with a global share of about 43 %, 32 % and 15 %, respectively (Kim and Dale, 2004). In

this regard, Van-Thuoc et al. (2008) used wheat bran and hydrolyzed it by enzymatic hydrolysis and the sugars produced were used for PHB production using *Halomonas boliviensis*. However, to increase the PHB yield, the carbon content in the medium was increased by the addition of sodium acetate and butyric acid, which was obtained from anaerobic digestate of solid potato waste. The authors reported a maximum biomass and PHB concentration of 8.0 and 4.0 g/L, respectively (Van-Thuoc et al., 2008). Other than wheat bran, wheat straw has also been used for PHB production using *Burkholderia sacchari*. In a study by Cesário et al. (2014), the authors hydrolyzed the wheat straw by ammonia fibre expansion (AFEX) process, and the cellulose and hemicellulose comprising mixture from the process mentioned above were further hydrolyzed using an enzymatic process. The final mixture comprises of hexose and pentose sugars, such as glucose, arabinose and xylose. In that study, the authors adopted a fed-batch strategy for PHB production, and a maximum PHB content of 72 % was observed along with a PHB to carbon source yield of 0.22 g/g and PHB productivity of 1.6 g/L·h.

1.3.7. Grassland refuse

Globally, nearly 69% of agricultural land accounts for about 3.4 billion hectares in the entire world is covered by grasslands. Particularly in Europe, out of 164 million hectares of agricultural area, 76 million hectares are permanently found to be the grassland (Obruca et al., 2014). Some of the major advantages of grasslands are: unlike agricultural land, these grasslands do not require any fertilizers; secondly, there is no need of annual ploughing and, finally, instead of greenhouse gas emissions, they act as the sink to reduce the carbon pollution in the atmosphere (Fischer et al., 2010). In a study reported by Davis et al. (2013), the authors used grass biomass as a feedstock for PHB production using *Pseudomonas* strains. The authors followed NaOH and hot water treatment for delignification, and, thereafter, the delignified biomass was treated with enzymes for sugar synthesis. The sugars

were subsequently used for the growth of *Pseudomonas* strains, which yielded a maximum *mcl*-PHA content of around 20-34 % (Davis et al., 2013). This study on grass biomass as the sole source of carbon and energy for PHB production was further developed by Koller et al. (2013) The authors used the juice extracted from the green grass and supplemented it with complex nitrogen and phosphate source for the enhancement of PHB production by *Ralstonia eutropha* (Koller et al., 2013). In another study by Radhika and Murugesan, (2012) reported on saccharification of water hyacinth, the authors reported that enzymatic hydrolysis is more preferred than acid hydrolysis for growth and PHB accumulation using *Ralstonia eutropha*. The authors optimized the process by using response surface methodology and found that with an initial sugar concentration in the hydrolysate of about 35 g/L and at the end of 72 h of fermentation, a maximum biomass and PHB concentration was estimated to be 12 g/L and 7 g/L, respectively (Radhika and Murugesan, 2012).

1.3.8. Waste date seeds and citrus biomass

Annually, 7 million tonnes of dates are produced across 30 countries, and each fruit comprises of 10 -15 wt% of seed in it. More than 1 million dates seeds are refused annually from the dates processing industries. Date seeds that are obtained after harvesting the date fruit are considered to be a waste; however, it has a high nutrient content that can be harnessed for PHB production. The date seed contains 50-70% carbohydrates, 20-40% proteins and 10-12% oil. Therefore, the carbohydrate can be readily hydrolyzed into sugars and protein, which can be used as a substitute for the growth of microorganisms. Yousuf and Winterburn, (2016) used date extract for PHB production using *Cupriavidus necator*, and reported a maximum biomass and PHB concentration of 6.3 g/L and 4.6 g/L, respectively, in the presence of an initial sugar concentration of 10.8 g/L.

Furthermore, the citrus processing industry during the production of orange juice refuses orange peel as one of the main waste material. Every year it was perceived that 50

million tonnes of orange fruits are produced and out of which 3 million tonnes were considered to be the edible portion and 1.5 million tonnes were refused as waste from these industries. Guzman Lagunes and Winterburn (2016) reported that the extract from the skin, seed and pulp of the orange resulted in a biomass and PHB concentration of 9.58 g/L and 7.8 g/L, respectively. In another study by Saratale et al. (2019), utilization of kenaf fibre (a non-edible crop and lignocellulosic biomass) was reported for PHB production using *Ralstonia eutropha*. A maximum biomass and PHB concentration of 18.3 g/L and 13.12 g/L, respectively were reported.

The initial assessment of different industrial refuse/waste biomass reported in the literature on utilization of these biomasses for PHB production revealed that the gap in the research side was converting the waste biomass to PHB production without paying attention to by-products and other useful resources generated from the process. Therefore, there is a need for a holistic approach toward the conversion of waste biomass into PHB, which can be brought about by introducing an integrative approach wherein a sequence of operation is cascaded so that the by-product of one process acts as the feedstock for the next immediate operation. Likewise, there is a need for biorefinery approach, which will support to unravel the full potential of waste biomass by deriving a maximum number of products and ensuring zero waste discharge. Thus waste biomass offers a promising means for PHB production at reduced production costs, however in order to realize the actual potential, further studies on the scale-up of the PHB production process from shake flask to bioreactors are inevitable. Hence, appropriate bioreactor systems should be chosen with respect to the nature of feedstock used for PHB production. In connection with this, the following section describes the different types of bioreactors used for PHB production.

1.4. Closed-loop biorefinery

In a conventional biorefinery, provision for cascading or recycling for an efficient utilization of materials derived from a process are usually not available. Moreover, several materials are excluded or even discarded, leaving the process an open linear type (Venkata Mohan et al., 2020). Due to rapid increase in population, which is expected to touch 9.8 billion in the year 2050 (Buchmann et al., 2019), production processes must be environmental friendly, sustainable and economical. Thus, there is a worldwide promotion for strategies like zero waste discharge, wealth from waste and resource recovery. In this regard, a closed-loop approach integrates different unit processes and operations by involving products and by-products derived from different units, thereby reutilizing the materials and minimizing the use of external resources. Hence, closed-loop biorefinery operations are frequently marked as economically viable, environmentally safe and self-sustainable in nature (Venkata Mohan et al., 2020).

Bioprocesses involving closed-loop approach are very recent to the field of biotechnology and bioengineering. And only a handful of reports are available in the literature (Fig. 1.5), which necessitates further research in this subject area. For instance, Socha et al. (2014) hypothesized the use of lignocellulosic biomass for the production of ionic liquids and its consecutive use in the same process for pretreatment of feedstock. Venkata Mohan et al. (2020) envisaged a blue-bioeconomy using algae as a self-sustainable source in a closed-loop approach. As illustrated in Fig. 1.5b, microalgae were cultivated on wastewater, and following extraction of various value-added products from the algal biomass, the by-products obtained were recycled back into the process for microalgal cultivation.

Similarly, Buchmann et al. (2019) developed a closed-loop biorefinery concept for continuous production of protein from microalgae by using a pulsed electric field

technique. Instead of harvesting the microalgae and extracting protein out of it, the authors reversibly treated the microalgal cells to extract protein into the broth (Fig. 1.5c). Reversible treatment of microalgae maintained the integrity of the microalgal cells, thereby enabling the biomass to be recycled back into the process for protein production. Other than these reports, there is no literature available on closed-loop biorefinery operations. Hence, this study envisages a closed-loop biorefinery approach for sustainable and economical production of PHB from waste carob pods.

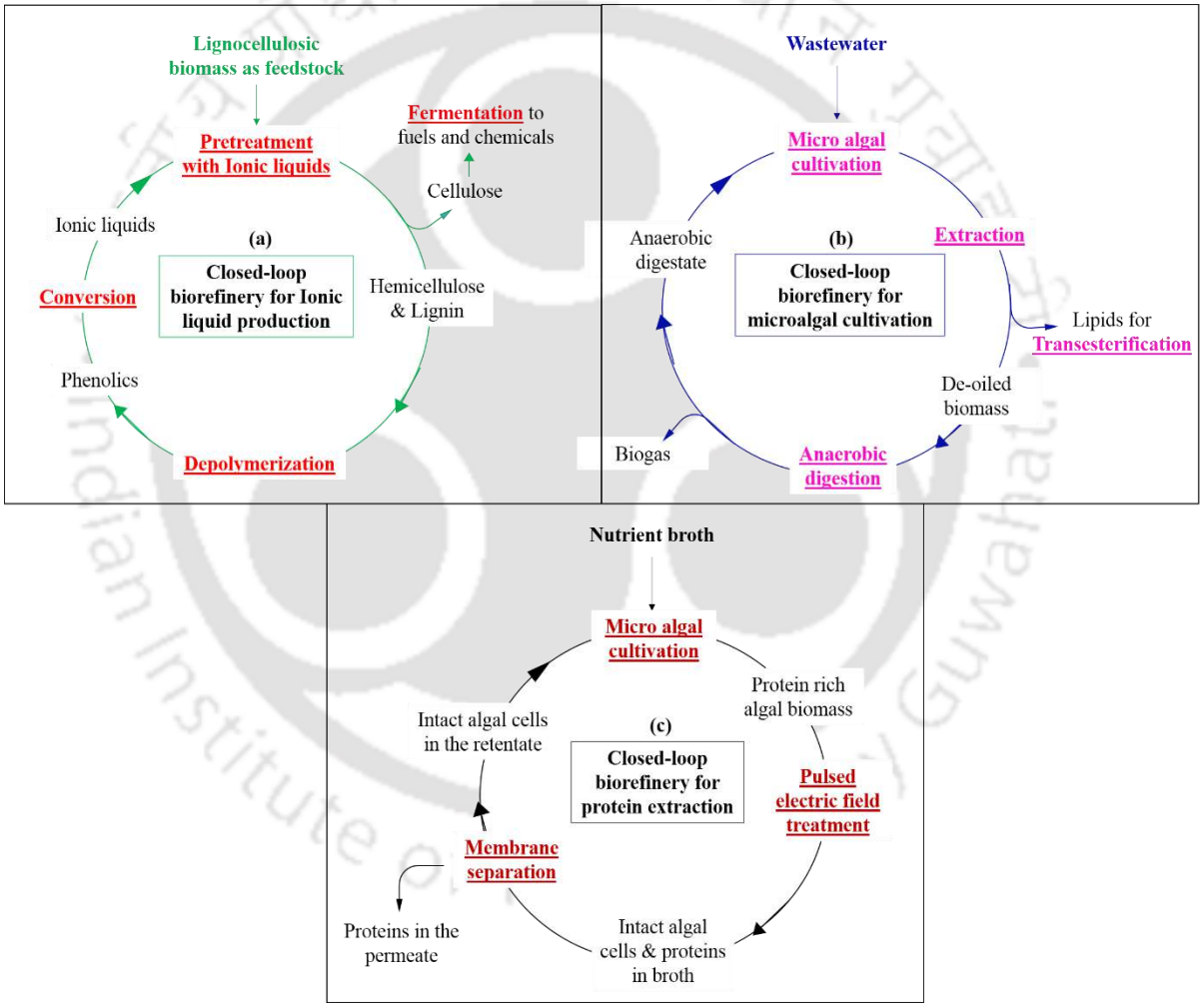

Fig. 1.5. Closed-loop biorefinery for (a) ionic liquid production, (b) microalgal production and (c) protein extraction (Underlined texts denote processes and regular ones are process derivatives).

1.5. Reactor considerations for upstream processing of PHB

Over the past decades, a variety of bioreactors have been studied for PHB production, and amongst which stirred tank bioreactor, airlift bioreactor, bubble column bioreactor and two-phase partitioning bioreactor stand out to be very common. Furthermore, these bioreactors were operated in various modes, viz. batch, continuous, continuous with cell recycle and fed-batch. All the aforementioned bioreactors used for PHB production are described briefly as follows:

1.5.1. Stirred tank bioreactor

Stirred tank bioreactors (STBRs) are most often used bioreactor for any biological processes and more specifically for aerobic fermentation. This bioreactor system comprises of a vessel (often made from glass) to hold the culture medium; air is sparged at the bottom of the vessel through a sparger, and it is dispersed uniformly by an impeller connected to a rotating shaft (Fig. 1.6a). Baffles of varying number from four to six are used to ensure sufficient mixing in the reactor. Increasing the impeller speed improves the oxygen transfer to the medium; however, beyond a certain speed, shear stress is imposed on the microorganism due to the sharp edges in the impeller and the baffles. On the increase in oxygen transfer also increases the biomass production and therefore PHB accumulation inside. Many studies have been carried out on PHB production using stirred tank bioreactors. Khanna and Srivastava, (2005) employed stirred tank bioreactor for the cultivation of *Ralstonia eutropha* with an initial fructose concentration of 40 g/L. The authors observed a maximum biomass and PHB concentration of 20.73 g/L and 9.35 g/L, respectively. Furthermore, PHB to fructose yield of 0.24 g/g was achieved (Khanna and Srivastava, 2005).

1.5.2. Airlift reactor

Unlike stirred tank bioreactor, airlift reactors (ALRs) are unique in its design as there are no rotating parts inside, and air circulation inside serves to bring about the necessary mixing. Because of this feature, they are often classified as pneumatic reactors. In its basic design, ALR comprises a draft tube in a long vertical cylinder with air sparger located at the bottom of the cylinder (Fig. 1.6b). However, ALR can be classified into two types: inner loop airlift reactor (ILALR) and external loop airlift reactors (ELALR). In the ILALRs, a partitioning wall is placed within the vertical cylinder, thereby separating the fluid medium into two regions, where one region is called as the upcomer and other one is called as the downcomer. These two regions give enough chance for the medium to circulate, thereby creating a well-defined fluid flow pattern. In the case of ELALR, a downcomer is placed as a separate arm to the airlift reactor and thereby, the fluid circulation is established in the reactor. Due to its simplicity in design and the absence of energy-intensive parts (e.g. impellers and shaft), both capital cost and operating cost are found to be relatively low. The modified flow of fluid introduced in the ALR ensures an enhancement in oxygen and nutrient supply from liquid medium to solid biomass. Furthermore, better heat transfer, quick mixing time and cell retention are the added advantage of using ALRs. Compared to stirred tank bioreactors, ALRs are observed to maintain a high level of sterility inside the reactor.

Many studies compare the performance of stirred tank bioreactor (STBRs) with that of ALRs for the growth of various microorganisms production of different metabolites and even for the degradation of different pollutants. These studies reported that though ALR operation is both simple and economical, it is slightly inferior in terms of efficiency. In line with these studies, ALRs were also used for PHB production by numerous authors. For instance, Tavares et al. (2004) cultivated *Ralstonia eutropha* in ALRs with a superficial gas

velocity of 10 m/s. They observed a maximum PHB productivity of 0.6 g/L·h along with a PHB cell content of 50% (Tavares et al., 2004). Nevertheless, the authors reported slightly higher productivity of 0.82 g/L·h with STBR. Finally, the authors concluded that the performance of ALR is better than STBR owing to its low energy demand. In another study by Pradella et al. (2010), the authors cultivated *Burkholderia sacchari* in an airlift reactor and operated the reactor under high cell density cultivation mode. A maximum PHB productivity of 1.7 g/L·h with a PHB to sucrose yield of 0.2 g/g was observed (Pradella et al., 2010). In another study by Du et al. (2004), the authors used short-chain fatty acids obtained from an anaerobic digester as a substrate for the growth of *Ralstonia eutropha* in ALR. A maximum biomass concentration of 22.7 g/L with 72.6% PHB content present in the biomass was reported (Du et al., 2004). Gahlawat et al. (2012) cultured *Azohydromonas australica* using a modified airlift reactor, with provision for in situ cell retention (Table 1.3). Performance of this novel airlift reactor was compared with that of STBR. The results demonstrated that the maximum biomass and PHB concentration of novel airlift reactor (10.76 g/L; 7.81 g/L) is superior in comparison with that of the STBR (8.31 g/L; 5.45 g/L) (Gahlawat et al., 2012).

1.5.3. Bubble column reactor

Bubble column bioreactors (BLBRs) can be classified under the category of multi-phase bioreactors. BLBRs consists of a long vertical cylinder similar to that of ALRs, however without any draft tube or partition contained in it (Fig. 1.6c). These reactors are also not having any moving parts similar to ALR but comprise of air distributor. The air distributor ensures uniform mixing in the reactor by proper distribution of gas and liquid phase, thereby leading to excellent mass and heat transfer in the reactor system. The reactor design is not only simple, but also it's capital and operation cost is considerably low. BLBRs in PHB production have certain advantage, such as they impart less shear stress on the PHB

producing microorganisms, easy to maintain the sterility as there are no moving parts or sealing present in the reactor. Last few years, many studies have been conducted using BLBRs for PHB production. For instance, Rahnama et al. (2012) utilized natural gas for PHB production using a bubble column bioreactor with *Methylocystis hirsute.* The authors observed a very low PHB concentration of 1.4 g/L This was attributed to the source (natural gas) used that was not a favourable substrate for the microorganism (Rahnama et al., 2012). Furthermore, in a study by García-Pérez et al. (2018), the authors used the same strain and substrate as mentioned before; however, a slight modification in the bubble column bioreactor was brought by adopting an internal gas recycling strategy. Through this recycling strategy, the authors observed an enhanced delivery of methane from the gas phase to the liquid phase, which resulted in a maximum PHB productivity of 1.4 ± 0.4 kg/m^3·d and a PHB content of $34.6 \pm 2.5\%$ (García-Pérez et al., 2018).

1.5.4. Two-phase partitioning bioreactor

In two-phase partitioning bioreactors (TPPBs), a non-aqueous phase is added along with the aqueous media in stirred tank bioreactor, which supports biological processes. The non-aqueous phase serves to overcome the limitation of the substrate or product toxicity experienced by the microorganisms (Zúñiga et al., 2011). In some other cases, when the substrate is insoluble in water, the non-aqueous phase is supplemented to increase the substrate bioavailability. Many organic solvents, polymer and copolymers have been used as a non-aqueous phase. Initially, TPPBs were designed to enhance the oxygen transfer in the culture medium with a final goal of achieving a maximum product yield. These reactors were used for producing citric acid and ethanol, and for polyaromatic hydrocarbons (PAHs) degradation.

Table 1.3 Comparison of PHB production on various bioreactors reported in the recent literature

Substrate	Bioreactor	Microorganism	PHB concentration (g/L)		Ref.
			Batch	Fed-batch	
Glucose	Real-time reaction biocalorimeter (BioRC1e)	*Ralstonia eutropha*	4.33	ND	Anusha et al. (2016)
Waste glycerol	Stirred tank bioreactor	*Cupriavidus necator*	ND	51.15	Cavalheiro et al. (2009)
Glucose	Stirred tank bioreactor	*Escherichia coli*	2.48	ND	Inan et al. (2016)
	Microbubble bioreactor		1.12		
Sucrose	Stirred tank bioreactor	*Azotobacter vinelandii* (Wild type)	5.1	ND	Díaz-Barrera et al. (2016)
		Azotobacter vinelandii (Mutant)	4.4		
Sucrose	Airlift reactor	*Azohydromonas australica*	7.81	ND	Gahlawat et al. (2012)
	Stirred tank bioreactor		5.45		
Sucrose	Stirred tank bioreactor	*Azotobacter vinelandii*	6.6	22.9	Castillo et al. (2017)

Recently, TPPB has been employed for the cultivation of PHB producing *Methylobacterium organophilum* using methane as a substrate. PHB accumulation in the range of 34-38% (w/w) was observed. However, this value was improved even up to 57% (w/w) in the limited nitrogen condition (Zúñiga et al., 2011). Thus, different types of bioreactor systems have been utilized for the production of PHB accumulating biomass: despite the fact that stirred tank reactor is the most widely recognized one, bubble column and airlift reactors were also likewise been investigated for PHB production. However, there are few bioreactors with a special mechanical framework, which are not considered for PHB production. For instance, Taylor and Couette reactor or annular bioreactor has different mechanical frameworks that permit efficient oxygen exchange without including any shear stress to the microorganisms. This reactor has been used in a wide array of applications, such as water purification, emulsion polymerization, liquid-liquid extraction, pigment preparation, photocatalysis, animal cell culture, and cultivation of microalgae (Ramezani et al., 2017, 2015). However, this reactor system has not been utilized for PHB production and hence using these bioreactors would result in enhanced PHB production.

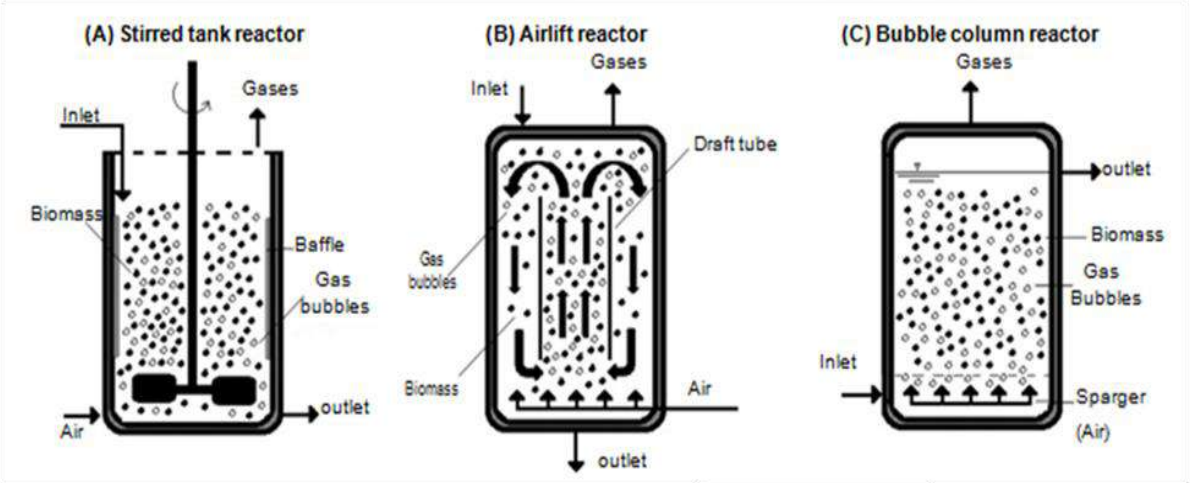

Fig. 1.6. Different bioreactors used for PHB production

1.6. Downstream processing for PHB recovery

Following biosynthesis of PHB, the separation of microorganisms from culture broth is the first step in the downstream operation, which is normally achieved by centrifugation, sedimentation and crossflow microfiltration (Nath, 2017; Waszak and Gryta, 2016). The initial separation of biomass from the culture broth during the downstream processing phase is very crucial for PHB production. This is mainly because the PHB producing bacteria are small in size (0.4 x 0.7 μm), and it poses a significant problem during its separation. Furthermore, in relation to culture volume, the microbial biomass produced is very less. Consequently, a large volume of culture broth needs to be processed in order to recover the whole (intact) biomass from the broth (Elcik et al., 2016).

In general, 20-30% of the total biomass production cost is utilized for separation of biomass from the culture broth (Pragya et al., 2013). In this scenario, an upcoming process like membrane separation seems to be more attractive and suitable for industrial application, particularly in the field of biotechnology (Piry et al., 2008; Pragya et al., 2013; Roshanida et al., 2018; Vasanth et al., 2011). However, membrane resistance due to fouling is a serious issue with membrane separation processes. Several studies have been carried out in the literature to address this problem either by varying the pore size and porosity of such membranes (Pragya et al., 2013; Dizge et al., 2011), or changing the pore shape/geometry from circular to rectangular pore (Bromley et al., 2002), or the length of the membrane (Piry et al., 2008; Piry et al., 2012). Almost all the strategies mentioned above were tested with polymeric membranes, the cost of these polymeric materials was often found to be very high, incorporation of these membranes will increase the final cost of the separation processes (Harabi et al., 2016; Issaoui et al., 2017; Kumar et al., 2015). However, ceramic membrane fabricated with low-cost starting materials viz. ball clay and kaolin remain unnoticed for the separation of PHB rich bacterial biomass. Some significant

advantages of the low-cost ceramic membrane include isothermal operation, zero addition of chemical agents; furthermore, the microfiltration process is regarded as safe for shear-sensitive bacterial cells with intracellular products (Pragya et al., 2013; Kumar et al., 2015; Kumar et al., 2016; Piry et al., 2012).

Following biomass separation from the culture broth, solvent extraction for PHB recovery and purification is highly successful for large scale processes (Koller et al., 2013). Modernly, high utilization of unstable solvents and toxic solvents are regular elements in PHB extraction (Table 1.4).

Table 1.4. Comparison of various PHB extraction protocols as mentioned in the literature

Method	Cost for chemicals	Time	Recovery yields	Product purity	Impact on molar mass	References
Chloroform method	High	Medium	High	High	Low	Fiorese et al. (2009)
Hypochlorite digestion	Medium	Medium	Medium	Medium–high	Medium–high	Saratale and Oh, (2015)
Cyclic carbonates	Medium	Medium	Medium	High	High	Koller et al. (2013)
Fusel alcohol	Low	High	High	Low–medium	Medium–high	Nonato et al. (2001)
Lactic acid method	High	Medium–high	Low–medium	Medium	Medium–high	Koller et al. (2013)
Enzymatic digestion	High	Low	High	Low before refining	No	Koller et al. (2013)
Mechanical disintegration	Medium	Low	Medium–high	Medium	No	Pradhan et al. (2017)

The dissolvable blend remaining after PHB precipitation, comprising of ethanol and chloroform, is usually discarded. Also, reutilization of solvents by distillation is not attractive from the financial perspective. This alienates the character of PHB biosynthesis as "green" innovation. Therefore, the use of green solvents such as lignin that makes the PHB production process both green as well as economical.

1.7. Polymeric nanocomposites for food packaging application

Since 40% of the entire plastic source was used for packaging applications, high interest is shown in recent years for preparing biodegradable polymers from renewable sources (Bomrungnok et al., 2019). In this context, PHB extracted from the process mentioned above can be used for food packaging application. However, its application in the food packaging sector lacks due to its moderate barrier, thermal and mechanical properties. In order to overcome the demerits associated with the PHB for food packaging applications, several fillers, ranging from natural pigments/biochemical compounds to advanced nanomaterials like silver nanoparticles and other nanoclays, were added to form PHB based polymeric composites/nanocomposites (Table 1.5). However, the results of polyhydroxybutyrate (PHB) or polyhydroxybutyrate valerate (PHBV) based composites/nanocomposites have not been successful thus far. Graphene is considered the best as it is the most robust material ever tested, and it offers exceptionally high barrier, thermal and mechanical properties. Further, there are no studies on the preparation of PHB based graphene nanocomposites in the context of food packaging applications with barrier properties and shelf life simulation studies.

Table 1.5. Polymeric nanocomposite with novel nanomaterials for food packaging application

S. No.	Polymer	Filler material	Remarks	Reference
1	Smart fortified PHB and chitosan-based biopolymer	✓ Thymus vulgaris leaf extract ✓ Zinc oxide (ZnO) ✓ Silver (Ag)	• Increase in degradability more than 15% in comparison with pristine PHBV. • Antibacterial property	(Zare et al., 2019)
2	Naturally biodegradable PHBV	✓ Multifunctional Cellulose Nanocrystals ✓ Graphene Oxide	• A 170.2% increment in the tensile strength and 52.1% increment in elongation to break in comparison with pristine PHBV. • 26.3°C increment in the maximum degradation temperature.	(Li et al., 2019)

3	PLA	✓ Reduced graphene oxide (rGO) ✓ Polyvinylpyrroli-done binder	• Water vapour permeability significantly declined by 87.6%. • At least eight-fold extension in the shelf life.	(Goh et al., 2016)
4	PHA	✓ Long alkyl chain quaternary salt (LAQ) functionalized graphene oxide	• Antibacterial rate of 99.9% against Gram-negative and Gram-positive bacteria. • Increase in tensile strength of 60% and storage modulus by 140%.	(Xu et al., 2020)

1.8. Research Gap

The significant cost associated with the PHB production is majorly due to the high capital cost involved in establishing an efficient aerobic fermentation process as well as the considerable cost involved in procuring sugar feedstock for biomass production and organic solvents for polymer extraction. Hence, there is a need to evaluate cheaper PHB production methods utilizing suitable industrial waste/refuse as a potent source for biomass production and PHB extraction. Further, in order to increase the fermentation efficiency, a non-conventional bioreactor with a different framework is needed for PHB production. Additional research on the integration of the upcoming techniques like ceramic-based membrane separation process for the separation of PHB rich bacterial biomass is required.

Besides, incorporation of advanced nanofillers in the PHB matrix to boost the properties to realize its potential for food packaging applications is essential.

1.9. Aim and objectives

The main aim of the present project is to utilize bean gum industry refuse/waste as a sustainable biomass feedstock for PHB production using *Ralstonia eutropha* and its application in food packaging. A novel bioreactor system and ceramic-membrane based separation process for reducing the cost associated with the PHB production was developed in this study. Furthermore, this study aims to develop a sustainable strategy for its possible application in the food packaging sector (Fig. 1.7). To fulfil this aim, the following objectives are framed:

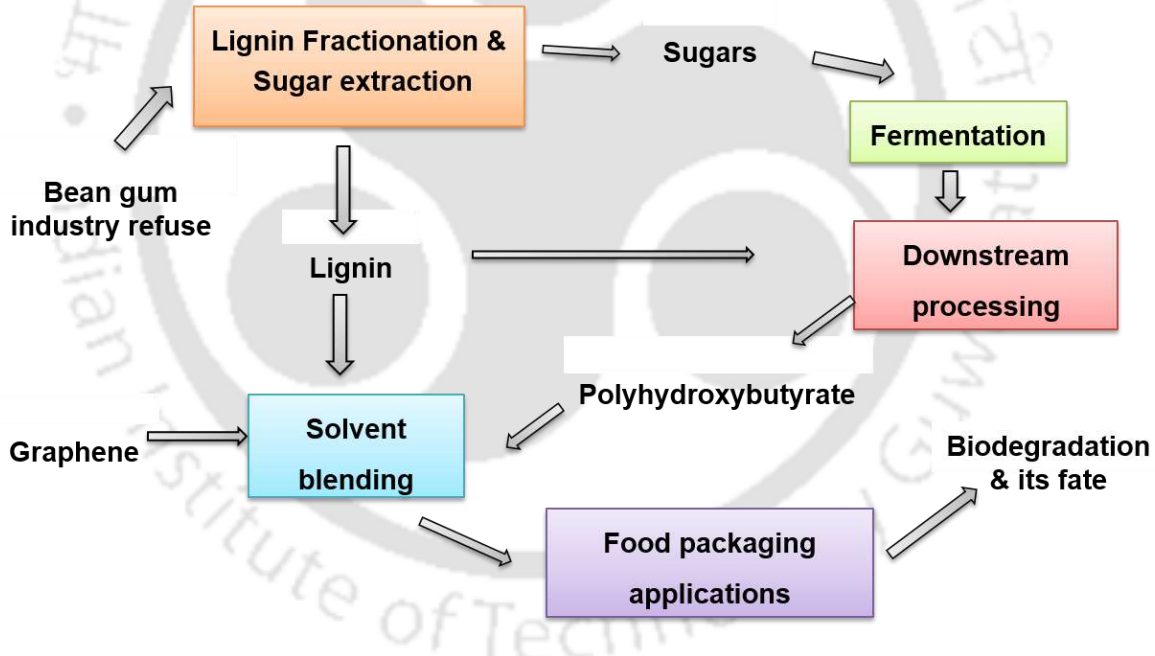

Fig. 1.7. Overall scheme and different steps involved in the present project

1. Strategy development for upstream to downstream processing in PHB production using lignocellulosic biomass as the cheap feedstock

- Lignin fractionation and sugar release from carob pods using methanol and water-based extraction

- Screening of process parameters employing Taguchi experimental design for biomass growth and PHB production using *R. eutropha* and *B. megaterium*
- Extraction of PHB granules from bacterial biomass using lignin from pretreated carob pods

2. Process intensification of PHB production using a non-conventional reactor system

- Design and fabrication of indigenous annular bioreactor for biomass cultivation and PHB production
- Evaluation of hydrodynamics of the annular bioreactor
- Biomass growth and PHB production using the annular bioreactor operated under fed-batch mode

3. Separation of PHB rich bacterial biomass from culture broth using tubular ceramic membrane

- Preparation and characterization of tubular ceramic membrane for biomass separation
- Performance evaluation of tubular ceramic membrane for biomass separation at different operating parameters
- Enhancing the throughput by introducing novel membrane assembly with multiple ceramic membranes

4. Application of bacterial PHB in food packaging

- Enhancement in PHB properties by including graphene nanoplatelets (Gr-NPs) of varying concentration
- Biocompatibility of the prepared polymer for its potential use in food packaging
- Shelf-life simulation studies of oil/dairy-based food items packed with PHB/Gr-NPs nanocomposite

- Biodegradation of PHB/Gr-NPs nanocomposites in the soil environment

5. Techno-economic assessment of polyhydroxybutyrate (PHB) production from carob pods

- Full-scale process design for PHB production using carob pod biomass as the feedstock for PHB production in a closed-loop biorefinery approach
- Feedstock and key component analysis for PHB production along with its capital and annual operating cost
- Techno-economic assessment of PHB production under different scenarios.

1.10. Organization of thesis

The present work is divided into seven chapters. The **first chapter** gives a general introduction and presents the available literature on properties of PHB, applications of PHB, various industrial refused for PHB production, reactor considerations for upstream processing of PHB, downstream processing in PHB recovery. Finally, the objectives of this work with the organization of the thesis are presented. C**hapter 2**, details on the development of a novel closed-loop biorefinery strategy to use carob pods as the cheap feedstock for upstream to downstream processing involved in PHB production. Tuning of process parameters like sugar concentration, C/N ratio, Inoculum percentage and nutrient adjunct using a statistically significant Taguchi experimental design for enhanced biomass and PHB production is discussed. Systematic characterization of the PHB extracted under the present closed-loop biorefinery approach using various characterization techniques is elaborated.

In **chapter 3**, a novel wide gap annular bioreactor (ABR) is fabricated, and experimental investigations and CFD simulations are carried out to understand hydrodynamic of the present bioreactor. Operation of ABR under the batch and fed-batch

mode for PHB production is examined. Simultaneously, a comparison of ABR performance with that of the stirred tank bioreactor (STBR) is made and finally, and the properties of PHB produced in this work are compared with that of the commercially available pure PHB. **Chapter 4** describes the use of low-cost ceramic membranes for the separation of PHB rich biomass from the culture broth. Effect of membrane arrangement and applied pressure on water/broth flux, biomass and PHB recovery is also investigated.

Chapter 5 reports on the preparation of PHB/Gr-NPs nanocomposite using simple solution cast technique. Analysis of barrier, thermal, mechanical and optical properties of the prepared PHB/Gr-NPs nanocomposite is performed. Cytotoxicity and biodegradation experiments of the nanocomposites are carried out. Finally, shelf-life simulation studies are undertaken to demonstrate the exceptional performance of the present PHB/Gr-NPs nanocomposite in food packaging applications. **Chapter 6** provides a detailed techno-economic analysis of the various novel strategies for PHB production from carob pods. Effectiveness of PHB production under various scenarios is evaluated based on its pay-out period and turnover accumulated at the end of 7^{th} year of a PHB plant operation

Chapter 7 draws summary and appropriate conclusions based on the previous chapters. This chapter also provides some useful recommendations for future research in the relevant area.

Chapter 2

A closed-loop biorefinery approach for polyhydroxybutyrate (PHB) production using sugars from *ceratonia siliqua* pods as the sole raw material and downstream processing using the co-product lignin

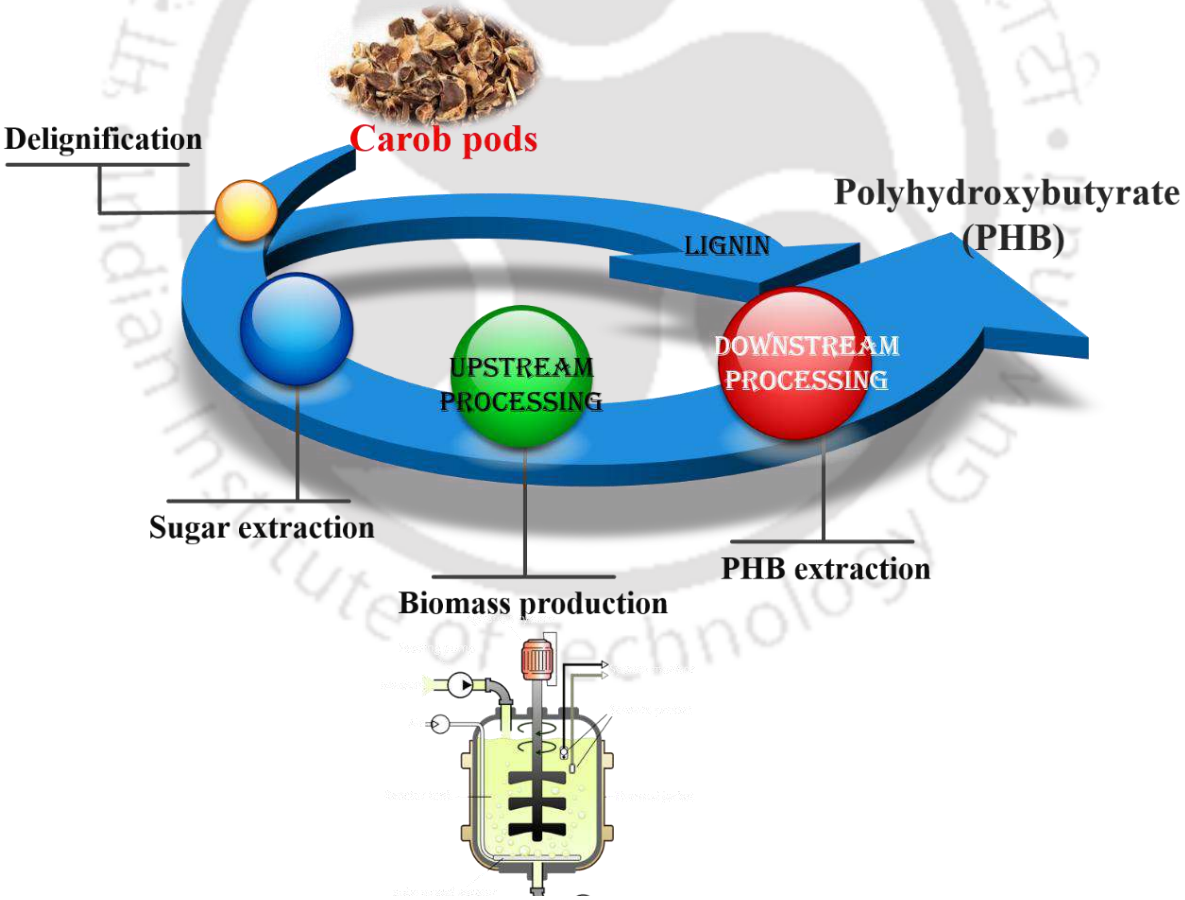

Abstract

A major challenge of the polymer sector is to develop a polymeric material without compromising the environmental safety and sustainability of the product. Therefore, in this chapter, we approach this challenge via novel closed-loop biorefinery model using carob pods as the feed material. The carob pods were first treated with methanol to recover lignin, which was found to be 3 g/L in terms of Gallic acid equivalents (GAE). As the second step, sugars present in the delignified carob pods were extracted using water, which yielded ~ 40 g/L of sugars and ~ 1 g/L of proteins and other nutrients. *R. eutropha* and *Bacillus megaterium* were then grown on carob extract under an optimized condition of 10 C/N ratio, 10% (v/v) inoculum size, 40 g/L sugar concentration and no added adjunct in the medium as concluded from the results of Taguchi experimental design. *R. eutropha* outperformed *B. megaterium* in terms of its capability to grow at a maximum initial sugar concentration of 40 g/L with a maximum PHB production of 12.2 g/L. Finally, the concentrated lignin from the first step was diluted with different proportions of chloroform to extract PHB from the bacterial biomass. The PHB yield and purity obtained were more than 90% respectively using either *R. eutropha* or *B. megaterium*. However, the PHB yield and purity due to *R. eutropha* were better than with *B. megaterium.* Properties of the PHB produced in this study were examined to establish its application potential. This study showed that closed-loop biorefinery model based on carob pods for PHB production is sustainable and environmentally safe for value addition to wastes.

2.1. Introduction

Worldwide pollution due to plastics is from the extensive use of plastics in food packaging sectors. In the year 2014, 40% of the entire plastic source was used for packaging applications (Bomrungnok et al., 2019). Therefore, high interest is shown in recent years for preparing biodegradable polymers from renewable sources. In this context, polyhydroxybutyrate (PHB) is well known for its excellent properties akin to the polymers of petrochemical origin. Besides, PHB is well known for its biodegradability, biocompatibility and renewable nature (Arul Manikandan et al., 2019a; Khanna and Srivastava, 2005). PHB belongs to the class of polyhydroxyalkanoates (PHAs), and they are generally classified as polyesters. Recently, these polyesters have gained significant attention and frequently referred as intracellular microbial polymers, as these are produced and stored inside the cell wall of heterotrophic bacteria as the carbon and energy source.

Ralstonia eutropha and *Bacillus megaterium* are well known for PHB production for the last 50 years (Arul Manikandan et al., 2019a; Khanna and Srivastava, 2005). However, pure glucose used for the PHB production limits commercial production of the product as raw material cost in the process accounts for 40-50% of the total production cost (González- García et al., 2011), which may even extend up to 70-80% of the total production cost (Al-Battashi et al., 2019; Annamalai and Sivakumar, 2016). In order to reduce the overall production cost incurred during PHB production, various renewable carbon sources from waste lignocellulosic biomass, such as rice straw (Al-Battashi et al., 2019), wheat straw (Soto et al., 2019), kenaf biomass (Saratale et al., 2019), softwood (Al-Battashi et al., 2019; Vaidya et al., 2019), etc., have been studied as a cheap carbon source for PHB production. However, there is still a need to explore more such renewable feedstock for PHB production for keeping the economic and environmental impact of the

process low. In this regard, the present study focuses on the utilization of carob pod extract as a renewable source for PHB production.

Carob pods are refused from the locust bean gum industry (Carvalho et al., 2016, 2014), which deals with the production of highly viscous polysaccharide from the carob seeds. In food sectors, this highly viscous syrup is used as a thickener, stabilizer and gelling agent. Thus, after dehulling of carob pods, seeds are separated for thickener production and carob pods are derived as a secondary product. Approximately 400,000 tons of carob pods are produced annually around the world (Carvalho et al., 2014). These carob pods are partially used as animal feed and as a substitute for cocoa in the food industry (Loullis and Pinakoulaki, 2018). However, a majority of the carob pods is refused from industries, and therefore, it can serve as an inexpensive carbon source for microbial fermentation process (Carvalho et al., 2016, 2014). Different biotechnological/value-added products have been produced using carob pod extract as a cheap carbon source (Yatmaz and Turhan, 2018), including dextran (Lule et al., 2016), bioethanol (Bahry et al., 2017; Germec et al., 2015), citric acid (Show et al., 2015) and succinic acid (Carvalho et al., 2016, 2014). However, PHB production using carob pod extract has not been reported thus far.

Generally, lignocellulosic material with a considerable amount of lignin is delignified through various treatment steps and subsequently used as a fuel source in boilers (Kumar et al., 2016; Sasaki et al., 2015; Wu et al., 2015). Very recently, lignin biorefinery operations have boomed due to the use of lignin in various fields (Hu et al., 2018). However, when the lignin content in the feedstock is less, extracting it as a single product is not economical. For instance, from Fig. 2.1, cotton stalk, barley straw, sugar cane bagasse and, rice straw contains 22.8%, 19.86% 15.2% and 15.25% relative weight of lignin, respectively (Chandel et al., 2018; Hu et al., 2018; Ragauskas et al., 2014). Compared with these biomass carob pod contains a very low lignin content (only 5%) (Fig. 2.1).

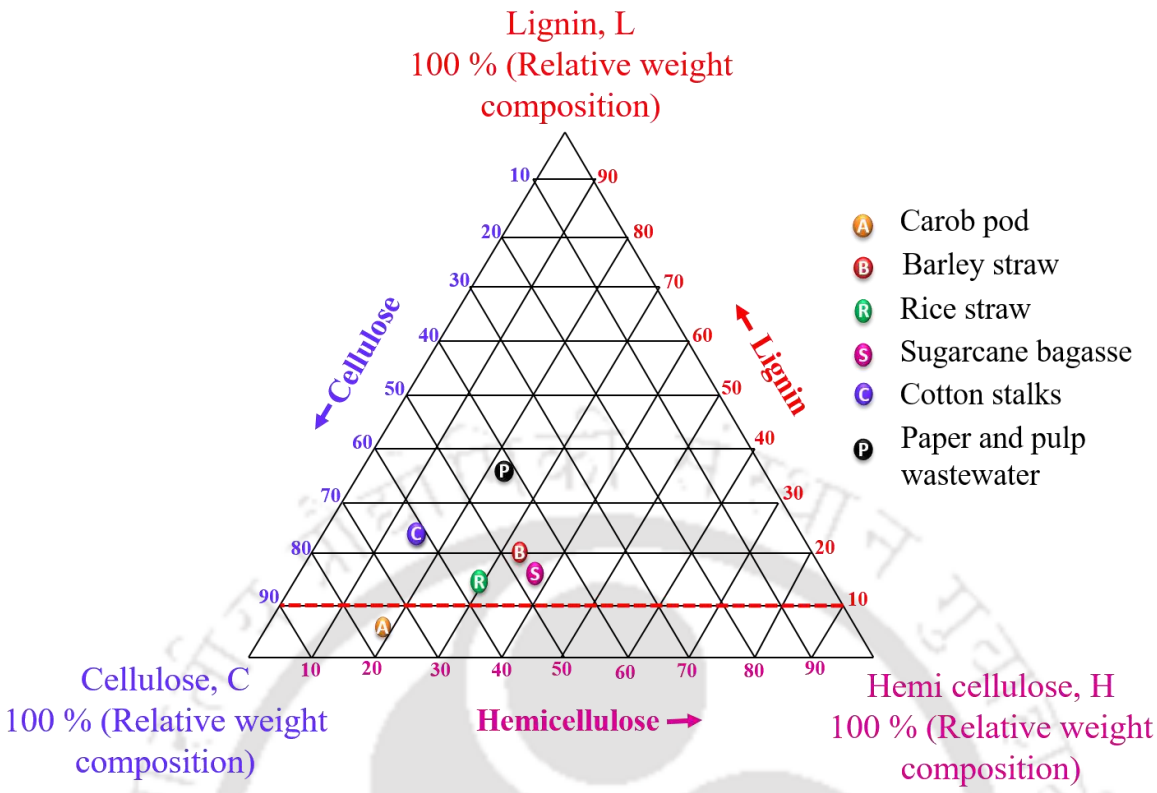

Fig. 2.1. Fraction of cellulose, hemicellulose and lignin in various lignocellulosic biomass

Negligence to separate lignin will not only result in the loss of lignin but also makes the final extract recalcitrant to PHB production. Conventionally, this recalcitrance due to lignin is removed via hydrolyzation coupled to adsorption (Kosa and Ragauskas, 2013; Liu et al., 2012; Meziani et al., 2015). However, a better alternative is to reuse the lignin recovered from the biomass in the same process for a suitability of the process. Hence, the present study strategizes a novel closed-loop biorefinery model, wherein, the lignin recovered from carob pods was neither purified and isolated as a separate product nor neglected during pretreatment, but used as a precursor for extracting PHB produced by bacterial fermentation of sugars present in the delignified biomass. Moreover, for efficient utilization of the nutrients present in the carob pod extract, bacterial growth factors, including sugar concentration, C/N ratio, Inoculum percentage and nutrient adjunct, were screened employing the statistically significant Taguchi experimental design. PHB

extracted under the present closed-loop biorefinery approach was characterized in detail using various instrumentation techniques to establish its application potential.

2.2.Materials and methods

2.2.1. Materials

Pottasium dihydrogen phosphate (KH_2PO_4), di-sodium hydrogen phosphate (Na_2HPO_4), Magnesium sulphate heptahydrate ($MgSO_4 \cdot 7H_2O$), calcium chloride ($CaCl_2$), yeast extract, bovine serum albumin, gallic acid, zinc sulphate heptahydrate ($ZnSO_4 \cdot 7H_2O$), ferrous sulphate heptahydrate ($FeSO_4 \cdot 7H_2O$), ammonium molybdate tetrahydrate ($(NH_4)_6Mo_7O_{24} \cdot 4H_2O$), boric acid ($H_3BO_3$), urea ($CO(NH_2)_2$), ammonium chloride ($NH_4Cl$), chloroform ($CHCl_3$), deuterated chloroform ($CDCl_3$), sodium hypochlorite (NaOCl), hydrochloric acid (HCl), sulphuric acid (H_2SO_4), sodium hydroxide (NaOH), tetrahydrofuran (C_4H_8O) and nutrient broth used in this study were bought from Himedia™, India. Commercial PHB and corn steep liquor were purchased from Sigma-Aldrich™, India.

2.2.2. Preparation of carob pod extract

Carob pods were acquired locally from IIT Guwahati, Assam, India (26.1879° N, 91.6916° E). With a specific goal to recover lignin from carob units, 10% (w/v) of carob biomass was suspended overnight in methanol solution. Thereafter, the delignified carob units were washed with water and subsequently dried at 60 ˚C until a constant weight is achieved without any further weight loss. The dried samples were then powdered and extracted using water; during this step sugars present in the carob pods are extracted by adding 40% (w/v) of powdered carob pods into water. Unlike the delignification process, the sugar extraction process was carried out in an incubator shaker maintained at an agitation rate of 200 rpm and under an ambient temperature of 28 ˚C (Arul Manikandan et al., 2019b; Carvalho et al., 2014). Finally, the sugars extracted from the carob pods were filtered using a muslin

cloth and stored at 4 ˚C till the actual experimental use, in order to avoid unwanted microorganisms growth in the extract.

2.2.3. Analysis of sugar and other constituents

Sugars (glucose, fructose and sucrose) present in the carob extract were analyzed by high-performance liquid chromatography (HPLC) equipped with RI detector. For this analysis, HPLC (Series 200 Model, Perkin Elmer) attached with Hi-plex H column was used. 0.01 M sulphuric acid was used as the mobile phase with a flow rate of 0.6 ml min^{-1}. All the samples were filtered using 0.45 µm Whatman® filters before the analysis. Protein concentration in the carob pod extract was measured following Lowrys method as described by Hazarika et al. (2015). Bovine serum albumin served as a standard for the protein estimation analysis. Lignin concentration in the extract was estimated as gallic acid equivalents (GAE) by following the Folin-Ciocalteu method as portrayed in the literature (Carvalho et al., 2016).

2.2.4. PHB production

The microbial strains, *R. eutropha* and *B. megaterium* used for PHB production were obtained from Microbial type culture collection® (MTCC), Chandigarh. The cultures are maintained at 5 °C on plates containing nutrient agar. PHB production using carob pod extract as the sole carbon source was studied by supplementing the raw extract with mineral salt medium (MSM). MSM consists of (g/L): pottasium dihydrogen phosphate (KH_2PO_4), 2.0; di-sodium hydrogen phosphate (Na_2HPO_4), 0.6; magnesium sulphate heptahydrate ($MgSO_4 \cdot 7H_2O$), 0.2; calcium chloride ($CaCl_2$), 0.2; and 10 mL L^{-1} of trace metal solution. The trace metal solution comprised of (mg/L): zinc sulphate heptahydrate ($ZnSO_4 \cdot 7H_2O$), 1.3; ferrous sulphate heptahydrate ($FeSO_4 \cdot 7H_2O$), 0.2; ammonium molybdate tetrahydrate ($(NH_4)_6Mo_7O_{24} \cdot 4H_2O$), 0.6 mg; and boric acid (H_3BO_3), 0.6. A stock solution of major components in the MSM and the entire trace metal solution was autoclaved separately and

added before performing the experiments. Carob pod extract served as the carbon source, and it was used in the range of 20 - 40 g/L for PHB production. Urea and ammonium chloride at their respective C/N ratio was used as the nitrogen source for *R. eutropha* and *B. megaterium*, respectively (Khanna and Srivastava, 2005; Kulpreecha et al., 2009).

2.2.5. Optimization of PHB production employing Taguchi experimental design

Screening and optimization of process parameters for PHB production using carob pod extract as the carbon source were carried out employing Taguchi orthogonal experimental design comprising of four basic operational parameters. The experimental design matrix consisted of a total of nine experimental runs with the following four parameters: C/N ratio, inoculum size % (v/v), carbon source concentration (g/L) and nutrient adjunct. All these four parameters in the study were tested at three different levels: carbon source concentration was varied as 20, 30 and 40 (g/L); C/N ratio was varied as 10, 40 and 100; inoculum volume was 3, 5 and 10% (v/v) and, finally, the nutrient adjuncts tested were yeast extract (YE), corn steep (CS) liquor and a medium without any nutrient adjunct (Null). The lower and upper limits of all the parameters were chosen based on the earlier reports of PHB production by *R. eutropha* and *B. megaterium* (Khanna and Srivastava, 2005; Kulpreecha et al., 2009; Saratale et al., 2019).

All these experiments were carried out in a 2-L stirred tank bioreactor with a working volume of 1.5 L, with a sparging and agitation rates of 0.8 vvm and 250 rpm, respectively. The pH in the bioreactor was maintained at 7.0 by the addition of 0.1N HCl or NaOH, and the bioreactor was operated at an ambient temperature of 28°C. All the experiments were continued out for 60 h, and after which the biomass in the bioreactor was harvested and analyzed for its PHB content (Arul Manikandan et al., 2019). Both biomass and PHB concentration (g/L) were recorded as the responses for optimizing the process. For the analysis of biomass and PHB, the bioreactor contents were harvested at the end of

60 h by centrifuging samples in polypropylene centrifuge bottles of 250 mL capacity at 6000×g for a total period of 10 min. Thereafter, the supernatant in the centrifuge bottles was slowly discarded, and the bacterial biomass was dried overnight at 60 ^{o}C in a hot air oven. The final weight of the bacterial biomass (M_b) was determined by gravimetric method. Likewise, PHB mass (M_s) in the bacterial biomass was analyzed following the crotonic acid method as reported in the literature (Arul Manikandan et al., 2019b; Balakrishna Pillai et al., 2018). In this crotonic acid method, the bacterial biomass was chemically digested using 98% sulphuric acid for 1 h in a boiling water bath. The sulphuric acid in the aforementioned reaction converts polyhydroxybutyric acid to crotonic acid, which was measured spectrophotometrically at 235 nm using a UV - Vis spectrophotometer (Lamda35 model, Perkin Elmer, USA) with pure sulphuric acid as the reference. Commercial PHB, as mentioned in section 2.2.1 was used for the construction of PHB standard curve. All the responses were analyzed thrice and reported as mean ± standard deviation. Taguchi experimental design with varying process parameters along with responses in each experimental run is presented in Table 2.1.

Although both biomass and PHB concentration (g/L) were recorded as the responses in this study, parameters and their levels were optimized for maximum PHB. The signal to noise (S/N) ratio of each process parameters are calculated by using the following equation (2.1) (Sinharoy et al., 2015):

$$\frac{S}{N} = -10\left[\log\left(\frac{1/Y^2}{n}\right)\right] \qquad (2.1)$$

Where Y is the PHB concentration (g/L) and n is the number of experimental runs. The Taguchi experimental analysis was carried out under the strategy “largest is the best”. The

statistical software Minitab® (version 16, PA, USA) was used for designing the experiments and analysis of the responses.

2.2.6. PHB extraction

PHB extraction from dried biomass using lignin as a by-product obtained from the carob pods was carried out for making the process greener and viable from the conventional method based on hydrolyzation. The methanol extracted lignin from carob pods were used for this purpose following its evaporation and drying at 60 ˚C. Later, suitable concentration 1-3% (w/v) of the lignin obtained was mixed in the chloroform solution (Kurosawa et al., 2015). The extraction efficiency of the lignin mixed chloroform extractant was compared with the other conventional solvents, i.e. 100% chloroform and 2% (v/v) NaOCl in chloroform.

All extractions were conducted using 100-ml glass tubes with screw tops and by agitating the tubes on a rotating shaker at 150 rpm. The dried cell mass (M_d = 5 g) was blended with 75 mL of a suitable solvent. Following incubation for 12 h, the mixture obtained was centrifuged at 4000 ×g for 15 min, and the organic phase containing PHB dissolved in chloroform was poured into a petri dish. The petri dish was placed in a fume hood for evaporating the solvents at ambient temperature to get PHB polymeric films, which were then weighed gravimetrically to get the mass of PHB (M_g). The PHB polymeric film obtained as above was characterized using various analytical techniques, as mentioned in the next section. Furthermore, the PHB polymer extracted was tested for its purity and yield by using the following equations (2.2 - 2.4) (Balakrishna Pillai et al., 2018; Fei et al., 2016):

$$P_{PHB}(\%) = \frac{M_s}{M_b} \times 100 \qquad (2.2)$$

Table 2.1. Taguchi experimental design showing the combinations of different parameters and their levels in each experimental run along with the responses

Run No.	Process parameters				Response			
					R. eutropha		***B. megaterium***	
	C/N ratio	**Sugars concentration (g/L)**	**Nutrient adjunct**	**Inoculum size (%v/v)**	**Biomass concentration (g/L)**	**PHB concentration (g/L)**	**Biomass concentration (g/L)**	**PHB concentration (g/L)**
1	10	20 ± 0.74	Corn steep liqour	3	12.8 ± 0.05	7.8 ± 0.017	10.49 ± 0.8	5.31 ± 0.02
2	10	30 ± 0.77	Yeast-extract	5	15.4 ± 0.07	9.93 ± 0.05	13.2 ± 1.05	5.82 ± 0.49
3	**10**	**40 ± 1.0**	**Null**	**10**	**22.7 ± 1.28**	**12.2 ± 0.44**	16.9 ± 0.05	5.76 ± 0.7
4	**40**	**20 ± 0.74**	**Yeast extract**	**10**	17.4 ± 0.05	10.16 ± 0.6	**15.92 ± 0.5**	**6.6 ± 0.05**
5	40	30 ± 0.77	Null	3	13.2 ± 3.5	7.65 ± 0.45	11.8 ± 0.79	5.01 ± 0.82
6	40	40 ± 1.0	Corn steep liqour	5	9.1 ± 1.75	6.54 ± 0.89	11.1 ± 0.21	4.7 ± 0.50
7	100	20 ± 0.74	Null	5	7.2 ± 0.77	5.21 ± 0.73	6.7 ± 1.4	3.5 ± 1.62
8	100	30 ± 0.77	Corn steep liqour	10	9.2 ± 0.032	6.52 ± 0.05	7.2 ± 0.06	3.67 ± 1.12
9	100	40 ± 1.0	Yeast extract	3	8.7 ± 1.12	6.41 ± 0.21	7.99 ± 0.92	4.23 ± 0.05

$$P_{purity}(\%) = \frac{M_s}{M_g} \times 100 \qquad (2.3)$$

$$Y_{yield}(\%) = \frac{M_g \times P_{purity}}{M_d \times P_{PHB}} \times 100 \qquad (2.4)$$

Where P_{PHB} (%) is percentage of PHB content in PHB rich bacterial biomass, P_{purity} (%) is the percentage purity of PHB, Y_{yield} (%) is the final percentage yield of PHB, M_s (mg) is the mass of PHB as quantified by spectrophotometry, M_b (mg) is the mass of biomass, M_g (mg) is the total mass of PHB as quantified by gravimetric analysis and M_d (g) is dried cell mass taken for PHB extraction.

2.2.7. Characterization of PHB polymer

Fourier transform infrared spectroscopy (FTIR) analysis was carried out in attenuated total reflectance (ATR) mode using IRAffinity-1 model, Shimadzu, Japan. All the polymeric films were subjected to scanning wavelength ranging from 400 to 4000 cm^{-1} with an average of 20 scans. Proton - Nuclear magnetic resonance (NMR) analysis was carried out by dissolving 50 to 100 mg of the polymer samples in 2 ml of deuterated chloroform ($CDCl_3$). These samples were then analyzed using ^1H nuclear magnetic resonance (NMR, ASCEND 600 model, Bruker 600 MHz). The molecular weight of the extracted PHB samples was analyzed using Gel Permeation Chromatography (GPC) (LC-10AD GPC model, Shimadzu). For this analysis, the Viscotek RI Detector equipped with PL-gel column was used with an injection volume of 100 µl. All the samples were filtered using 0.45 µm Whatman® filter before injecting into the equipment. Tetrahydrofuran was used as the eluent with a flow rate of 0.5 mL/min. Standard polystyrene monodispersed in tetrahydrofuran was used for calibration.

Powder X-ray diffraction (XRD) analysis was carried out using X-ray diffractometer (Make: Rigaku, model: SmartLab, USA) which was operated at a voltage of 45 kV and 112 mA Ni filtered on Cu-Kα radiation (λ = 0.15418 nm). The samples were scanned in the 2 theta range of 5 to 80^{o} along with a scan rate of 5^{o} min^{-1}. Both TGA and DSC analyses were carried out simultaneously using a High-Temperature Differential Scanning Calorimetry (DSC)/ Thermo Gravimetric (TG) System (STA449F3A00 model, Netzsch). All the analysis were carried out under argon atmosphere over a temperature range of 30 – 600 ^{o}C with a heating rate of 10 ^{o}C min^{-1}.

Since the PHB in the present study was extracted using lignin, its inherent bactericidal activity was examined on Gram-positive bacteria and Gram-negative bacteria like *Staphylococcus aureus* and *Escherichia coli*, respectively. For this analysis, 0.1 g of the extracted PHB was suspended aseptically into a test tube containing 10 ml of sterile nutrient broth. Thereafter, 10% (v/v) inoculum of the respective bacterial cultures were added into the test tube under an aseptic condition in a laminar flow chamber. The organisms were allowed to grow for 24 h under 37 ^{o}C with an agitation rate of 120 rpm (Dharmalingam et al., 2019). At the end of 24 h, the growth of the microorganisms was measured by determining optical density (OD) of the cultures at 600 nm by using UV – Vis spectrophotometer (Lamda35 model, Perkin Elmer, USA). All the analysis were repeated thrice, and the data were presented as mean ± standard deviation. The difference in the OD values was subjected to statistical analysis using Turkey's test. Mechanical properties of the polymeric samples, viz. tensile stress and tensile strain were analyzed using 5 kN Electromechanical Universal Testing Machine (Z005TN model, Zwick Roell). The samples for this analysis were prepared according to the ASTM D882-12 standard, and the thickness of the films was measured using a digital micrometre (Mitutoyo, Japan). All the samples were of length 80 mm, gauge length 50 mm, width 5 mm and thickness 0.2 mm

for this UTM analysis, which was carried out at a strain rate of 5 mm min^{-1}. Tensile stress (τ) and elongation (ε) were calculated from the stress-strain curve by using the following equations (2.5 and 2.6) (Chandra Mohan et al., 2018):

$$\tau = \frac{F_{max}}{A} \quad (2.5)$$

$$\varepsilon = \frac{\Delta L}{L} \times 100 \quad (2.6)$$

Where τ is tensile stress in MPa, F_{max} is the maximum force needed to pull the sample apart, and A is the initial cross-sectional area of the sample in m^2, ε is the elongation in percentage, ΔL is the extension of the sample at the time of rupture in mm and L is the original length of the sample, which is 50 mm for the present study. Optical property of the polymeric film in the present study was analyzed using UV-Vis spectrophotometer (Lambda 35, PerkinElmer, Germany). Sample analysis was carried out in the range of 200 – 600 nm with a scan rate of 50 nm min^{-1} and bandwidth of 2 nm.

2.3. Results and discussion

2.3.1. Screening and optimization of process parameters using Taguchi experimental design

Aqueous extraction of sugars from carob pods yielded 21.87 ± 2 g/L of sucrose, 14.79 ± 0.5 g/L of glucose and 4.23 ± 0.5 g/L of fructose. Total phenolics in the carob pod extract was measured as 0.1 ± 0.05 g/L gallic acid equivalent (GAE). A total 0.95 ± 0.1 g/L of protein was obtained in the carob pod extract, which may be due to the presence of various amino acids in the carob extract such as asparagine, leucine, alanine, glutamine and valine (Ayaz et al., 2009). Table 2.1 shows the combined level of the parameters in each

experimental run, according to the Taguchi experimental design, which also presents the biomass and PHB production as the responses in each experimental run.

Fig. 2.2 outlines the impact of the four parameters on PHB production by *R. eutropha* and *B. megaterium* utilizing the carob pod extract as the carbon source. It can be seen that for each of the parameters tested at three distinct levels, specific levels of the parameters affected PHB production by the bacteria. For instance, at level 3 of all the factors (sugar concentration, nutrient adjunct and inoculum size), PHB production was significantly affected. However, C/N ratio was optimum for PHB production by both *R. eutropha* and *B. megaterium* only at level 1. It can be seen from Table 2.1 that in case of *R. eutropha*, experimental run - 3 yielded the best results in terms of biomass production (22.7 ± 1.28 g L^{-1}) and PHB production (12.2 ± 0.44 g L^{-1}). In the case of *B. megaterium*, the best response was obtained for the experimental run 4 with a biomass and PHB production of 15.9± 0.5 g L^{-1} of 6.6 ± 0.05 g L^{-1}, respectively.

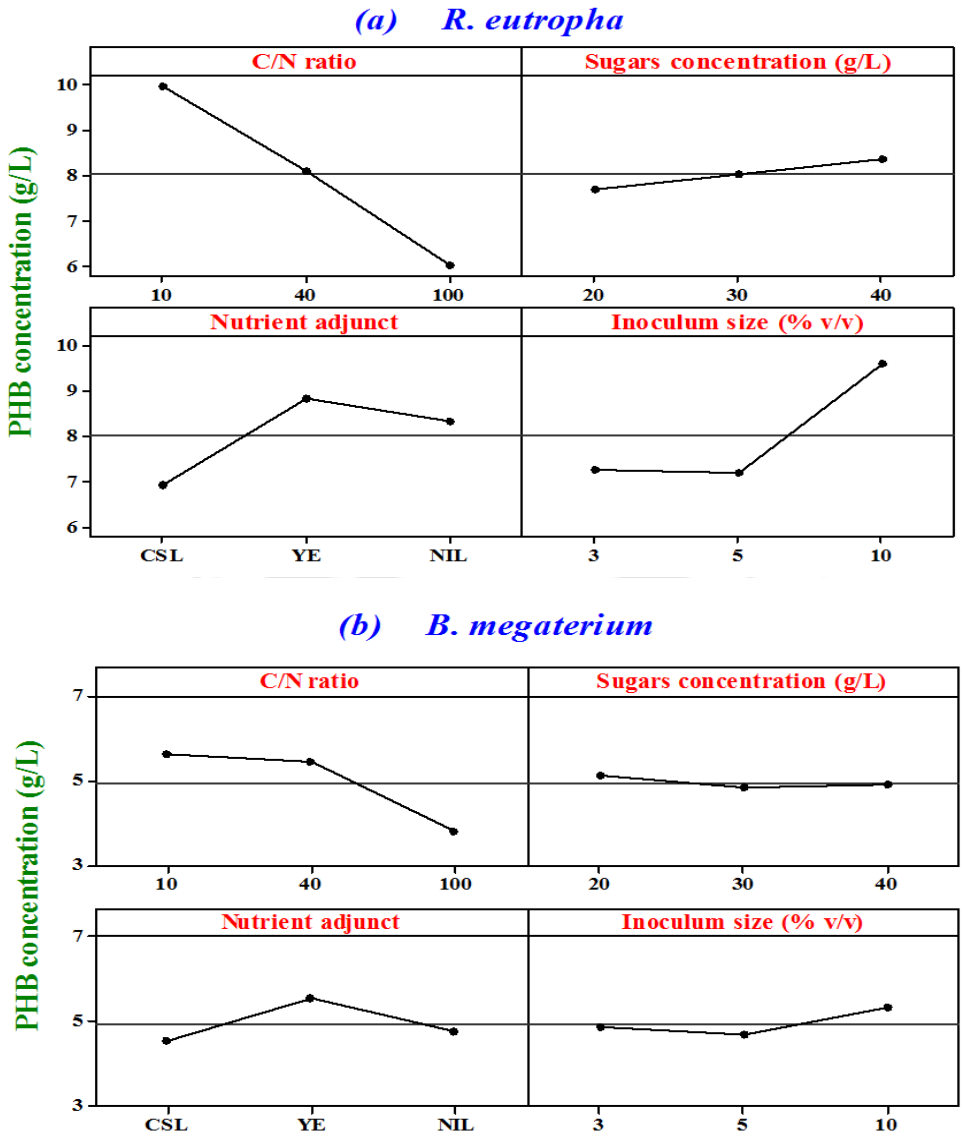

Fig. 2.2. Mean effect plot of the different process parameters on PHB production using: (a) *R. eutropha* and (b) *B. megaterium.*

Table 2.1 presents the input sugar concentration used in this study, whereas statistical analysis of the results obtained from Taguchi experimental design followed in the study, in the form of signal to noise (S/N) ratio for each factor and each level are given in Table 2.2. Delta S/N ratio value for each factor was calculated from S/N ratio values of the factors for their ranking. Accordingly, S/N ratio estimated for different levels of sugar concentration for *R. eutropha* and *B. megaterium* did not vary much, and from the delta S/N ratio value

for the same was found to be low indicating that it played a less significant role than the other factors for PHB production by the bacteria. A high PHB titer due to *R. eutropha* and its ability to consume sugar-rich feedstock (40 g L^{-1}) with no additional supplements concluded that *R. eutropha* is suitable than *B. megaterium*. Hence, *R. eutropha* was considered further for PHB production with the following optimum conditions: 10 C/N ratio, 10% (v/v) inoculum size, 40 g L^{-1} sugar concentration and no added adjunct in the medium.

Table 2.2. Values of average signal to noise (S/N) ratio for PHB production using (a) *R. eutropha* and (b) *B. megaterium* and their ranking based on delta S/N ratio

a) *R. eutropha*

Level	**C/N ratio**	**Sugar concentration**	**Nutrient adjunct**	**Inoculum size**
1	19.89	17.48	16.85	17.25
2	18.04	17.97	17.94	16.87
3	15.60	18.08	18.74	19.41
Delta	4.29	0.61	1.89	2.54
Rank	1	4	3	2

b) *B. megaterium*

Level	**C/N ratio**	**Sugar concentration**	**Nutrient adjunct**	**Inoculum size**
1	15.01	13.98	13.10	13.73
2	14.66	13.53	13.38	13.23
3	11.62	13.79	14.82	14.34
Delta	3.39	0.45	1.73	1.11
Rank	1	4	2	3

2.3.2. Integrated downstream processing using lignin as a green solvent for PHB recovery

Due to the intracellular nature of PHB, it is necessary to break the cells in order to facilitate its extraction and further purification. Therefore, in the present study, lignin, a co-product obtained during the pretreatment of carob pods was integrated with downstream processing for the recovery of PHB produced by *R. eutropha* and *B. megaterium* (Fig. 2.3). The effect of lignin content (1 & 3 wt %) in chloroform on yield, purity and average molecular weight (M_w) of the biopolymer was studied. Among the studied concentration of lignin, the highest yield (92.7%) and purity (91.5%) of PHB were obtained with the combination of 1% (w/v) lignin mixed in chloroform for *R. eutropha* used as the microbial strain. Under these conditions, the extracted PHB had an average molecular weight of 560 Kg/mol, which was slightly lower than the average molecular weight (584.6 Kg/mol) of the polymer extracted using 100% chloroform. Low values of PHB yield and purity were observed with an increase in the lignin content in the chloroform, whereas its molecular weight was high, which may be due to the formation of PHB-lignin composites.

Similar results were reported in a recent study conducted by Kai et al. (2018); the authors synthesized PHB-lignin composite by addition of a known amount of lignin to the PHB polymer. In the case of *B. megaterium* PHB, its purity matched with that from *R. eutropha*; however, the PHB yield was found to be slightly less with the combination of 1% (w/v) lignin in chloroform as the extracting solvent. The reduced yield of *B. megaterium* PHB in comparison with the *R. eutropha* PHB can be attributed to the fact that the Gram- positive bacterium *B. megaterium* has a highly resistant peptidoglycan layer in its cell wall, which makes the biomass less susceptible to the solvent extraction process (Dharmalingam et al., 2019). On the other hand, PHB extraction using the conventional

chlorinated solvent (NaOCl) resulted in a drastic reduction of molecular weight (Fig. 2.3). Thus, the lignin - a green solvent used in the present study can be considered as an alternative to the commonly used highly corrosive chlorinated (NaOCl) solvents for PHB extraction.

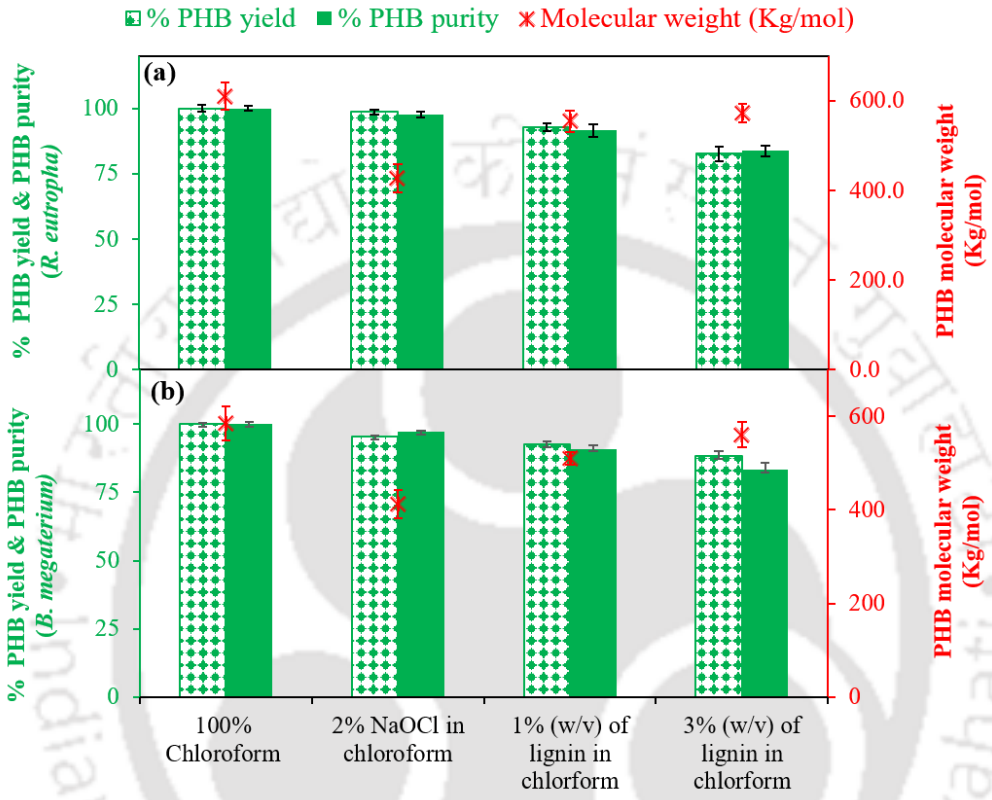

Fig. 2.3. Yield, purity and average molecular weight (M_w) of the biopolymer obtained from (a) *R. eutropha* and (b) *B. megaterium* by extraction using chloroform, chlorinated chloroform and lignin mixed with chloroform in various proportion

2.3.3. Characterization of extracted PHB

2.3.3.1. Fourier transform infrared spectroscopy (FTIR) analysis

To identify the chemical species and confirm the incorporation of phenolic compounds in the PHB product. FTIR spectra of the samples were measured in the wavelength of 400–4000 cm^{-1}. The FTIR spectra of the PHB extracted from *R. eutropha* and *B. megaterium* were compared with that of the commercial PHB, which are shown in Fig. 2.4 a and b,

respectively. The doublet peak observed in the FTIR spectra at 2900 to 3000 cm^{-1} corresponds to the C-H vibration in PHB polymer, and these peaks were commonly observed on all FTIR spectra irrespective of the microorganisms or the type of solvents used in the present study. Similarly, the characteristic peak observed at 1740 cm^{-1}, 1380 cm^{-1} and 1278 cm^{-1} can be attributed to the presence of carbonyl bond (C-O), methyl group (CH_3) and carbon-oxygen elongation (C-O-C), respectively, observed in any typical PHB sample. For instance, all the aforementioned peaks can be seen even in the synthetically produced commercial PHB. The detected peak at 3400 cm^{-1} corresponds to the -OH stretch of the phenolic compounds presents in lignin, and the peak due to phenolic compounds is observed only in PHB extracted from the bacterial biomass using a varying concentration of lignin in the extractant. The observed results are in correlation with the results presented in the literature (Pradhan et al., 2017; Saratale and Oh, 2015; Saratale et al., 2019).

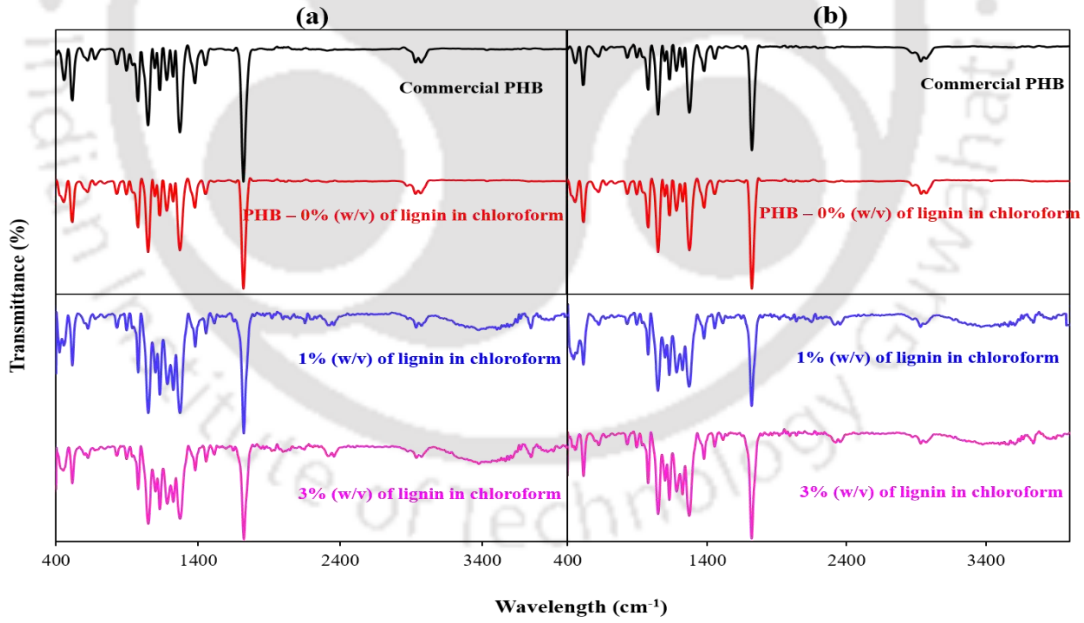

Fig. 2.4. FTIR spectra of commercial PHB and polymer extracted from (a) *R. eutropha* and (b) *B. megaterium* by solvent extraction with chloroform and lignin mixed with chloroform at varying proportion

2.3.3.2. Nuclear magnetic resonance (NMR) analysis

PHB polymer extracted from *R. eutropha* and *B. megaterium* using different solvent was characterized by ^{1}H NMR, and the results were compared with the spectrum obtained due to the commercial PHB (Fig. 2.5). The peak observed at 7.26 and 0 ppm are due to the reference compound, i.e. deuterated chloroform ($CDCl_3$) and tetramethylsilane (TMS), respectively. The characteristic peaks of PHB at 1.26 ppm, 2.50 ppm and 5.24 ppm correspond to the protons of $–CH_3$, $-CH_2$ and –CH in PHB chains of both commercial PHB and the biopolymer produced in the study (Kai et al., 2018; Pradhan et al., 2017). When lignin concentration in the extracting solvent was increased, the carbon signal at 3.85 ppm (methoxyl groups) corresponding to lignin is observed in PHB extracted from the bacterial biomass. Results of both FTIR and NMR analyses suggest that the lignin used in the extracting solvent does not impose any modification to the primary structure of PHB by forming any chemical bonds. However, the additional peaks observed in the presence of lignin confirms its role as a non-reactive filler in the PHB matrix (Vaidya et al., 2019).

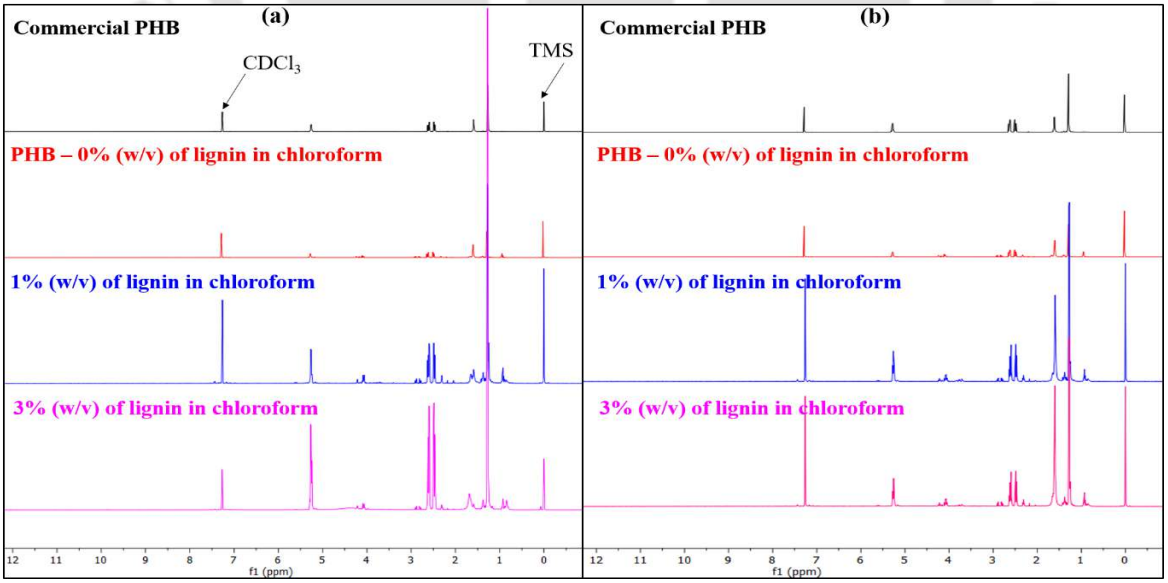

Fig. 2.5. ^{1}H NMR spectra of the commercial PHB and the biopolymer extracted from (a) *R. eutropha* and (b) *B. megaterium* by solvent extraction with chloroform and lignin mixed with chloroform at varying proportion

2.3.3.3. X-ray diffraction (XRD) analysis

XRD analysis was carried out for the commercial PHB, and PHB extracted from *R. eutropha* and *B. megaterium* using chloroform and varying concentration of lignin in chloroform and the results are presented in Fig. 2.6. The strong crystalline peaks observed at 2θ values of 13.4°, 16.8°, 25.4° can be attributed to (020), (110) and (111) planes of PHB crystal structure, respectively. These peaks were also observed in the commercial PHB, thus comprising the purity of the biopolymer production in the study. On the other hand, PHB extracted using chloroform exhibited crystalline peaks with strong intensity at 22.5°, and 23.9°. However, with the addition of lignin in the extracting solvents, amorphous halos of low intensity were noticed at 2θ values of 30.2° and 42.5°. These differences in the peaks can be attributed to the distortion in the polymeric chain and increase in the mobility of the polymeric chain by the intrusion of lignin into the PHB matrix (Kai et al., 2018).

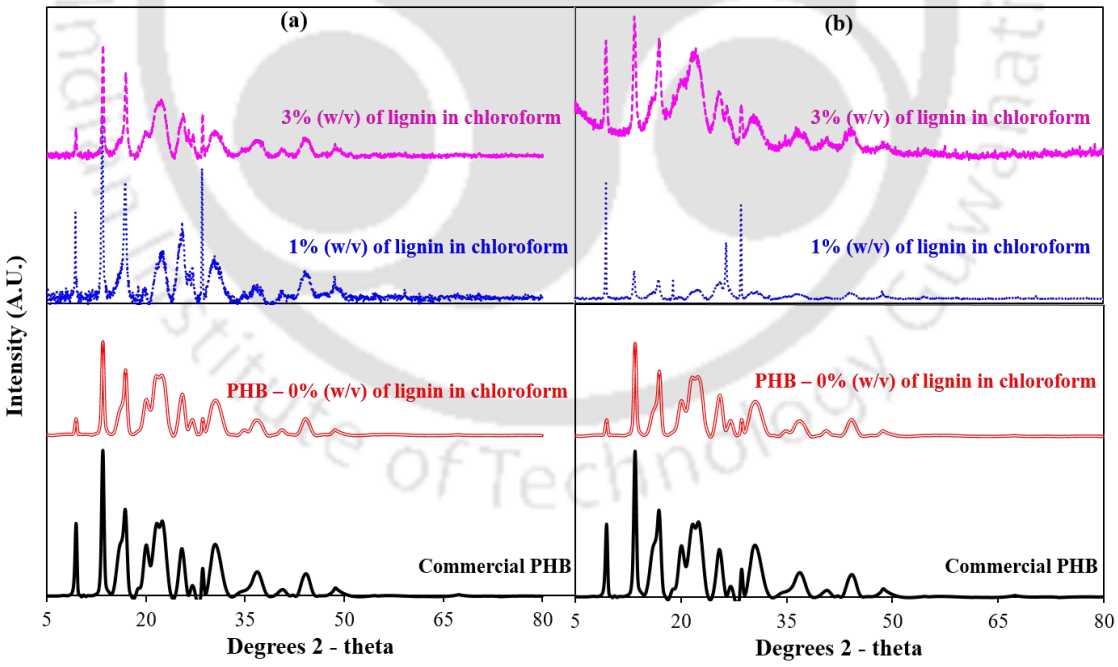

Fig. 2.6. XRD spectra of the commercial PHB and the biopolymer extracted from (a) *R. eutropha* and (b) *B. megaterium* by solvent extraction with chloroform and lignin mixed with chloroform at varying proportion

2.3.3.4. Antibacterial activity

PHB extracted from the bacterial biomass using varying concentration of lignin in the extractant yielded an inhibition zone with the microorganism *S. aureus*, whereas the PHB extracted using 100% chloroform did not cause any inhibition of the bacterium (Fig. 2.7). Furthermore, the results of antibacterial activity test carried out on PHB extracted from *R. eutropha* and *B. megaterium* using a varying proportion of lignin in chloroform revealed a strong reduction in the growth of the Gram-negative bacterium *E. coli*, whereas only a slight reduction in the growth of the Gram-positive bacterium *S. aureus* was observed. The strong antibacterial activity observed in case of the Gram-negative bacterium can be attributed to the absence of peptidoglycan layer in the cell wall of such bacteria. On the contrary, a slight reduction in the Gram-positive bacterium is due to the presence of peptidoglycan layer and lipopolysaccharides in its cell wall, which makes it rigid and highly lipophilic, thereby avoiding the entry of lignin into the cell wall for exerting any inhibitory effect (Dharmalingam et al., 2019). The antibacterial activity of the lignin is due to the presence of different functional groups like –OH, –CO and –COOH in its structure, which was also confirmed earlier by FTIR analyses. These functional groups present in the lignin-containing PHB impose severe bactericidal effect due to oxidation of cell wall and thereby resulting in the lysis of cell wall and consequently leading to the release of cell content (Fig. 2.7d) (Fortunati et al., 2016).

2.3.3.5. DSC/TGA analysis

Change in the melt behaviour of the commercial PHB and PHB extracted from the bacterial biomass using a varying concentration of lignin in the extractant were studied using DSC analysis, and the results are shown in Fig. 2.8. The endothermic peak shown in Fig. 2.8 (a & b) reveals the melting area of PHB with a T_m value of 172^oC, which shows the crystalline nature of PHB (Castro-Mayorga et al., 2018; Kuntzler et al., 2018).

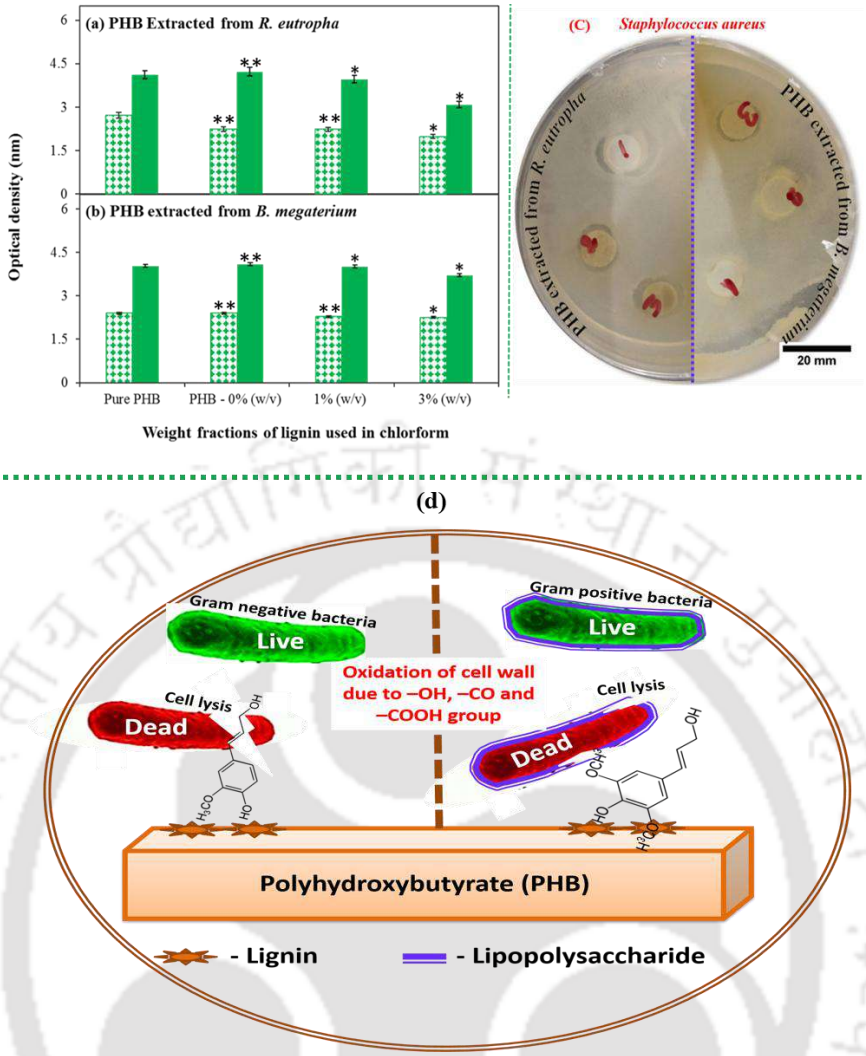

Fig. 2.7. Antibacterial activity of the commercial PHB and polymer extracted from (a) *R. eutropha* and (b) *B. megaterium* by solvent extraction with chloroform and lignin mixed with chloroform at varying proportion over *Eschercia Coli* (Filled bars) and *Staphylococcus aureus* (Patterned bars) (c) Zone of inhibition noticed on *Staphylococcus aureus* plate culture upon placing the PHB films extracted using chloroform containing varying concentration of lignin (1 – 0%, 2- 1% and 3- 3%) (d) Mechanism of bactericidal effect of lignin present in PHB. * symbol above the bars in (a) and (b) indicates that the differences in the values are statistically significant at $P < 0.05$ and ** symbol above the bar indicates that the differences in the values are statistically insignificant at $P > 0.05$ by employing Turkey's test.

The use of different extractant reduced the T_m value by 2-3 ^oC. This is due to the presence of lignin in the PHB loosens the PHB polymeric chain and makes it more amorphous, as confirmed earlier by XRD analysis. These results signify that the presence of lignin decreases the melting point of PHB. The TGA plots (Fig. 2.8 (c & d)) clearly demonstrate that the degradation temperature (thermal stability) of the PHB extracted using a varying concentration of lignin in the extractant is reduced by 3^oC. This reduction in thermal stability can be attributed to the carbonizing action of lignin in the thermal degradation process of PHB (Kai et al., 2019). However, the small reduction in melting point and thermal stability is insignificant in comparison with the other interesting properties offered by the extractant.

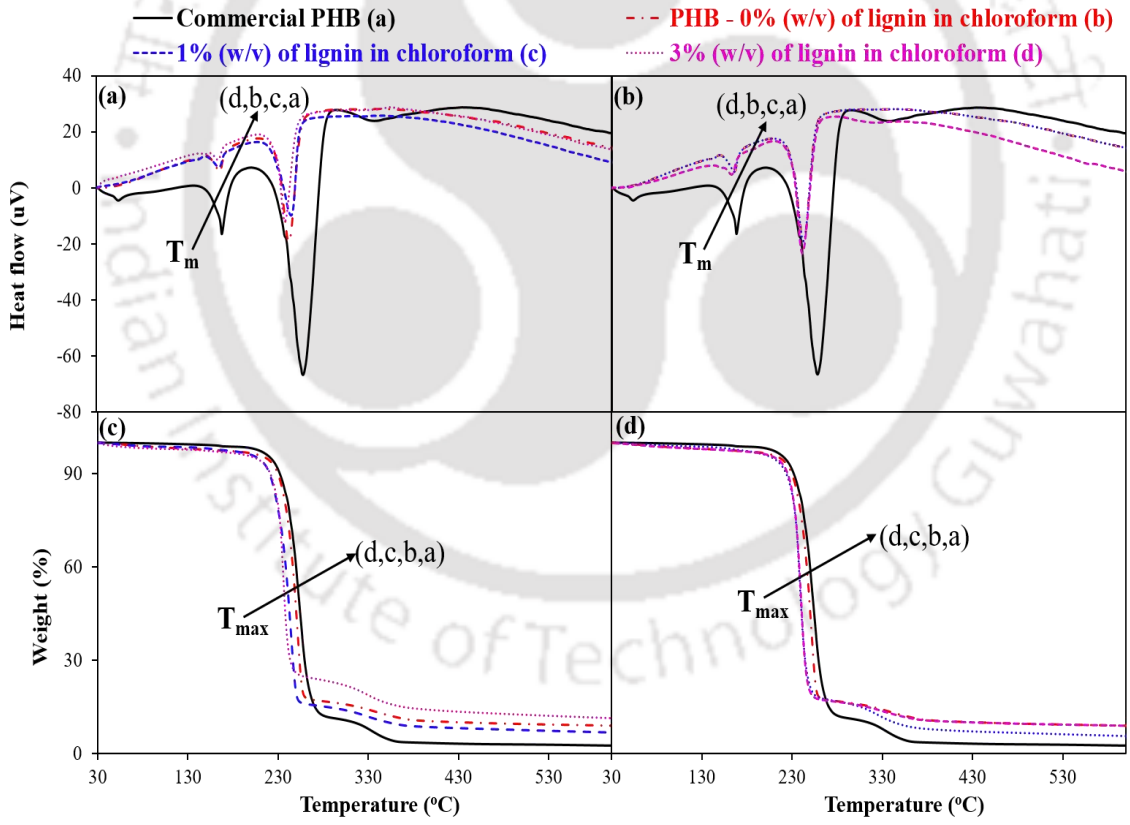

Fig. 2.8. TGA and DSC spectra of commercial PHB and polymer extracted from (a & c) *R. eutropha* and (b & d) *B. megaterium* by solvent extraction with chloroform and lignin mixed with chloroform at varying proportion

2.3.3.6. Mechanical properties

Tensile test of the polymer films was performed to determine the mechanical properties of the commercial PHB and PHB extracted from the bacterial biomass using a varying concentration of lignin in the extractant (Fig. 2.9). The PHB had a tensile strength of 2.2 ± 0.04 MPa and elongation at break of 10 ± 1%. The PHB extracted using chloroform containing 1% (w/w) of lignin increased the tensile strength and elongation at break. However, a further increase in lignin concentration to 3% (w/w) in the extracting solvent weakened the tensile strength of the sample; however, the elongation property of the polymer was enhanced. A two-fold increase in elongation at break was observed for the PHB samples in comparison with that of the commercial PHB. This result clearly suggests that the presence of lignin added ductility to the PHB by acting as a bridge to prolong the fracture process (Kai et al., 2018). PHB extracted from both the microorganisms yielded nearly the same results.

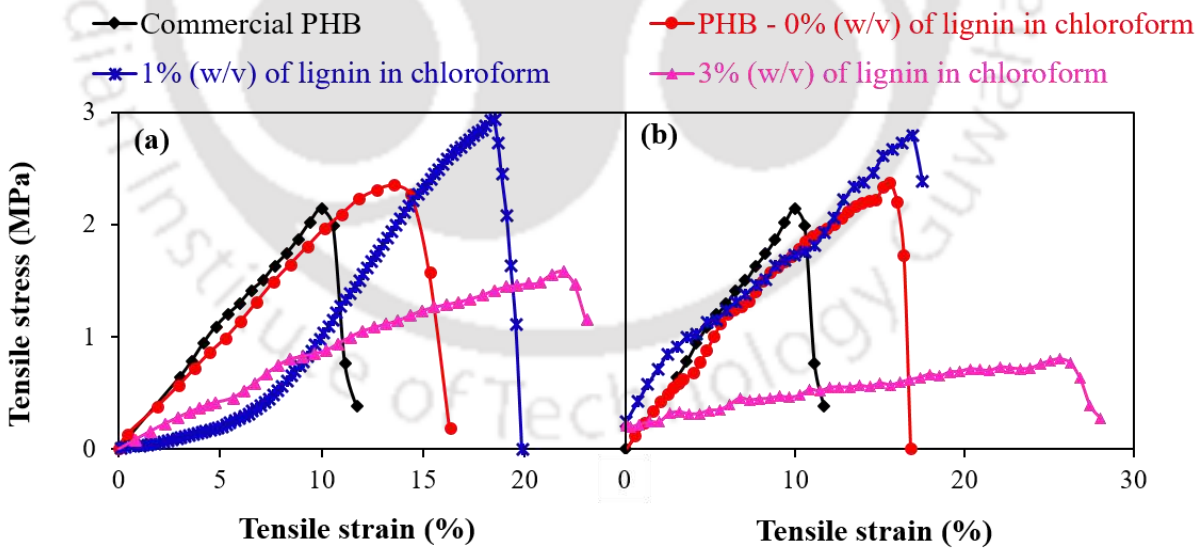

Fig. 2.9. Mechanical property of the commercial PHB and biopolymer extracted from (a) *R. eutropha* and (b) *B. megaterium* by solvent extraction with chloroform and lignin mixed with chloroform at varying proportion

2.3.3.7. Optical properties

Optical property of a polymeric material is essential for realizing its potential in food packaging applications. Under a high UV (200 - 400 nm) light irradiation, photochemical degradation of the polymeric material can occur, whereas high transparency to visible (400 -700 nm) light may adversely affect the food by its rapid deterioration (Valapa et al., 2015). Fig. 2.10 shows the optical properties of the PHB extracted from *R. eutropha* and *B. megaterium*. In the commercial PHB film, a 90% transparency to UV light was observed at 400 nm. This value of transparency is nearly the same for the biopolymer extracted from both the bacterial biomass using chloroform as the solvent. However, the presence of lignin in the extracting solvent and its intrusion into the extracted PHB samples significantly reduced the UV light penetration to nearly half (45%) of its original transparency. Thus, the extraction of PHB from bacterial biomass using varying proportion of lignin gives an added advantage to the polymeric film of low transmission to UV light.

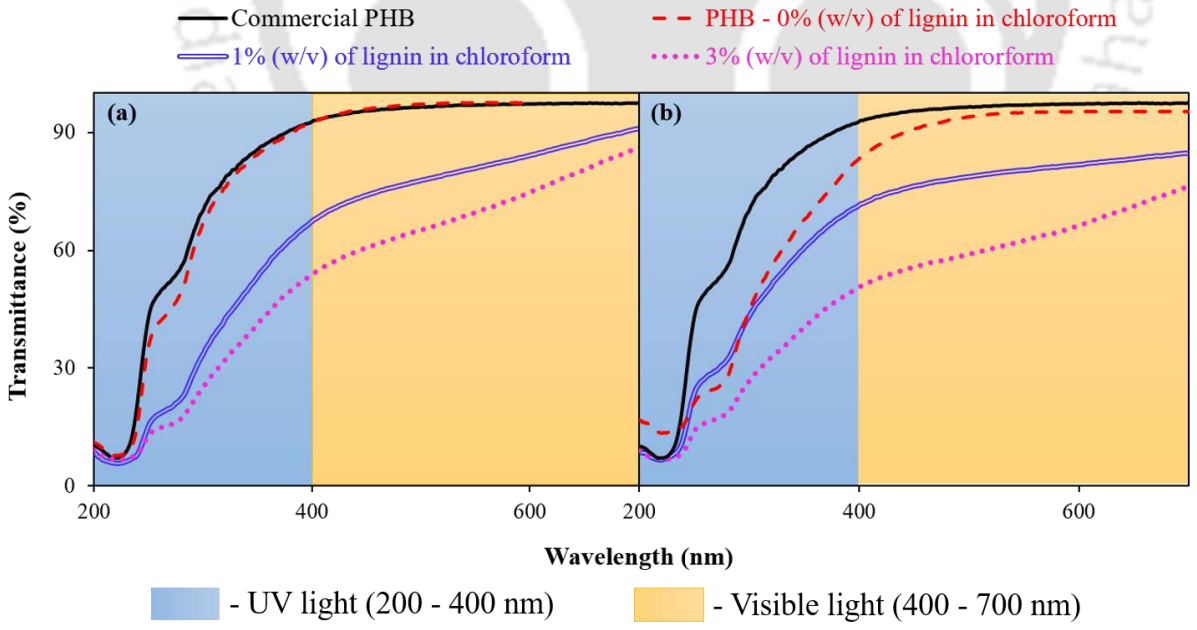

Fig. 2.10. Optical properties of the commercial PHB and biopolymer extracted from (a) *R. eutropha* and (b) *B. megaterium* by solvent extraction with chloroform and lignin mixed with chloroform at varying proportion

Kuntzler et al. (2018) developed an antibacterial polyhydroxybutyrate fibres by producing PHB using the microalgae *Spirulina***.** The authors used the intrinsic phenolic nature of the *Spirulina* biomass to intrude into the PHB polymeric film for antimicrobial property of the fibre. Moreover, the authors adopted electrospinning technique in the second stage to produce PHB nanofibers (Kuntzler et al., 2018), thus demonstrating the advantage of the intruded phenolic compound in food packaging application. In another study, Castro-Mayorga et al. (2018) added silver nitrate in the fermentation broth of *Cupriavidus necator*, a PHB producing bacterium. They found that silver nanoparticles were embedded into PHB granules even inside the bacterial biomass itself. The authors demonstrated antimicrobial activity of the *insitu* silver nanoparticle loaded PHB composites.

A similar strategy based on the addition of silver nitrate during the fermentation stage for preparing antimicrobial PHB-Ag composite materials was demonstrated by Jayakumar et al. (2019) using *B. megaterium* as the PHB producing bacterium. The authors achieved a maximum biomass concentration of 5.8 g/L, which is very less compared with that obtained in the present study (15.9 g/L) for *B. megaterium*. Moreover, in all these literature reported studies, the PHB titre is very low compared with that obtained in the present work. This is due to the fact that a high phenolic content or silver nitrate content during the growth stage of microorganisms retards its growth, thereby reducing the biomass as well as PHB concentration. In contrast to adding such inducers during fermentation or in the upstream of the production process, the present study strategically used lignin in a downstream processing step, thereby reducing the producer organism from any unwanted stress. In a recent study by Kai et al. (2019) and Vaidya et al. (2019), the effect of addition of a controlled amount of lignin into PHB matrix on antimicrobial film preparation was

examined. However, as the antimicrobial films were prepared by adopting a different method, i.e. by carrying out unique chemical reactions like ring-opening polymerization, the results obtained cannot be compared with the present study. Thus, the present study with its novel strategy based on closed-loop biorefinery approach for PHB production stands out to be unique by offering various advantages for its application in the food sector as detailed in the next section.

Fig. 2.11 shows the mass balance analysis of carbon for PHB production following the closed-loop biorefinery approach. It is found that 100 g of carob pods yielded a PHB mass of 2.79 and 1.09 g with *R. eutropha* and *B. megaterium*, respectively. Moreover, lignin extracted from the delignification step was sufficient at 1% w/v along with chloroform for extracting PHB. Furthermore, PHB extracted using 1% w/v lignin in chloroform showed antimicrobial activity due to incorporation of lignin in the PHB matrix. PHB extracted from *R. eutropha* and *B. megaterium* contained 0.26 and 0.16 g lignin in the respective PHB-lignin mass of 3.05 and 1.25 g, respectively. Thus, for scaling up the PHB-lignin production to 1 ton/year, the use of *R. eutropha* and *B. megaterium* as the PHB producers require 32.69 and 80 tons of carob, respectively. The annual world production of carob pods is reported to be 315, 000 tons on a total area of 200, 000 hectares (El Batal et al., 2016). Furthermore, the present cost of carob is 1-5 USD/ton with a minimum supply of about 13 tons (Bitat, 2020). It can also be observed in Fig. 2.11 that on use of every 100 g of carob pods, near about 85 g of sugar-free carob pods were obtained as a by-product from the present strategy, which can further be hydrolyzed using enzymes/acids to get fermentable sugars (Saratale et al., 2019). After PHB extraction, the spent bacterial biomass of 2.63 and 1.28 g were obtained from *R. eutropha* and *B. megaterium*, respectively. In recent years, promising strategies were developed to convert the spent bacterial biomass to bio-oil via pyrolysis and hydrothermal liquefaction techniques were reported in the literature (Wei et al., 2015).

Thus, the carob pods used in the present study under a closed-loop biorefinery can be envisaged as a potential feedstock for commercial PHB production.

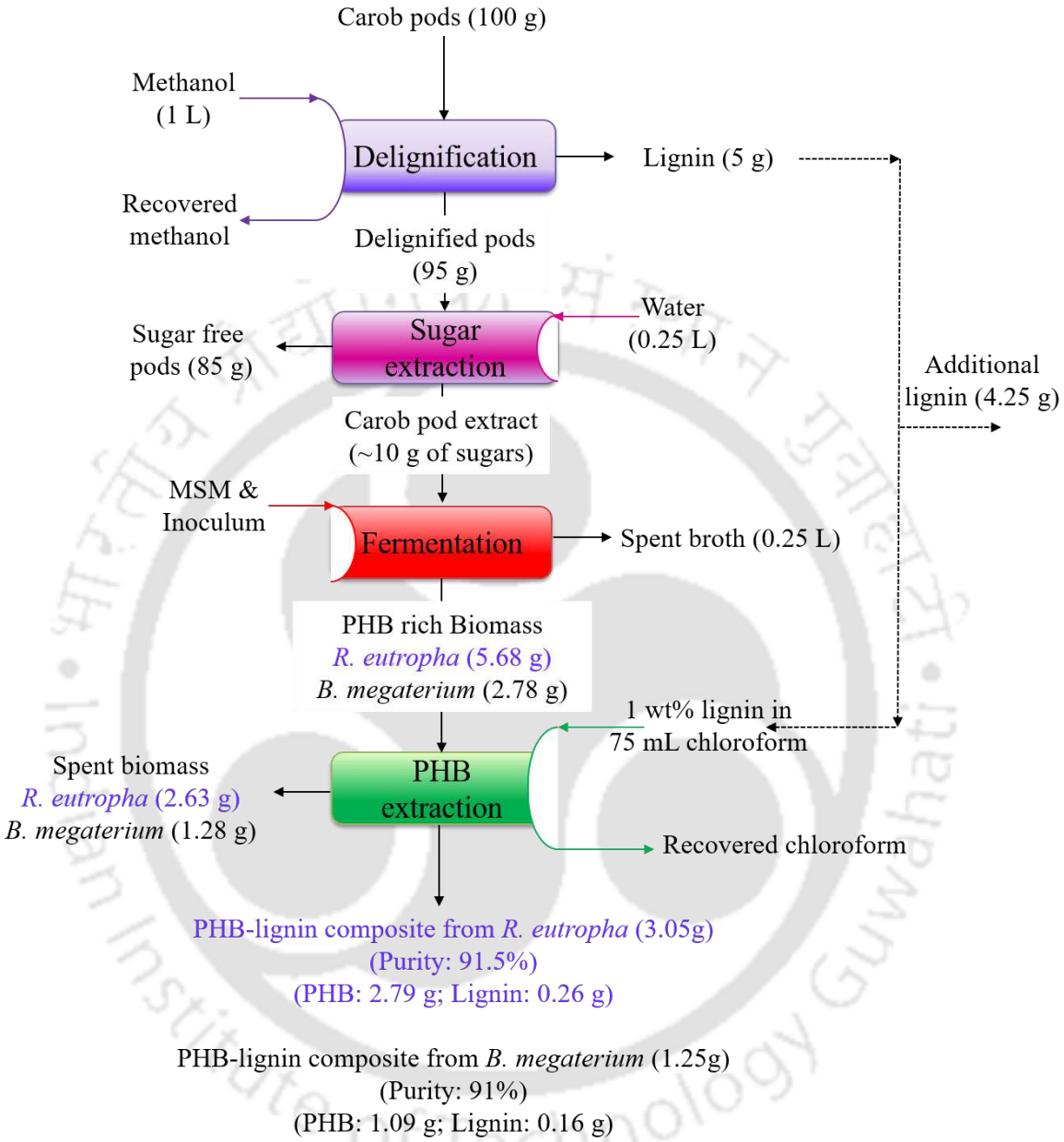

Fig. 2.11. Mass balance analysis of carbon for PHB production following the closed-loop biorefinery approach

The strategy of using carob pods as the feedstock for upstream to downstream processing for PHB production in a closed-loop biorefinery setup is the highlight of this

work. Further, a holistic view of the present strategy on closed-loop biorefinery can be developed by extending the current approach to other lignocellulosic biomass. Bacterial biomass produced using sugars sourced from carob pods and the lignin source used for PHB extraction can be used as a unique technique to cater the polymer requirement in the packaging field. Excellent properties offered by the PHB polymeric film produced in this study demonstrate its suitability in packaging applications. For instance, the exceptionally high antibacterial activity provided by the PHB film proves its application as antimicrobial packaging films. Furthermore, the extended tensile strain at the cost of reduced tensile stress observed in the polymeric film is an added advantage, as the packaging material often invokes higher elongation at break than the tensile strength. As discussed earlier, optical property, i.e. the reduced transparency to UV light observed in the PHB films can be used for packaging of sensitive food products such as vitamins, pigments, flavours and lipids. Thus, the strategy developed in the present study for PHB production will open a new door in the research of biobased polymeric packaging films. However, further investigations on barrier property analysis and shelf life of the polymeric product would be essential to fulfil its application in food packaging.

2.4. Summary

The present study reports a novel strategy based on closed-loop biorefinery model for using lignocellulosic biomass, particularly carob pods, as a self-sufficient feedstock for upstream to downstream processing in polyhydroxybutyrate (PHB) production. Initial Taguchi experimental design demonstrated that *R. eutropha* outperformed the *B. megaterium* in terms of its capability to grow under sugar-rich medium along with a maximum PHB concentration without any added nutrient adjunct in the medium. PHB extraction from dried cell mass using lignin (a cogenerated product in the present process) can be considered as an alternative to the commonly used highly aggressive chlorinated solvent,

including NaOCl. The biopolymer showed excellent properties akin to a commercially available product. Thus, the present closed-loop biorefinery model is highly suited for the sustainable and environmentally safe production of PHBs.

Chapter 3

Taylor and Couette flow mediated improved hydrodynamics in an annular bioreactor for shear stress-free biomass growth and PHB production by *Ralstonia eutropha*

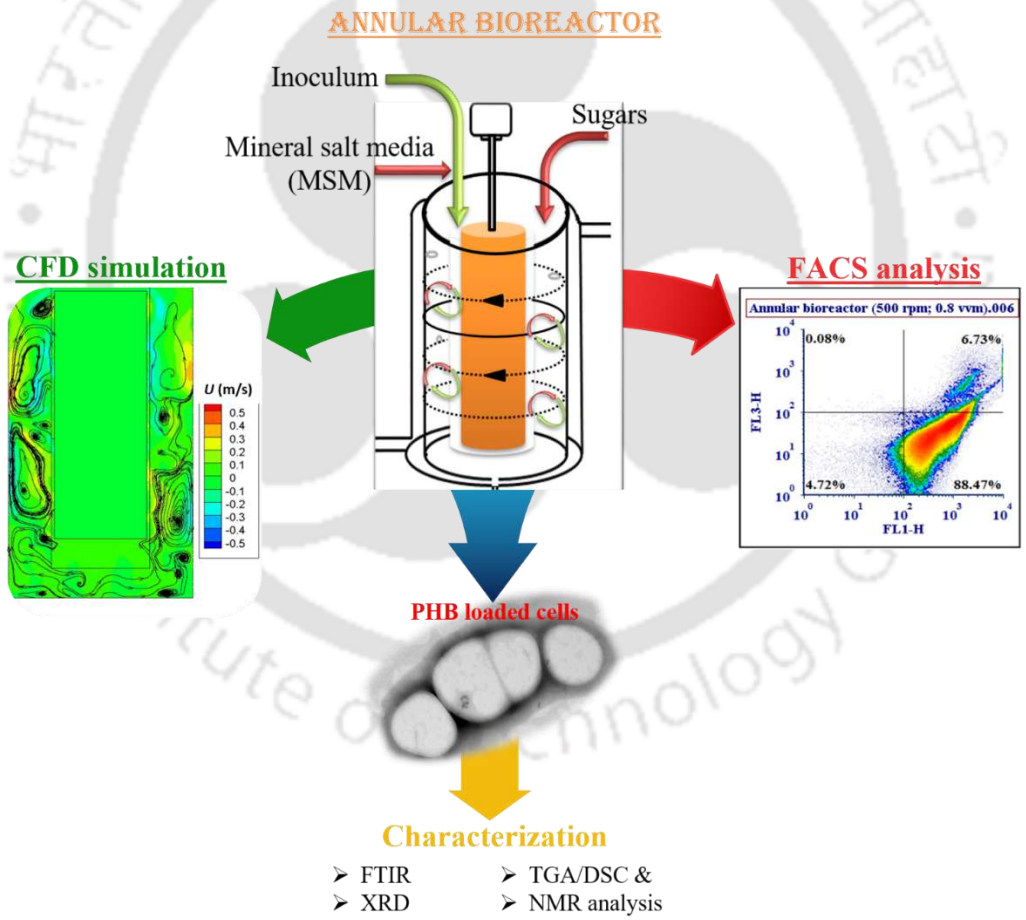

ABSTRACT

In the present chapter, a novel annular bioreactor (ABR) with a wide gap was used for the cultivation of *Ralstonia eutropha*, which produces PHB as an intracellular product. Hydrodynamic studies with the ABR were carried out by analyzing the response in terms of tracer (KCl) concentration, bubble size and dissolved oxygen. Moreover, computational fluid dynamics (CFD) simulations were carried out to analyze the type of flow in the ABR. Initial experiments with the reactor demonstrated uniform distribution of fluid due to the Taylor and Couette flow in the bioreactor. Thereafter, the ABR was operated at different agitation and sparging rates to study its effect on *R. eutropha* growth and PHB production. The ABR operated at 500 rpm with an air sparge rate of 0.8 vvm yielded a maximum PHB concentration of 14.89 g/L, which was nearly 1.4 times that obtained using a conventional STBR. Furthermore, performances of the bioreactors were compared by operating the reactors under fed-batch mode in single as well as dual cycles and by dosing once or twice during the operation (50 g of sugars in 50ml, at each dosage). At the end of 90 h of operation, the ABR with double dosage resulted in a very high PHB production of 70.8 g/L. Due to oxygen transport limitations in the STBR, the reactor performed poorly, thereby resulting in a low PHB concentration of 44.2 g/L. The highest PHB volumetric productivity observed with the ABR (0.74 g/L·h) is 1.6 times the PHB volumetric productivity (0.46 g/L·h) observed using the STBR. Finally, the PHB extracted in the present study was characterized using different techniques, and its characterization results were compared with that of a commercially available pure PHB. The superior performance of the ABR in terms of *R. eutropha* biomass and PHB production over the conventional STBR was mainly attributed to an enhanced oxygen and nutrient mass transfer in the system.

3.1. Introduction

Polyhyroxybutyrate is a thermoplastic biopolyester of microbial origin that offers several exciting properties, such as biocompatibility, biodegradability and it shares features similar to those of the petroleum-based polymers (Arul Manikandan et al., 2019a; Deepthi et al., 2018). Under nutrient limiting conditions, i.e. due to the insufficient amount of nitrogen and phosphorus sources in the medium, few microorganisms start to accumulate the excess carbon source intracellularly as water-insoluble polyhydroxybutyrate (Fiorese et al., 2009; Serafim et al., 2004). These microorganisms are later harvested, and the PHB accumulated inside is recovered by a liquid-liquid extraction method. The process of growing microorganisms for intracellular accumulation of PHB is often referred to as upstream processing. Harvesting of the biomass and extraction of PHB from the microorganism are referred to as downstream processing (Arul Manikandan et al., 2019a). Owing to its sustainable nature, for the past few decades, PHB occupies a top position in the area of contemporary research. Unlike the petroleum-based polymers which use depleting fossil resource as its feedstock, PHB is sustainable as it can be sourced from a variety of biomass, agro-industrial refuse and even waste materials (Annamalai and Sivakumar, 2016).

Many microorganisms have been reported to feast on sugar source and accumulate PHB inside the cell. Among these microorganisms, *Ralstonia eutropha* is a very well-known PHB producer of all time (Khanna and Srivastava, 2005). Some of the interesting features of *R. eutropha* are: it is capable of growing on readily available sugar source (sucrose, fructose and glucose) as well as using more recalcitrant compounds (Bisphenol A and many other aromatic compounds) (Annamalai and Sivakumar, 2016; Babatabar et al., 2019; Heidari et al., 2017), *R. eutropha* can accumulate PHB up to 80% of its cell dry weight (Vidal-Mas et al., 2001), and it is generally regarded as safe (GRAS) (Abd-El-haleem et al., 2007). Many large scale biotechnological products, e.g. bioethanol and

succinic acid are often produced by anaerobic/facultative microbes with low biomass production (Bahry et al., 2017; Kumar et al., 2009). The low biomass production is due to less oxygen requirement in these microorganisms. On the other hand, *R. eutropha* being aerobic bacterium (Babatabar et al., 2019; Satagopan and Tabita, 2016), requires an elevated amount of oxygen in the medium for both biomass and PHB production, i.e., high biomass produced results in high PHB production by the bacterium (Saratale et al., 2019). Due to the high oxygen requirement for PHB production, the use of conventional stirred-tank bioreactors is doubtful. Any efforts to increase the oxygen availability in the traditional stirred-tank bioreactors by increasing the agitation rate would result in imparting shear stress on the microorganisms. In some cases, the sharp edges and corners contributed by baffles and impeller in such conventional stirred-tank bioreactors result in cell death and loss of PHB (Curran and Black, 2005; Follonier et al., 2012; Inan et al., 2016).

In order to overcome the limitation in the transfer of oxygen and other nutrients, different types of bioreactors have been proposed for PHB production. For instance, Gahlawat et al. (2012) used a novel airlift reactor (ALR) for PHB production. Using this bioreactor, the authors reported a K_La value of 57.6 h^{-1}, which is very high compared with the K_La value of 18 h^{-1} observed in the stirred tank reactor. Secondly, Inan et al. (2016) used a microbubble generator system for PHB production. Due to a reduction in the bubble size, the authors observed an enhancement in the K_La value. The K_La value increased from 23.93 h^{-1} using a conventional air sparged bioreactor system to 43.14 h^{-1} with the bioreactor assisted with a microbubble generator system. In a more recent study, García-Pérez et al. (2018) used a novel gas-recycling bubble column bioreactor for PHB production from methane as the substrate; efforts were laid to increase the methane solubility. In addition to these studies, many other novel bioreactors for enhancing the K_La value were reported in the literature for the production of other biotechnological products such as arachidonic acid

(ARA) -rich oil (Li et al., 2018), sophorolipid (Jia et al., 2017) and peroxin (PEX) protein (Qiao et al., 2014), etc. However, all the bioreactors have been reported to have one or more serious drawbacks for PHB production.

Hence, in the present study, the performance of annular bioreactor with Taylor and Couette flow was evaluated for PHB production. Furthermore, the bioreactor was fitted with a membrane-based sparger system to achieve enhanced K_La value. The use of annular bioreactor with Taylor and Couette flow is interesting because of its ability to improve the oxygen and nutrient delivery solely by means of the fluid agitation. This mechanism of agitation in ABR is quite contrary to the impeller driven agitation in a stirred tank bioreactor, where an increase in agitation rate may impart shear stress on the microorganisms (Curran and Black, 2005). This type of bioreactor with Taylor and Couette flow has been reported for various biotechnological applications ranging from animal cell culture (Qiao et al., 2014), microalgae cultivation (Kong et al., 2013), biopolymerization (Douaire et al., 2011) to biohydrogen production, etc. (Wen et al., 2017). For instance, Paule et al. (2011) used a novel annular bioreactor with Taylor and Couette flow for the development of phototrophic biofilm cultures. Qiao et al. (2014) used Taylor-Couette bioreactor for peroxin (PEX) protein production from quail muscle clone 7 (QM7) cells. Recently, Ramezani et al. (2017) examined oxygen transfer and bubble size distribution using a narrow annular gap Taylor-Couette vortex bioreactor. Qiao et al. (2018) carried out a computational study using computational fluid dynamics on oxygen transport in a narrow annular gap Taylor-Couette bioreactor. Very recently, Naseem et al. (2019) investigated a wide gap turbulent rotating Taylor-Couette flow reactor. However, the study was limited only to the fluid flow analysis using Particle Image Velocimetry (PIV). To the best of our knowledge, no study has been reported on the use of wide gap annular bioreactor with Taylor and Couette flow for biotechnological application. The wide annular space is an

added advantage in carrying out biochemical reactions as it offers very high volumetric productivity. Moreover, it is worth noting that other than the conventional stirred tank bioreactor (Kalaiyezhini and Ramachandran, 2015), membrane bioreactor (Haas et al., 2017), bubble column bioreactor (García-Pérez et al., 2018a; Ghoddosi et al., 2019), microbubble bioreactor (Inan et al., 2016) and airlift bioreactor (Gahlawat et al., 2012), there is no study reported in the literature on PHB production using Annular bioreactor or Taylor and Couette bioreactor.

Therefore, in the present study, a novel wide gap annular bioreactor (ABR) was fabricated and its hydrodynamics, including mixing, bubble size distribution and dissolved oxygen (DO) analyses at various operating conditions, were initially carried out. In order to understand the flow pattern prevailing in the ABR, CFD studies using Ansys^{TM} software were performed. Thereafter, the ABR was operated in batch mode under various agitation and sparge rate to optimize the biomass and PHB production. Under the optimized condition, Fed-batch experiments were carried out to analyze its potential for PHB production. The performance of the ABR was compared to that of a stirred tank bioreactor. Finally, PHB produced in the study was examined and its characteristics were compared with that of a commercially available pure PHB using techniques such as Fourier transform infrared spectroscopy (FTIR), Proton - Nuclear magnetic resonance (NMR), X-ray diffraction analysis and DSC/TGA analysis.

3.2. Materials and Methods

3.2.1. Chemicals

The chemicals, pottasium dihydrogen phosphate (KH_2PO_4), di-sodium hydrogen phosphate (Na_2HPO_4), magnesium sulphate heptahydrate ($MgSO_4 \cdot 7H_2O$), calcium chloride ($CaCl_2$), yeast extract, zinc sulphate heptahydrate ($ZnSO_4 \cdot 7H_2O$), ferrous sulphate heptahydrate ($FeSO_4 \cdot 7H_2O$), ammonium molybdate tetrahydrate ($(NH_4)_6Mo_7O_{24} \cdot 4H_2O$), boric acid

(H_3BO_3), Urea ($CO(NH_2)_2$), ammonium chloride (NH_4Cl), chloroform ($CHCl_3$), deuterated chloroform ($CDCl_3$), sodium hypochlorite (NaOCl), hydrochloric acid (HCl), sulphuric acid (H_sSO_4), sodium hydroxide (NaOH), tetrahydrofuran (C_4H_8O), pottasium chloride (KCl), safranin, sudan black, fluorescein diacetate (FDA), propidium iodide (PI), nutrient broth™ were bought from Himedia™, India. Pure PHB was purchased from Sigma-Aldrich™, India.

3.2.2. Hydrodynamic studies with the ABR

The STBR used in the present study is a commercial fermenter (Biotron™, Spectrochem, India), which consisted of a single-stage Rushton impeller and four baffles. The same STBR was modified by replacing Rushton impeller with a cylinder and by removing all the four baffles to fabricate the ABR for this study. While the external cylinder/ bioreactor vessel was stationary, the inner rotating cylinder served as the stirrer for the ABR (Ramezani et al., 2015). The inner cylinder of the ABR was made of aluminium covered plywood and attached to a motor for rotating the cylinder in the range 250–500 rpm. Air sparging in both STBR and ABR was ensured by a tubular ceramic membrane installed at the bottom of the bioreactors, and the sparge rate was controlled manually by adjusting the flow meter connected to a compressor. The airflow rate was varied by setting the flowmeter to 0.6 and 1.2 LPH so as to get a sparge rate of 0.4 and 0.8 vvm, respectively. Fig. 3.1 shows the images of the STBR, ABR and membrane sparger used in the present study, and Table 3.1 presents the specifications of the ABR and the membrane sparger.

Table 3.1. ABR specifications and input parameter for the CFD simulation

Descriptions	**Values**
Annular bioreactor specifications	
Outer cylinder diameter (cm)	15
Inner cylinder diameter (cm)	9
Axis	Symmetric axis
Operating volume (L)	1.5
Agitation rate (rpm)	250, 350, 500
Sparging rate (LPM)	0.6, 1.2
Initial and saturated oxygen concentration in the liquid (mg/L)	7.8
Media specifications	
Water viscosity (Pa·s)	0.00083
Tracer (KCl) concentration (N)	0.1
Operating pressure (atm)	1
Sparger specifications (Arul Manikandan et al., 2019) [1]	
Outer diameter (cm)	1.15
Channel diameter (cm)	0.55
Length (cm)	7
Pore size (µm)	0.309
Porosity (%)	53

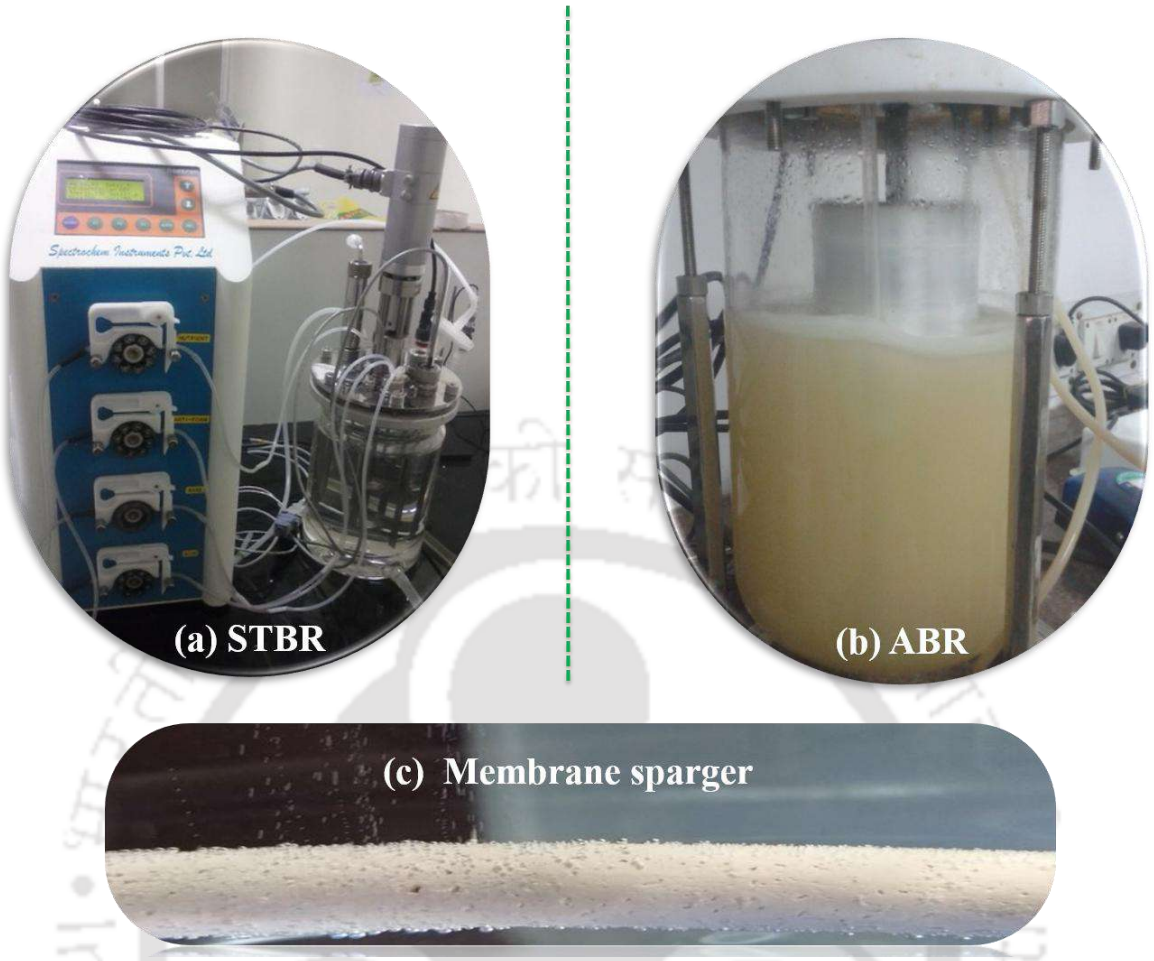

Fig. 3.1. Image showing of (a) stirred tank bioreactor (STBR), (b) annular bioreactor (ABR) and (c) membrane sparger used in this study

PHB production using *R. eutropha* was investigated using the ABR operated at different agitation rates of 250, 350, or 500 rpm and air-sparge rates of 0.4 or 0.8 vvm. As shown in Fig. 3.2(a), based on the investigations, i.e., tracer analysis, DO measurement or biomass-cum-PHB production, the probe fitted with the bioreactor was changed from conductivity probe, DO probe or pH probe, respectively. Tracer analysis was carried out by injecting 10 mL of 0.1 N KCl into the stem of the bioreactor using a glass pipette. Thereafter, the conductivity of the solution was analyzed for every 5 s using a conductivity meter (Eutech, Singapore). Prior to this study, a calibration curve relating the conductivity and KCl concentration was obtained.

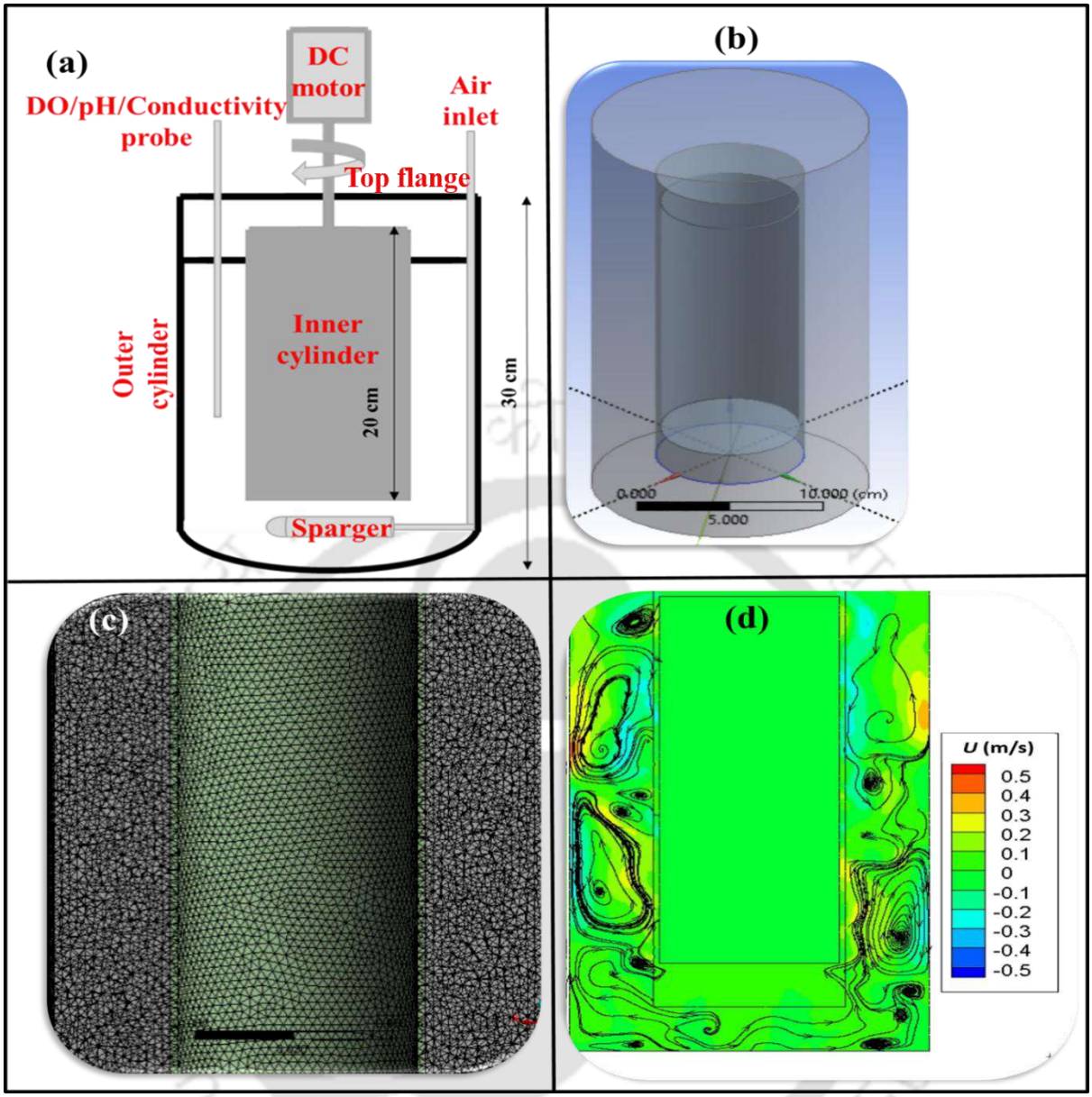

Fig. 3.2. (a) Schematic of ABR, (b) Reactor geometry of ABR, (c) ABR mesh and (d) velocity profile of ABR operated at 500 rpm

The tracer analysis was carried out for ABR operated under batch mode with agitation rates of 250, 350, or 500 rpm and air-sparge rates of 0.4 or 0.8 vvm. Similarly, DO measurement using a DO probe (Hach, India) was carried out with the ABR operated under batch mode and agitation rates of 250, 350, or 500 rpm and air-sparge rates of 0.4 or 0.8 vvm. However, before carrying out the DO measurement, DO in the bioreactor solution was brought down almost to 0 mg/L by continuous sparging of nitrogen gas through the

sparger. Once the DO in the bioreactor solution was brought down to 0 mg/L, quickly nitrogen sparge was replaced with an air sparge into the bioreactor. After that, DO in the bioreactor solution was measured for every 25 s using a DO probe, as mentioned earlier. From the DO profile, k_La estimation was carried out by using the following equation (1) (Ramezani et al., 2015):

$$\ln\left(1-\frac{C_t}{C_*}\right)=-k_La \times t \qquad (1)$$

Where, C_t is the dissolved oxygen concentration in the bioreactor solution at a given time, C_* is the saturated dissolved oxygen concentration (7.8 mg/L), t is the arbitrary time, k_L is the mass transfer coefficient, and 'a' is the specific air-liquid interfacial surface area. For the tracer analysis and DO measurement, 1.5 L of Millipore water having a saturated DO concentration (C_* = 7.8 mg/L) and pH value of 7.0 was used. Both the tracer analysis and DO measurement were carried out as per the protocol reported in the literature by Ramezani et al. (2015) and Saravanan et al. (2010). Besides, bubble size distribution in the ABR at different operating conditions was analyzed using a high-speed camera (VEO 640, Phantom, USA). The images were captured by mounting focus lens on to the camera, and the lens was placed in close proximity to the outer cylinder of the ABR. Furthermore, the reactor was properly illuminated to get clear bubble images. The image analysis software ImageJ® was used to analyze the size of the bubbles.

3.2.3. Computational fluid dynamic (CFD) simulation

CFD simulation was carried out to analyze the flow pattern in the annular bioreactor (ABR) operated at an agitation rate of 500 rpm. Simulation studies were carried out using Ansys® Fluent 14.5. Both geometry creation and meshing were done using an in-built software interface available with Ansys®. Meshing was done in a 3D domain, with the inner cylinder set as a moving wall and outer one as the stationary wall. The dimensions of the ABR used

for simulation were the same shown in Fig. 3.2a and Table 3.1. Simulation strategy, as described by He et al. (2018) and Paule et al. (2011), was used for this CFD study, which involved a combination of Navier–Stokes equations and the k-ε Reynolds Stress model at steady-state.

3.2.4. Microorganisms

The microorganism (*R. eutropha*) used in the present study was purchased from Microbial Type culture collection (MTCC®), Chandigarh, India (30.7489° N, 76.7337° E). The culture was initially grown under constant agitation rate of 150 rpm, temperature 30 ^{o}C and a total cultivation period of 24 h in a 250 mL Erlenmeyer flask containing 100 mL working volume of Nutrient broth™. Exponentially growing cells of *R. eutropha* were used as the inoculum for carrying out the bioreactor experiments.

3.2.5. ABR and STBR study

Throughout the reactor study, 150 mL of *R. eutropha* in their mid logarithmic phase was used as the seed culture in both STBR and ABR containing 1.5 L of sugar-rich carob pod extract with mineral salt medium (MSM) as described in chapter 2. The composition of the carob pod extract is 40 g/L of sugar concentration, out of which sucrose shares the largest concentration of 20 g/L, followed by glucose and fructose concentrations of 15 g/L and 5 g/L, respectively. Composition of the MSM is as follows (g/L): pottasium dihydrogen phosphate (KH_2PO_4), 2.0; di-sodium hydrogen phosphate (Na_2HPO_4), 0.6; magnesium sulphate heptahydrate ($MgSO_4{\cdot}7H_2O$), 0.2; calcium chloride ($CaCl_2$), 0.2; and 10 mL/L of trace metal solution. Further, the trace metal solution comprised of (mg/L): zinc sulphate heptahydrate ($ZnSO_4{\cdot}7H_2O$), 1.3; Ferrous sulphate heptahydrate ($FeSO_4{\cdot}7H_2O$), 0.2; ammonium molybdate tetrahydrate ($(NH_4)_6Mo_7O_{24}{\cdot}4H_2O$), 0.6; and boric acid ($H_3BO_3$), 0.6. A stock solution of major components in the MSM and the trace metal solution was autoclaved separately and added aseptically before performing the experiments.

ABR was operated in batch mode under various agitation rates (250, 350 and 500 rpm) and sparge rates (0.4 and 0.8 vvm). Following batch culture for 60 h, PHB rich *R. eutropha* cells from the bioreactor were harvested by centrifuging the biomass taken in a 250 ml polypropylene bottle. Centrifugation was carried out at 6000×g for a total time span of 10 min, and thereafter, the supernatant from the bottles was discarded to get biomass pellet, which was oven-dried at 60 ^{o}C for 12 h to obtain the final biomass concentration in g/L. PHB from the biomass was extracted by suspending the bacterial biomass in a solution mixture containing 100 mL of chloroform and 100 mL of NaOCl (4% w/v). The suspension was incubated at 30 ^{o}C for 2.5 h in a shaker incubator set at 150 rpm followed by centrifugation at 8000×g for 10 min. After centrifugation, three distinct phases were formed and the bottom phase containing PHB rich chloroform was separated using a separating funnel. After that, the chloroform containing PHB was transferred into ice-cold ethanol to get a white precipitate of PHB. The precipitates were then weighed to obtain the PHB concentration in g/L (Saratale and Oh, 2015). In addition to the gravimetric analysis for biomass estimation, turbidimetric analysis at OD_{600} was carried out using a UV – Vis spectrophotometer (Lamda 35 model, Perkin Elmer, USA).

For an efficient PHB production, fed-batch experiments were further carried out by following pulse feeding strategy, similar to that reported by Castillo et al. (2017). Feeding was started with an initial working volume of 1.5 L and at the end of 25-hour batch a single substrate pulse containing 50 g of sugar-rich carob extract dissolved in 50 mL Millipore water was added to the bioreactor and thereafter, at the end of 60th hour, a double substrate pulse containing each 50 g of reenacted carob extract dissolved in 50 mL Millipore water was added into the bioreactor. Samples were withdrawn from the bioreactor with a time interval of 6 h and analyzed for biomass concentration (g/L) and total organic carbon (TOC) concentration (g/L) for understanding biokinetics of the process. Biomass analysis

followed for this biokinetic study was the same as described before, PHB concentration was estimated by the crotonic acid assay method, as described in chapter 2 (Arul Manikandan et al., 2019). For PHB analysis, the biomass was treated with 98% sulphuric acid for 1 h in a boiling water bath to convert polyhydroxybutyric acid to crotonic acid, which was then measured spectrophotometrically at 235 nm using a UV - Vis spectrophotometer (Lamda 35 model, Perkin Elmer, USA). Pure sulphuric acid served as the reference in this UV - Vis spectroscopy analysis.

Commercial PHB was used to construct the calibration curve and thereafter PHB yield was estimated. The supernatant drained for getting the biomass pellet was used to analyze the total organic carbon (TOC) concentration (g/L) in the sample using a TOC analyzer (model no. 1030, O-I-Analytical, Aurora, USA). Change in solution turbidity of the ABR operated at an agitation rate of 500 rpm and a sparge rate of 0.8 vvm due to the *R. eutropha* growth inside was monitored using a digital camera (J8 model, Samsung, Korea) to observe the increase in the turbidity. Furthermore, enhancement in PHB accumulation during *R. eutropha* growth was checked using safranin and Sudan black staining. Whereas the safranin stains with the biomass, Sudan black stains only with the PHB granules, which were then visualized using a Nikon eclipse TS-100 inverted microscope (Japan) and images were obtained separately using Nikon L22 (Nikon Corp., Japan) digital camera. Confirmation of PHB accumulation in the *R. eutropha* cell was made using a field emission transmission electron microscope (FETEM). For this analysis, *R. eutropha* cells during the culture growth were placed in a copper grid and analyzed using FETEM (JEOL, JEM 2100F, Japan) operated at 200 kV. All the samples for biomass and PHB concentration (g/L) were analyzed thrice and mean ± standard deviation (SD) values of the results were reported. The performance results of the batch and Fed-batch experiments of ABR were compared with that of the conventional STBR. However, batch operations with the STBR

were carried out only for two agitation rates of 250 and 300 rpm and at a single sparge rate of 0.8 vvm.

3.2.6. Analytical techniques

Changes in the viability of *R. eutropha* cells due to different agitation conditions in ABR and STBR were investigated by flow cytometry analysis of the cells (BD Calibur™ Flow Cytometer, BD Biosciences, USA). Exponentially growing cells from both the reactors operated under batch mode were analyzed using 488 nm laser and 530 nm emission filter. Fluorescein diacetate (FDA) and Propidium Iodide (PI) fluorescent dyes were used to distinguish between the live and dead cells. FL1-H detector detects the FDA stained cells, which are proportional to the fraction of live cells in the population, and FL3-H detector detects the PI stained cells that are proportional to the fraction of dead cells in the population.

For sodium dodecyl sulfate-polyacrylamide gel electrophoresis (SDS- PAGE) analysis, at the end of batch experiments with ABR, biomass sample was centrifuged at 6000×g for 10 min. And the biomass was resuspended and diluted in phosphate buffer saline (PBS) at pH 7.0 so as to get a final OD_{600} around 10. The treated biomass was then taken for tip sonication to lyse the cells and expel proteins out of it. Sonication was carried out in 6 rounds with 20 s on-cycle (50% amplification) and 20 s off-cycle (Wu et al., 2019). After that, 15 µL of the lysed cultures were subjected to SDS-PAGE analysis. The gel was later stained with Coomasie brilliant blue R- 250 to locate the protein bands. Finally, the gel was visualized using a gel documentation system (Bio-Rad) (Yoganand et al., 2019). All the aforementioned experiments were repeated at least twice, and the representative results were presented.

In order to compare the PHB produced in this study using ABR with a commercially available PHB, various characterization techniques including Fourier transform infrared

spectroscopy (FTIR), thermogravimetric/differential scanning calorimetric (TGA/DSC), X-ray diffraction (XRD) and proton nuclear magnetic resonance (NMR) analyses were employed. For all these characterizations, PHB extracted from the ABR operated at an agitation rate of 500 rpm and a sparge rate of 0.8 vvm was used. Further, all these characterizations were carried out as per the methodology mentioned in section 2.2.7.

3.3. Results and discussion

3.3.1. Hydrodynamic studies of ABR

Tracer experiments were first carried out with the ABR operated under batch mode by circulating the liquid inside while the air sparged into the system was allowed to escape through a vent placed at the top flange of the bioreactor. The tracer injected in the stem of the bioreactor was evenly distributed within the bioreactor due to the continuous air sparging and liquid agitation in the bioreactor. Therefore, tracer concentration measured at the top of the bioreactor represented the hydrodynamic conditions and flow pattern within the bioreactor. The increase in tracer concentration as detected by conductivity meter during the bioreactor operation at various air sparge and agitation rates is shown in Fig. 3.3.

The overall pattern of tracer study conducted at different agitation and sparge rates resembles an exponential curve. However, variations in the mixing pattern due to the change in agitation and sparging rates are observed. For instance, a change in agitation rate from 250 to 500 rpm at a fixed sparge rate of 0.8 vvm resulted in the enhancement of KCl concentration from 55 to 70.5 mg/L. Similarly, a change in the sparge rate from 0.4 to 0.8 vvm at a fixed agitation rate of 250 rpm resulted in a hike in the KCl concentration from 52 to 55 mg/L. Similar tracer patterns were observed by Saravanan et al. (2010) in their study on the hydrodynamics of an internal loop airlift bioreactor. In contrary, Jamshidi et al. (2001) on their hydrodynamic study using downflow jet loop bioreactor reported an

initial sharp increase in the KCl concentration followed by a reduction in the value until a steady-state reached. This change in the tracer pattern might be due to the position of the conductivity probe placed in the bioreactor system. As mentioned earlier, the conductivity probe in the present study was placed on the top while the tracer was injected at the stem of the bioreactor. However, keeping the probe close to the injection area might have resulted in a steep increase in the KCl concentration. Therefore, it can be concluded from these tracer experiments that ABR operated at a sparge rate of 0.8 vvm and agitation rate of 500 rpm resulted in a better mixing than at other conditions. Since the ABR used in the present study was aimed at achieving a maximum growth of fragile bacterial cells, the agitation rate was not increased beyond this point. This observation is consistent with those of Qiao et al. (2014) for culturing of QM7 cells in a Taylor-Couette bioreactor and Ramezani et al. (2017) on using multiphase Taylor-Couette vortex bioreactor.

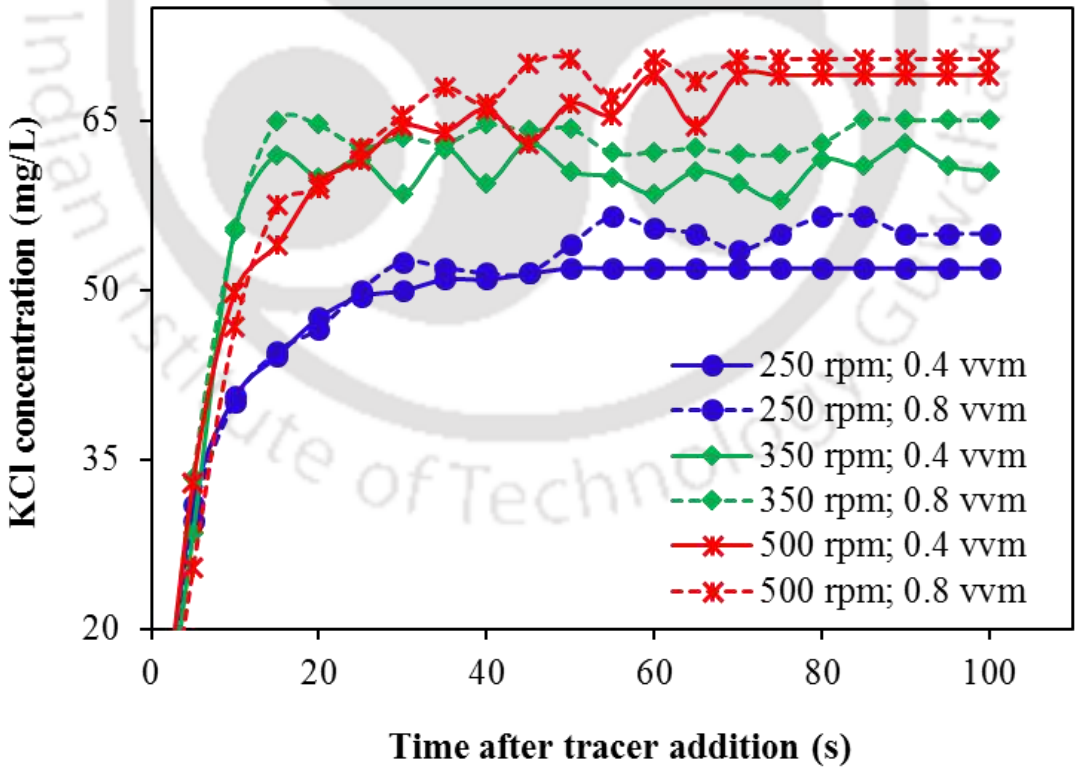

Fig. 3.3. Results of tracer (KCl) experiments with the ABR operated at varying operating conditions

In order to determine the capability of the bioreactor to efficiently deliver oxygen to the microorganism, K_La and dissolved oxygen measurements were carried out. Fig. 3.4(a) portrays that at the end of 600 s of operating the ABR at a sparge rate of 0.4 vvm and agitation rate of 250 rpm, the DO level in the liquid was 74% of the saturation efficiency. An increase of agitation rate from 250 to 350 rpm by keeping the sparge rate at 0.4 vvm resulted in 93% of the saturation efficiency. At all other operating conditions, the DO profile reached 100% saturation efficiency, i.e., a maximum DO concentration of 7.8 mg/L. A similar trend of DO profile (achieving the 100% saturation efficiency) was reported by Ramezani et al. (2015) in a narrow gap Taylor-Couette vortex bioreactor.

Fig. 3.4(b) shows the linearized form of DO profile for estimating the volumetric mass transfer coefficient (K_La) in ABR. K_La in the ABR increased with an increase in the agitation and sparge rates. For instance, an increase in the agitation rate from 250 to 500 rpm with a constant sparge rate of 0.4 vvm resulted in 5.6 times enhancement in K_La value from 8.12 to 45.2 h^{-1}. The highest K_La of 70 h^{-1} was observed at a maximum agitation and sparge rate of 500 rpm and 0.8 vvm, respectively. The increased K_La with agitation rate is due to an efficient mixing in the ABR (Curran and Black, 2005; Qiao et al., 2018; Ramezani et al., 2015). K_La values obtained at various operating conditions of ABR were presented in Table 3.2. Air bubbles in the ABR were observed using a high-speed camera, and the images along with the bubble size distribution are shown in Fig. 3.5. It can be inferred from the figure that any effort to increase the turbulence in the ABR by varying the agitation rate resulted in a shift in the bubble size to a larger size. However, variation in the sparge rate at a given agitation rate displayed only a slight increase in the bubble size.

Table 3.2. Comparison of ABR performance with that of the STBR at varying operating conditions

Agitation rate (rpm)	**250**	**250**	**350**	**350**	**500**	**500**	**250 (STBR)**	**300 (STBR)**
Air sparge rate (vvm)	**0.4**	**0.8**	**0.4**	**0.8**	**0.4**	**0.8**	**0.8 (STBR)**	**0.8 (STBR)**
OD_{600} (60h)	9.64 ± 0.1	27.96 ± 1.47	21.9 ± 0.81	37.3 ± 0.89	53.16 ± 1.6	70.2 ± 2.0	50.16 ± 1.02	44.2 ± 1.0
PHB % (60 h)	70.43	64.5 ± 0.49	67.0 ± 0.70	60.1 ± 0.50	54.2 ± 1.00	50.1 ± 0.8	49.8 ± 0.52	47.5 ± 0.52
K_La (h^{-1})	8.12	24.1	16	32	45.2	70	42	45.2

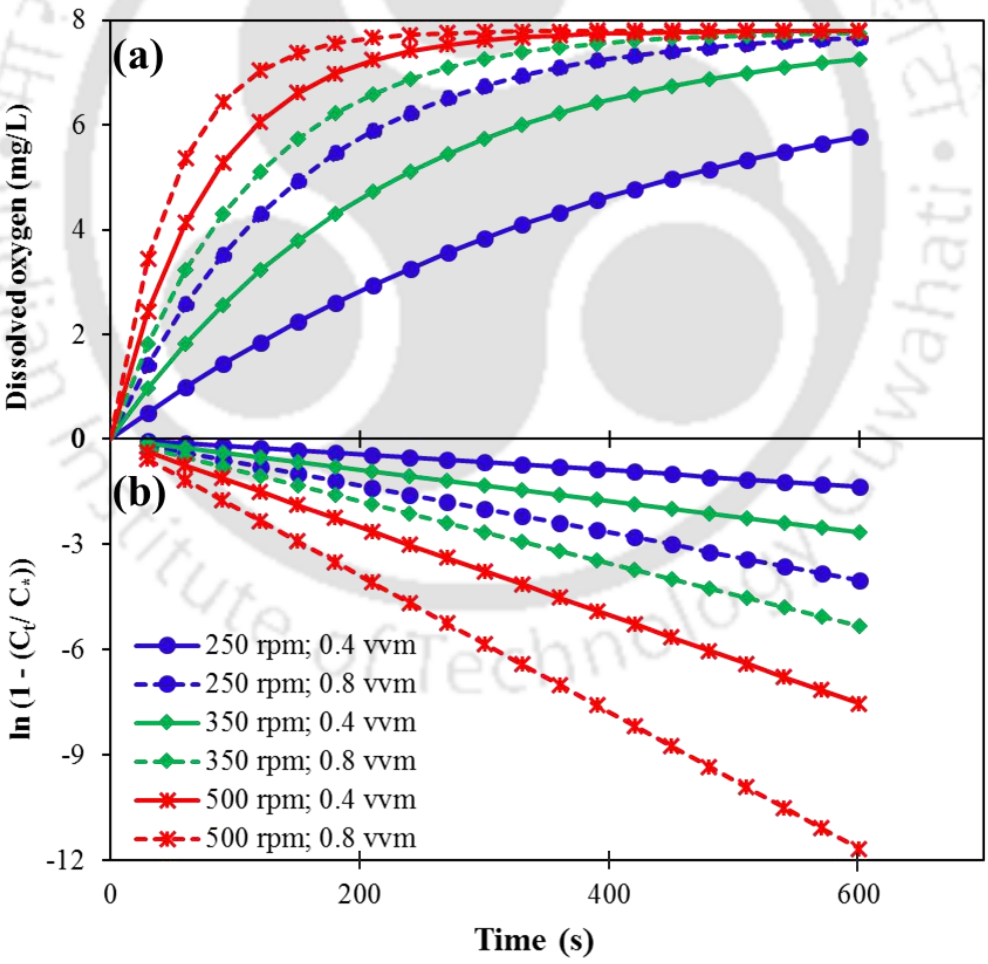

Fig. 3.4. (a) DO profile and (b) linearised profile for K_La determination in the ABR operated at varying operating conditions

The increase in bubble size with an increase in the agitation rate is typically found only in such bioreactor having Taylor and Couette flow, but not in other conventional STBR or ALR (Saavanan et al., 2009). For instance, a narrow gap annular bioreactor having Taylor and Couette flow also resulted in a continuous shift in bubble size to a higher value with an increase in agitation/sparge rate (Ramezani et al., 2015). Similar results were observed by the same authors for a different study carried out using the same bioreactor with Taylor and Couette flow (Ramezani et al., 2017). Bubble size analysis in another horizontal bioreactor with Taylor and Couette flow was also found to match with the results obtained in this study (Hubacz and Wroński, 2004). The increase in bubble image and enhancement in oxygen K_La is attributed to the bubble coalescence (Fig. 3.5(b)) due to the Taylor flow and increased gas hold up in the Taylor vortices, respectively (Ramezani et al., 2015). These results further confirm the presence of Taylor and Couette flow in the present ABR with a wide annular gap. In order to further ascertain the flow pattern in ABR, CFD simulation was performed on the bioreactor geometry and the results were discussed in the next section.

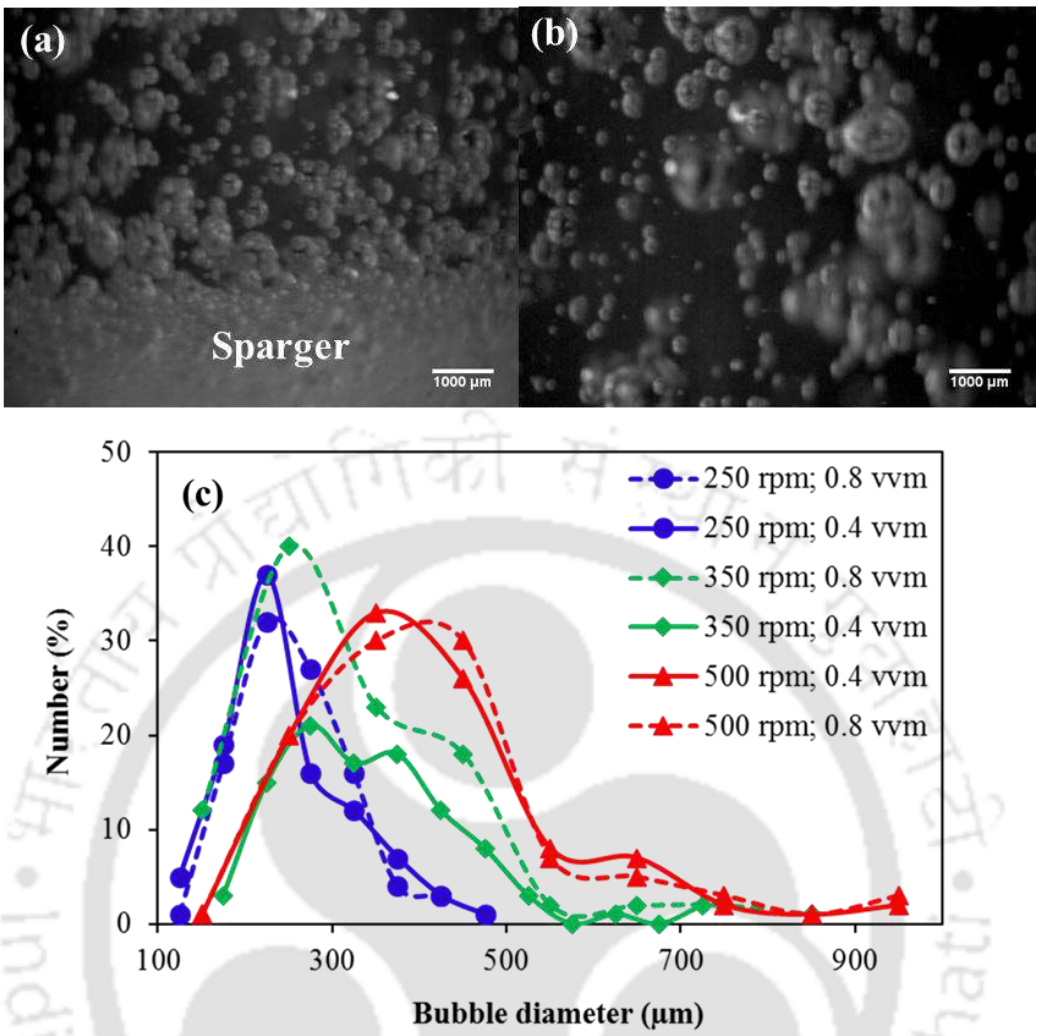

Fig. 3.5. Images showing (a) air bubbles originating from the sparger, (b) air bubbles at the stem of the ABR and (c) plot of bubble size distribution in the ABR operated at varying operating conditions

3.3.2. CFD analysis

Fig. 3.2 (b - d) shows the various components involved in CFD simulation, viz. reactor geometry, meshing and velocity profile contour. The reactor geometry consisted of an outer stationary cylinder and a solid rotating cylinder placed inside. The outer cylinder was considered as a stationary mesh and the inner cylinder was considered as a moving mesh. Finer mesh was chosen to get accurate results. Also, the grid density on the boundary was increased to avoid inaccuracy in the iteration. Mesh size was increased and reduced on a

trial and error basis. It was found to converge finally at a grid size of 1 x 10^{-3} m and 3 x 10^{-3} m for the central computational domain and boundary layer, respectively. The contour plot (Fig. 3.2(d)) showed the velocity profile when the ABR was rotated at an agitation rate of 500 rpm. Also, the well-connected swirls and whirls on the sides of the inner cylinder displayed the presence of Taylor and Couette flow (Paule et al., 2011). Based on the K_La results presented in the previous section and the CFD simulation results, it can be concluded that the wide gap annular bioreactor exhibited Taylor and Couette flow.

3.3.3. Performance of ABR in batch mode

Changes in the *R. eutropha* cells during different phases of its growth in the batch operated ABR are shown in Fig. 3.6. Turbidity of the culture was maximum during the stationary growth phase. The cells at this phase were harvested and stained with Sudan black and safranin dye, which revealed an impressive purple shading, in Fig. 3.6. It also revealed the Gram-negative nature of *R. eutropha*. However, blue inclusion of the cells, as shown in these images, indicates the presence of PHB inside the cells. It could be seen from the images that cells at the stationary phase showed more blue colour than at the logarithmic growth phase, signifying that PHB production was more pronounced following the exponential phase. These findings confirm that after achieving the exponential growth period, the substrate flux deviated towards PHB production by the cells (Fig. 3.6). For a clear visualization of the PHB granules, the *R. eutropha* cells were observed under FETEM, which revealed a moderately high number of well defined PHB granules inside the cells.

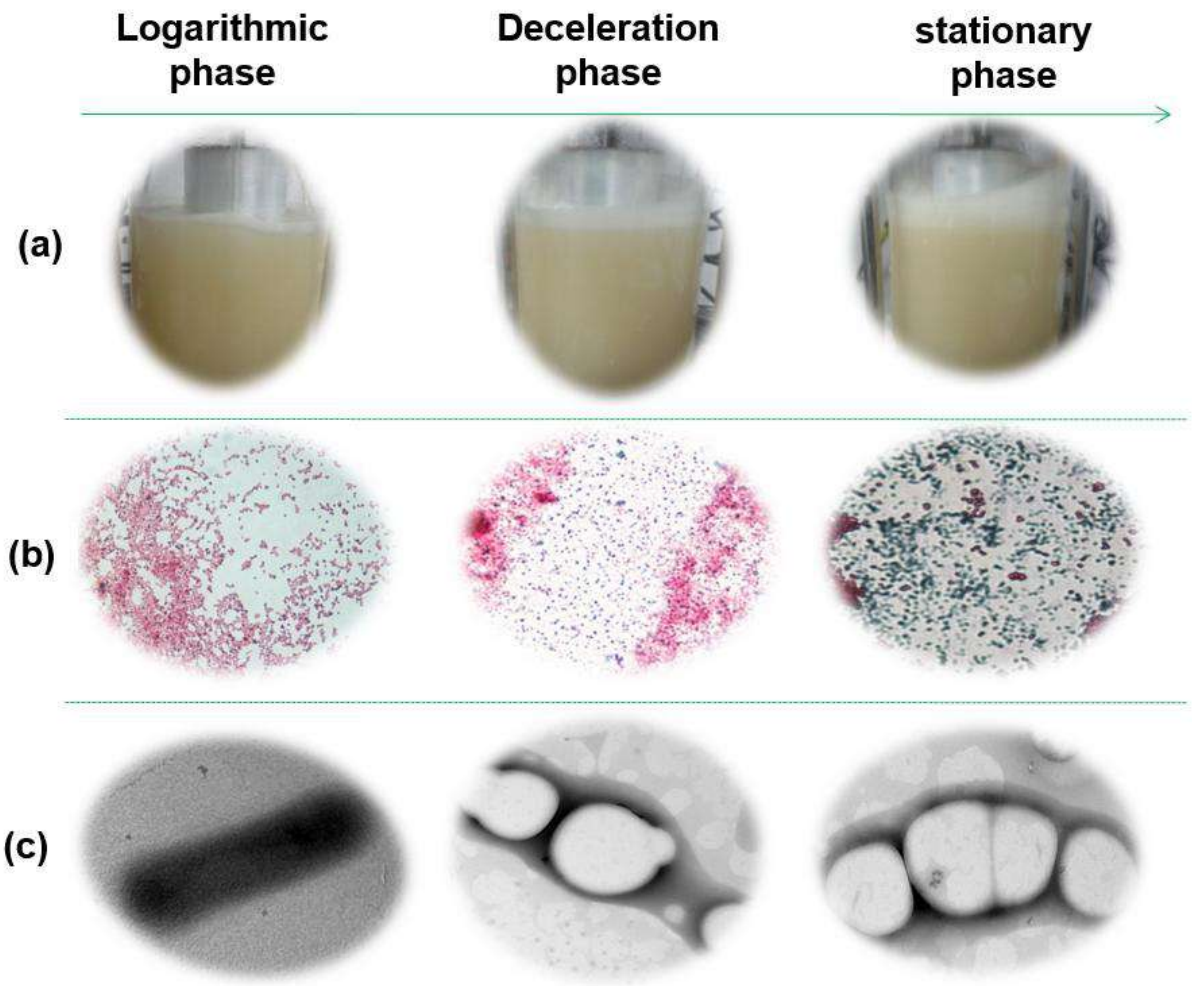

Fig. 3.6. Images showing changes observed in *R. eutropha* cells at a different phase of its growth in the batch-operated ABR: (a) culture broth, (b) light microscopy (100 X) magnification and (c) FETEM showing PHB granules

At the end of the 60 h batch fermentation in ABR, operated at 500 rpm and a sparging rate of 0.8 vvm, *R. eutropha* biomass production was observed to be exceedingly high (OD_{600} around 70.2). Even at 250 rpm and 0.4 vvm, the biomass produced was high (OD_{600} = 9.64). The high biomass titre obtained is due to the increased K_La value from 8.12 h^{-1} to 24.1 h^{-1} when sparging rate raised from 0.4 vvm to 0.8 vvm at 250 rpm (see Table 3.2). It is expected that a minimum agitation rate and air sparge rate in a fermentor yield the least biomass production owing to the oxygen limitation condition in the bioreactor, and for the same reason, deploying an unconventional reactor like ABR is favoured as it

helps in the production of *R. eutropha* biomass by increasing oxygen uptake by the microorganisms. However, it could be inferred from Table 3.2 that at low DO conditions, PHB accumulation by the bacterial biomass increased due to the change in substrate flux from biomass production to PHB accumulation by the bacteria. Similar observations were made by Díaz-Barrera et al. (2016), wherein an increase in agitation rate reduced PHB accumulation from 84 to 65 % (w/w). This observation on increased PHB accumulation at a low agitation rate was confirmed from the results of the gel electrophoresis analysis (Fig. 3.7). Since the bacterial cells used for the analysis were obtained at the end of the batch cultivation, protein bands were less intense. However, the band due to histone-like protein at 40 kDa is found to be intense and the intensity decreased along with an increase in the agitation rate.

Histone is a protein known to bind the DNA. In Fig. 3.7, the band at 40 kDa is a representation of histone-like proteins because these proteins bind the PHB inside the bacterial cell to form granules (Luengo et al., 2003). A schematic showing the role of histone-like proteins in *R. eutropha* along with TEM image of the actual *R. eutropha* is shown in Fig. 3.7(b-c). Thus, a decreased intensity of the band corresponding to histone-like proteins in Fig. 3.7(a) at a high agitation rate indicates reduced accumulation of PHB. After 60 h of batch fermentation, the average PHB production values at 0.4 vvm air-sparge rate and agitation rates of 250, 350 and 500 rpm were 4.14, 8.47 and 21.18 g/L, respectively (Fig. 3.8). At the same agitation rates with an increased air sparging rate of 0.8 vvm, the PHB concentrations were increased to 12.25, 16.2 and 29.72 g/L, respectively.

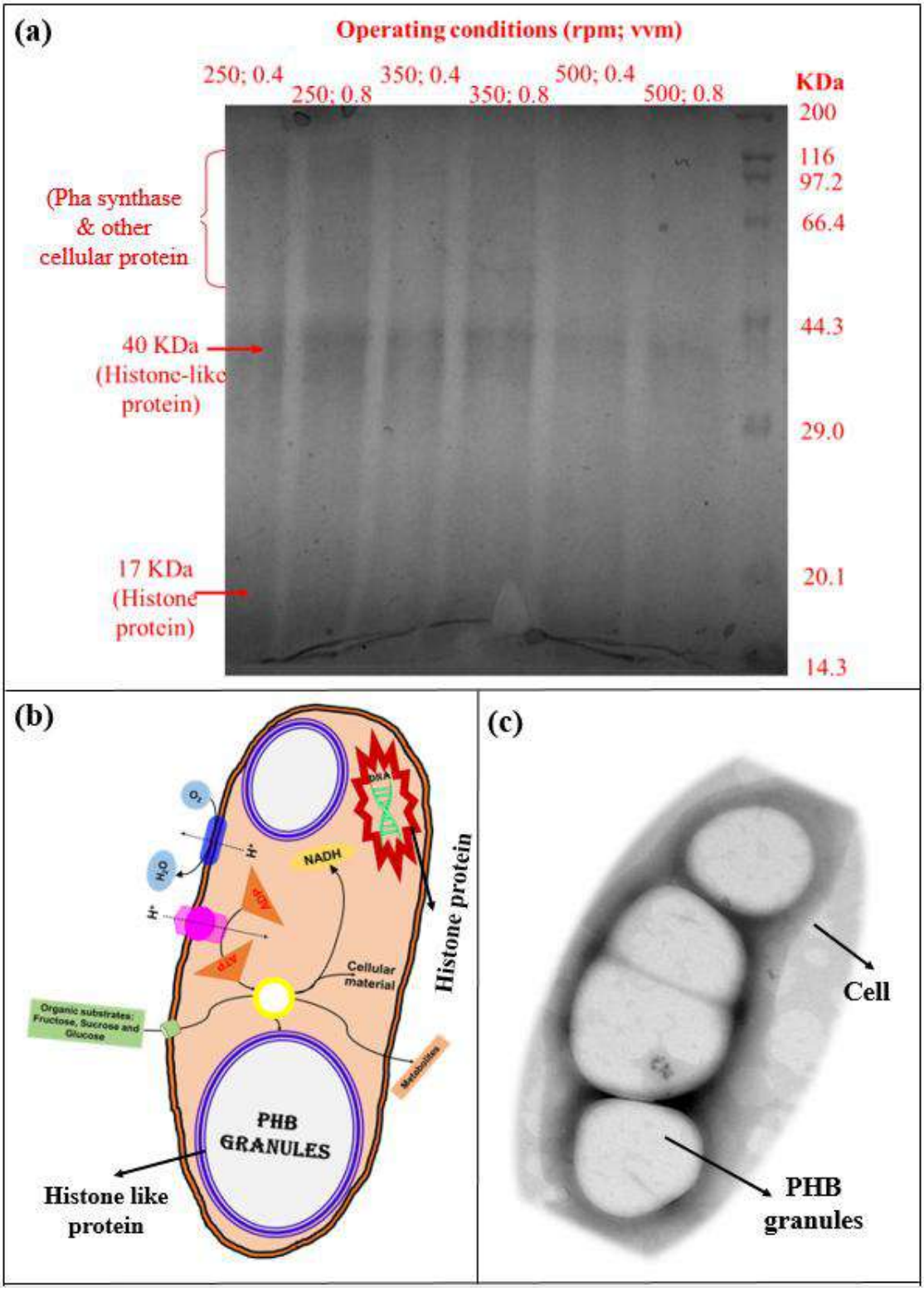

Fig. 3.7. (a) Results of gel electrophoresis analysis of *R. eutropha* cells obtained from the batch operated ABR at varying agitation and air sparge rates, (b) Schematic showing *R. eutropha* cell with PHB granules enclosed inside a histone-like protein and (c) FETEM image of an actual *R. eutropha* cell with PHB granules accumulated inside its cell wall

The bioreactor operated at 350 rpm, and at increased air sparge rate from 0.4 to 0.8 vvm did not yield significant enhancement in PHB accumulation. However, at the other two agitation rates, i.e., 250 and 500 rpm, an increase in air sparge rate significantly improved the PHB accumulation (Fig. 3.8). Similar results were reported in the literature, which suggests that oxygen constrained cultivation conditions result in low biomass production and PHB yields (Cavalheiro et al., 2009; Díaz-Barrera et al., 2016). Moreover, reduction in available oxygen could altogether influence native metabolic pathways in *R. eutropha*, including ATP generation, which further reduces biomass and PHB production (Anusha et al., 2016; Cavalheiro et al., 2009). The results obtained from the batch operated ABR were compared with the results obtained from STBR operated at 250 rpm and 0.8 vvm air sparge rate. Increasing the STBR agitation rate resulted in lowered biomass concentration (Fig. 3.8). Whereas, ABR yielded 1.3 times higher biomass production and PHB production than the STBR operated at the optimized conditions.

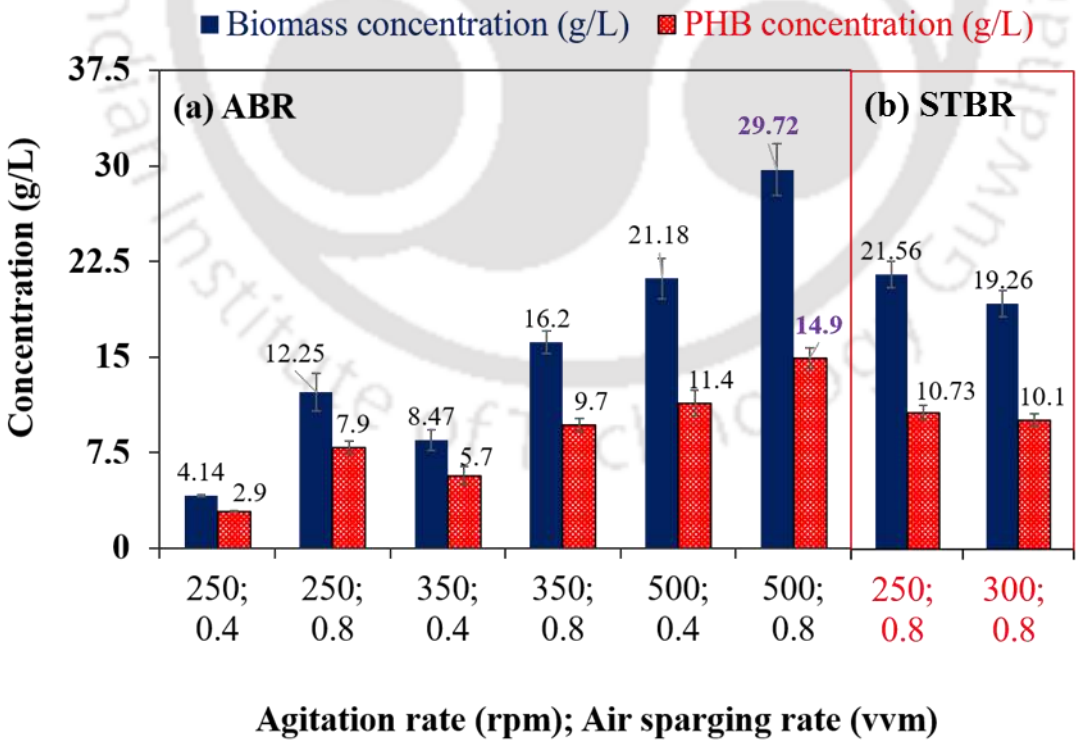

Fig. 3.8. Biomass and PHB concentration at various operating conditions in the batch operated (a) ABR and (b) STBR

The results of flow cytometry analysis of *R. eutropha* cells in (a) positive control, (b) fermentation in ABR and (c) in STBR are depicted in Fig. 3.9 (a - c), respectively. From Fig. 3.9(b), 7% of the values fall in the upper right quadrant, which implies that ABR did not inhibit the microbial growth or impose any stress on the microbial cells. However, the mortality rate of *R. eutropha* cells in STBR increased to 22%, which confirms the high stress imposed by STBR even at moderate agitation and aeration rates, resulting in cell death.

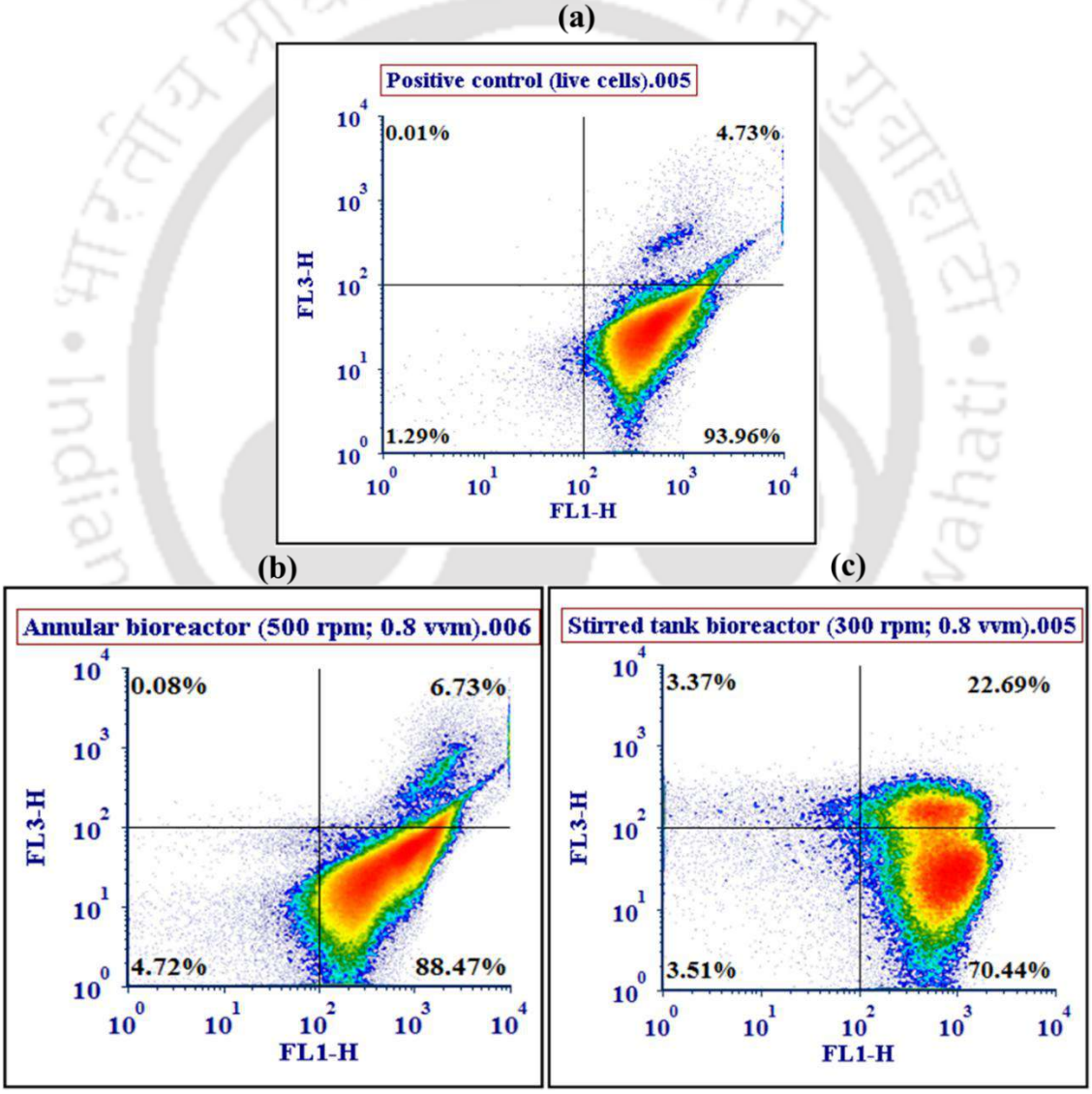

Fig. 3.9. Results of flow cytometry analysis of (a) positive control (b) ABR operated at an agitation rate of 500 rpm with sparge rate of 0.8 vvm and (c) STBR operated at an agitation rate of 500 rpm with sparge rate of 0.8 vvm.

3.3.4. Performance of ABR in fed-batch mode

In case of an intracellular product like PHB, Fed-batch experiments were preferred over continuous experiments to get very high biomass concentration and to avoid substrate toxicity and wastage of water. Therefore, a pulse feeding based fed-batch strategy was followed for evaluating the performance of both ABR and STBR by changing the number of feeding dosages. The pulse feeding strategy showed a significant positive effect on biomass growth, PHB production and TOC utilization (Fig. 3.10). In both the reactors (ABR and STBR), the TOC utilization profile increased after pulse addition. However, the TOC utilization profile was more drastic in the case of ABR than with STBR. As observed earlier in the batch study, a high oxygen transfer in ABR improved assimilation of the carbon source, thereby enhancing the biomass and PHB production. The highest concentrations of total biomass (94.1 g/L) and PHB (70.8 g/L) were thus achieved in the fed-batch experiments conducted with the ABR; on the other hand, a total biomass concentration of 60.9 g/L and PHB concentration of 44.2 g/L were achieved using the STBR. Moreover, the total sugars in the ABR were fully consumed with a residual TOC of 6.21 g/L at the end of the 90 h fed-batch experiment. In the case of STBR, the residual TOC was 62 g/L (Fig. 3.10).

These results demonstrate that the performance of STBR was at least ten times inferior to that of the ABR in delivering nutrients, in particular, oxygen, which is a limiting nutrient for biomass production to the microorganisms. A similar result of better sugar removal due to reactor framework has been reported by adopting fed-batch strategy in an airlift reactor (ALR) (Gahlawat et al., 2012); however, the biomass (39.17 g/L) and PHB production (29.64 g/L) values reported are low in comparison with the results obtained in the present study (Gahlawat et al., 2012). For large-scale production of PHB and reduction of production costs, the fermentation strategy must ensure high PHB concentration. For

organisms such as *A. lata*, values of PHB concentration as high as up to 98.8 g/L have been reported (Castillo et al., 2017). For *A. vinelandii*, the highest PHB concentration reported was 36 g/L. With the same strain (*R. eutropha*) used in the present study, the literature was reported a maximum value of PHB concentration of 93.5 g/L (Huschner et al., 2015), which is quite high as compared to the PHB concentration (70.8 g/L) observed in the present study. The high PHB value reported by Huschner et al. (2015) is because of the use of organic acids, such as acetic acid, as a substrate in their study. It was reported that unlike conventional carbon sources, such as glucose, fructose and sucrose, acetic acid could directly enter into the acetyl-CoA pathway, and thereby resulting in very high biomass and PHB production.

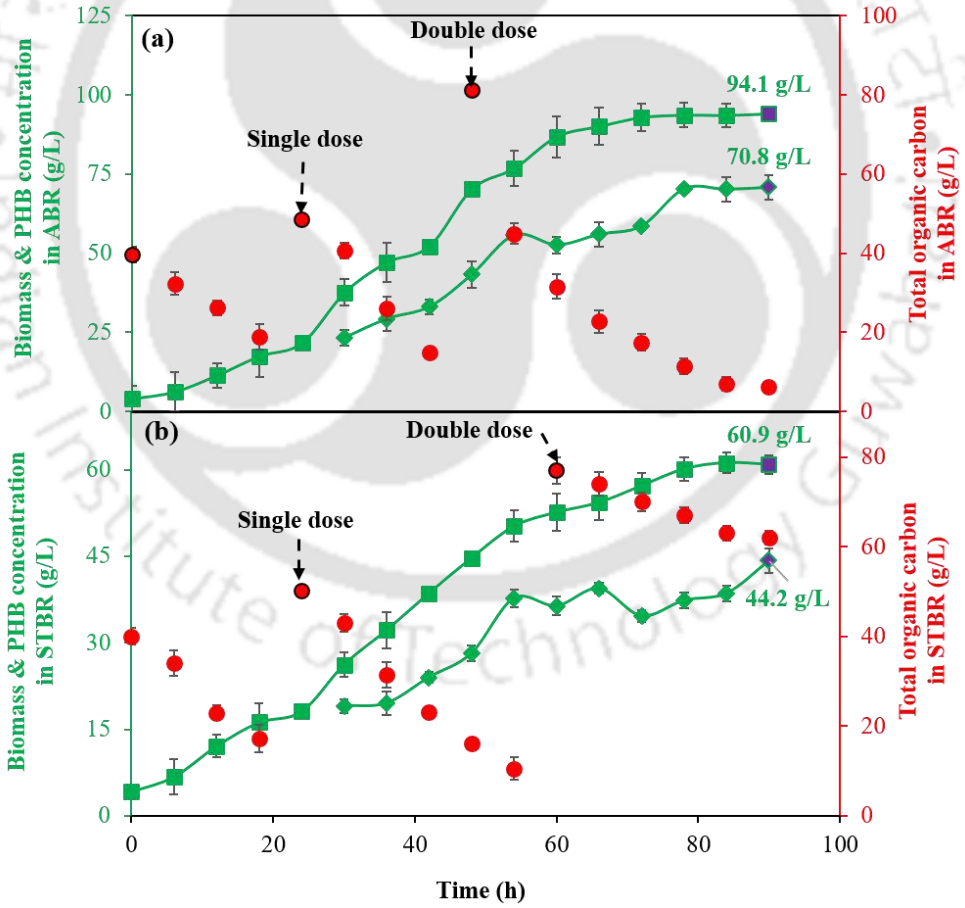

Fig. 3.10. Biomass and PHB and TOC profile in the fed-batch operated (a) ABR and (b) STBR. Biomass concentration (Square), PHB concentration (Diamond) and TOC concentration (Circle)

Comparison of the results obtained in this work with the literature data clearly revealed that the biomass (94.1 g/L) and PHB (70.8 g/L) production observed in the present study was substantially high. The least biomass (8.3 g/L) and PHB (4.33 g/L) concentration obtained by Anusha et al. (2016) is probably because of their use of real-time reaction biocalorimeter (BioRC1e) as a tool to understand the oxygen utilization rate and metabolic heat generation. Stirred tank bioreactor fed with waste glycerol was also reported to yield high biomass (82.5 g/L) and PHB (51.15 g/L) concentration (Cavalheiro et al., 2009). However, the values cannot be attributed to the performance of STBR, but due to the glycerol used, which is the most preferred substrate for biomass and PHB production by *Cupriavidus necator* (Balakrishna Pillai et al., 2018; Cavalheiro et al., 2009; Hu et al., 2013; Kalaiyezhini and Ramachandran, 2015).

The biomass and PHB production values with the ABR operated at batch mode were at least two times higher than the values obtained using an airlift reactor. Thus, the ABR with a wide annular gap is found to perform excellently in delivering air into the bioreactor by imparting Taylor and Couette flow, which enhanced biomass and PHB production by *R. eutropha*. However, an extraordinary performance of a membrane bioreactor for biomass (148 g/L) and PHB (112.8g/L) production can be attributed to the inherent cell retention and continuous media transfer nature of the membrane in the bioreactor, which is possible even with the present ABR (Haas et al., 2017). And this aspect could be studied using the current ABR with membrane for achieving even high biomass and PHB production. Furthermore, kinetic models development for continuous monitoring and control of ABR will yield enhanced biomass and PHB production.

3.3.5. Characterization of PHB

PHB extracted from the present study was characterized employing different techniques, and its properties were compared with that of a commercially available pure PHB. Fig.

3.11(a) compares the TGA/DSC results of the PHB from this study with that of the pure PHB. TGA plots for both the PHB follow a single step degradation at 284 ^{o}C, which is due to the cleavage of ester bonds in the polyhydroxybutyric acid to form crotonic acid. The maximum degradation temperature (T_{max} = 279.9 ^{o}C) and melting temperature (T_m = 172 ^{o}C) of the PHB obtained in this study were found to match closely with the T_{max} (279.4 ^{o}C) and T_m (174.4 ^{o}C) value of the pure PHB. Thermal properties of the PHB also matched well with the literature reports (Pradhan et al., 2017; Saratale and Oh, 2015). Fig. 3.11(b) compares the FTIR spectra of the PHB obtained with that of the pure PHB. It can be clearly seen that a sharp carbonyl peak was observed at 1740 cm^{-1} on both the PHBs, which is attributed to the C=O bond in the ester group (–COOR) of the biopolyester products.Doublet peaks observed at 2978 cm^{-1} on both the PHBs can be attributed to the presence of C-H functional group. Furthermore, the peak observed around 1278 cm^{-1} was due to the C-O-C elongation found in the backbone of the PHB. These results match with those reported in the literature on PHBs (Pradhan et al., 2017; Saratale and Oh, 2015; Saratale et al., 2019). Fig. 3.11(c) compares the XRD profiles of the PHB extracted in the present study with that of the pure PHB. Four major peaks predominantly found with both the PHBs are at the 2 theta values of 13.3^{o}, 16.8 ^{o}, 25.4^{o} and 28.5^{o}, which correspond to the planes of the crystal lattices (0 2 0), (1 1 0), (1 1 1) and (1 3 0), respectively (Díez-Pascual and Díez-Vicente, 2014; Pradhan et al., 2017). Furthermore, the well-defined crystalline peaks due to the PHB produced in this study reveals its crystalline nature. NMR results depicted in Fig. 311(d) compare the proton NMR spectrum of the PHB extracted from the present study with that of the pure PHB. In this time, the peaks observed at 7.26 and 0 ppm were considered as the reference peak for the NMR analysis, as the peaks are attributed to the presence of deuterated chloroform ($CDCl_3$) and tetramethylsilane (TMS), respectively. Characteristic PHB peaks observed at 1.26 ppm, 2.50 ppm and 5.24 ppm are attributed to

the presence of $–CH_3$, $-CH_2$ and –CH in the PHB polymeric chains (Kai et al., 2018; Pradhan et al., 2017).

3.4. Summary

The annular bioreactor (ABR) with wide annular gap has shown excellent hydrodynamic characteristics with the least mass transfer limitation for biomass and PHB production by *R. eutropha*. The Taylor and Couette flow pattern in the ABR proved beneficial for increasing the oxygen volumetric mass transfer coefficient (K_La). The ABR performance is much superior to the STBR operated under batch or Fed-batch modes. Even at high agitation and aeration rates, ABR did not impose any stress or damage to the cells in the reactor. Characterization results of the PHB clearly established its application potential akin to a pure PHB obtained commercially. The results obtained from this study demonstrate the utility of a wide gap annular bioreactor with Taylor and Couette flow for biotechnological applications.

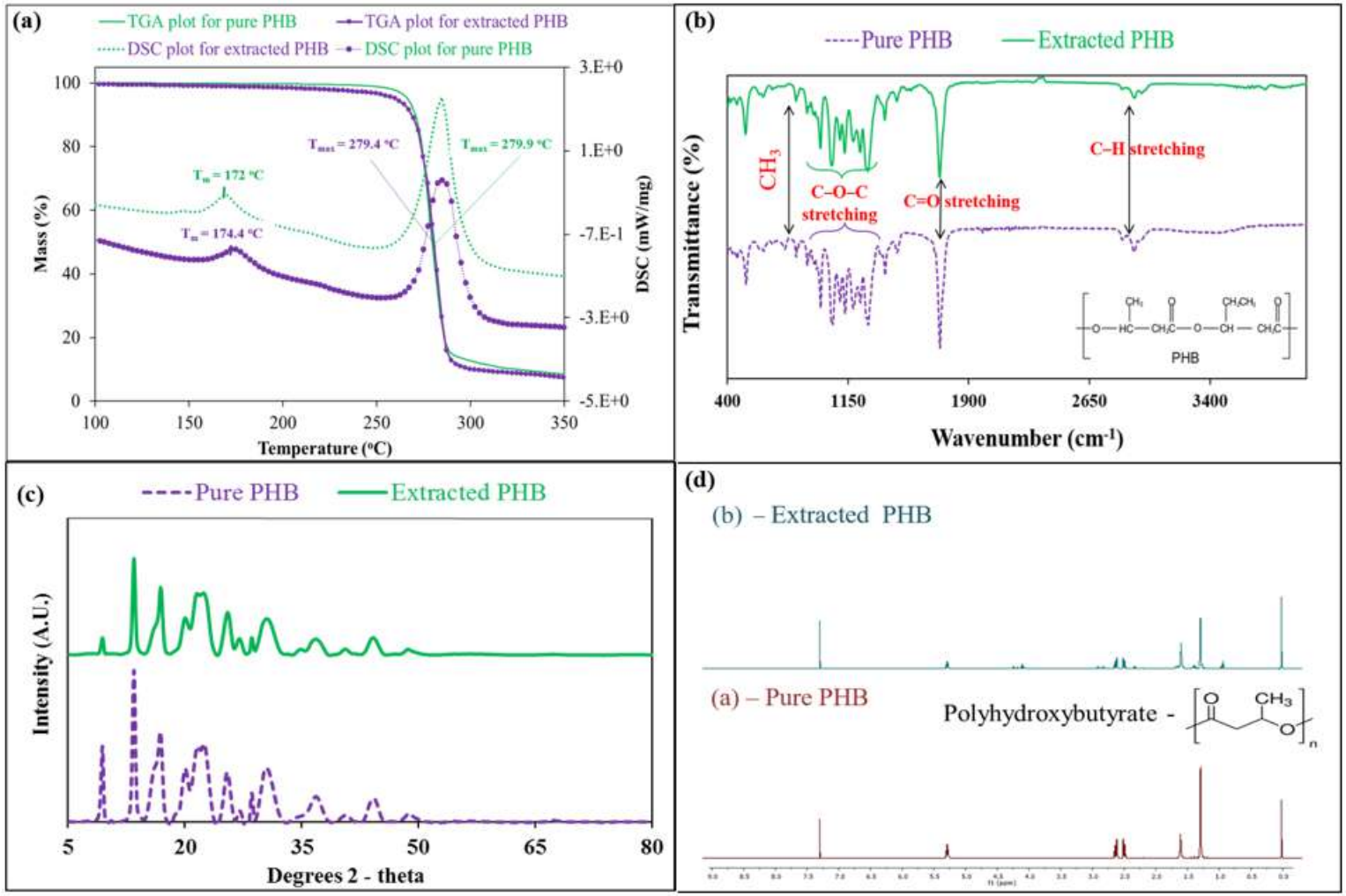

Fig. 3.11. Characterization results comparing the PHB extracted from the present study with that of the pure PHB: (a) TGA/DSC, (b) FTIR, (c) Powder XRD and (d) proton NMR analysis

Chapter 4

A novel ceramic membrane assembly for the separation of polyhydroxybutyrate (PHB) rich *Ralstonia eutropha* biomass from culture broth

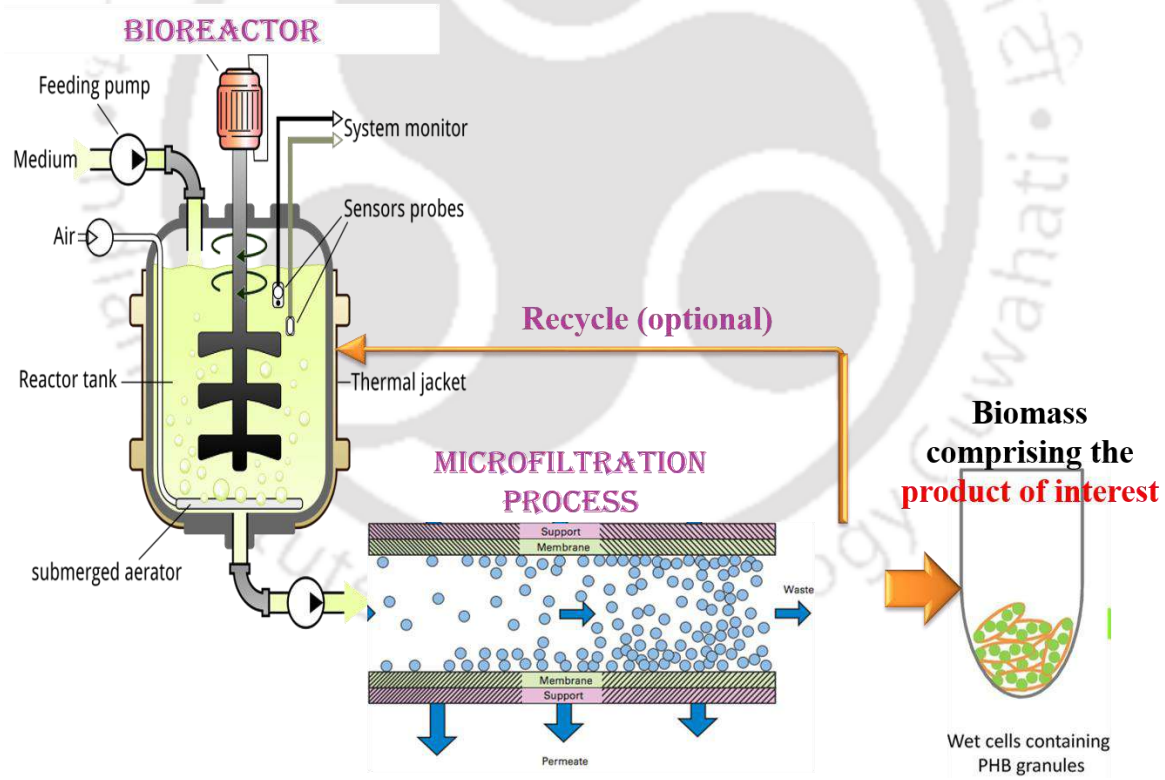

ABSTRACT

This chapter presents the investigation on the separation of polyhydroxybutyrate (PHB) containing *Ralstonia eutropha* cells from the culture broth using a novel ceramic-based tubular membrane assembly. The number of ceramic membranes in the assembly was raised from 1 to 4 and its performance was assessed by measuring the broth flux, biomass and PHB recovery as a function of applied pressure (49 - 196 kPa). The present ceramic membrane is found to be highly efficient (99.9%) in recovering the PHB from the culture broth. A maximum initial water flux of 444 $L/m^2 \cdot h$ and a permeate broth flux of 52 $L/m^2 \cdot h$ were observed at the maximum applied pressure (196 kPa) and with four number of ceramic membranes added to the membrane assembly. Both biomass and PHB recovery were observed to decrease with an increase in the applied pressure; on the contrary, a reduction in the applied pressure enhanced the biomass and PHB recovery, but it reduced the broth flux. However, both recovery and broth flux were enhanced by increasing the number of membranes in the membrane assembly. Further, an increase in the number of membranes resulted in a drastic reduction of the filtration resistance. Thus, the present study opens up a novel membrane-mediated separation process for the separation of intracellular product in the area of biotechnology.

4.1. Introduction

Polyhydroxybutyrate (PHB) is a green polymer, and unlike petroleum-based polymer, it is of natural origin, particularly from microorganisms (Raza et al., 2018). Properties of PHB are similar to that of petroleum-based plastics, and therefore it finds numerous applications in various industrial fields. Owing to its biodegradable, biocompatible, thermoplastic and nontoxic nature, it serves as the best alternative to the petroleum-derived polymers (Khanna and Srivastava, 2005; Raza et al., 2018). During fermentation and under nitrogen-limited conditions, the excess carbon source is converted to PHB by certain microorganisms. And these are stored as insoluble inclusion bodies in the cytoplasm of these microorganisms. Some microorganisms are capable of producing PHB, which includes *Ralstonia eutropha* and *Cupriavidus necator*. Fermentative PHB production is a two-stage process: with the individual growth and PHB accumulation inside as the first phase or upstream processing in PHB production. During the second phase or the downstream processing, the biomass produced during fermentation is separated from the culture broth and processed further to extract PHB out of it (Aramvash et al., 2015; Khanna and Srivastava, 2005; Raza et al., 2018). The initial separation of biomass from the culture broth during the downstream processing phase is very crucial for PHB production. This is mainly because the *R. eutropha*, a typical rod-shaped PHB producing bacteria, is small in size (0.4 x 0.7 μm), and it poses a significant problem during its separation. Furthermore, in relation to culture volume, the microbial biomass produced is very less. Consequently, a large volume of culture broth needs to be processed in order to recover the whole (intact) biomass from the broth (Elcik et al., 2016). In general, 20-30% of the total biomass production cost is utilized for the separation of biomass from the culture broth (Pragya et al., 2013).

In this scenario, membrane separation seems to be more attractive and suitable for industrial applications, particularly in the field of biotechnology (Piry et al., 2008; Pragya

et al., 2013; Roshanida et al., 2018; Vasanth et al., 2011). By integrating membrane with a bioreactor, separation of microbial biomass from culture broth can be carried out under batch or continuous mode based on the operation mode of the bioreactor. Microfiltration is generally employed for the separation of microorganisms from the liquid as the pore size of these membranes is in the range of 0.1 - 10 μm, which matches well with the size range of microorganisms (Piry et al., 2008; Vasanth et al., 2011). In microfiltration, cross-flow filtration is mostly preferred, because the flow in this mode is parallel to the membrane and perpendicular to the permeate, thereby reducing the membrane fouling (Piry et al., 2008). Membrane filtration offers numerous advantages over the conventional separation processes, such as sedimentation, filtration, flocculation-flotation and centrifugation processes. Some of these advantages are isothermal operation, zero addition of chemical agents. Furthermore, the microfiltration process is regarded as safe for shear-sensitive bacterial cells with intracellular products (Kumar et al., 2016; Piry et al., 2012; Pragya et al., 2013). Membrane separation is also relatively cheaper in comparison with centrifugation. This is because the major cost, including capital cost, operation and maintenance cost and depreciation cost, associated with centrifugation is reduced in cross-flow microfiltration just with membrane replacement and pumping cost (Barros et al., 2015; Pragya et al., 2013; Zhao et al., 2017). This has led to great interest among researchers and industrialists to develop a novel low cost as well as porous ceramic membranes exhibiting good filtration performance with excellent chemical and thermal stability, good mechanical strength and extended period of use without any environment pollution (Issaoui et al., 2017). Most of the research is focused on the development of ceramic membranes with starting material such as alumina, titania, silicon carbide, cordierite, and zirconia. However, the cost of these starting materials is very high, which increases the final cost of the prepared membranes (Issaoui et al., 2017; Medjemem et al., 2016; Vinoth Kumar et al.,

2015). In order to address the cost aspect, recent research interest is to explore low-cost starting materials for membrane preparation and its performance evaluation (Issaoui et al., 2017). Some of these materials include natural raw clay, dolomite, apatite powder, bauxite, and kaolin (Issaoui et al., 2017). Among these starting materials, kaolin seems to be a cost-effective and suitable material that is available abundantly in the earth (Emani et al., 2014; Issaoui et al., 2017; Vasanth et al., 2011; Vinoth Kumar et al., 2015). Previously, ceramic membrane prepared using a mixture of kaolin, feldspar, pyrophyllite, quartz, ball clay, and calcium carbonate was reported with an estimated cost of 69 $\$/m^2$ (Vinoth Kumar et al., 2015). Therefore, this study was focused on the application of the low-cost ceramic membrane for bioseparation of PHB rich biomass from the culture broth. This is mainly because an increase in membrane resistance due to fouling is a serious issue with membrane separation processes. Several studies have been carried out in the literature to address this problem by either varying the pore size and porosity of such membranes (Dizge et al., 2011; Pragya et al., 2013), or changing the pore shape/geometry from circular to rectangular pore (Bromley et al., 2002), or the length of the membrane (Piry et al., 2012, 2008). In the present study, water and broth flux along with the biomass and PHB recovery were examined using single, double and four membrane assembly as a function of applied pressure. To the best of our knowledge there is no previous literature available on application of ceramic membranes for PHB recovery and there is no study is reported on enhancing the flux by increasing the number of membranes using a modified membrane assembly. Therefore, this is the first study which reported the application of ceramic membranes for biomass and PHB recovery from the culture broth in a novel tubular ceramic membrane assembly. Furthermore, the resistance due to membrane was overcome without any change in pore size or pore geometry or length of the membrane, but with a change in the number of membranes.

4.2. Materials and methods

4.2.1. Materials

The starting materials used for the fabrication of ceramic membrane are kaolin [$Al_2Si_2O_5(OH)_4$], quartz (SiO_2), ball clay ($3SiO_2Al_2O_3$), pyrophyllite [$Al_2(Si_2O_5)_2(OH)_2$], calcium carbonate ($CaCO_3$) and feldspar (Na, Ca)($AlSiO_8$). All these materials were procured locally from Kanpur, India (26.4499° N, 80.3319° E). The chemicals used for *R. eutropha* culture growth are as follows: calcium chloride ($CaCl_2$), magnesium sulphate heptahydrate ($MgSO_4 \cdot 7H_2O$), di-sodium hydrogen phosphate (Na_2HPO_4), potassium dihydrogen phosphate (KH_2PO_4), yeast extract, ferrous sulfate heptahydrate ($FeSO_4 \cdot 7H_2O$), ammonium molybdate tetrahydrate ($(NH_4)_6Mo_7O_{24} \cdot 4H_2O$), boric acid ($H_3BO_3$) and zinc sulphate heptahydrate ($ZnSO_4 \cdot 7H_2O$). All these chemicals used were obtained from either Himedia®, India or Merck®, India. Hydrochloric acid and sodium hydroxide used for pH maintenance were purchased from Merck®, India. Pure PHB, which was used as a standard for PHB estimation, was procured from Sigma-Aldrich®, India. Carob pods used for the preparation of carob extract was acquired locally from IIT Guwahati, India. Methanol used for lignin extraction was obtained from Merck®, India.

4.2.2. *R. eutropha* culture growth

The culture broth used for the microfiltration was obtained as a result of the fermentation process carried out using *R. eutropha*. The microbial strain was purchased from Microbial type culture collection (MTCC), Chandigarh. The culture was grown in a medium containing carob pod extract as the cheap carbon source. A slightly modified procedure, as reported by Carvalho et al. (2014), was followed in the present study for preparing the carob pod extract. Dried carob fruits acquired locally from IIT Guwahati were soaked overnight in methanol to solubilize lignin present in the units. The delignified carob pods were then dehulled to remove seeds and the pods were subsequently washed thoroughly

with tap water followed by drying at 60 ˚C until a constant weight is attained. The dried carob units were powdered and suspended in distilled water at a solid/liquid ratio of 1:10 (w/v) and agitated at 28 ˚C in a rotating orbital shaker at 200 rpm for 1 h. The carob pod extract was then filtered using muslin cloth, and filtrate containing sugars were stored at 4 ˚C for further use. The initial carbon concentration measured as total organic carbon concentration and was found to be 20 g/L; whereas the initial nitrogen concentration was maintained at 4 g/L by the addition of Urea.

In addition to the above major nutrients, the following minor nutrients in the form mineral salt medium (MSM) as mentioned in Khanna and Srivastava (2007) was added to the carob extract: 20 mg/L $CaCl_2$, 0.2 g/L $MgSO_4 \cdot 7H_2O$, 0.6 g/L Na_2HPO_4, 2.0 g/L KH_2PO_4, 10 ml/L trace metal solution, 0.1 g/L yeast extract. The trace metal solution comprised of 0.2 mg/L $FeSO_4 \cdot 7H_2O$, 0.6 mg/L $(NH_4)_6Mo_7O_{24} \cdot 4H_2O$, 0.6 mg/L H_3BO_3 and 1.3 mg/L $ZnSO_4 \cdot 7H_2O$. The culture was grown in a stirred tank bioreactor with a working volume of 1.5 L and sparged at 0.8 vvm with an agitation rate of 250 rpm (Carvalho et al., 2014). The pH of the solution was maintained at 7.0 by the addition of 0.1 N HCl or NaOH. For all the experiments, 10% (v/v) of inoculum was provided for the biomass production. The biomass growth was monitored by measuring the biomass concentration at every 12 h interval. At the end of 60 h, the biomass was harvested and the final concentration was observed to be around 11.2 g/L. Substrate uptake by *R. eutropha* cells was measured in terms of total organic carbon (TOC) using a TOC analyzer (model no. 1030, O-I-Analytical, Aurora, USA). The intracellular structure of *R. eutropha* during its growth and various samples like retentate and permeate from the microfiltration system was visualized using the Field emission transmission electron microscopy (FETEM) (JEM- 2100F, JEOL, USA). For this FETEM analysis, a small drop of samples is placed on a carbon coated copper grid and allowed to dry overnight under ambient atmospheric conditions. The size

distribution analysis of *R. eutropha* cells was carried out using a particle size analyzer (Delsa nanoparticle analyzer, Beckman Coulter, Nyon, Switzerland).

4.2.3. Membrane preparation

The membrane used in this study was prepared as per the method reported in our previous work (Vinoth Kumar et al., 2015). The locally available low-cost material such as kaolin (15 wt%), ball clay (18 wt%), quartz (28 wt%), feldspar (6 wt%), pyrophyllite (15 wt%), and calcium carbonate (18 wt%) were used for the fabrication. The aforementioned materials were mixed with Millipore water so as to make a paste of uniform mixture; finally, the paste was packed in an extruder to draw ceramic tube having an inner diameter of 5.5 mm and an external diameter of 11.5 mm. The drawn tubes were dried in the open air for 12 h. These tubes were further oven-dried at 100 °C and 200 °C for a time period of 12 h each. Thereafter, the ceramic tubes were sintered for 6 h in a box furnace at 950 °C. The properties of the tubular ceramic membrane are as follows: 3 mm thickness, 0.309 µm average pore diameter, 53% porosity, 12 MPa mechanical strength, 3.8×10^{-3} m^2 area and 2.2 $L/m^2 \cdot h \cdot kPa$ pure water permeability (Vinoth Kumar et al., 2015).

4.2.4. Experimental setup and analytical techniques

Experimental setup for bioseparation of PHB rich biomass from the culture broth consisted of the fabricated tubular membranes with the aforementioned properties. Fig. 4.1 shows a schematic and actual cross-flow setup used in the present study. The number of membranes in the cartridges was varied from 1 to 4, as shown in Fig. 4.1. In order to study the effect of applied pressure on the flux and recovery, the applied pressure was varied from 49 to 196 kPa by controlling valves situated on both sides of the membrane assembly. A constant cross flow velocity of 20 L/h and ambient room temperature of 28 ± 2°C was maintained for all the experiments.

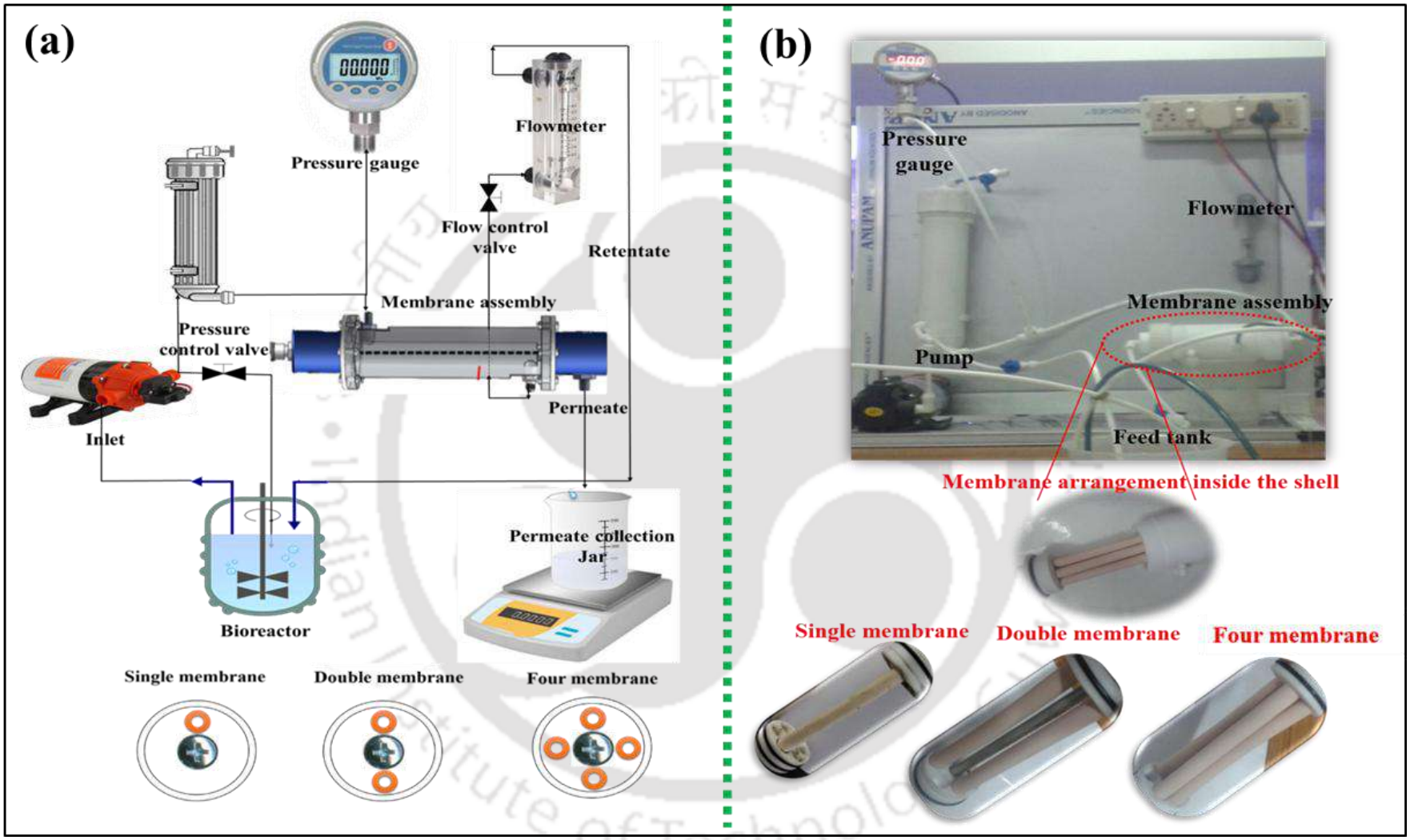

Fig. 4.1 (a) Schematic and (b) real image of cross flow microfiltration system

The cross-flow velocity (CFV) and applied pressure values chosen in the present study are in the microfiltration range as reported in the literature (Vasanth et al., 2011; Vinoth Kumar et al., 2015). Initially, pure water was permeated in the outer side of the membrane and the permeate was drawn from the inner side of the membrane to calculate the permeate flow rate and water flux. Likewise, the broth flux was measured by pumping the culture broth obtained from the bioreactor. Permeate collected through the membranes was weighed using a weighing balance for flowrate and flux calculation. The water and broth flux (J) were calculated by measuring permeate volume collected per unit time per unit membrane area according to equation 4.1 and 4.2 for pure water and broth, respectively (Kumar et al., 2016; Vasanth et al., 2011; Vinoth Kumar et al., 2015):

$$J_W = \frac{Q_W}{A \times t} \quad (4.1)$$

$$J_b = \frac{Q_b}{A \times t} \quad (4.2)$$

Where, J_W is water flux ($L/m^2 \cdot h$), Q_W is permeated water volume (L), J_b is broth flux ($L/m^2.h$), Q_b is permeated broth volume (L), A is the outer surface area of the membrane (m^2) and t is the filtration time (h).

All filtration experiments were carried out for 30 min. For each experiment, permeate samples were collected every 3 min and analyzed for biomass and PHB concentration. At the end of each experiment, the membrane was backwashed at a higher pressure of 400 kPa to restore its orginal flux value. The surface characteristics of raw/unused and fouled/used membranes were analyzed by Field emission scanning electron microscopy (FESEM) (Sigma, Zeiss, Germany). Prior to FESEM analysis, the samples were mounted on a double sided carbon tape and sputtered with a thin layer of gold. The biomass and PHB concentration in the feed and permeate solution were estimated

according to the process described in chapter 2 and section 2.2.5. as per the literature reports (Aramvash et al., 2015; Khanna and Srivastava, 2005). The analysis was carried out in triplicate and error bars denote mean ± standard deviation. Biomass and PHB recovery in the study were calculated using the following equations (4.3 and 4.4):

$$\text{Biomass recovery efficiency}\,(\%) = \frac{C_{ib} - C_{pb}}{C_{ib}} \times 100 \qquad (4.3)$$

$$\text{PHB recovery efficiency}\,(\%) = \frac{C_{iP} - C_{pP}}{C_{iP}} \times 100 \qquad (4.4)$$

Where, C_{ib} - initial biomass concentration (g/L), C_{pb} - permeate biomass concentration (g/L), C_{iP} - initial PHB concentration (g/L) and C_{pP} - permeate PHB concentration (g/L).

4.2.5. Calculation of filtration resistance

For determining the membrane resistance (R_M) and total resistance (R_T) during the separation of *R. eutropha* cells from the culture broth, the following equations (4.5 and 4.6) were used.

$$R_T = \frac{\Delta P}{\eta_b \times J_b} \qquad (4.5)$$

$$R_M = \frac{\Delta P}{\eta_w \times J_w} \qquad (4.6)$$

As total resistance (R_T) is the sum of membrane resistance (R_M) and filtration resistance (R_F). The filtration resistance (R_F) is given by the following equation (Eq. 4.7) (Piry et al., 2012, 2008):

$$R_F = R_T - R_M \qquad (4.7)$$

Where, R_T (m^{-1}), R_M (m^{-1}) and R_F (m^{-1}) are total resistance, membrane resistance, and filtration resistance, respectively; η_w (Pa s) and η_b (Pa s) are water and broth viscosity, ΔP (Pa) is applied pressure.

The viscosity of water and culture broth at 28 °C was found to be 8.3×10^{-4} Pa s and 8.8×10^{-4} Pa s, respectively, as measured by using a rheometer (Physica MCR 301 rheometer; Anton Paar, Europe). In actual terms, filtration resistance is the summary of resistance due to membrane fouling and other boundary variation in the membrane. A detailed study on the variation in the membrane boundaries during the microfiltration is outside the scope of the present study.

4.3. Results and Discussion

4.3.1. *R. eutropha* growth and biomass size distribution analysis

Fig. 4.2 shows typical growth and substrate utilization profile of *R. eutropha* for PHB production using a stirred tank bioreactor. The *R. eutropha* biomass reached a maximum concentration of 11.2 g/L at the end of 60 h of the batch experiment. Since the substrate - carob pod extract used in the study comprises three sugars, namely sucrose, glucose and fructose, a triauxic biomass growth and substrate utilization pattern are observed. The FETEM images provided as an inset into Fig. 4.2 clearly exhibits that the PHB granules were formed towards the end of the growth phase. Fig. 4.3(a) shows the size distribution of *R. eutropha* cells in the feed, permeate and the retentate.

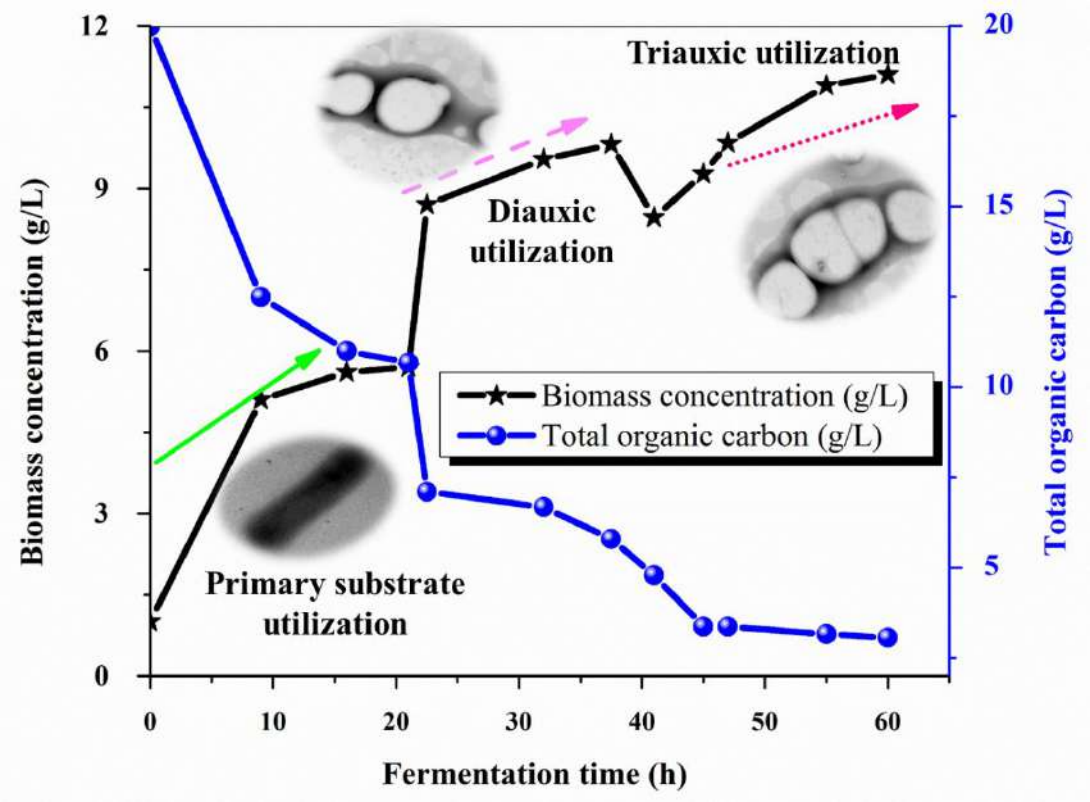

Fig. 4.2. *R. eutropha* growth and substrate utilization profile in the fermentation process (Inset - FETEM image shows the production of PHB granules inside the *R. eutropha* biomass)

Analysis of the size distribution of *R. eutropha* biomass clearly demonstrated that the size of *R. eutropha* cells in the feed is in the range of 0.3 - 0.7 µm. The majority of *R. eutropha* cells were around 0.5 µm size, which relates to the actual size of the *R. eutropha*. The lower size range observed is partly due to the lateral dimension of *R. eutropha*, which is 0.3 µm and partly due to immature cells in the feed. As the majority of the *R. eutropha* cells size is greater than the pore size (0.3 µm) of the membrane used in this study, only a small amount of the *R. eutropha* cells could pass through the membrane, which is confirmed from the biomass size distribution profile observed in the permeate stream. Moreover, the size of the *R. eutropha* cells in the permeate stream was even more reduced, which can be attributed to the presence of disrupted *R. eutropha* cells in the permeate stream. A slightly high size range of the cells observed in the permeate stream is due to the

presence of immature and deformed cells. The FETEM images of the biomass present in the permeate and retentate streams are shown in Fig. 4.3(b-c) and 4.3(d), respectively. These FETEM results reveal the presence of disrupted, deformed and immature cells in the permeate. In contrast, the membrane fully retained the completely grown *R. eutropha* cells containing PHB granules.

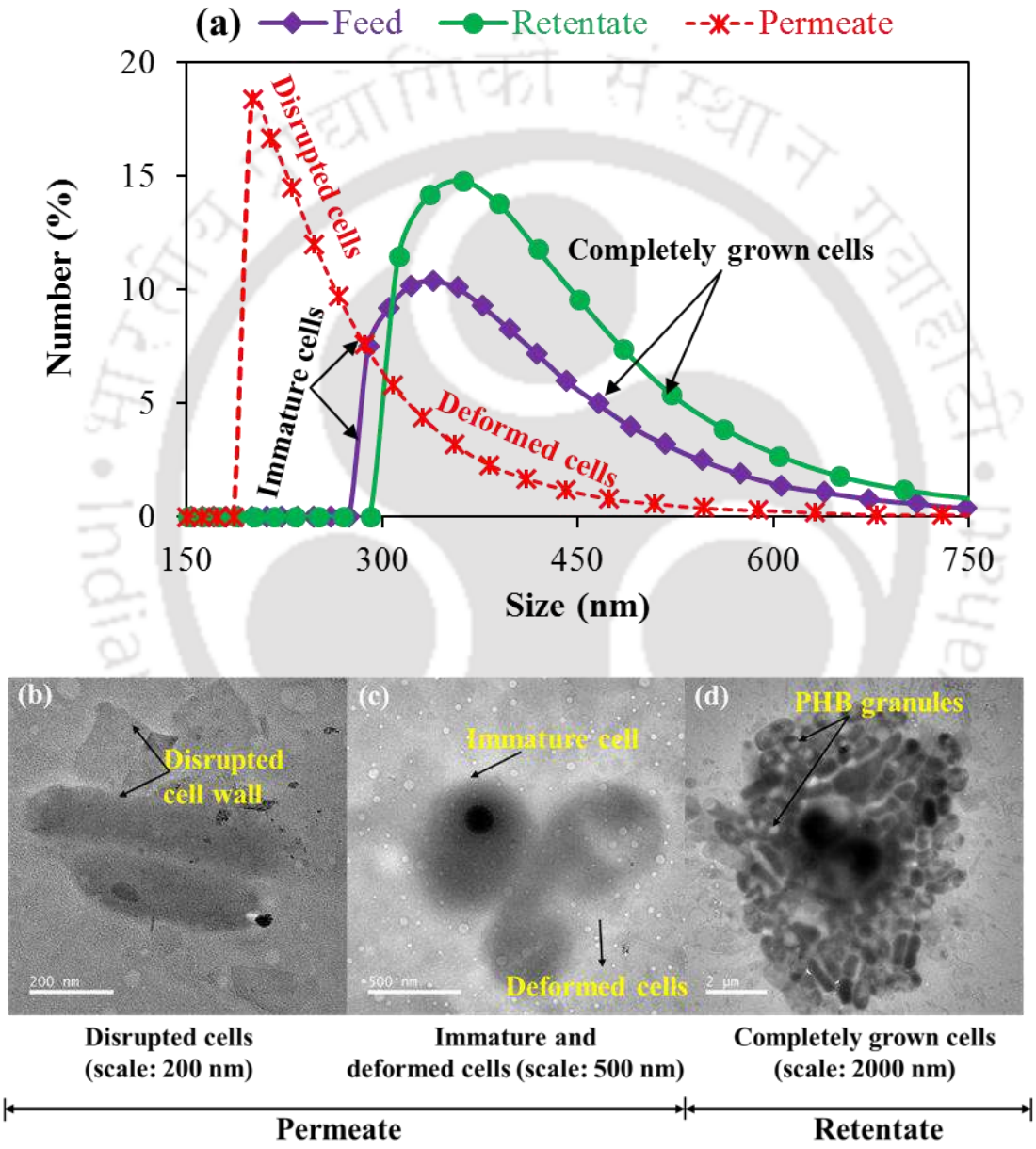

Fig. 4.3. (a) Size distribution analysis of various samples obtained from the microfiltration system and (b - d) FETEM images of various samples obtained from the microfiltration system

4.3.2. FESEM analysis

Field emission scanning electron microscopy (FESEM) technique is a well-known technique for examining the surface characteristics of membranes (Helling et al., 2017). Fig. 4.4 shows FESEM images of the raw and fouled membrane. Surface images of the fouled membrane with bacterial cells on the feed side/outer surface as well as that on the permeate side/inner surface at two different magnifications (10 and 25 KX) are also presented in Fig. 4.4. A clear difference in surface morphology of the raw and fouled membranes are observed from these images. In the case of fouled membrane, the membrane surface is clogged with a bed of bacteria, as clearly evidenced in Fig. 4.4 (c and e). The figure also clearly reveals that large or completely grown *R. eutropha* biomass of size 0.4×0.7 μm is sieved by the ceramic membrane with a pore diameter of 0.3 μm. Whereas the feed side of the membrane is covered by a bed of bacteria and very few bacteria are found on the inner side of the membrane (Fig. 4.4 (d and f)). The bacteria passing through the membrane were also smaller than the pore diameter of the ceramic membrane. From these observations, it could be concluded that only completely grown *R. eutropha* cells comprising of PHB granules were retained by the membrane, whereas the immature cells devoid of PHB were quickly passed through the membrane. These results were further confirmed by the analysis of biomass and PHB recovery, as detailed in a later section. Moreover, the deposition of bacteria as a bed on the surface of the membrane mainly resulted in the fast decline of flux through the membrane.

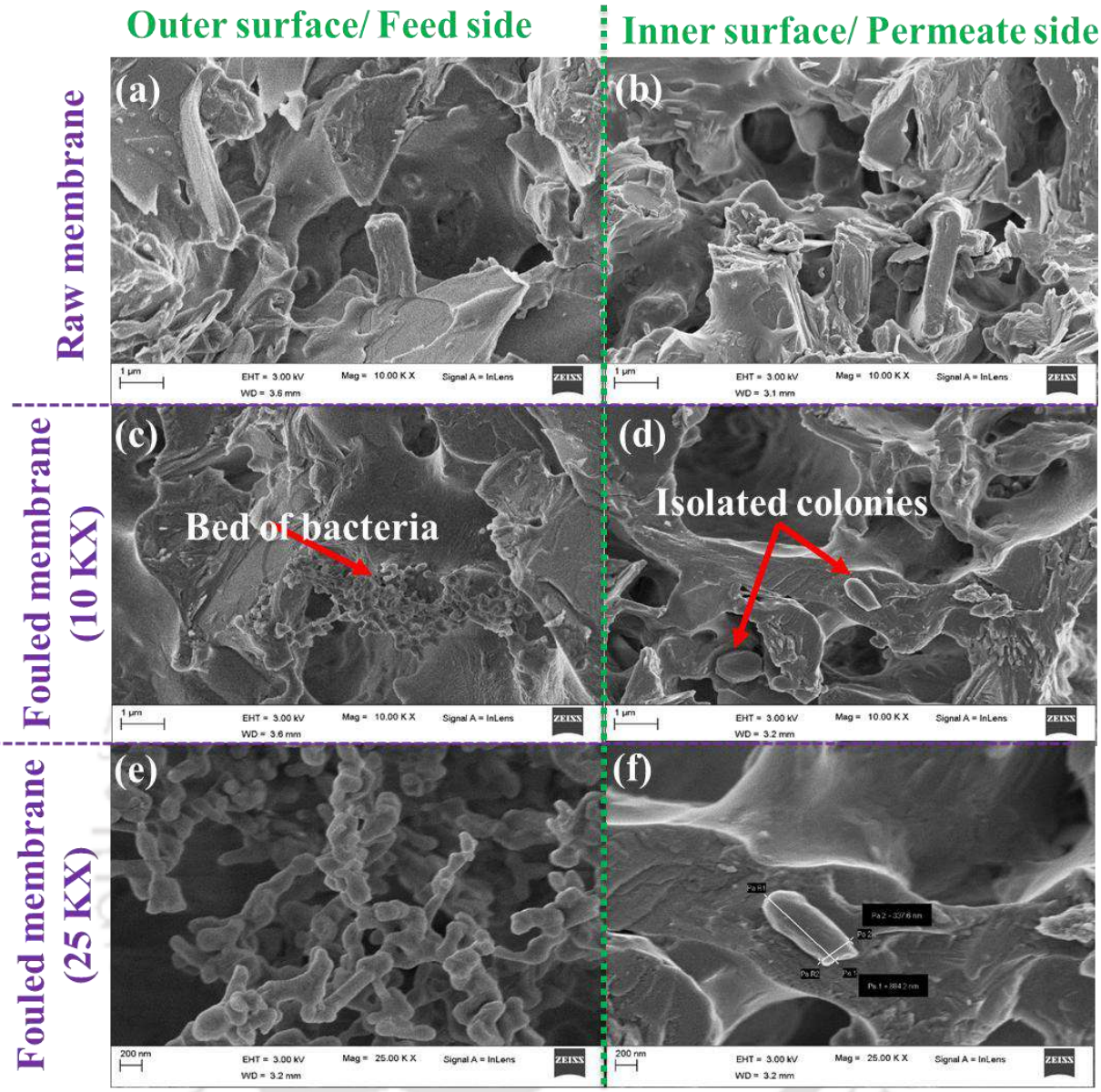

Fig. 4.4. FESEM images of (a - b) outer and inner surface of raw membrane, (c - d) outer and inner surface of fouled membrane at 10 KX magnification and (e - f) outer and inner surface of fouled membrane at 25 KX magnification

4.3.3. Permeate water flowrate and water flux analysis

Performance of any membrane based separation is evaluated by passing pure water and finding its permeability, which determined the membrane's ability to process solution. A large value of membrane permeability indicated very good capacity and throughput of the membrane. Before carrying out the actual experiment on permeability assessment of the

membrane in this study, fresh membranes were compacted by passing pure water at a pressure higher than usually applied in the separation experiments. This was carried out to cleanse the membrane from any adhered/clogged particles in the pores of the membrane.

Following compaction of membrane, the membrane was operated under the selected operating pressure until a steady permeate flow rate was achieved. Fig. 4.5(a) shows an increase in the permeate flowrate along with an increase in the applied pressure for all the three different membrane assemblies. The permeate flowrate also increased with an increase in the number of membranes in the membrane assembly. In the single membrane assembly, the permeate water flow rate increased from 0.42 to 1.68 L/h with an increase in the applied pressure from 49 to 196 kPa, respectively. Similarly, a two-fold and four-fold increase in the permeate water flow rate were observed with the double and four membrane assemblies, respectively. Furthermore, as reported by Helling et al. (2017), an excellent fit observed between the permeate flow rate and applied pressure across all the membrane assemblies in the present study clearly reveals a steady performance of the membrane over the entire range of applied pressures. Besides, the straight-line fit clearly demonstrates that the pore size or pore structure and porosity of the membranes remain unchanged with an increase in the applied pressure.

Fig. 4.5(b) shows the pure water flux of various membranes assemblies with respect to the different applied pressures. In line with Darcy's law, pure water flux increased steadily with increasing applied pressure (Mirbagheri et al., 2015). The pure water flux values are 110, 216, 327, and 441 $L/m^2 \cdot h$ for the applied pressure values of 49, 98, 147 and 196 kPa, respectively. However, the pure water flux remains almost unaltered for the different membrane assemblies studied over the various applied pressures. This is due to the fact that the flux is calculated for a unit membrane area.

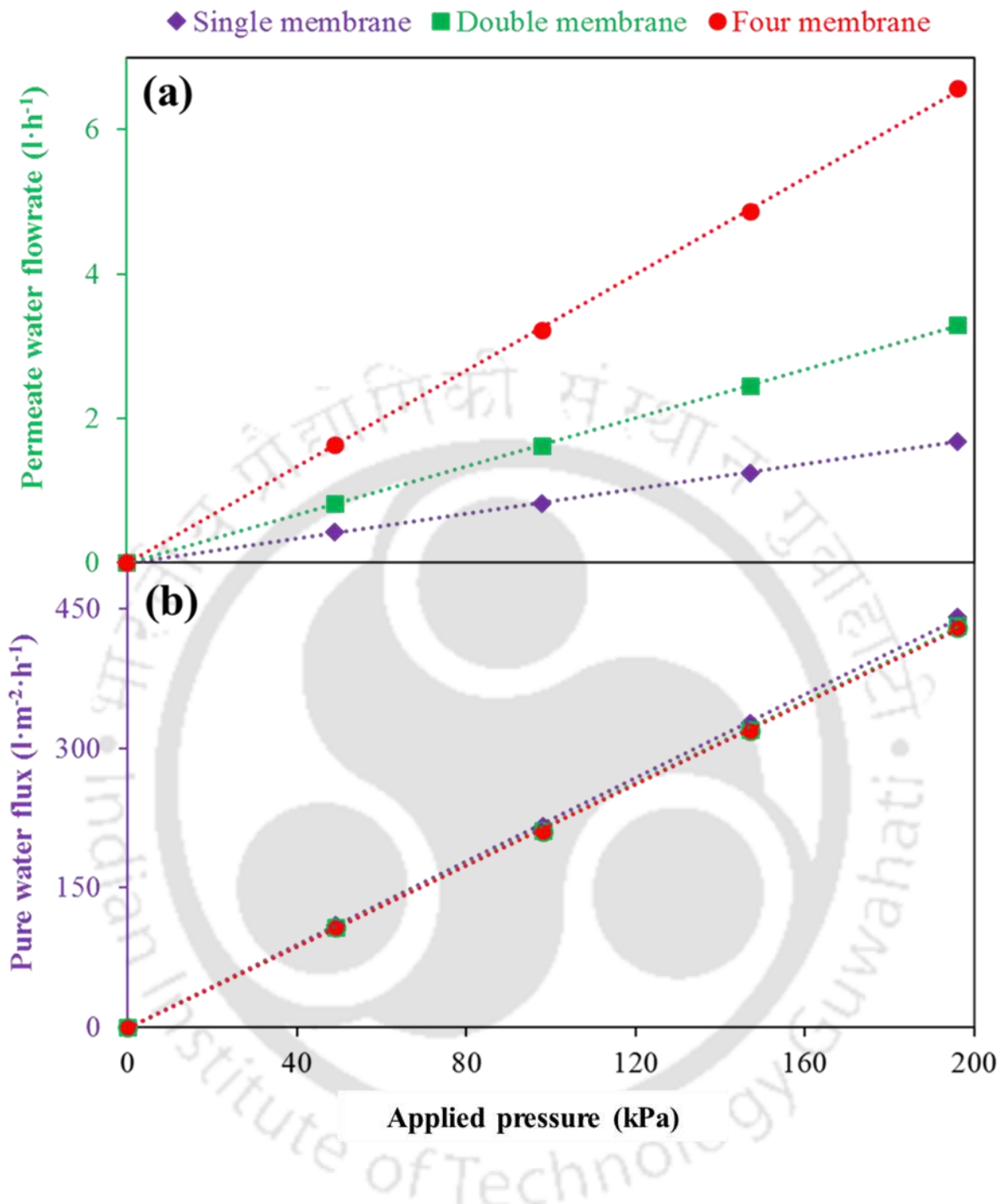

Fig. 4.5. (a) Permeate water flow rate and (b) water flux versus applied pressures for three different membrane assemblies

4.3.4. Effect of applied pressure on broth flux

Fig. 4.6 shows the effect of applied pressure in cross-flow microfiltration of broth flux using different (single, double and four) membrane assemblies. As mentioned earlier, the cross-flow velocity was maintained constant at 20 L/h. At the beginning of the

microfiltration experiments, the broth flux reduced drastically due to blockage of pore due to deposition of *R. eutropha* cells on the membrane surface by adsorption. The formation of a fouled layer on the membrane surface lasted for the initial fifteen minutes of the filtration experiment. After which, the flux decreases further due to compression of the fouled layer on the membrane surface. Following 25 min of filtration, the decline in flux rate was very less and it remained the same towards the end of the filtration experiment. This trend in flux decline was the same with all the four different applied pressures and the three different membrane assemblies investigated in the present study. This reduced flux decline at the end of the microfiltration experiment can be attributed to the high tangential/lift force acting on *R. eutropha* cells due to the cross-flow filtration operation. At this stage, the magnitude of the friction forces which is making *R. eutropha* cells to deposit on the membrane surface is greatly reduced and the tangential force carries the *R. eutropha* cells to the retentate (Fraga et al., 2017; Mukherjee et al., 2018; Vasanth et al., 2013).

Even though the trend in flux decline is found to be same, the broth flux at the end of 30 min is found to increase with an increase in the applied pressure. For instance, in the single membrane assembly, the final broth flux increased from 3.1 to 7.8 $L/m^2 \cdot h$ with an increase in the applied pressure from 49 to 196 kPa. A similar increase in broth flux with an increase in the applied pressure is observed in case of the double and four membrane assemblies as well. The observed result complies with Darcy's law, which states that broth flux during filtration is proportional to the applied pressure. These results further suggest that the increased mass transfer resistance and reduced broth flux due to the adsorption of *R. eutropha* cells can be overcome by increasing the applied pressure.

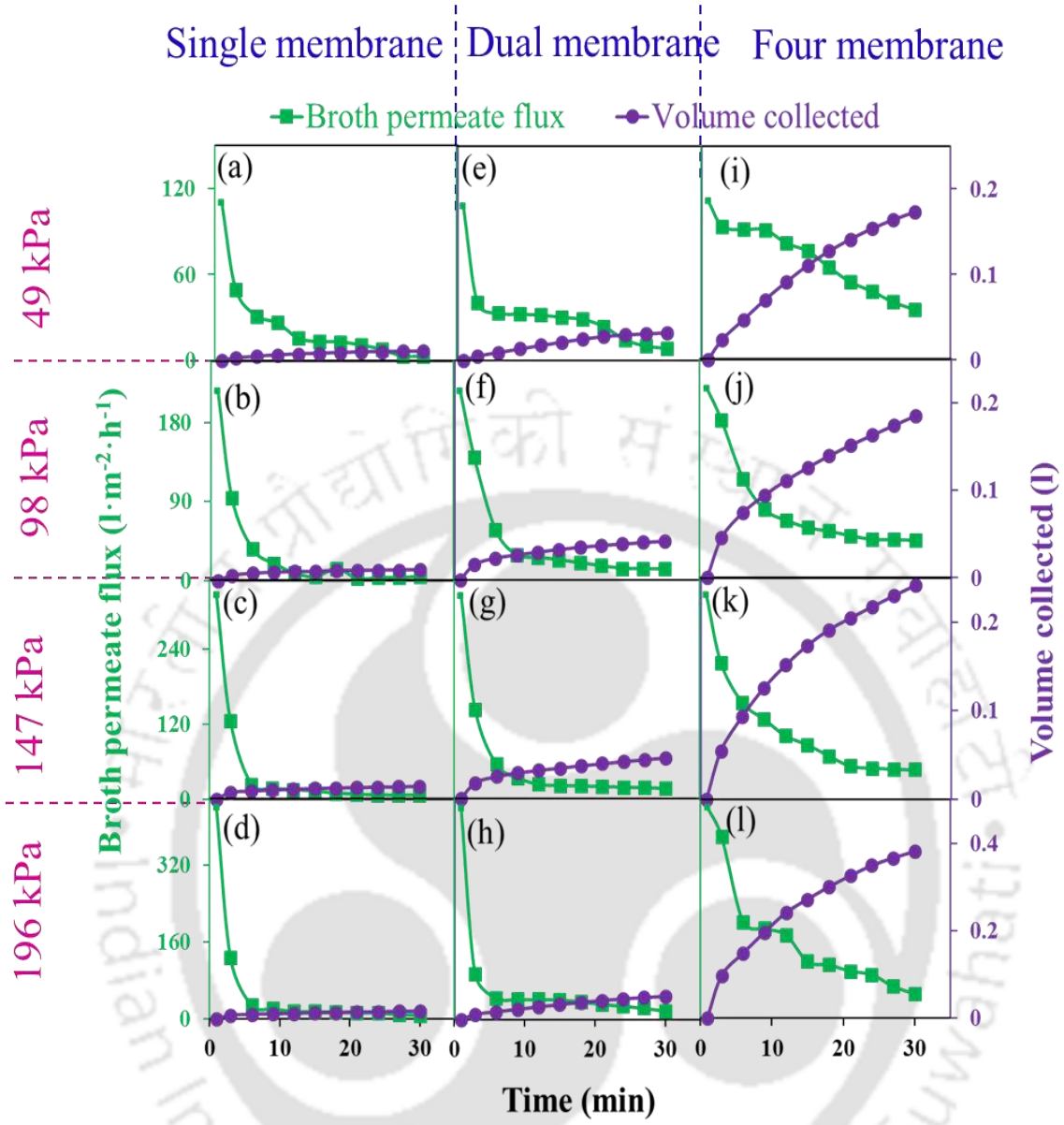

Fig. 4.6. Influence of applied pressure (49 -196 kPa) on broth flux: (a - d) single membrane assembly, (e - h) double membrane assembly and (i-l) four membrane assembly

Babel and Takizawa, (2010) reported a similar result of higher broth flux with increased applied pressure during microfiltration of suspension containing algal cells. The authors further suggested that an increase in broth flux with increasing applied pressure can be attributed to the compressible nature of the *Chlorella* cells investigated in the study. Similarly, Kim et al. (2007) in their study, attributed this to the compressible nature of organic matter considered for separation.- In contrast, a study by Hwang and Hsueh, (2003)

revealed a decrease in broth flux with an increase in the applied pressure and this reduced flux was attributed to the formation of incompressible and compact skin-like layer on top of the membrane surface, which changed the membrane to an asymmetric geometry having different characteristics. Hence, in the present study, an increase in the broth flux observed with increasing applied pressure is owing to the compressible nature of *R. eutropha* cells at high applied pressure. This also supported by the presence of a compressible extracellular matrix (ECM) on the surface of *R. eutropha* cells (Wang and Yu, 2007). Fig. 4.7(a) clearly depicts an increase in the cake concentration (Cc) with an increase in the applied pressure, which is due to a decrease in the filtration rate (calculated by taking the slope of broth flux Vs time) with an increase in the applied pressure. The low filtration rate and broth flux observed at a low applied pressure resulted in reduced deposition of *R. eutropha* cells. However, at a high applied pressure, *R. eutropha* cells deposited in larger quantities, layer by layer and as stated earlier, forming a highly compressed layer of cake. The resistance offered by the biomass cake was further examined and the results are reported in section 4.3.8.

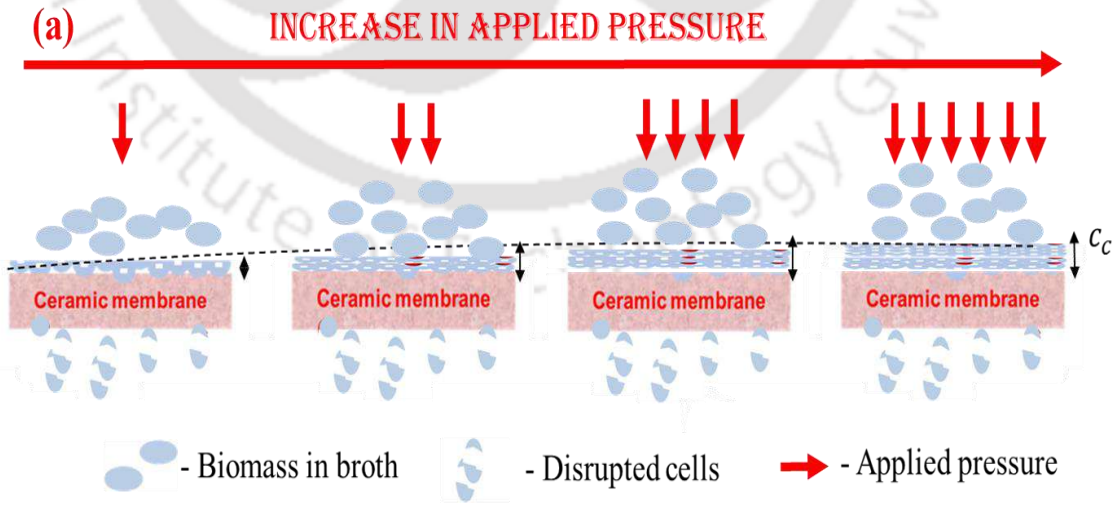

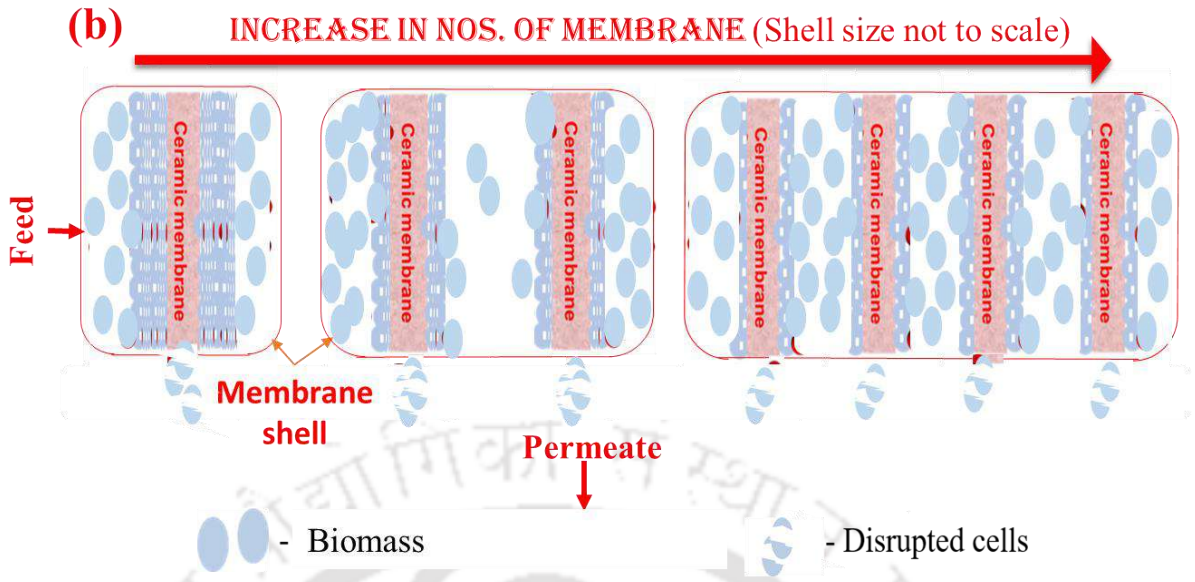

Fig. 4.7. Mechanism of membrane fouling as a function of (a) applied pressure and (b) number of membranes

4.3.5. Effect of number of membranes on the broth flux

To study the impact of number of membrane tubes in different membrane assemblies, experiments were carried out using the same experimental set up for a filtration time of 30 min and at a set cross-flow velocity of 20 L/h. Table 4.1 presents a comparison of initial and final broth flux values for each experimental run. The final broth flux in the single membrane assembly increased from 3.1 $L/m^2 \cdot h$ to 7.8 $L/m^2 \cdot h$ with an increase in the applied pressure from 49 to 196 kPa. In the double membrane assembly, the final broth flux varied from 8.3 $L/m^2 \cdot h$ to 18.4 $L/m^2 \cdot h$ for an applied pressure of 49 to 196 kPa, respectively. In case of the four membrane assembly, the final broth flux varied from 35.7 $L/m^2 \cdot h$ to 52 $L/m^2 \cdot h$ for an increase in the applied pressure from 49 to 196 kPa. Despite a four-fold increase in applied pressure from 49 to 196 kPa, only a two-fold increase in the final broth flux is observed for all the three membrane assemblies. However, when increasing the number of membranes to four-fold, a nine-fold increase in the final broth flux is observed at all the applied pressures. Reduction in the pore blockage and membrane

fouling along with an increase in the number of membranes resulted in very high final broth flux for the membrane assembly with four number of membranes. These results also suggest a uniform distribution of bacterial biomass on all the membranes, thereby avoiding fouling of the membranes. A schematic showing bacterial separation with respect to the different membrane assemblies is shown in Fig. 4.7(b). The single membrane assembly first showed major signs of fouling; upon increasing the number of membranes, the membrane fouling reduced drastically. These experiments suggest that during microfiltration of culture broth, a high number of membranes is desirable to reduce fouling, achieve a higher broth flux and an extended filtration rate. This result differs from the results of the experiment with an increase in applied pressure (Fig. 4.7(a)), which shows that the membrane fouling steadily increased with an increase in the applied pressure. However, it is to be noted that membrane fouling due to cake formation and pore plugging is inevitable and, therefore, a periodic backwashing with advanced control system is needed to restore the original performance of the membrane (Bagheri et al., 2019).

The trend followed and volume of permeate collected during the experiment, as a function of applied pressure and number of membranes, are presented in Fig. 4.6. It can be seen that the volume of permeate collected increased with an increase in the applied pressure as well as with an increase in the number of membranes. For instance, at the end of 30 min, in the single membrane assembly, an increase in the applied pressure from 49 to 196 kPa resulted in the enhancement of permeate volume collected from 0.01 to 0.017 L. In double membrane assembly, this value increased from 0.03 to 0.05 L, and with the four membrane assembly, the value further increased from 0.17 to 0.38 L.

Table 4.1. Comparison of pure water flux and final broth flux in different membrane assemblies as a function of applied pressure

S. No.	Applied pressure (kPa)	Flux (l m^{-2} h^{-1})					
		Single membrane		Double membrane		Four membrane	
		Pure water flux	Broth flux*	Pure water flux	Broth flux*	Pure water flux	Broth flux*
1	49	110	3.1	108	8.3	112	35.7
2	98	216	4.6	215	12.7	217	43.1
3	147	327	5.9	326	16.6	330	47.9
4	196	441	7.8	439	18.4	444	52

*- Broth flux measured at the end of 30 min.

4.3.6. Biomass and PHB recovery

Performance of any membrane cannot be assessed only based on broth flux of the membrane as a maximum broth flux can be attained even without any biomass recovery. Therefore, the results of broth flux were evaluated along with biomass and PHB recovery efficiency in this study. Fig. 4.8 shows the efficiency of *R. eutropha* biomass and PHB recovery observed at the end of 30 min in each experimental run. The permeate sample collected at the end of each experimental run was subjected to the analysis of biomass and PHB concentrations. This analysis of biomass and PHB recovery efficiencies in each experimental run was carried out by increasing the applied pressure and with an increase in the number of membranes. In each case, the biomass, as well as PHB recovery efficiency values were found to decrease with an increase in both the applied pressure and the number of membranes. For instance, in the single membrane assembly, the biomass recovery

efficiency decreased from 94.3 ± 0.72 to 84.9 ± 0.89% and the PHB recovery efficiency decreased from 99.9 ± 0.03 to 90.5 ± 0.5% with an increase in the applied pressure from 49 to 196 kPa. In the case of the double membrane assembly, the values of biomass and PHB recovery efficiency reduced from 94.2 ± 0.8 to 81.8 ± 1% and 99.2 ± 0.03 to 88.1 ± 0.6%, respectively. But in case of the four membrane assembly, the reduction in biomass and PHB recovery efficiency was from 94.2 ± 1.2 to 80.6 ± 1.4% and from 99.2 ± 0.03 to 87.1 ± 0.7%, respectively.

As described earlier, the enhanced PHB recovery efficiency in comparison with the biomass recovery efficiency in all the experiments is attributed to the loss of immature *R. eutropha* cells to the permeate stream that is void of PHB granules. Therefore, 99% of PHB recovery efficiency is observed for all the three membrane assemblies at a low applied pressure of 49 kPa. However, an increase in the applied pressure resulted in the reduction of both biomass and PHB recovery efficiency. At elevated pressures, the disruption of PHB containing *R. eutropha* cells as well as the deformation of peptidoglycan layer present in the cell wall of the Gram-negative *R. eutropha* cells is more likely that enables its passage through the permeate side. Many such reports on the passage of bacterial biomass due to the disruption and deformation of Gram-negative bacteria are well documented in the literature (Gaveau et al., 2017). A schematic showing the mechanism of passage of *R. eutropha* cells through the ceramic membrane used in this study is depicted in Fig. 4.9. The reduction of biomass and PHB recovery efficiency with an increase in the number of membranes can be attributed to the reduced secondary layer formation on the membrane. It is understood that reduced formation of secondary layer results in large pore size and consequently reduced biomass and PHB recovery. Many authors reported a similar effect on the secondary layer formation with an increase in filtration time and applied pressure;

reduction in secondary layer is also reported with an increase in the membrane length (Goswami et al., 2018).

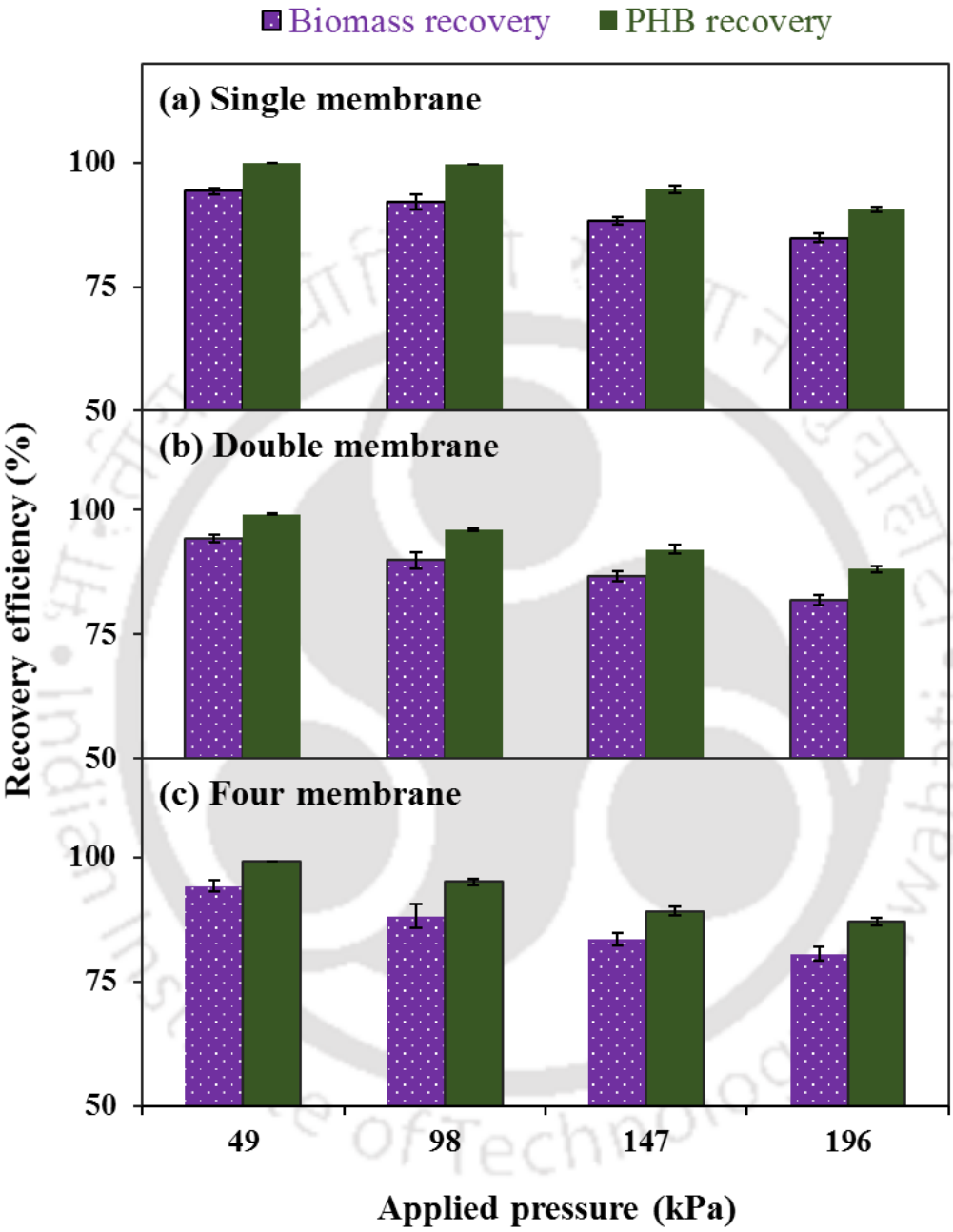

Fig. 4.8. Influence of applied pressure on biomass and PHB recovery efficiency: (a) single membrane assembly, (b) double membrane assembly and (c) four membrane assembly

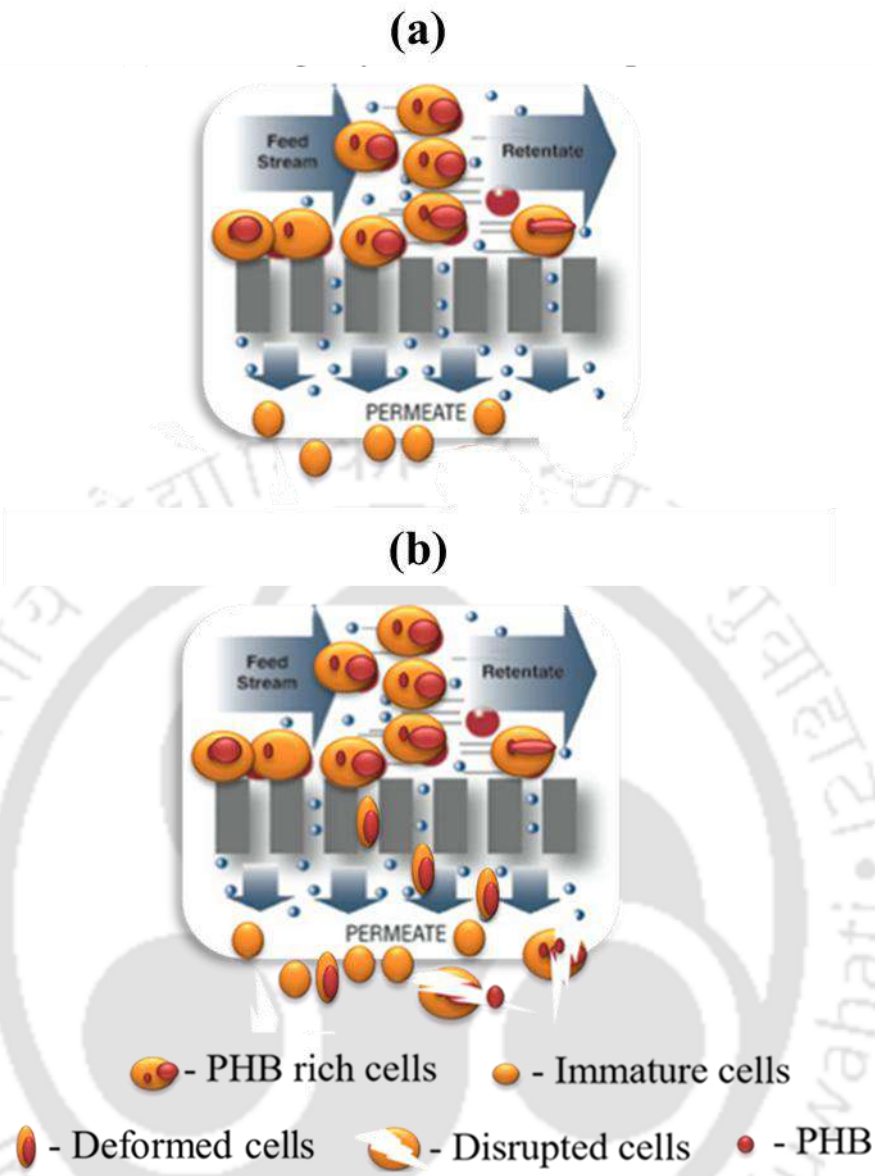

Fig. 4.9. Mechanism of biomass and PHB recovery by microfiltration: (a) Plausible mechanism for enhanced PHB recovery in comparison with biomass recovery and (b) Plausible mechanism for effect of pressure on PHB recovery

Piry et al. (2012) observed a very good enhancement in broth flux due to an increase in the separation of whey protein during casein fractionation. Furthermore, such secondary membrane formation is reported not only during separation of biological material, such as bacteria and algae, but also during the separation of oil in water emulsion and heavy metals (Mukherjee et al., 2018; Vasanth et al., 2013, 2011; Vinoth Kumar et al., 2015). Hence, it

could be concluded that reduction in biomass and PHB recovery efficiency mainly depended on the applied pressure rather than the number of membranes in the assembly.

4.3.7. Relationship between recovery efficiency and broth flux

Both recovery efficiency and permeate flux are critical parameters that determine the performance of any separation processes. But in general, an inverse relationship exists between these two parameters; that is, any attempt to increase the flux would result in a reduction in the recovery and vice-versa. Therefore, few recent researchers focused on maintaining a balance between the two to achieve an optimum performance of membranes. Hu et al. (2018) and Engtrakul et al. (2016) modified surface charge on a stainless steel membrane to achieve maximum flux and recovery of hydrocarbon from water. Piry et al. (2008) and Piry et al. (2012) increased the length of ceramic membrane and achieved an enhancement in separation of whey proteins along with an improved broth flux. Further, Bromley et al. (2002) demonstrated an increase in bacterial removal efficiency with an increase in the broth flux by changing the pore geometry of a membrane from a round shape to a slotted one.

Compared with the literature study, the present study achieves enhancement in biomass recovery and broth flux by increasing the number of membranes. Fig. 4.10 shows the relationship between PHB recovery efficiency and final broth flux. In this analysis, the biomass recovery efficiency is neglected as PHB is the product of interest. With a single membrane assembly, the PHB recovery (90.4 ± 0.5%) achieved is low at high applied pressure, but the final broth flux (7.8 $L/m^2 \cdot h$) is high. Using a single membrane and at low applied pressure, a high PHB recovery (99.9 ± 0.03%) and low final broth flux (3.1 $L/m^2 \cdot h$) is obtained. Using more number of membranes operated at a high applied pressure, PHB recovery of 87.1 ± 0.7% and a very high broth flux of 52 L m^{-2} h^{-1} was obtained. At low applied pressure, more number of membranes yielded a maximum PHB recovery of 99.2 ±

0.03% and final broth flux of 35.7 L/m^2·h. These results clearly reveal that the inverse relationship between recovery efficiency and broth flux with a single membrane assembly is overcome by increasing the number of membranes. Thus, it can be concluded that microfiltration carried out at a low applied pressure and maximum number of membranes results in the best PHB recovery and final broth flux.

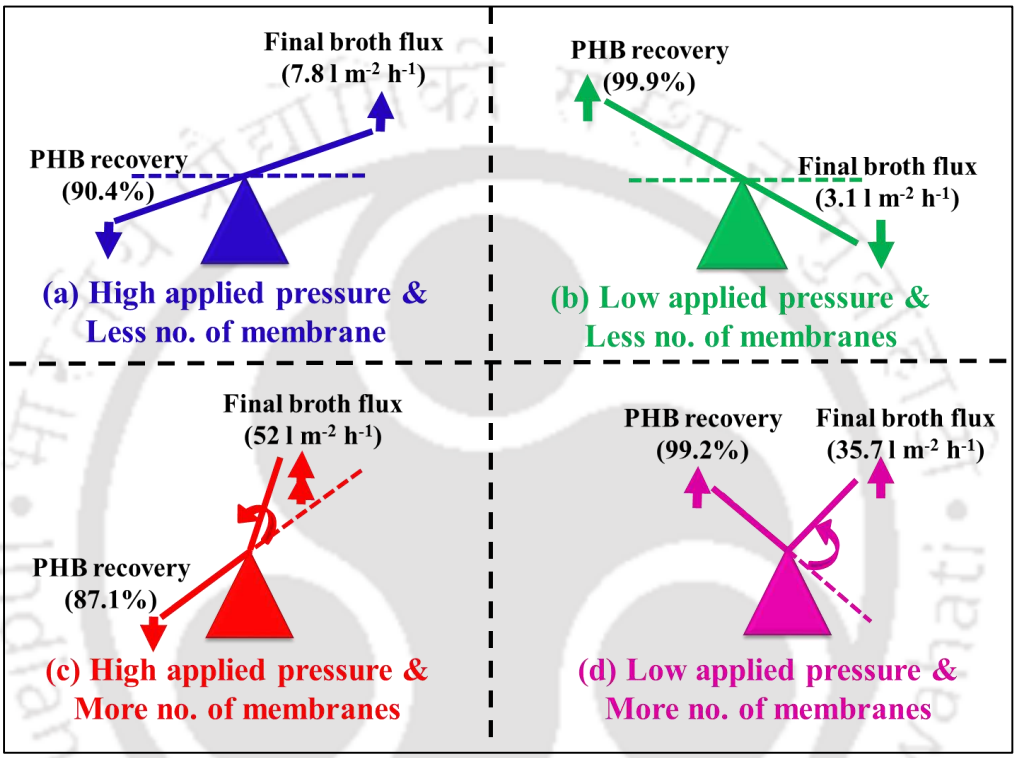

Fig. 4.10. Relationship between PHB recovery and broth flux in the present cross-flow microfiltration system

4.3.8. Resistance analysis

Fig. 4.11 shows the effect of applied pressure and the number of membranes on various resistance, such as filtration resistance, cake resistance and membrane resistance (Piry et al., 2012, 2008). Membrane resistance is the intrinsic resistance of the present ceramic membrane, which does not vary with change in the process conditions. In the present study, the membrane resistance is calculated to be 0.19×10^{13} m^{-1}. The total resistance varies with the process conditions and the difference between total resistance and membrane resistance

is the filtration resistance (Piry et al., 2012, 2008). At all the applied pressures, the magnitude of filtration resistance followed the order: single membrane > double membrane > four membranes. Filtration resistance increased with an increase in applied pressure for all the three membrane assemblies. However, in the case of the single membrane assembly, it can be clearly seen that filtration resistance increases initially and it remained constant at high applied pressure (Fig. 4.11); The filtration resistance increased drastically from 6.4×10^{13} m^{-1} to 10.13×10^{13} m^{-1} with an increase in the applied pressure from 49 to 147 kPa. A further increase in the applied pressure results in almost the same filtration resistance value of 10.28×10^{13} m^{-1}. This initial increase in the resistance can be attributed to the compressible nature of the *R. eutropha* cells. The constant values of resistance obtained at a high applied pressure indicate a highly compacted form of the *R. eutropha* cells. In contrast with this result obtained using the single membrane assembly, the filtration resistance increases steadily with an increase in the applied pressure for the other two membrane assemblies. This result suggests that the *R. eutropha* cells are not fully compacted even at very high applied pressure in the case of double and four membrane assemblies. A constant value of the resistance at a high applied pressure observed in the single membrane assembly is also attributed to the extracellular matrix in the *R. eutropha* cells that remains fully compacted.

Babel and Takizawa, (2010) in their study observed fouled membrane at different applied pressures. They found through the microscopy analysis that the algal cells are well dispersed at low applied pressure. However, at high applied pressure, the authors reported that the void space between the algal cells is greatly reduced because of the extracellular organic matrix produced. A similar phenomenon was observed by Kim et al. (2007) in their study on the separation of natural organic matter (NOM) using membranes. In another study by Morineau-Thomas et al. (2002), compression of algal cells due to the soft polymer

shell covering the biomass was reported. However, the authors reported that the secondary membrane formed due to the compression of algal cells or NOM on the membrane restricted the passage of algal cells. In contrast, the water passage towards the permeate side remained unhindered.

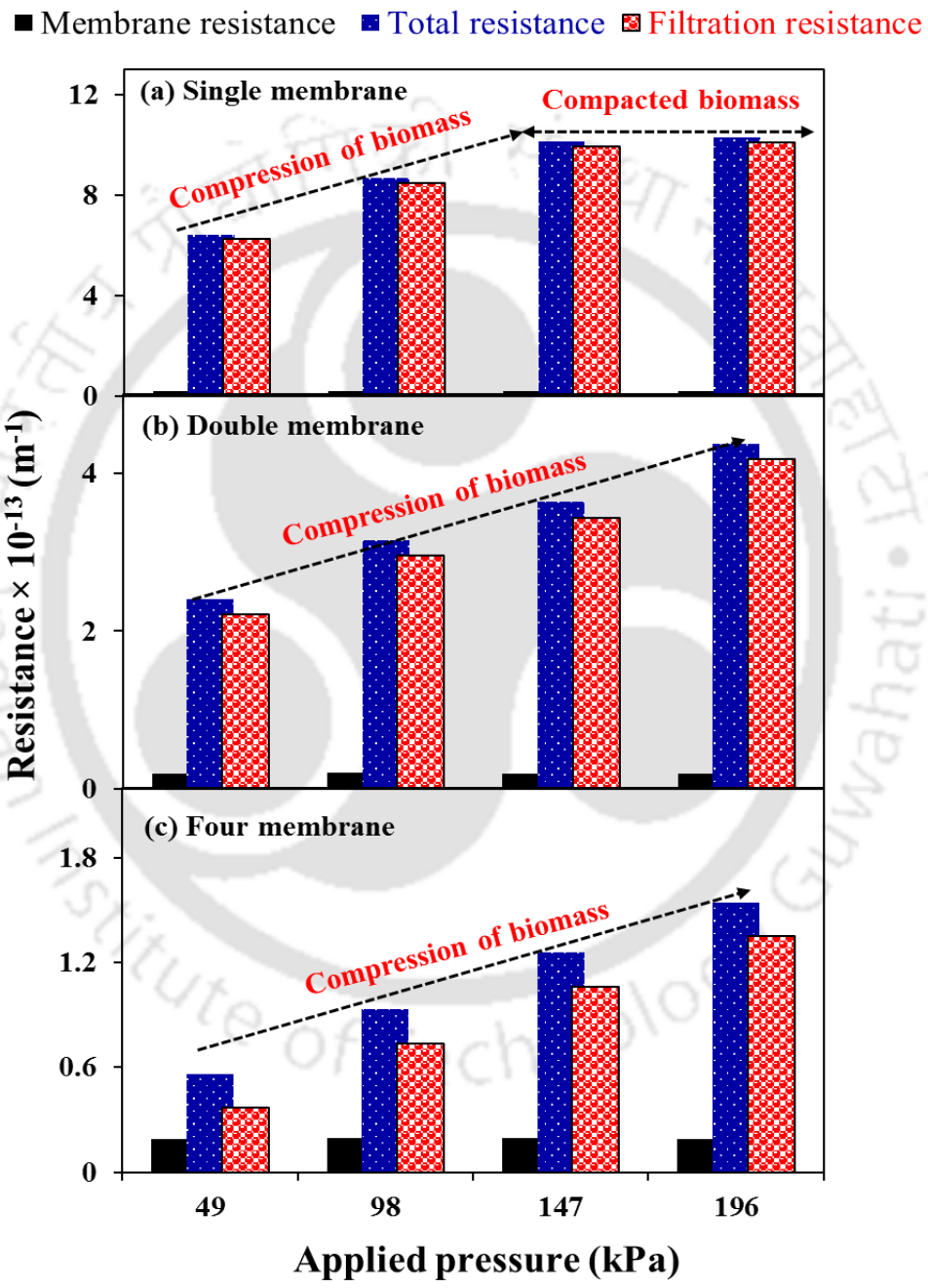

Fig. 4.11. Influence of applied pressure on different membrane resistances: (a) single membrane assembly, (b) double membrane assembly and (c) four membrane assembly

4.4. Practical applications and future research perspectives

The conventional processes including centrifugation and coagulation are customarily used for the separation of bacterial biomass from the culture broth (Barros et al., 2015; Pragya et al., 2013; Zhao et al., 2017). However, these techniques were found to be either energy-intensive or the coagulants used in the process give rise to secondary pollutants (Pragya et al., 2013). Therefore, the application of membrane technology is found to be more attractive by making the process cost-effective and also without addition of chemical additives into the system. However, it is noteworthy to mention that the raw materials used for the fabrication of ceramic membrane are expensive (Harabi et al., 2016; Issaoui et al., 2017; Kumar et al., 2015a,b). Hence, we have developed a low-cost ceramic membrane by utilizing cheap starting materials that resolves the issue of high membrane cost associated with the ceramic membranes. Further, a very high PHB recovery efficiency proposes the suitability of the membrane in separating the present product of interest. The novel ceramic membrane assembly containing multiple numbers of membranes exhibits a very good broth flux along with the maximum biomass and PHB recovery in comparison with the conventional single membrane assembly. The low applied pressure suggested in the present study to attain a balance between flux and recovery garnered the additional strength of low pumping cost and thereby resulting in the reduction of overall cost of the membrane separation process.

The present study mainly focuses on the separation of *R. eutropha* bacterial biomass that is rich in polyhydroxybutyrate. This study conducted on bacterial separation can also be extended for the separation of other biomass such as yeast, algae, and actinomycetes comprising of value-added products. The high efficiency exhibited for bacterial separation in the present investigation assures similar or even better efficiency in the case of other microbial biomass, as their size is several folds larger in comparison with

the bacteria (Barros et al., 2015; Pragya et al., 2013; Katla et al., 2019). For instance, intermediate value products like single cell protein and lipids produced by the algal biomass can be readily investigated for its separation using the existing tubular ceramic membrane assembly. It is to be noted that the separation of very high-value products like bioactive compounds and pharmaceutical compounds produced in the yeast can also be studied using the present system (Katla et al., 2019). The tubular membrane assembly used in this work can also be integrated with the bioreactor, which will reduce the major problem of fouling faced by the current practice of high cell density cultivation carried out in the membrane bioreactor. However, proper experiments and continual up gradation are needed for its installation in the bioprocess industries.

4.5. Summary

Application of membrane technology was found to be more attractive in separation of PHB rich biomass by making the process highly efficient (> 99%) and also without any generation of secondary pollutants from the system. Unlike the conventional fabrication method using expensive raw materials. The present developed a low-cost ceramic membrane by utilizing cheap starting materials that resolves the issue of high membrane cost associated with the ceramic membranes. The novel ceramic membrane assembly containing multiple numbers of membranes exhibits a very good broth flux along with the maximum biomass and PHB recovery in comparison with the conventional single membrane assembly. The low applied pressure suggested in the present study to attain a balance between flux and recovery garnered the additional strength of low pumping cost and thereby resulting in the reduction of overall cost of the membrane separation process.

Chapter 5

Preparation and characterization of environmentally safe and highly biodegradable microbial polyhydroxybutyrate (PHB) based graphene nanocomposites for potential food packaging applications

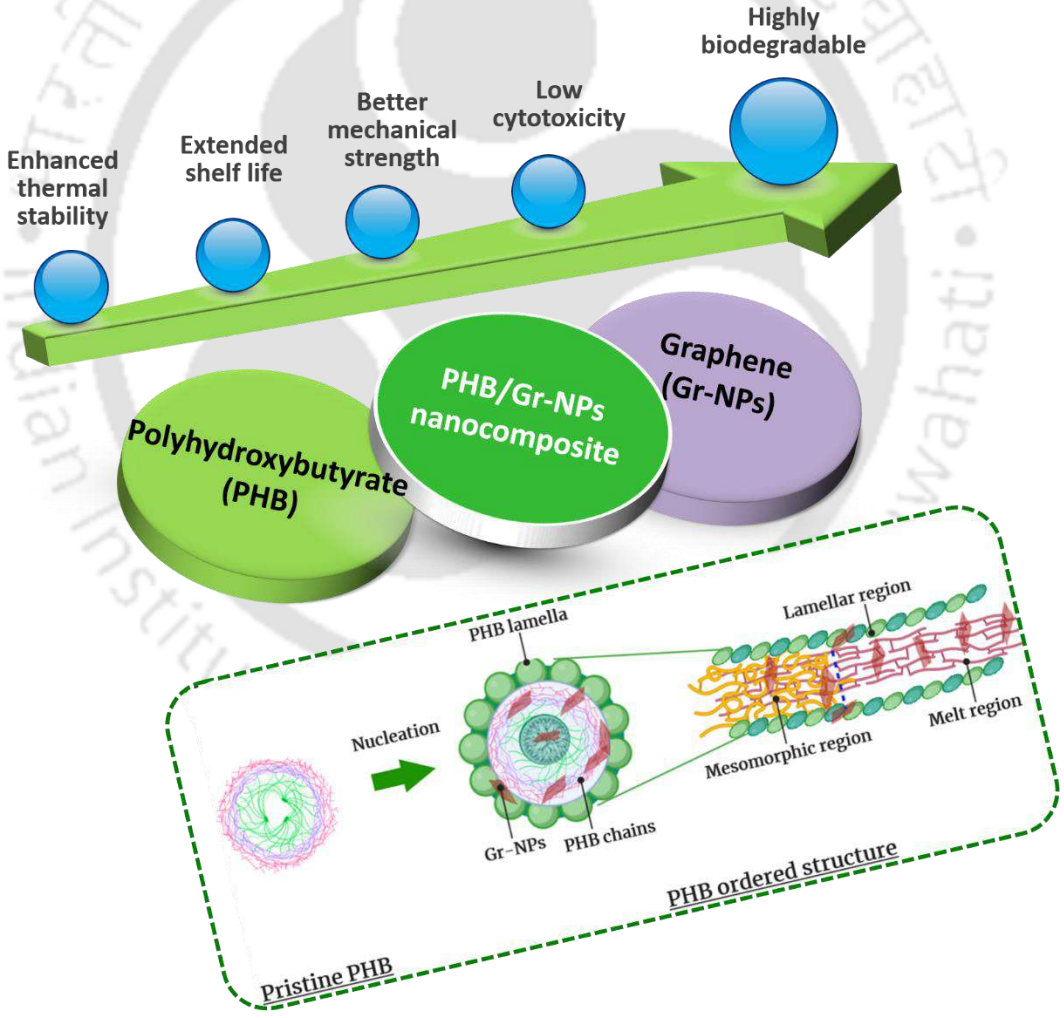

Abstract

Polyhydroxybutyrate (PHB) is a natural polyester of microbial origin and is an excellent substitute for petroleum-based food packaging materials. However, moderate mechanical, thermal and barrier properties limit utilisation of PHB for commercial food packaging applications. In order to overcome these drawbacks, the present study evaluated the solution casting method for the preparation of PHB nanocomposite by incorporating various concentration (0-1.3 wt%) of graphene nanoplatelets (Gr-NPs). The prepared nanocomposites were tested for their morphology, mechanical, thermal, barrier, cytotoxicity and biodegradable properties. A Gr-NPs concentration of 0.7 wt% was found to be optimum without any agglomeration. In comparison with pristine PHB, the PHB/Gr-NPs nanocomposite showed a higher melting point (by 10 ^{o}C), thermal stability (by 10 ^{o}C), tensile strength (by 2 times) along with 3 and 2 times reduction in oxygen and water vapour permeability, respectively. The penetration of UV and visible light was greatly reduced with the addition of Gr-NPs. Furthermore, cytotoxic effect of the prepared nanocomposite was found to be statistically insignificant in comparison with the pristine PHB. A four-fold increase in the shelf life was demonstrated by a simulation study conducted using moisture and oxygen-sensitive food items (potato chips and milk product).

5.1. Introduction

The use of plastics concomitantly increases with its accumulation in the environment every year and it is predicted to reach 33 billion tons in the year 2050 (Goh et al., 2016). Many efforts are being made to reduce the dependency of the conventional petroleum-based polymer, so as to avoid its environmental impact (Goh et al., 2016; Li et al., 2019; Xu et al., 2020). In this context, the use of biopolymers with properties derived to meet the standards of food packaging materials is considered as the best solution (Goh et al., 2016; Li et al., 2019). Biopolymers including starch, chitosan, cellulose and few other multipurpose polymers such as polylactic acid (PLA), polyglycolic acid (PGA), polybutylene succinate (PBS), polyhydroxybutyrate (PHB) are well studied for their biocompatible, biodegradable and ecofriendly nature (Xu et al., 2020). In particular, the fully biodegradable, non-toxic and highly crystalline nature of the bacterial polyhydroxybutyrate makes it more attractive and is at the forefront of the contemporary research (Acevedo et al., 2018; Xu et al., 2020). Unlike the petroleum-based plastics, PHB is completely produced from sustainable biomass resources. Secondly, the PHB properties are similar to that of the conventional petroleum-based polymers such as polypropylene (PP), polystyrene (PS), polyethene (PE) and polyethene terephthalate (PET) (Serafim et al., 2004). Among the many biodegradable polymers that have been researched thus far, PHB has reached commercial level of production with a wide array of applications ranging from manufacturing of routine use commodities like razors and bottles to more sophisticated biomedical items such as sutures and bone implants, etc. (Ganapathy et al., 2018). However, its application in the food packaging sector is lacking due to the moderate barrier, thermal and mechanical properties of this biopolymer (Xu et al., 2020).

In order to overcome the demerits associated with the PHB for food packaging applications, several fillers ranging from natural pigments/biochemical compounds to

advanced nanomaterials like silver nanoparticles and other nanoclays were added to form PHB based polymeric composites/nanocomposites. However, the results of PHB based composites/nanocomposites have not been successful thus far. For instance, Zare et al. (2019) prepared a smart fortified PHB and chitosan-based biopolymer by using *Thymus vulgaris* leaf extract as the stabilising agent along with the addition of high functionality nanoparticles such as zinc oxide (ZnO) and silver (Ag). The authors reported a remarkable reduction in oxygen permeability (OP) from 6 to 3.5 $cm^3 \cdot mm/m^2 \cdot d^2 \cdot atm$, which is still very high compared with the OP value limit (1 $cm^3 \cdot mm/m^2 \cdot d^2 \cdot atm$) for food packaging applications (Xu et al., 2020). Dhar et al. (2017) tested cellulose nanocrystal addition to PHB and found 2 fold decrease in OP value, but the value was higher than the index value of 1 $cm^3 \cdot mm/m^2 \cdot d^2 \cdot atm$. Tripathi et al. (2019) investigated the effect of nutritional supplements on PHB produced using sugar refinery wastewater for potential food packaging applications. The melting point of the PHB produced following this approach was found to be 179 ^oC, which is only slightly above the melting point of pristine PHB. In comparison with the conventional fillers, viz. leaf extract (Zare et al., 2019), biochemical compound (Arrieta et al., 2014) and nanoparticles (Castro-Mayorga et al., 2014; Jayakumar et al., 2019); graphene is considered the best as it is the most robust material ever tested and it offers exceptionally high barrier, thermal and mechanical properties (Goh et al., 2016). Even after 15 years of its discovery, graphene is still a novel high-performance material not exploited for preparing biopolymer-based nanocomposites. Though only a few studies have reported on the preparation of PHB/graphene nanocomposites, the scope of these studies was limited to morphology analysis, crystallisation kinetics and phase transition analysis, etc. (Barrett et al., 2014; Beć et al., 2018; Jing and Qiu, 2012). To the best of our knowledge, there are no studies on the preparation of PHB based graphene

nanocomposites in the context of food packaging applications with barrier properties and shelf life simulation studies.

Therefore, the present study aims at the preparation of PHB/Gr-NPs nanocomposite using simple solution casting technique with the help of tip sonication and without the addition of any external modifiers or chemical coupling agents. The prepared nanocomposites were characterised by using various techniques, including atomic force microscopy (AFM), Field emission scanning electron microscopy (FESEM), field emission transmission electron microscopy (FETEM), X-ray diffraction (XRD) and Fourier transform infrared (FTIR) spectroscopy. Furthermore, thermal, mechanical and optical properties of the prepared PHB/Gr-NPs nanocomposite were evaluated; In particular, barrier properties viz. water vapour permeability (WVP) and oxygen permeability (OP) analyses were carried out. In addition to the aforementioned physicochemical, thermal and mechanical analyses, cytotoxicity and biodegradability of the prepared PHB/Gr-NPs nanocomposites were performed. Finally, shelf-life simulation studies were undertaken to establish the potential of PHB/Gr-NPs nanocomposite in food packaging applications.

5.2. Materials and methods

5.2.1. Materials

Polyhydroxybutyrate (PHB) with an average molecular weight (M_w) of 610 Kg/mol used in the study was of microbial origin and the preparation procedure was described in chapter 2 and 3. Graphene nanoplatelets (Gr-NPs) was procured from United Nanotech Innovations Pvt. Ltd., Bangalore, India (12.9724° N, 77.5806° E). Graphene of different grades viz. typical grade, predominant grade, premier grade and superior grade graphene (Gr-NPs) were first subjected to trial experiments; based on the results obtained, only superior grade graphene was considered throughout the study. The properties of the superior grade graphene (Gr-NPs) are as follows: 1 - 4 layer thickness, > 99% of purity, 5 µm length, 2-3

nm thickness and a surface area greater than 300 m^2/g. Chloroform ($CHCl_3$) and phosphate buffer saline (PBS) with pH 7.4 used in the study were purchased from Himedia^{TM}, India, and used without any further purification. Trypan blue, propidium iodide (PI), Dulbecco's modified Eagle's medium (DMEM), fetal bovine serum (FBS), methemoglobin (MetHb), the antibiotics penicillin and streptomycin, fluorescein diacetate (FDA) and 3-(4,5-dimethylthiazol-2-yl)-2,5-diphenyltetrazolium bromide (MTT) used in the cytotoxicity experiments were purchased from Sigma-Aldrich^{TM}, India.

5.2.2. Preparation of PHB/Gr-NPs nanocomposite

PHB/Gr-NPs nanocomposite with varying concentrations of Gr-NPs (% w/w), i.e., 0.3, 0.5, 0.7, 1.0 and 1.3 wt% were prepared by solution casting technique as follows: PHB (0.1 g) was first dissolved in 10 mL of chloroform by continuous mixing for 60 min (Solution A). Superior grade graphene (Gr-NPs) of concentration in the range of 0.3 - 1.3 wt% with respect to PHB was dispersed in chloroform (1 mL) by sonication for 45 min (15 s on cycle: 45 s off-cycle) (Solution B). And the resulting mixture (Solution B) was then added to PHB–chloroform mixture (Solution A) with stirring at 100 rpm for 60 min (Solution C). Finally, after stirring for an hour, the solution C was poured on a petri dish, and the solvent was evaporated by placing it into a fume hood. Thereafter, these films were peeled off and taken for further characterization. A polymer sample without any added Gr-NPs served as the control in this study, and the same is mentioned as pristine PHB. The steps followed for the preparation of PHB/Gr-NPs nanocomposite was depicted in Fig. 5.1.

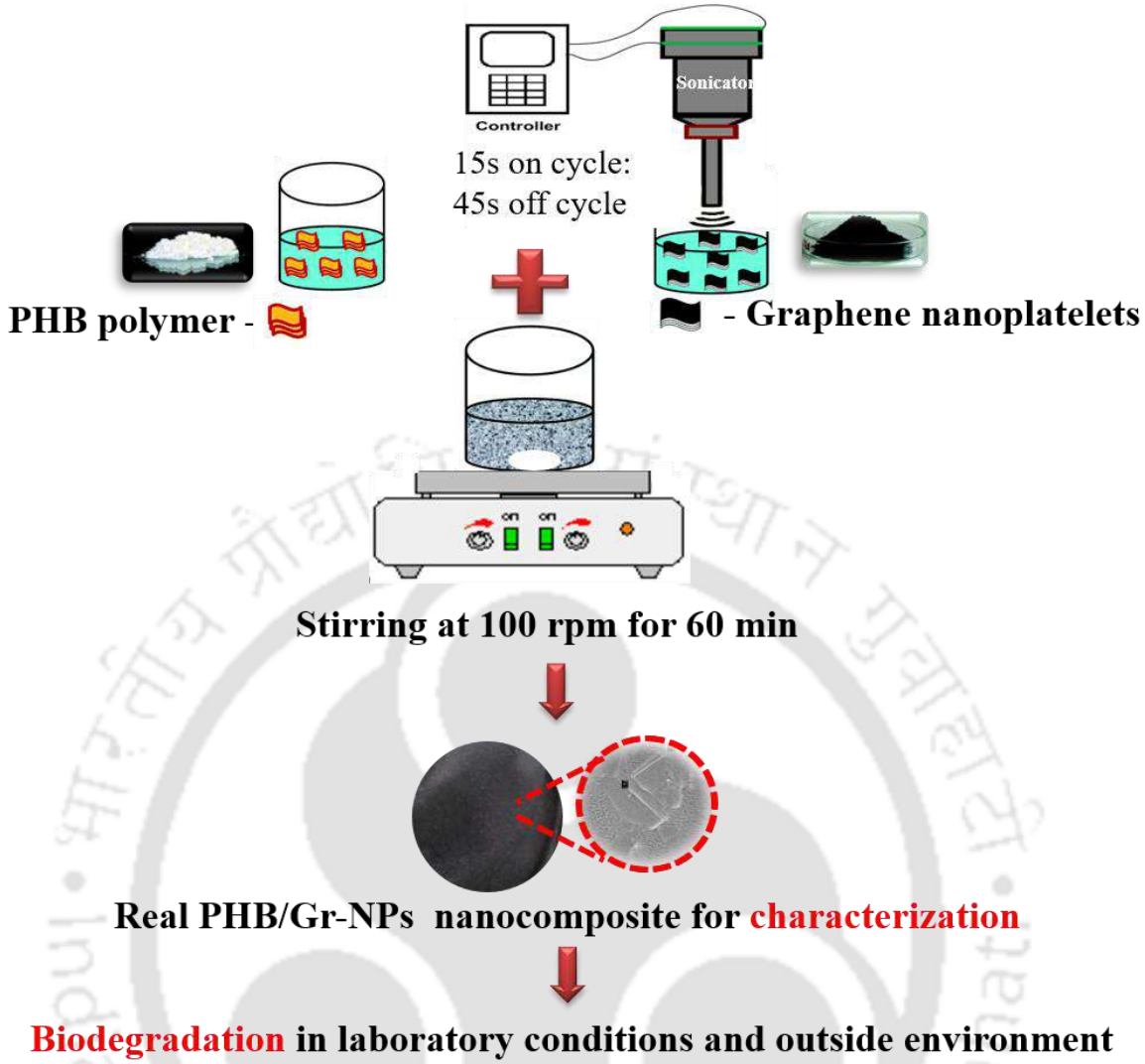

Fig. 5.1. Steps followed for PHB/Gr-NPs nanocomposite preparation

5.2.3. Characterization

5.2.3.1. Physico-chemical characteristics

Dispersion of Gr-NPs and morphology of the PHB/Gr-NPs nanocomposites and pristine PHB were studied using imaging techniques - atomic force microscopy (AFM), field emission scanning electron microscopy (FESEM) and field-emission transmission electron microscopy (FETEM). PHB micro-grain structure was analysed by using AFM (Oxford, Cypher model, United Kingdom) operated under non-contact mode. 1 mL of PHB dissolved in chloroform was cast on a coverslip prior to the AFM analysis. For FESEM

analysis, either PHB or PHB/Gr-NPs nanocomposite was cast directly on double-sided carbon tape and mounted on a stainless steel stub. These stubs were gold-sputtered to form a thin layer of gold on the sample. Gold-coated samples were finally analysed using FESEM (Zeiss, Sigma model, Germany) operated at 2 kV. For FETEM analysis, the samples were dropped directly onto a copper grid and dried overnight. These dried samples were used for observation under FETEM (JEM 2100F, JEOL, Japan) operated at 200 kV.

Fourier transform infrared (FTIR) (Shimadzu, IR-affinity 1 model) analysis under attenuated total reflection (ATR) mode was carried out to identify the functional groups present in the pristine PHB and PHB/Gr-NPs nanocomposites. An average of 60 scans with a resolution of 4 cm^{-1} was performed for all the samples over the wavelength range of 400 to 4000 cm^{-1}.

Contact angle analysis was carried out using Drop shape analyser – DSA 25, Kruss model, Germany. The droplet size of 4 µL with a dropping rate of 0.16 mL/min was maintained for all the analysis. Image for the contact angle analysis was captured after 30 s from the dropping of the liquid. X-ray diffraction (XRD) analysis of pristine PHB and PHB/Gr-NPs nanocomposites was carried out under an ambient atmosphere using powder XRD (Rigaku, SmartLab, USA) instrument operated at 40 kV and 40 mA with Cu-Kα radiation wavelength of 0.15406 nm. The samples were scanned in the 2- theta degrees ranging from 5 to 60^{o} along with a scanning rate and step size of 0.1^{o} s^{-1} and 0.5 s, respectively.

5.2.3.2. Oxygen permeability and water vapour permeability

Oxygen permeability (OP) analysis was carried out using Ox-Tran Modular System, India operated at 25 ^{o}C and relative humidity of 50%. Prior to this analysis, the pristine PHB and PHB/Gr-NPs nanocomposites films were equilibrated for a total period of 2 days at a

relative humidity value of 50% (Chandra Mohan et al., 2018). Polymeric films were mounted between two stainless steel mould having a circular opening in the centre so as to have an active surface area of 5 cm^2. On one side of the stainless steel mould, oxygen was passed while on the other side, nitrogen gas was passed. Nitrogen gas connected to the coulometric sensor and analysis was carried out after attaining steady-state to calculate oxygen transmission rate (OTR). Finally, oxygen permeability (OP) values were estimated by using equation (5.1) (Hema Prabha and Ranganathan, 2018):

$$\text{Oxygen permeability (OP)} = \frac{\text{OTR}}{\Delta P} \times L \qquad (5.1)$$

Where OP is the oxygen permeability ($cm^3 \cdot mm/m^2 \cdot d^2 \cdot atm$), OTR is the oxygen transmission rate ($cm^3/m^2 \cdot d$), ΔP is the difference in partial pressure of oxygen on both sides of the film (atm) and L is the film thickness (mm).

Water vapour permeability (WVP) analysis of the samples was carried out as per the ASTM E96/E96 M gravimetric method, which is generally referred as "cup method". For this analysis, the respective films were placed over a steel mould having a circular opening of 2.9 cm^2. Free space in the cup underneath the polymeric film was filled entirely with calcium chloride having a relative humidity value of 0% (Jha et al., 2019). This permeation cup was thereafter placed in a desiccator having a surrounding temperature of 25 ^oC and relative humidity of 75% maintained through sodium chloride solution. The increase in weight of the permeability cup was measured for 2 days with a regular time interval of 12 h. The increase in weight of the permeation cup was measured as a function of time divided by the transfer area to get the water vapour transmission rate (WVTR). Finally, water vapour permeability (WVP) values were estimated by using equation (5.2) (Hema Prabha and Ranganathan, 2018):

$$\text{Water vapour permeability (WVP)} = \frac{\text{WVTR}}{\Delta P} \times L \qquad (5.2)$$

Where WVP is the water vapour permeability (g·mm/m^2·d^2·atm), WVTR is the water vapour transmission rate (g/m^2·d), ΔP is the difference in partial pressure of oxygen on both sides of the film (atm) and L is the film thickness (mm).

5.2.3.3. Shelf life (Θ) simulation test

Shelf life (Θ) simulation of the pristine PHB and PHB/Gr-NPs nanocomposites was determined for the packaging of potato chips and milk products and by interrelating the oxygen permeability values with the rate of oxidation as specified in the following models (eqs. 5.3 and 5.4):

$$\theta = \frac{O_{2(max)}}{k_{O_2} \cdot p_{O_2}} \qquad (5.3)$$

$$p_{O_2} = \frac{0.21 \times \left(\frac{OP}{d}\right) \times A}{k_{O_2} + \left(\frac{OP}{d}\right) \times A} \qquad (5.4)$$

$O_{2\,(max)}$ is the maximum concentration of oxygen that can react with the food items and can finally lead to its spoilage. Oxidation rate constant (k_{O_2}) values of the potato chips and milk products were obtained based on the literature (Andersson H, 2006; QUAST et al., 1972). Matlab™ 2015a software was used for this shelf simulation study. In equation (5.4) the term p_{O_2}, OP, A and d are the partial pressure of oxygen, oxygen permeability value, surface area and thickness of the film, respectively. For this simulation study, the thickness of the PHB/Gr-NPs composite films was fixed as 100 µm and the film surface area of 1L capacity was taken as 0.1 m^2.

5.2.3.4. Thermal characteristics

The thermo-gravimetric analysis (TGA) was performed under a nitrogen atmosphere with a flow rate of 40 mL/min on a TG 209 F1, Libra Analyser, Germany with a heating rate of 10 ^{o}C/min and a temperature range of 30-500^{o}C. The sample was placed in a 900 µL ceramic crucible for analysis. Differential thermogravimetric analysis (DTG) was carried out to find the maximum thermal degradation temperature (T_{max}) of the samples. Differential scanning calorimetry (DSC) measurement was done on Mettler Toledo - 1 series, Switzerland in the temperature range of 25-200 ^{o}C with a heating rate of 5 ^{o}C/min. For this analysis, all the samples were first heated from 25 to 200 ^{o}C and maintained at the same temperature for 5 minutes to eliminate the processing and thermal history associated with the samples. Melting temperature (T_m) of the samples was later obtained from the DSC thermographs.

5.2.3.5. Transmittance and tensile characteristics

Transparency of the pristine PHB and PHB/Gr-NPs nanocomposites films was analysed using a UV-visible spectrophotometer (Perkin Elmer, Lambda 35 model, USA). For this analysis, the samples were scanned in the wavelength ranging from 200 - 600 nm with a scan rate and bandwidth of 50 nm/min and 2 nm, respectively. $BaSO_4$ coated plate was used as a reference for this analysis. Tensile test of the pristine PHB and PHB/Gr-NPs nanocomposites films was measured using 5 kN Electromechanical Universal Testing Machine (Z005TN model, Zwick Roell, USA). Samples for this analysis were prepared according to ASTM D882-12 standard. The dimensions of the sample specimens are as follows: length 80 mm, gauge length 50 mm, width 5 mm and thickness 0.2 mm. Sample thickness was measured using digital micrometre (Mitutoyo, Japan), and the sample elongation rate for all the analysis was maintained at 5 mm/min. Tensile stress (τ) and

elongation (ε) were calculated from the stress-strain curve by using the following equations (5.5 and 5.6) (Chandra Mohan et al., 2018):

$$\tau = \frac{F_{max}}{A} \tag{5.5}$$

$$\varepsilon = \frac{\Delta L}{L} \times 100 \tag{5.6}$$

Where τ is tensile stress in MPa, F_{max} is the maximum force (MPa) needed to pull the sample apart, A is the initial cross-sectional area of the sample in m^2, ε is the elongation in percentage, ΔL is the extension of the sample at the time of rupture in mm and L is the original length of the sample, which is 50 mm for the present study. Change in surface morphology of the polymeric samples during the course of elongation was analysed only for PHB/Gr-NPs nanocomposite with 0.7 wt% Gr-NPs loading using FESEM analysis.

5.2.4. Cytotoxicity test

Cytotoxicity test of the pristine PHB, Gr-NPs and PHB/Gr-NPs nanocomposites was carried out using mouse macrophage cell line J774A.1. Cell line for this study was kindly provided by Malaria research group of Department of Biosciences and Bioengineering, Indian Institute of Technology (IITG), Guwahati, India. The cell lines were grown using Dulbecco's modified Eagle's medium (DMEM), and to which 10% fetal bovine serum (FBS) and 1% penicillin-streptomycin antibiotic were added. The cells were then incubated at 37 ^oC in a CO_2 incubator containing balanced air and CO_2 composition of 5%. Cytotoxicity analysis of the samples was performed following the MTT assay method. For this assay, ten thousand cells were seeded in a 48 well-containing plate having 0.2 mL of complete media and incubated for 40 h at 37 ^oC in a CO_2 incubator containing balanced air and CO_2 composition of 5%. On the day of culture, MetHb was added to the medium. Prior to the cell culture, polymeric samples were placed in the wells, and the well-containing

only medium served as the control for this assay. Thereafter, the cell viability was measured by the MTT reduction test, as described in the literature (Arkusz et al., 2006; Deshmukh and Trivedi, 2013). For microscopic analysis, a separate 48 well plate was taken and all the aforementioned steps were followed, but at the end of the culture period, i.e. at 40^{th} h, media from the 48 well plates were discarded and treated with the dyes fluorescein diacetate (FDA) and propidium iodide (PI), in order to differentiate the live cells from the dead ones. After staining with these dyes, the 48 well plate was directly examined in 40x magnification using a Nikon eclipse TS-100 inverted microscope, Japan. Bright-field and fluorescent images were captured separately using Nikon L22 (Nikon Corp., Japan) digital camera and finally merged using a software interface accompanied with the instrument.

5.2.5. Biodegradation test

Biodegradability of the pristine PHB and PHB/Gr-NPs nanocomposites films was analysed by soil burial method (Zhijiang et al., 2011). For this study, preweighed polymeric samples of four numbers each with specimen dimensions of 130 × 12 × 3 mm were cut and placed on a wooden frame. Thereafter, these samples were buried in the soil under a depth of 10 - 15 cm from the surface. All these experiments were conducted under an ambient atmospheric condition of 28 ^{o}C temperature and 80% relative humidity. During the study period of 30 days, samples were withdrawn on 5^{th}, 10^{th}, 15^{th} and 30^{th} days. Four numbers of each sample were placed in the soil, and on the sampling days, one sample from each test was withdrawn for the analysis. After retrieving from the soil, samples were washed with distilled water and oven-dried at 70 ^{o}C until a constant weight was achieved. The loss in weight of the samples before and after the test was calculated as represented in the equation (5.7) to obtain their percentage biodegradation. Change in surface morphology of the polymeric samples during biodegradation was analysed for 0.7 wt% PHB/Gr-NPs nanocomposite sample by FESEM analysis.

$$\text{Biodegradation}\,(\%) = \frac{W_i - W_t}{W_i} \times 100 \qquad (5.7)$$

Where W_i (g) is initial weight and W_t (g) is weight of the polymeric sample at time t. All the aforementioned analysis was carried out thrice and mean ± standard deviation values were reported. Furthermore, statistical analysis of the results in the form of one-way ANOVA and Turkey's test were carried out using Origin™ Pro 9.0 software. For this analysis, a comparison was made between pristine PHB and the respective PHB/Gr-NPs nanocomposites. Where, * represents the $P < 0.05$ and ** represent $P > 0.05$. A P-value greater than 0.05 indicates that the value observed for the respective PHB/Gr-NPs nanocomposites was not statistically different as compared with the value obtained using the pristine PHB sample.

5.3. Results and discussion

5.3.1. Physico-chemical characteristics

5.3.1.1. Dispersion analysis

The dispersion of Gr-NPs in the polymer matrix and their interfacial bonding are essential for improving the physical, mechanical and barrier properties of composite materials. In order to confirm the dispersion of graphene in the PHB lattice, FESEM, AFM and FETEM analysis of various grades of Gr-NPs, pristine PHB and PHB/Gr-NPs composite films were carried out and the results are shown in Fig. 5.2. The Gr-NPs are self-assertively dispersed in the PHB matrix. Agglomeration was observed for a Gr-NPs concentration above 0.7% (w/w) in the PHB matrix dispersed with superior grade graphene. This aggregation of Gr-NPs in PHB matrix is generally regarded as the overcrowding effect, which occurs when the concentration of filler material in the polymer matrix exceeds its optimum level. This can be overcome to a certain extent by appropriate surface functionalisation of Gr-NPs or

increased time of exposure to the sonication process utilised for the preparation of PHB/ Gr-NPs nanocomposite. For instance, Xu et al. (2020) added 5 wt% of graphene oxide in PHBV matrix by functionalisation of graphene oxide with a long alkyl chain quaternary (LAQ) salt. Any further attempt to increase the graphene oxide concentration above 5 wt% resulted in agglomeration of graphene oxide, which deteriorated the nanocomposite properties. Similarly, Li et al. (2019) grafted graphene oxide with cellulose nanocrystal (CNC) and with which a maximum filler concentration of 1wt% was used without affecting the material properties. Also, Valapa et al. (2015) achieved better loading of graphene into PLA matrix by adopting a modified sonication strategy.

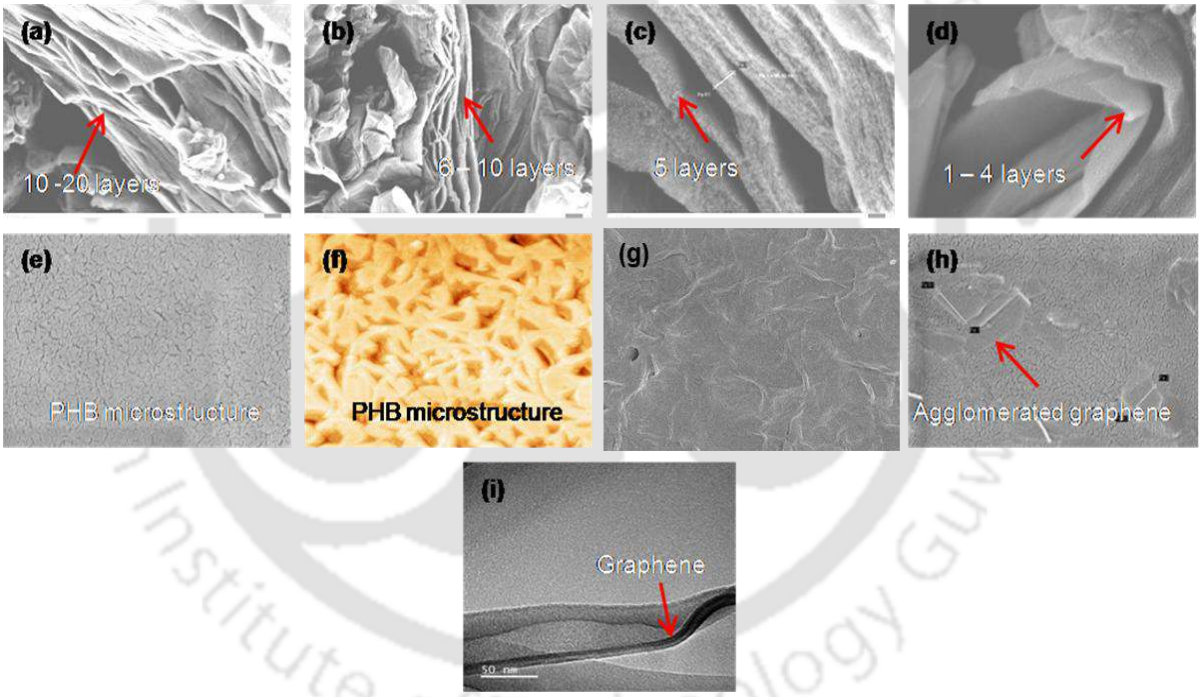

Fig. 5.2. FESEM images of (a) typical grade graphene, (b) predominant grade graphene, (c) premier grade graphene, (d) superior grade graphene, (e) pristine PHB and AFM images of (f) pristine PHB, (g) composite made of PHB at Gr-NPs concentration of 0.7wt%, (h) composite made of PHB at higher Gr-NPs concentration, and (i) TEM image of PHB/Gr-NPs composite at 0.7 wt% concentration

5.3.1.2. FTIR analysis

FTIR spectra of the pristine PHB and PHB/Gr-NPs nanocomposites portrayed in Fig. 5.3(a) shows dominant peaks at around 2978 cm^{-1} due to the presence of C-H stretching in the PHB. PHB being a biopolyester, a strong band noticed at 1720 cm^{-1} corresponds to the carbonyl (C=O) stretch of the ester (-COOR) group (Pradhan et al., 2017). The peaks that are visible around 1450 and 1049 cm^{-1} in the spectra are attributed to the presence of the amide group, which are prevalent in microbial PHB (Hu et al., 2013). Furthermore, the –C–O stretch in the pristine PHB is indicated by the band at 1180 cm^{-1} (Saratale and Oh, 2015). All the aforementioned peaks in the pristine PHB were observed in the PHB/Gr-NPs nanocomposites without any modification or shift in the peaks. Even with increasing Gr-NPs concentration, no additional or shift in the peaks was observed. These FTIR results confirm that the addition of Gr-NPs did not change the main backbone structure of the PHB. Moreover, no chemical interaction between pristine PHB and Gr-NPs was evident due to the lack of functional groups present in Gr-NPs to react and bond with it. Hence, it could be laid that the interaction between PHB and Gr-NPs was primarily due to physical interactions and without any covalent bond formation. A similar observation was made by Jiang et al. (2010), on the addition of graphene onto polyvinyl alcohol (PVA), which yielded no change in the FTIR spectra. In the same study, changes in the nanocomposites were observed when graphene oxide was used instead of graphene due to chemical interaction between the PVA matrix and the functional groups present on the graphene oxide (Jiang et al., 2010).

5.3.1.3. XRD analysis

Fig. 5.3(b) shows the XRD spectra of the Gr-NPs, pristine PHB and PHB/Gr-NPs nanocomposites. Reflection observed at 2 theta value of 26.4^{o} is due to the (0 0 2) planes present in the Gr-NPs. Similar results were reported in the literature by Azra et al. (2014).

Four major peaks observed in the XRD spectra corresponding to the 2 theta values of the pristine PHB are as follows: (0 2 0) at 13.3^{o}, (1 1 0) at 16.8 ^{o}, (1 1 1) at 25.4^{o} and (1 3 0) at 28.5^{o}. The aforementioned peaks were observed on all the PHB/Gr-NPs nanocomposites but at varying intensities. The peak due to Gr-NPs at 2 theta value of 26.4^{o} consistently increases with an increase in the Gr-NPs concentration. However, up to a Gr-NPs concentration of 0.7 wt% in the PHB/Gr-NPs nanocomposites, the PHB peaks are found to be prominent. Above 0.7 wt% concentration, Gr-NPs peaks in the XRD spectra dominated over the PHB peaks, which further confirmed the uniform dispersion of Gr-NPs in the PHB matrix upto an optimum concentration of 0.7 wt%. Further increase in the Gr-NPs concentration resulted in stacking of Gr-NPs in PHB matrix.

Crystallinity of the pristine PHB and PHB/Gr-NPs nanocomposites was estimated by dividing the area of the four major peaks observed by the reflection of (0 2 0), (1 1 0), (1 1 1) and (1 3 0) planes to that of the cumulative area of all the peaks present in the spectra. Crystallinity values of the pristine PHB and PHB with 0.3, 0.5 0.7, 1.0, 1.3 wt% of Gr-NPs are 40, 42.18, 47.5, 46.7 and 36.4%, respectively. Similar results on the increase in crystallinity with an increase in the nanofiller concentration have been reported in the literature (Bera and Maji, 2017). Increase in the crystallinity is indeed desirable as it enhances the thermal stability of a product (Pradhan et al., 2017) as discussed in the later section of this work.

5.3.1.4. Contact angle analysis

Hydrophilicity of the pristine PHB and PHB/Gr-NPs nanocomposites was estimated as water contact angle to study the surface change induced due to the addition of Gr-NPs into the PHB matrix. Gr-NPs are often considered as a hydrophobic material with a water contact angle of 127^{o} (Lan et al., 2016). Thus, the addition of Gr-NPs in the PHB matrix increased the contact angle of the pristine PHB from 62^{o} to a maximum value of

73.4, 73.4 and 75° with the addition of 0.7, 1.0 and 1.3 wt% of Gr-NPs, respectively. Contact angle results are displayed in Fig. 5.4, and the mechanism involved is shown in Fig. 5.4(c). This type of increase in contact angle with the addition of nanofillers has been reported in the literature. Goh et al. (2016) added reduced graphene oxide into the polylactic acid (PLA) matrix by forming a sandwich architecture, which resulted in an enhancement of contact angle to a few degrees in decimals. However, the steep increase in the contact angle from 62° to 75° due to the addition of Gr-NPs is advantageous for application in food packaging sectors. Polymeric films with a low contact angle are often not considered for food packaging applications as it may lead to unnecessary growth of foodborne microorganisms, thereby resulting in food spoilage (Han, 2005).

5.3.2. Barrier properties

As mentioned in the previous section, various semi-crystalline regions such as mesomorphic and melt regions in the PHB are permeable to oxygen molecules and water vapour. Entry of oxygen and water vapour through the packaging films is known to accelerate food deterioration, and, therefore, an ideal packaging film must be impervious to the surrounding atmosphere. In this study, the barrier properties of the PHB were enhanced by the addition of impermeable Gr-NPs to the PHB matrix. Presence of Gr-NPs made the polymeric film impervious to oxygen and water by creating a tortuous structure/pathway inside, thereby leading to a reduction in oxygen and water vapour permeability; however, above a certain concentration of Gr-NPs led to agglomeration which turned the pathway from tortuous to a direct one. A detailed schematic showing the influence of Gr-NPs concentration on barrier properties of the nanocomposite is depicted in Fig. 5.4(c).

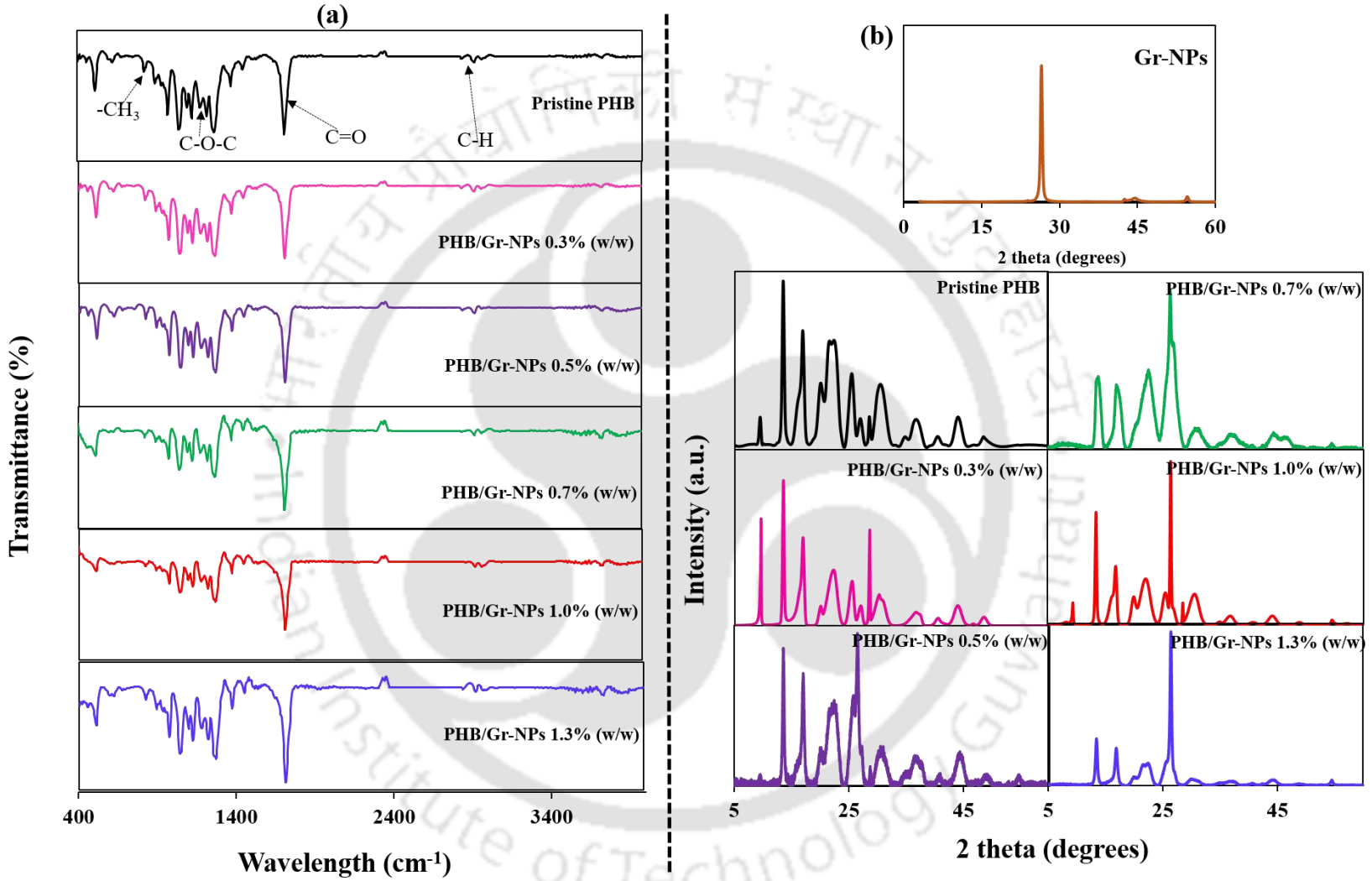

Fig. 5.3. (a) FTIR spectra and (b) XRD patterns of pristine PHB and PHB/Gr-NPs nanocomposite with varying concentration of Gr-NPs

Oxygen permeability (OP) and water vapour permeability (WVP) values of the pristine PHB are 1.53 $cm^3 \cdot mm/m^2 \cdot d^2 \cdot atm$ and 9.26 $g \cdot mm/m^2 \cdot d^2 \cdot atm$, respectively. Upon addition of 0.7 wt% of Gr-NPs, OP and WVP values of the PHB were reduced to 0.4 $cm^3 \cdot mm/m^2 \cdot d^2 \cdot atm$ and 4 $g \cdot mm/m^2 \cdot d^2 \cdot atm$, respectively. These values of OP and WVP were again high due to an increase in the Gr-NPs concentration to 1.3 wt%, and the values were 0.63 $cm^3 \cdot mm/m^2 \cdot d^2 \cdot atm$ and 5.8 $g \cdot mm/m^2 \cdot d^2 \cdot atm$, respectively (Fig. 5.4b). Hence, PHB matrix with 0.7 wt% of Gr-NPs was confirmed to be the optimum.

At an optimum concentration, the OP and WVP values obtained in the present study are comparable and, in many cases, even better than the reports available in the literature. For instance, the OP values of films made out of amylopectin, polyethene terephthalate, amylose and graphene oxide reinforced PLA are 1.4, 1.3, 0.7 and 0.6 $cm^3 \cdot mm/m^2 \cdot d^2 \cdot atm$, respectively (Goh et al., 2016). All these values are higher than the OP value (0.4 $cm^3 \cdot mm/m^2 \cdot d^2 \cdot atm$) observed in the present study. However, a study by Goh et al. (2016) (Goh et al., 2016) reported a high OP value of 0.2 $cm^3 \cdot mm/m^2 \cdot d^2 \cdot atm$, which was achieved at an elevated cost by preparing a sandwich PLA film of many layers laminated one over the other. It is worth mentioning that the permissible limit of OP value is 1.0 $cm^3 \cdot mm/m^2 \cdot d^2 \cdot atm$ (Xu et al., 2020), and the value reported in the present study is well below the permissible limit. The trend of change in OP value with variation in Gr-NPs concentration was found to be similar for variations in the water vapour permeability (WVP) value of the nanocomposites.

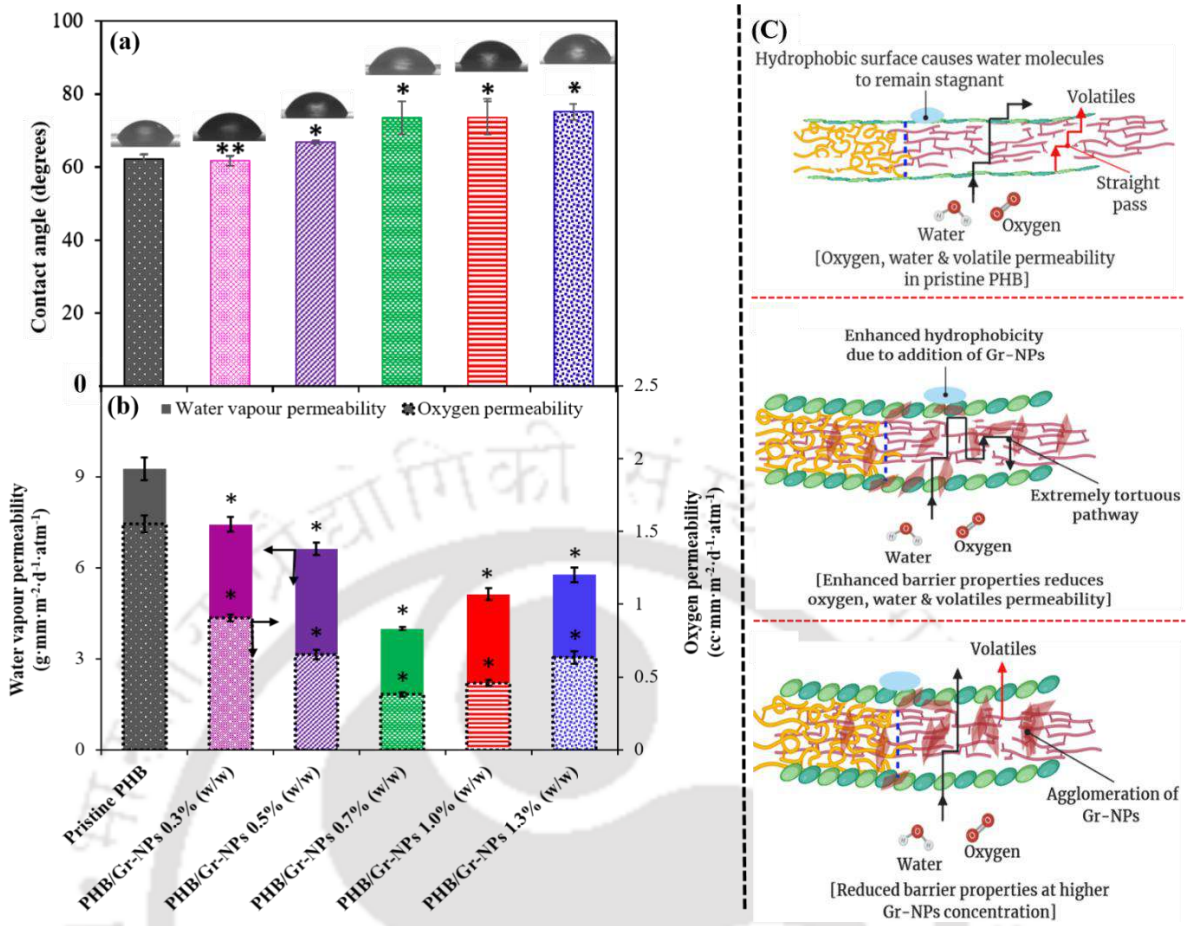

Fig. 5.4 (a) Contact angle and (b) barrier properties of pristine PHB and PHB/Gr-NPs nanocomposite with varying concentration of Gr-NPs and (c) schematic showing the effect of Gr-NPs concentration on PHB/Gr-NPs nanocomposite (* symbol above the bars indicates that the differences in the values are statistically significant at $P < 0.05$ and ** symbol above the bar indicates that the differences in the values are statistically insignificant at $P > 0.05$ by employing Turkey's test)

5.3.3. Shelf life (Θ) simulation

From the previous results of barrier property analysis, it was concluded that reinforcement of PHB with Gr-NPs improved both the oxygen and water vapour barrier properties. However, in order to realise the actual potential of the prepared PHB/Gr-NPs nanocomposite films for food packaging applications, it is essential to know the shelf life of food products packed using such film. In the present study, two different food products,

i.e. one quickly perishable milk product and other long-lasting potato chips were evaluated of their shelf life upon packaging with the current PHB/Gr-NPs nanocomposites films. In general, both these food products are sensitive to oxygen and moisture environment, and, therefore, it was assumed that these products deteriorate only due to the presence of oxygen and water vapour. All other environmental factors and microbial effects were neglected in the present study (Dhar et al., 2017; Goh et al., 2016). The shelf life with the pristine PHB for potato chips and milk products were 60 days and 6 days, respectively (Fig. 5.5). The low shelf life of the milk product is due to its quick deteriorating nature. With the addition of Gr-NPs, the shelf-life times were enhanced to 245 days and 26 days for potato chips and milk products, respectively, which is more than four times higher than with the pristine PHB.

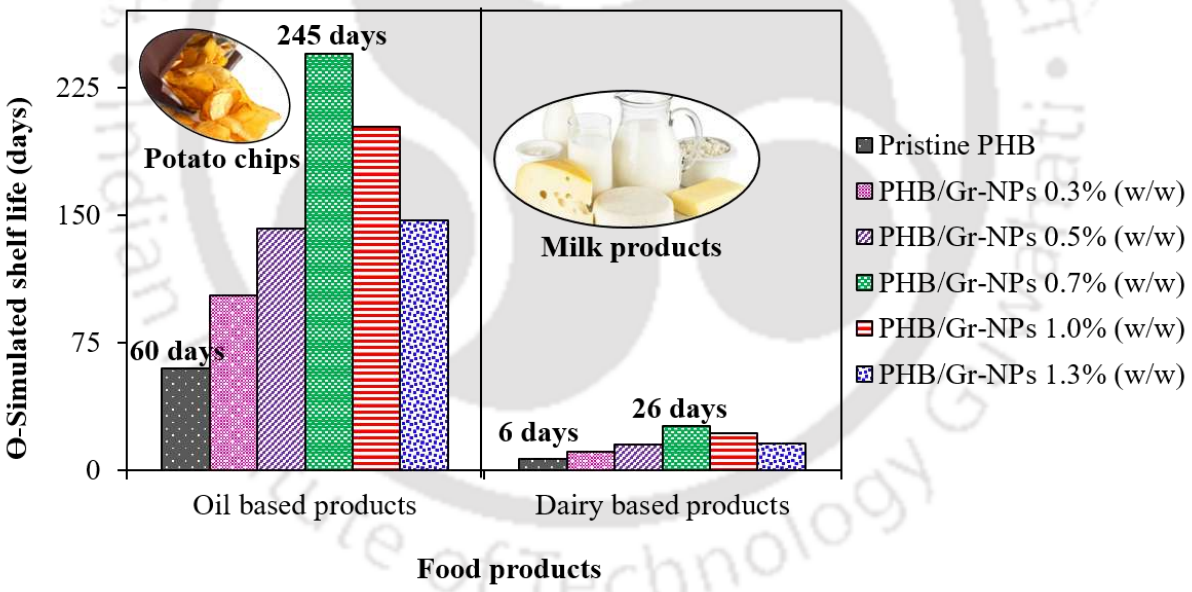

Fig. 5.5. Results of shelf life (Θ) simulation study of oil and dairy based food items packed using pristine PHB and PHB/Gr-NPs nanocomposite with varying concentration of Gr-NPs

This enhancement can be correlated to the reduction in the oxygen and water vapour permeability values observed with the addition of Gr-NPs. Dhar et al. (2017) (Dhar et al., 2017) on their study on preparation of packaging film by addition of olive oil to PLA by

reactive extrusion observed a maximum shelf life of 151 days and 17 days for oil-based products and milk-based food products, respectively.

5.3.4. Thermal characteristics

5.3.4.1. TGA analysis

The TGA plots shown in Fig. 5.6 clearly demonstrate that there is negligible weight loss observed for Gr-NPs due to an increase in the temperature. On the contrary, a steady single-step thermal degradation is observed for pristine PHB and PHB/Gr-NPs nanocomposites, which is identified by a single peak in the DTG analysis result (Fig. 5.6(a)). As reported by Pradhan et al. (2017) (Pradhan et al., 2017), the maximum degradation of the PHB based nanocomposites observed above 280 ^{o}C is due to the cleavage of the ester bonds to form crotonic acid from PHB. The temperature which relates to the extreme rate of weight reduction (T_{max}) is viewed as another critical property for the polymer composite framework.

The T_{max} is characterised as the peak value that is acquired from the first derivative of TGA thermograph. The T_{max} of the pristine PHB and PHB nanocomposite with varying Gr-NPs concentrations of 0.3, 0.7 and 1.3 wt% are 279.4 ^{o}C, 283.1 ^{o}C, 289.5 ^{o}C and 284.1 ^{o}C, respectively. The extended thermal stability can be attributed to the delayed release of volatiles upon addition of Gr-NPs (Fig. 5.4(c)). This increased thermal resistivity is an added advantage of the present PHB/Gr-NPs nanocomposites for extending its use in packaging of hot food materials even at an elevated temperature. Improvement in the thermal stability behaviour of the nanocomposites is further attributed to the presence of high-performance graphene material (Valapa et al., 2015).

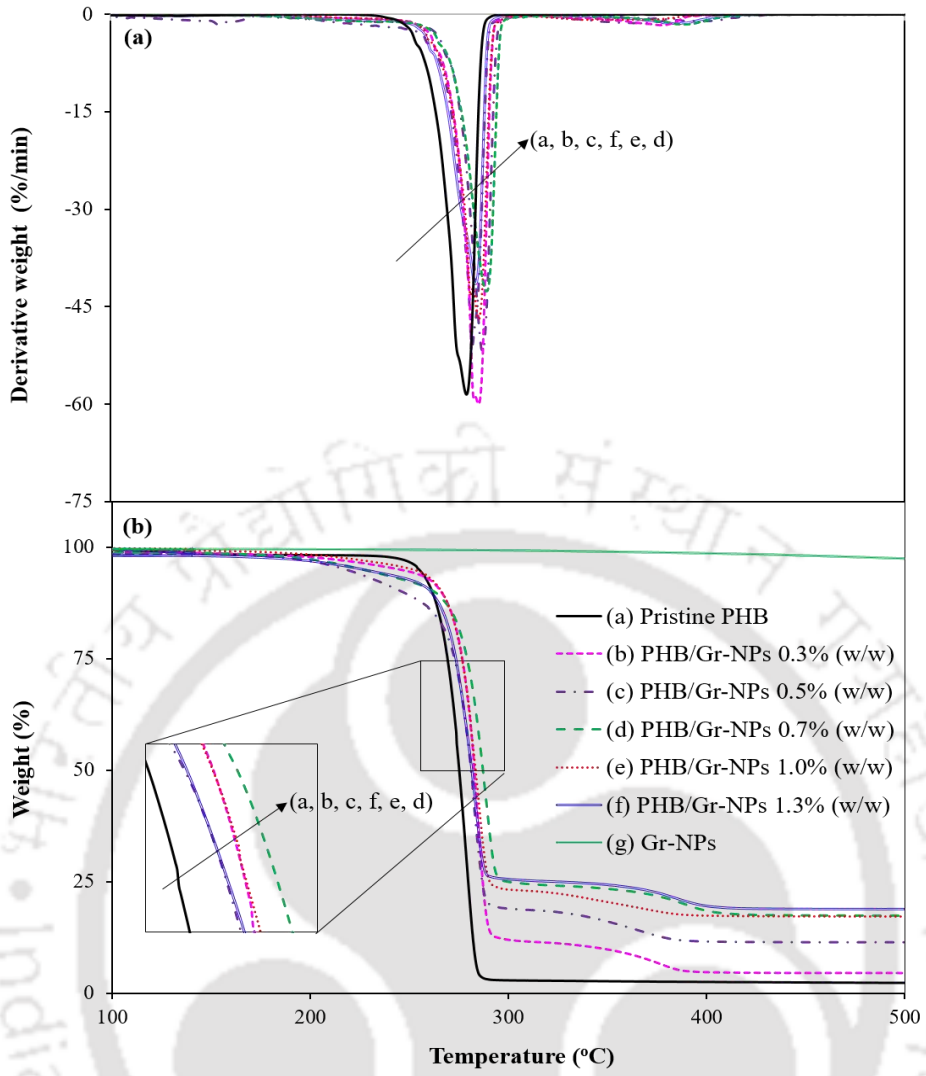

Fig. 5.6. (a) DTG and (b) TGA plots of pristine PHB and PHB/Gr-NPs nanocomposite with varying concentration of Gr-NPs

5.3.4.2. DSC analysis

Change in melt behaviour of pristine PHB and PHB/Gr-NPs nanocomposites were studied by DSC analysis and the DSC thermographs for these materials are shown in Fig. 5.7(a). The bimodal peak of the pristine PHB is unified to form a unimodal endothermic peak (Fig. 5.7(a)) upon addition of Gr-NPs. This can be seen in the melting area of PHB (T_m 172°C), which indicates the crystalline type of PHB. This type of formation of unimodal endotherm peak from bimodal peak shows the absence of heterogeneous passage of crystal and uniform crystal thickness created after reinforcement of Gr-NPs.

A simple schematic showing the different phases of PHB, viz. lamellar, mesomorphic and melt region and nucleation brought about by the addition of Gr-NPs is shown in Fig. 5.7(b). The mechanism illustrated in Fig. 5.7(b) is in agreement with the reports available in the literature by Xu et al. (2015) and Valapa et al. (2015). The increase in Gr-NPs concentration from 0.1 wt% to 0.7 wt% in the PHB matrix enhanced the melting temperature (T_m) value by 10 ^oC (Fig. 5.7(a)), which can be attributed to the reduction in the basic core measure required for the arrangement of a thick and stable core in PHB (Valapa et al., 2015; Xu et al., 2015). These results reveal that Gr-NPs act as a nucleating agent by improving T_m. Similar results were observed by Xu et al. (2015) during the reinforcement of polyethylene glycol (PEG) grafted graphene oxide into PLA matrix. The 10 ^oC increase in the T_m observed in this study is an added advantage of the PHB/Gr-NPs nanocomposites for extending its use in packaging of hot food materials even at an elevated temperature.

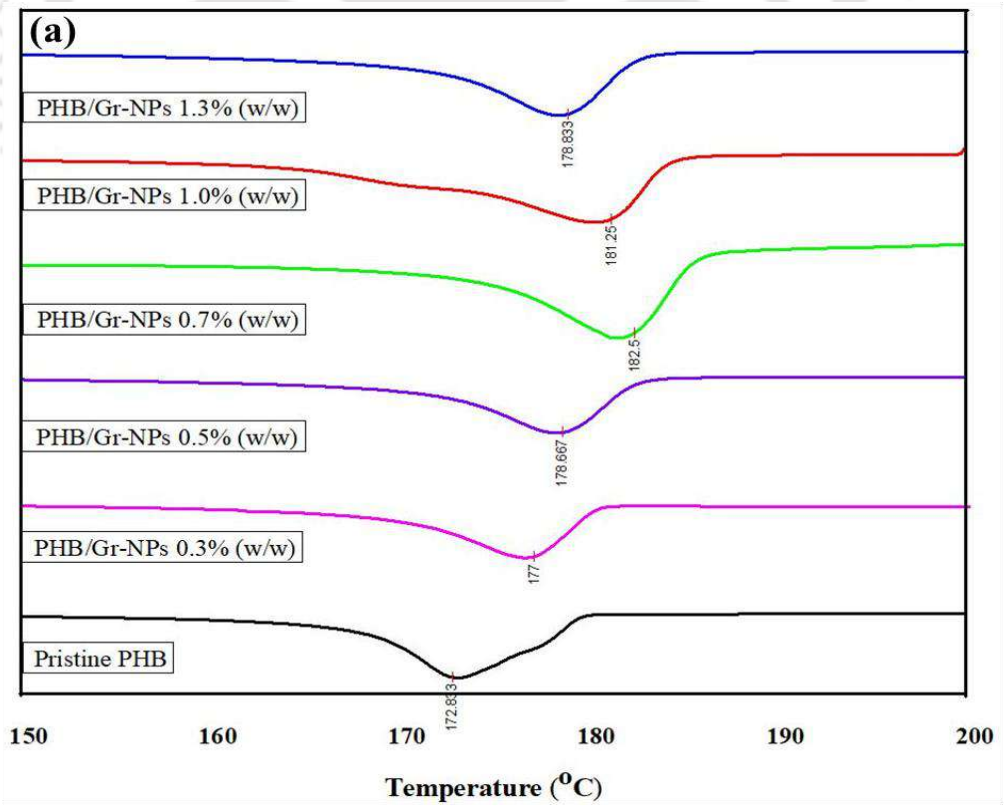

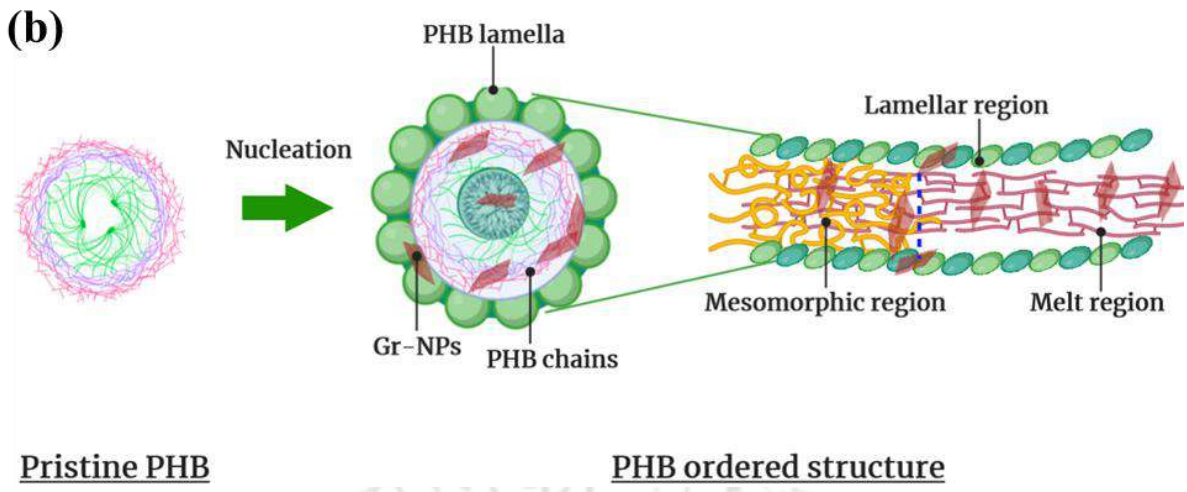

Fig. 5.7. (a) DSC thermographs for PHB and PHB- graphene composites made with varying concentrations of Gr-NPs and (b) mechanism showing the nucleating action of Gr-NPs

5.3.5. Transmittance and Tensile characteristics

5.3.5.1. Transmittance analysis

Transparency to visible and UV lights is a crucial parameter in preparing polymeric material for food packaging applications. Exposure of polymeric material to an intense UV irradiation of wavelength ranging from 200 to 400 nm may result in photochemical degradation of the polymeric material. Whereas strong transparency to visible light of wavelength ranging from 400 to 600 nm may result in deterioration of light-sensitive food products. Almost 90% of transparency in the UV region and 95% of transparency to visible light is observed for the pristine PHB (Fig. 5.8). Being an opaque material, increasing Gr-NPs concentration in the PHB matrix drastically reduced transparency to both visible and UV lights. For instance, Gr-NPs concentration of 0.7 wt% in the PHB matrix resulted in a three times reduction in the transparency value to both visible and UV lights.

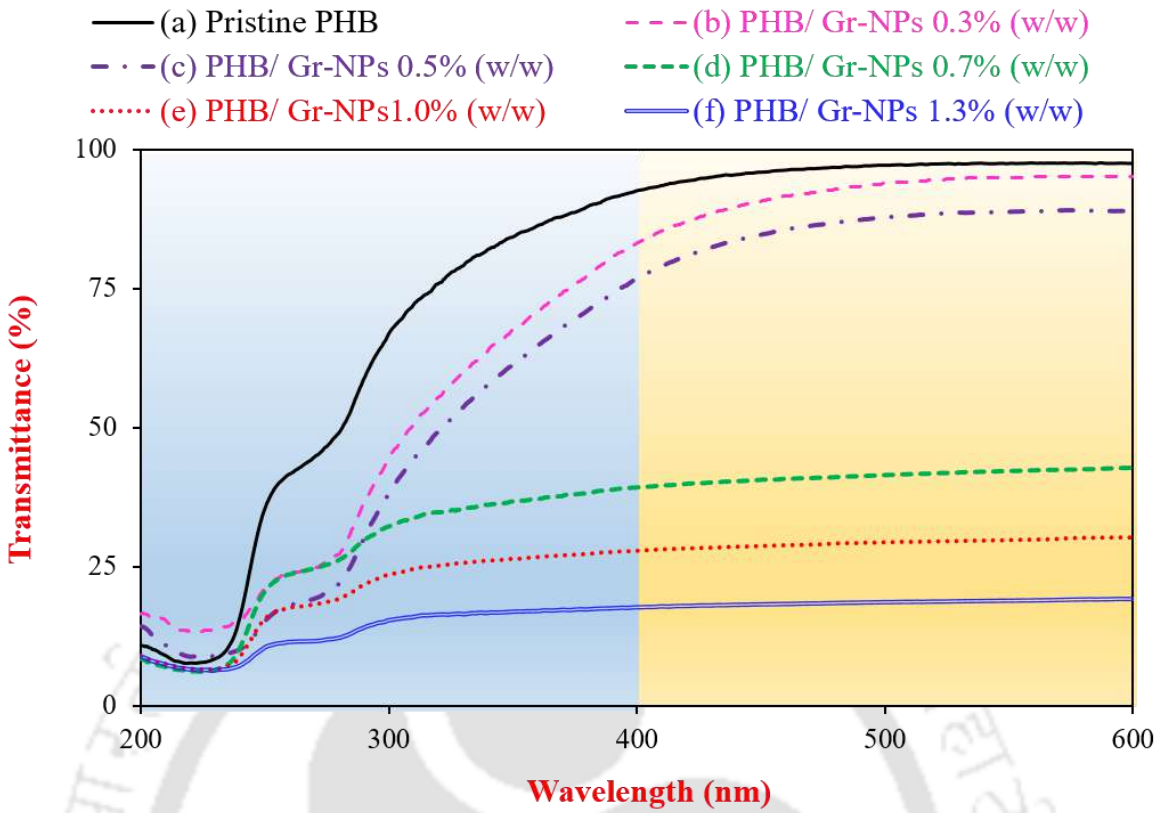

Fig. 5.8. Transparency of pristine PHB and PHB/Gr-NPs nanocomposite with varying concentration of Gr-NPs to UV/visible lights

Further increase in Gr-NPs concentration resulted in a drastic decrease in the transparency value. However, due to its effort on other properties and agglomeration effect above 0.7 wt%, the same Gr-NPs concentration was chosen as the optimum. This reduction in transparency to the visible and UV lights is in line with a study by Valapa et al. (2015); the addition of 0.5 wt% of graphene in the PLA matrix was reported to reduce transparency by nearly 50%. Such reduction in transparency is desirable as these polymeric films can be suited for storing light-sensitive food materials, including vitamins, lipids, flavours and pigments (Valapa et al., 2015).

5.3.5.2. Tensile properties

The tensile properties of the pristine PHB and PHB/Gr-NPs nanocomposites are shown in Fig. 5.9(a). The tensile stress and elongation at break of the pristine PHB are found to be

4.5 MPa and 15%, respectively, and the values match well with the literature reports (Kai et al., 2019, 2018). The value of tensile stress steadily increased with the addition of Gr-NPs to the PHB matrix, however at the cost of reduced tensile strain. For instance, increase in Gr-NPs concentration from 0.3 wt% to 1.3 wt% resulted in the increase in tensile stress value from 7.5 MPa to 12.2 MPa, but at the same time, the tensile strain dropped from 14.9% to 8.5%. These results further confirm that 0.7 wt% of Gr-NPs concentration is optimum, and at this concentration, the tensile stress and tensile strain values are found to be 9 MPa and 12.2%, respectively.

Incorporation of graphene, which is the strongest material ever tested, in the PHB matrix with uniform dispersion resulted in the enhancement of tensile stress. The drop in elongation at break can be attributed to the brittleness due to the addition of Gr-NPs in the PHB matrix. Similar observations of reduction in elongation at break with an increase in the concentration of graphene-based nanomaterials were reported in the literature (Javanbakht and Namazi, 2018). In order to understand the role of Gr-NPs in imparting mechanical strength to the PHB/Gr-NPs nanocomposites, FESEM analysis of PHB/Gr-NPs (0.7 wt%) was carried out during different stages of elongation and the same is depicted in Fig. 5.9(b). It is clearly noticed that in the initial step, (i.e., specimen before subjecting it to tensile load) Gr- NPs were uniformly dispersed in the PHB matrix. And in the second step upon application of tensile load, Gr-NPs loses its grip to form passages of blank PHB. Finally, on passages of blank PHB, crevices are created, thereby leading to specimen fracture. The FESEM analysis results shown in Fig. 5.9b clearly established the role of Gr-NPs in binding the PHB polymeric chains.

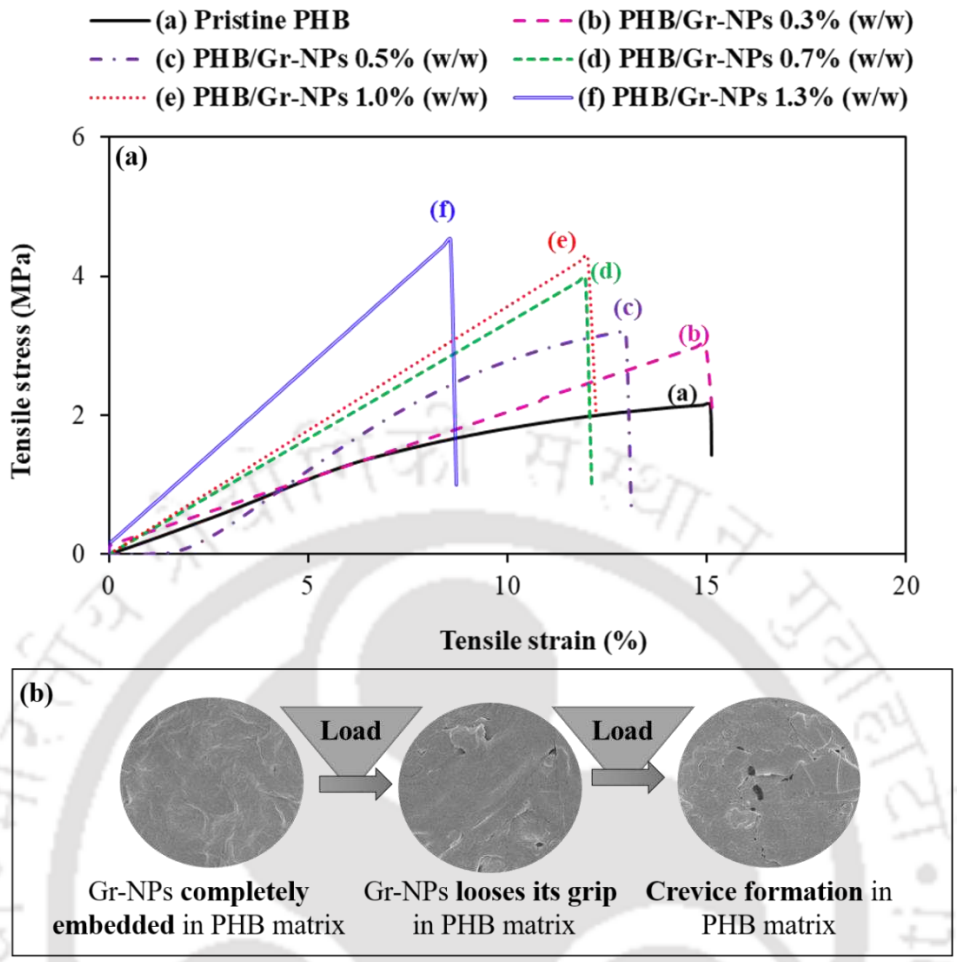

Fig. 5.9. Results of (a) tensile strength analysis of pristine PHB and PHB/Gr-NPs nanocomposite with varying concentration of Gr-NPs, and (b) FESEM analysis on the elongation of PHB/Gr-NPs nanocomposite

5.3.6. Cytotoxicity analysis

Cytotoxicity analysis of the pristine PHB, Gr-NPs and PHB/Gr-NPs nanocomposites was carried out to examine the suitability of the present polymeric nanocomposites in food packaging applications (Shahbazi et al., 2016). Cell viability of the pristine PHB, Gr-NPs and PHB/Gr-NPs was reported in Fig. 5.10(a). Cytotoxicity is referred to as percentage cell viability subtracted with cent percentage. For instance, the 100% cell viability observed for the control experiments denotes no cytotoxicity in that particular experiment. However, a drastic reduction in cell viability (21%) with test sample containing only graphene, portrays

cytotoxicity of 79%. In comparison with the control experiment, cell viability of the pristine PHB and PHB/Gr-NPs nanocomposite with Gr-NPs concentration of 0.7 wt% showed no cytotoxic effect with a statistical difference P value less than 0.05. However, above this concentration, the polymeric nanocomposite showed some cytotoxic effect on the treated cells.

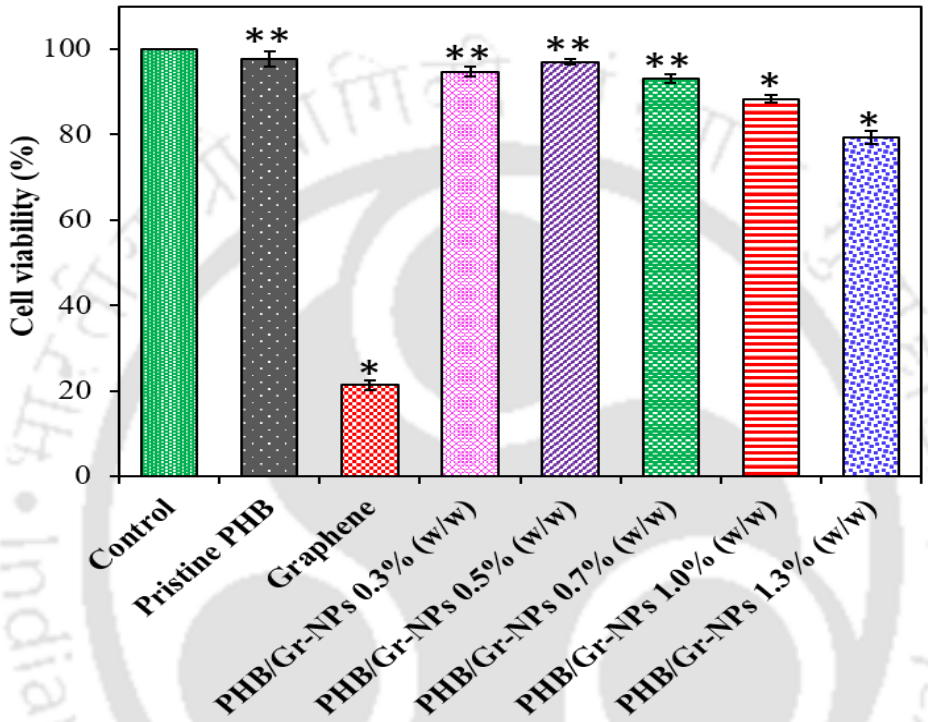

Fig. 5.10. Cytotoxicity analysis of pristine PHB and PHB/Gr-NPs nanocomposite with varying concentration of Gr-NPs (* symbol above the bars indicates that the differences in the values are statistically significant at $P < 0.05$ and ** symbol above the bar indicates that the differences in the values are statistically insignificant at $P > 0.05$ by employing Turkey's test)

Fluorescent microscopy analysis was carried out as a support to the aforementioned MTT assay, and the results are shown in Fig. 5.11. The results clearly demonstrate the presence of only trypan blue stained macrophage cells in control experiments and other experiments conducted using pristine PHB and PHB/Gr-NPs nanocomposites with a maximum Gr-NPs concentration of 0.7 wt%. Trypan blue-stained cells with green colour

indicate live cells. Above Gr-NPs concentration of 0.7 wt% cells stained with red coloured propidium iodide are seen. The red colour cells indicate dead cells. Furthermore, the experiment carried out with only Gr-NPs clearly showed the mortality effect of Gr-NPs on cells. This adverse effect observed due to the excess concentration of Gr-NPs or with Gr-NPs only can be attributed to the sharp edges and corners present in the Gr-NPs, which act as a blade in slicing away the live cells (Pham et al., 2015). This effect of Gr-NPs on cells was further confirmed by TEM and AFM analyses, which revealed that the cells followed treatment with Gr-NPs contained corroded or ruptured cell wall (Fig. 5.11).

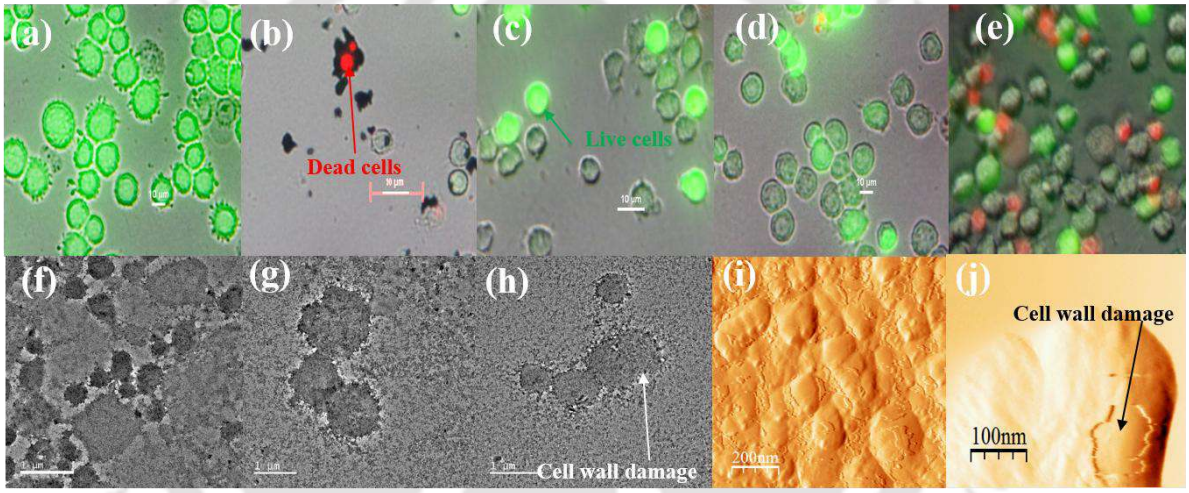

Fig. 5.11. Fluorescent microscopy analysis of the cells from (a) medium only well, (b) graphene only well, (c) pristine PHB, (d) PHB/Gr-NPs 0.7% (w/w), (e) PHB/Gr-NPs 1.3% (w/w), (f) TEM analysis of cells from medium only well, (g) TEM analysis of cells from well containing PHB/Gr-NPs 0.7% (w/w), (h) TEM analysis of cells from well containing PHB/Gr-NPs 1.3% (w/w), (i) AFM analysis cells from well containing PHB/Gr-NPs 0.7% (w/w) and AFM analysis of cells from well containing PHB/Gr-NPs 1.3% (w/w)

5.3.7. Biodegradation experiment

Being a biodegradable polymer, it is necessary to study the change in the biodegradability of PHB due to the addition of Gr-NPs to the PHB matrix. The results of biodegradation

experiments performed in the mid of February till the end of March 2019, as shown in Fig. 5.12. Morphological changes in PHB/Gr-NPs 0.7% (w/w) during the course of the experiment were analysed by FESEM analysis, and as shown as inset to Fig. 5.12. Biodegradation of the nanocomposite was observed even from the very first withdrawal of sample on 5^{th} day of the experiment. The biodegradation of all the samples increased steadily and lasted for a total time period of about 30 days. At the end of 30 days, all the samples were 100% degraded, though some polymeric remains were found with PHB/Gr-NPs nanocomposites, which were, however, statistically insignificant ($P > 0.05$) (Fig. 5.12).

Compared to pristine PHB, PHB/Gr-NPs nanocomposites showed resistance to degradation by soil microorganisms, which is due to antimicrobial activity of Gr-NPs added in the polymeric nanocomposite. Morphology analysis of the samples clearly showed degradation of PHB with no effect on Gr-NPs. This type of degradation is due to the secretion of extracellular enzymes by the soil microorganism. In the case of PHB degradation, PHB depolymerase enzyme selectively converts PHB polymer to hydroxybutyrate monomeric units, and thereafter, which is then utilised as carbon source by the soil biota (Joyyi et al., 2017). Thus, the present study on incorporation of Gr-NPs into PHB matrix resulted in PHB based polymeric nanocomposites having a superior barrier, thermal and tensile properties. Further, the prepared nanocomposite was found to be environmentally safe and highly biodegradable. However, in the present study, PHB/Gr-NPs nanocomposite was prepared by following a laboratory-scale solution casting method. Hence future research on the use of melt processing techniques such as extrusion-cum-blow moulding for large scale production of PHB/Gr-NPs nanocomposite is warranted to realise its commercial potential.

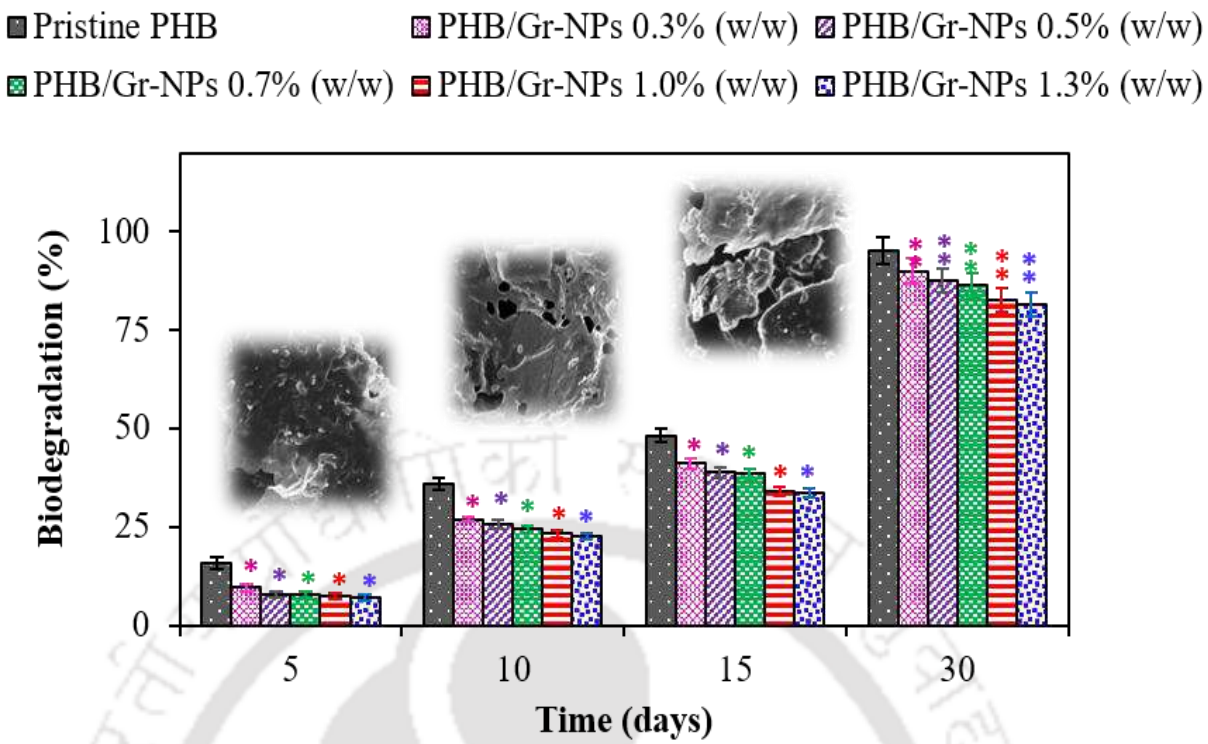

Fig. 5.12. Biodegradation result of pristine PHB and PHB/Gr-NPs nanocomposite with varying concentration of Gr-NPs (* symbol above the bars indicates that the differences in the values are statistically significant at $P < 0.05$ and ** symbol above the bar indicates that the differences in the values are statistically insignificant at $P > 0.05$ by employing Turkey's test). The inset image shows the change in surface morphology of the 0.7 wt% PHB/Gr-NPs nanocomposite during the course of biodegradation as noticed by FESEM analysis

5.4. Summary

PHB based nanocomposites were prepared by dispersing Gr-NPs in PHB matrix using a simple solution cast method. FESEM analyses revealed that Gr-NPs were uniformly distributed in the PHB matrix at an optimum concentration of 0.7 % (w/v). Above this concentration, the Gr-NPs were found to get agglomerated in the PHB matrix. PHB nanocomposites with 0.7 wt% Gr-NPs displayed improved melting point, thermal stability, tensile strength and barrier properties. Transparency to UV and visible light was significantly reduced with the addition of GR-NPs. In addition to negligible cytotoxic

effect, the PHB nanocomposite improved the shelf life of certain food products and showed high biodegradability by soil microorganisms. Thus, the nanocomposite based packaging film prepared in this study is highly used for packaging applications.

Chapter 6

Techno-economic assessment of large scale polyhydroxybutyrate (PHB) production from carob pods in a closed-loop biorefinery based setup with novel bioprocessing strategies

Abstract

High cost of feedstocks and processing steps/strategy limits realizing the commercial production of polyhydroxybutyrate (PHB). In this context, the use of lignocellulosic feedstock and novel bioreactor system, as well as downstream processing employing ceramic membranes, seem attractive for commercial PHB production. Therefore, the present study details the techno-economic analysis of the various novel strategies for PHB production from carob pods, which is a waste lignocellulosic biomass. This study compared different scenarios (SC1 to SC4), wherein SC1 involved the utilization of costly pure sugars as feedstock for PHB production, and SC2 to SC4 considered sugars extracted from carob pods as the cheap carbon source. The main features of SC2, SC3 and SC4 involve the use of a conventional stirred tank bioreactor (STBR), annular bioreactor (ABR) and novel ceramic membrane for biomass separation, respectively. Effectiveness of PHB production under the various scenarios was evaluated based on its pay-out period and turnover accumulated at the end of 7^{th} year of a PHB plant operation. Instead of the use of pure sugars as the feedstock (SC1), the use of carob pod extract (SC2) as the alternative feedstock reduced the pay-out period from 12.6 to 6.8 years. Likewise, switching onto ABR instead of the conventional STBR decreased the pay-out period from 6.8 to 4.8 years and increased the turnover from 0.06 to 1.35 billion USD. Finally, solid-liquid separation using ceramic membranes (SC4) instead of centrifugation resulted in a similar pay-out period of 4.8 years along with an increase in the turnover of about 1.4 billion USD. Thus, in SC4, a significant decrease in the cost of the sugar feedstock along with an improved PHB titre in ABR and incorporation of low-cost ceramic membrane technology for PHB rich biomass separation resulted in a highly cost-effective PHB production strategy.

6.1. Introduction

Polyhydroxybutyrate is well known as a successful substitute for the conventional petroleum-based polymer. Unlike other biodegradable polymers, which rely on crude oil for its production, PHB entirely relies on sustainable feedstock (Arul Manikandan et al., 2020). PHB is of microbial origin and shows high stereoregularity. Despite the many attractive features, PHB is unable to hit the commercial market because of the cost incurred in various stages of PHB production, starting with feedstock selection to its final preparation. On the other hand, waste generated from various agro-industries is gaining importance as a sustainable feedstock for PHB production (Al-Battashi et al., 2019). However, for establishing the commercial potential of such new technologies, techno-economic assessment is inevitable. For instance, Levett et al. (2016) evaluated the techno-economics of PHB production by thermophilic bioprocessing of methane as the cheap feedstock. The authors reported that the thermophilic process resulted in a three-fold reduction in the operating cost, which is otherwise incurred for heat removal in the mesophilic process for PHB production. Naranjo et al. (2014) studied the effect on carbon footprint and water utilization by replacing pure sugars as feedstock with sugars obtained from residual banana for PHB production in an integrated biorefinery approach. Finally, Shahzad et al. (2017) examined the techno-economic feasibility of polyhydroxyalkanoate (PHA) produced from slaughterhouse wastewater as the starting material. More specifically, the various components fractionated from lignocellulosic biomass can be well used for PHB production.

The genesis of polyhydroxyalkanoates (PHAs) dates back 1950s, and thereafter oil crises during the 1970s led to the development of industrial-scale PHB production (Ray and Kalia, 2017). Since then, various companies were started around the globe for PHAs production by initiating the production process with one or more of their own patented

bioconversion technologies. For instance, Enmat™ developed its own polyhydroxybutyrate valerate (PHBV) production using a novel water-based extraction technology, which the company patented in the year 2004. Recently, AirCarbon™ patented its award-winning microorganism based 9X biocatalyst for the conversion of greenhouse gases to bioplastic (Levett et al., 2016). Table 6.1 summarizes the PHA production firms across the world, along with their trade name and production capacity.

Table 6.1. Industrial production of polyhydroxyalkanoates (Dietrich et al., 2017; Levett et al., 2016; Ray and Kalia, 2017; Shogren et al., 2019)

Company name	**Country**	**Trade name**	**Carbon substrate**	**PHA type**	**Production capacity (tons/annum)**
Biomers	Germany	Seluma™	Canola oil	PHB	15,000
Metabolix	USA	Mirel, Mvera™	Switchgrass, camelina, sugar cane	PHAs	10,000
TianAn Biologic Material Co	China	ENMAT	Corn/cassava starch	PHBHV	10,000
Tianjin GreenBio	China	SoGreen™	Corn starch	P3HB4HB	10,000
Bio-on	Italy	Bio-on™	Beet or sugar cane	PHA	10,000

Shenzhen Ecomann Biotech. Co	China	-	Corn starch	PHA	5000
PHB Industrial	Brazil	Biocycle™	Sugar cane	PHB	2000
Kaneka	Japan	AONILEX™	Vegetable oil	PHAs	1000
Biomer		Biomer P™	Sugar (sucrose)		1000
Newlight Technologies	California	AirCarbon™	Waste methane	PHA	>500

In the present study, carob pod was used as a novel feedstock for upstream to downstream processing in PHB production (Arul Manikandan et al., 2020). Along with the replacement of pure sugars with raw carob pod extract, the incorporation of other innovative process alternatives such as the use of annular bioreactor (Arul Manikandan et al., 2018) and ceramic membrane based separation process (Arul Manikandan et al., 2019) was examined for this effect on the PHB production cost and economics. Fig. 6.1 thus depicts the different scenarios considered for studying this effect on PHB production cost and economics.

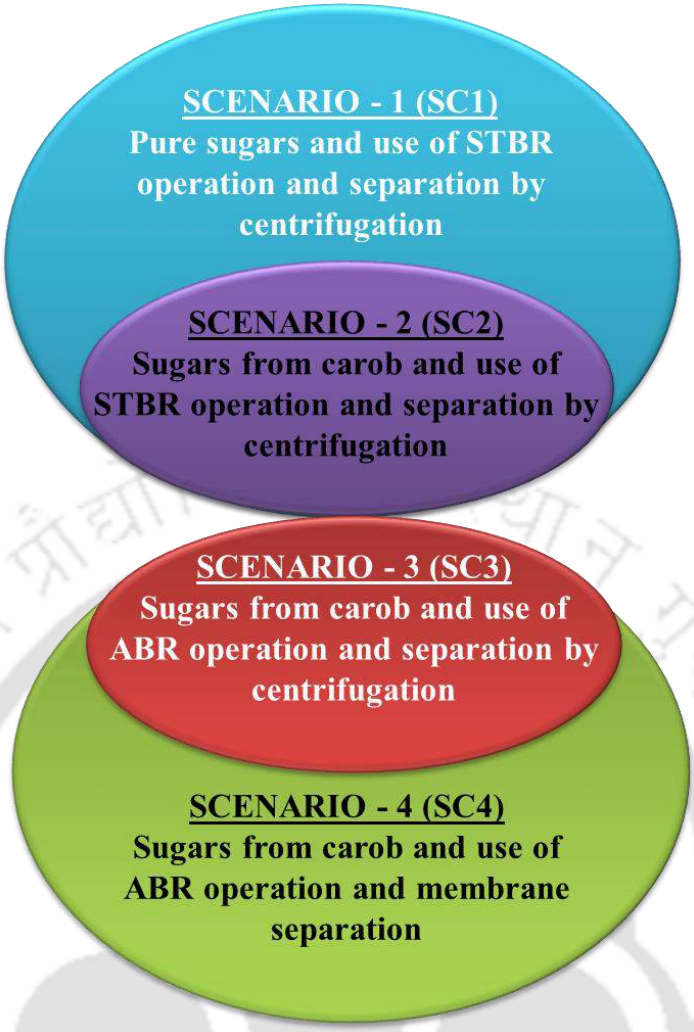

Fig. 6.1. Various scenarios considered for techno-economic assessment of PHB production in this study.

The key aspects of the present study on techno-economic assessment of polyhydroxybutyrate (PHB) production following a closed-loop biorefinery model involving novel process alternatives are as follows:

1) Full-scale process design for PHB production using carob pod biomass as the feedstock for PHB production in a closed-loop biorefinery approach.
2) Feedstock and key component analysis for PHB production along with its capital and annual operating cost.
3) Techno-economic assessment of PHB production under the different scenarios.

6.2. Methodology

6.2.1. Base cost for constructing a PHB producing plant

PHB production in this study is based on agro-industry residues, particularly from the bean gum industry. In order to transport the feedstock, an annual transportation cost of 0.38 million USD was allocated, as reported by Levett et al. (2016) for techno-economic assessment on PHB production. A yearly requirement of 0.1 TMC (thousand million cubic feet) of freshwater is estimated with an average cost of about 1.18 million USD. And further, it was stated that the water rate in Gujarat is lowest in comparison with other states in the country (Shah, 2010).

Due to a high PHB production capacity planned in this study, a total industrial space of 70 acres is chosen for the present study, which is quite higher than the 20 acres industrial area, Danimer Scientific®, Georgia - a Biotechnology company, for PHB production (Levett et al., 2016). Construction and erection of all components required for PHB production from upstream to downstream processing and product finishing are detailed in a later section. A nominal construction cost of 6.94 million USD was allotted to build the over cover for the industrial area and buildings to shelter administration and research arena. As water treatment facilities are inevitable for any process industry, a reasonable cost of 4 million USD was allotted. The cost estimate is based on a study by Shahzad et al. (2017) treating slaughter house wastewater (SHWW) as the feedstock for biopolymer production. Furthermore, an annual operation cost of 0.83 million USD was allotted for operating the wastewater treatment facilities, which comprise of various units viz. settler, aeration tank and sludge thickener to reduce the COD and BOD load to less than the permissible limit. Thus the base cost for the proposed industry as presented from Table 6.2 is calculated and found to be 23.06 million USD; the raw material and equipment cost needed for PHB

production were categorized under raw material and key-component requirement and detailed under a separate section.

Table 6.2. Base cost for the PHB production plant irrespective of the different scenarios considered in the study

S. No.	Components	Quantity/measure	Cost (USD in millions)
1	Industrial land for the proposed PHB plant	70 acres	9.72
2	Construction cost		6.94
3	Freshwater for industrial use	0.1 TMC*	1.18
4	Transportation cost		0.38
5	Wastewater treatment facilities and its annual operating cost		4 + 0.83
	Total base cost for the PHB plant		**23.06**

*TMC - Thousand million cubic feet

6.2.2. Background of the study

The techno-economic assessment was carried out on a novel PHB production strategy based on closed-loop biorefinery model utilizing lignocellulosic biomass, particularly carob pods, as a self-sufficient feedstock for upstream to downstream processing of the bioproduct. Compared with the costly sugars for polyhydroxybutyrate (PHB) production, carob pods are cheap and often refused from the locust bean gum industry (Carvalho et al., 2016, 2014). Approximately 400,000 tons of carob pods are produced annually around the world (Carvalho et al., 2014). In this closed-loop biorefinery model for PHB production, an innovative and unconventional annular bioreactor system and a novel ceramic-based

membrane separation processes were incorporated for PHB production. Key findings from the method followed for techno-economic assessment of PHB production are as follows: The carob pods are first treated with methanol to recover lignin, which is determined to be 3 g/L in terms of Gallic acid equivalents (GAE). As the second step, sugars present in the delignified carob pods are extracted using water, which yields ~ 40 g/L of sugars with 20 g/L of sucrose as the major sugar present in it, followed by glucose and fructose concentrations of 13 g/L and 7 g/L, respectively. Along with the aforementioned carob extract, several other minerals in the form of mineral salt medium (MSM) were provided in the production medium. The MSM composition is as follows (g/L): pottasium dihydrogen phosphate (KH_2PO_4), 2.0; di-sodium hydrogen phosphate (Na_2HPO_4), 0.6; magnesium sulphate heptahydrate ($MgSO_4 \cdot 7H_2O$), 0.2; calcium chloride ($CaCl_2$) 2.0; and 10 mL/L of trace metal solution. Furthermore, the trace metal solution comprised of (mg/L): zinc sulphate heptahydrate ($ZnSO_4 \cdot 7H_2O$), 1.3; ferrous sulphate heptahydrate ($FeSO_4 \cdot 7H_2O$); 0.2; ammonium molybdate tetrahydrate ($(NH_4)_6Mo_7O_{24} \cdot 4H_2O$), 0.6; and boric acid ($H_3BO_3$) 0.6. For techno-economic assessment, production medium consisting of these sugars and minerals is scaled up to 5000 m^3 bioreactor, planned to be operated in 96 batches, which is a year for PHB production.

Screening experiments concluded that *Ralstonia eutropha* outperformed the *Bacillus megaterium* in terms of its capability to grow on the carob pod extract containing MSM with a maximum PHB titre of 12.2 g/L (Arul Manikandan et al., 2020). Concentrated lignin from the first step was diluted with different proportions of chloroform to extract PHB from the bacterial biomass. Secondly, a novel annular bioreactor (ABR) with improved hydrodynamics was used for the cultivation of *Ralstonia eutropha* in pure carob pod extract supplemented with the MSM. It was found that at the end of 90 h of fed-batch operation, the ABR with double dosage of sugars resulted in a very high PHB production

of 70.8 g/L. However, with the same substrate, STBR performed poorly, thereby resulting in a low PHB concentration of 44.2 g/L (Arul Manikandan et al., 2020). Finally, ceramic membrane-based separation of PHB rich biomass from culture broth using a novel ceramic membrane assembly was opted owing to its low energy requirement. The ceramic membrane was found to be highly efficient (99.9%) in recovering the PHB from the culture broth along with an optimal permeate broth flux of 52 L/m^2h (Arul Manikandan et al., 2019). These results from laboratory studies were adopted for scaling up PHB production in a 5000 m^3 bioreactor that is planned to operate in 96 batches a year for carrying out the present techno-economic assessment analysis.

6.2.3. Cost for the raw materials requirement

The raw materials required for PHB production from upstream to downstream processing and product finishing under SC1 and SC2 to SC4 are portrayed in Fig. 6.2(a) and 6.2(b), respectively. It can be seen from Figure 6.2a that the pure sugars viz. sucrose, fructose, glucose and pure lignin were purchased only in SC1, whereas in SC2, SC3 and SC4, the necessary sugars are obtained from carob pods. The feedstock requirement for upstream processing of PHB production was calculated based on the results of Fed-batch experiments. Since the fed-batch experiment was lasted for 90 hours and nearly 96 batches of PHB production can be performed annually using a bioreactor of capacity 5000 m^3. The bioreactor capacity chosen in the present study is quite similar to that reported by Levett et al. (2016). The total number of batches, i.e., 96 in the present study was calculated based on the assumption that there is zero accident in a calendar year, which is quite achievable (Gupta et al., 2015). For instance, Biocon^{TM} India reported zero accidents in the last year, 2019 (Biocon Limited, 2019). Other than the upstream requirements, feedstock required for PHB extraction, finishing the product and various other elements like steam needed in the process flow was also included in Fig. 6.2. The cost of the chemicals is based on a

commercial supplier (Alibaba.com). Furthermore, a complete flowsheet for the PHB production using carob pods as feedstock considering SC4 was developed using Aspen plus^{TM} V10 software and is shown in Fig. 6.3.

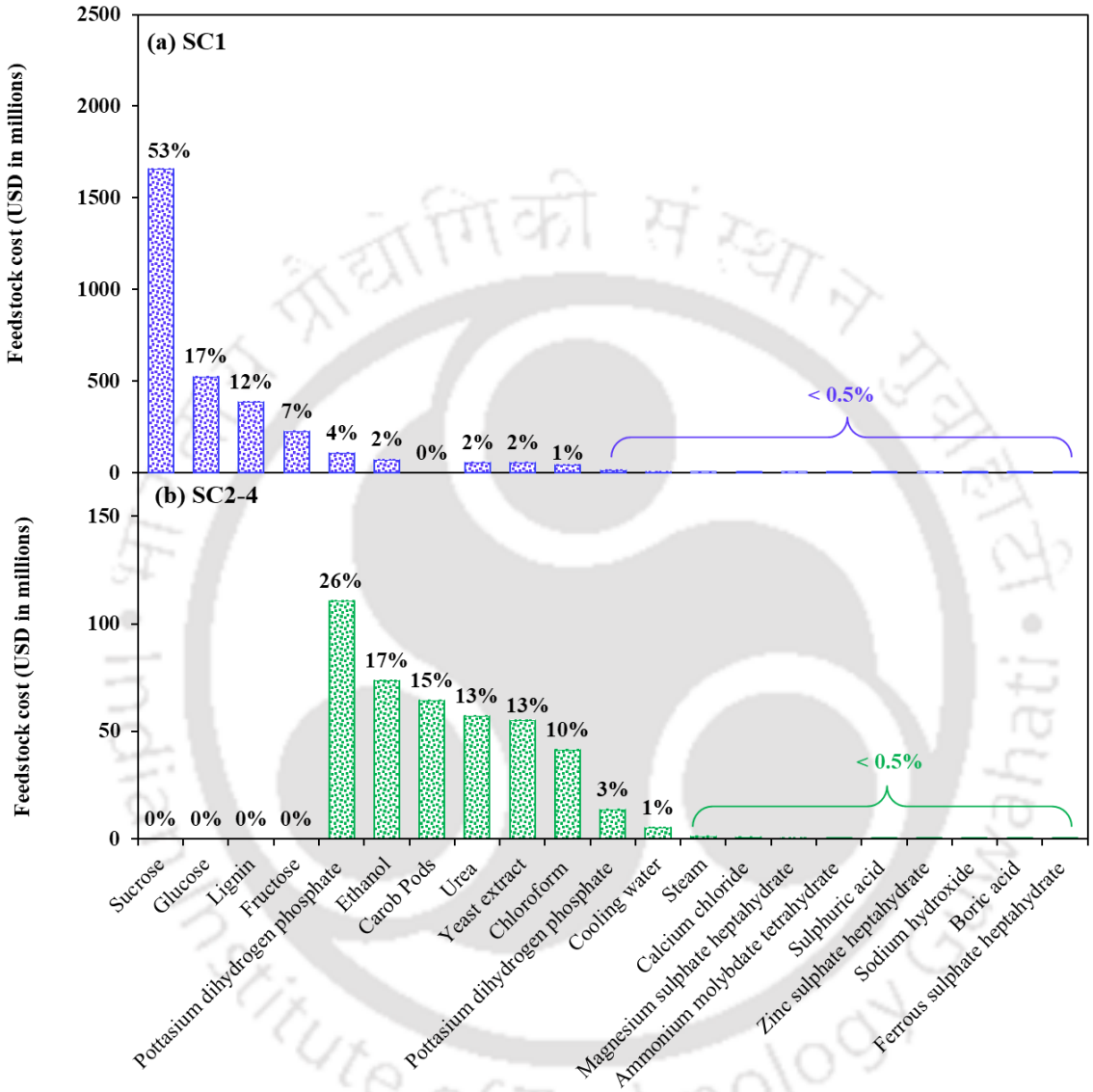

Fig. 6.2. Feedstock requirements for PHB production considering different scenarios: (a) SC1 and (b) SC2 to SC4.

6.2.4. Process flow in PHB production using carob pods under SC4

Fig. 6.3(a) shows a schematic of PHB production from carob pods considering SC4. The process flow consisting of carob pods (CAROBPOD) is first delignified by soaking it with methanol (METH1) in a soaking vessel (SVESSEL), outlet (SOUT) from the SVESSEL

comprises of delignified carob pods (DLPODS) and lignin-containing methanol (LIGMETH) solution, which are separated by passing the stream through screen 1 to get DLPODS and LIGMETH solution. The LIGMETH solution is then fractionated in a distillation column (DIST1) to obtain lignin (LIGNIN) and methanol (METH2) as the top and bottom product, respectively. Whereas the LIGNIN is reused later for extraction of PHB from bacterial biomass, METH2 stream is recycled back and mixed (MIX1) with fresh methanol (FMETH) for the delignification process. DLPODS separated from the screens were primarily crushed using a roll crusher (ROLLC) to get size reduced pods and further size reduced by employing a ball mill (BALLMILL) to obtain fine powders (SRPOD) of DLPODS. SRPOD is stirred (STIRRER) with water (WATER) to get sugar-rich carob pod extract. Thus, the outlet (SROUT) from the STIRRER comprises of sugar extracted carob pod biomass (SEPODS) and carob pod extract (CPEXTRAC). SEPODS was separated through a screen as a by-product, and the CPEXTRAC was used as a carbon source for the production of PHB rich biomass (PHBRBIO).

In the annular bioreactor (ANNULARB), as discussed in section 6.2.2, inoculum (INOC) for initial seeding, NaOH/HCl stream for pH control and air (AIR1) from a compressor (COMP) are added. Since the process is operated under the fed-batch mode, all the essential minerals in the form of MSM are added in ANNULARB prior to the beginning of the experiment. The temperature of the ANNULARB is maintained by circulating cooling water through cooling water inlet (CW1) and cooling water outlet (CW2) provided in the bioreactor sheathing. The outlet (BOUT) of the ANNULARB contains PHB rich biomass and spent media devoid (SPENTMED) of minerals and substrate.

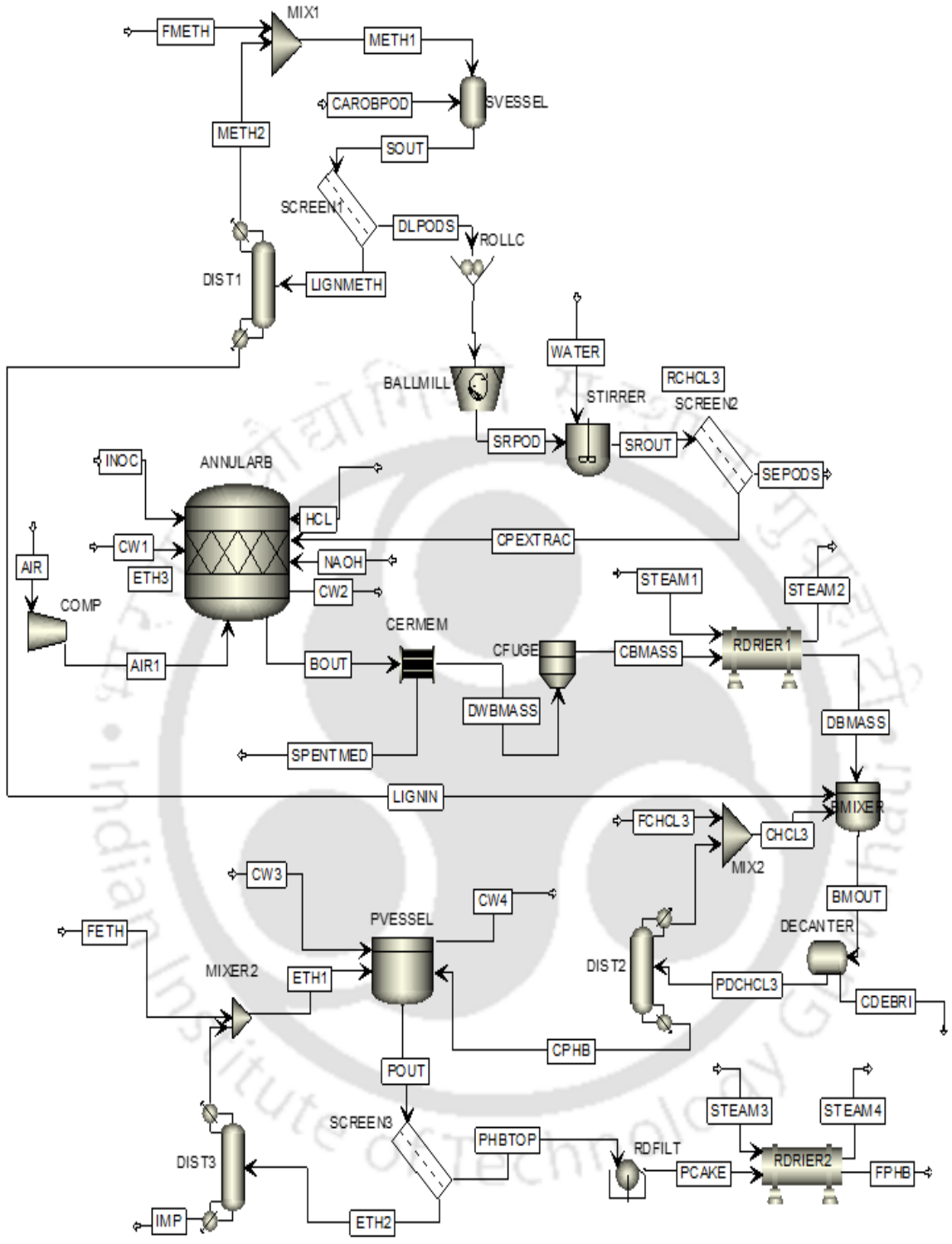

Fig. 6.3. Aspen Plus™ process flow sheet detailing the closed-loop biorefinery approach including novel bioprocessing strategies for PHB production considering SC4

The PHBRBIO is separated from SPENTMED using a ceramic membrane (CERMEM) based separation process. Dewatered biomass (DWBMASS) from CERMEM

is centrifuged (CFUGE) to get biomass cake (CBMASS) and it is dried using a rotary drier (RDRIER1) by introducing hot steam in (STEAM1) and steam out (STEAM2). Dried biomass (DBMASS) is then mixed with chloroform (CHCL3) and LIGNIN in a batch mixer (BMIXER) to expel polyhydroxybutyrate out of DBMASS. The outlet (BMOUT) of the BMIXER containing polyhydroxybutyrate and lignin dissolved in chloroform (PDCHCL3) and the cell debris (CDEBRI) are separated by subjecting BMOUT to a decantation process (DECANT). Whereas the CDEBRI is isolated as a by-product, the PDCHCL3 stream is distilled (DIST2) to separate chloroform and obtain concentrated PHB (CPHB). Distilled chloroform is recycled (RCHCL3) and mixed (MIX2) with fresh chloroform (FCHCL3) and used to feed-in BMIXER.

CPHB from the distillation column is taken to a precipitation vessel (PVESSEL) and counter precipitated with ethanol (ETH1) in cold condition maintained bypassing of colling water in (CW3) and cooling water out (CW4). Outlet (POUT) from PVESSEL is passed through a screen to separate PHB (PHBTOP) in the top layer and ethanol solution (ETH2) at the bottom. This ETH2 solution is distilled (DIST3) to get ethanol (ETH3) in the distillate and negligible amount of chloroform and lignin as an impurity (IMP) in the bottom portion. ETH3 is mixed (MIX3) with fresh ethanol (FETH) and used to feed PVESSEL. PHBTOP is filtered using a rotary drum filter (RDFILT) to get PHB cake (PCAKE) which is then dried using a rotary drier (RDRIER 2) by passing hot steam through inlet (STEAM3) and outlet (STEAM4) to obtain final dried PHB (FPHB) for bagging and storage.

6.2.5. Capital and maintenance cost of the key components needed for PHB production

6.2.5.1. Key components involved in the preparation of carob pod extract

Various unit operations and processing steps involved in the present PHB production process are depicted in Fig. 6.3. The variation in the key components of the different scenarios (SC1 - SC4) is clearly portrayed in Fig. 6.4. The capital cost and annual maintenance cost were estimated based on previous techno-economic assessment studies published in the literature (Baawuah et al., 2019; Levett et al., 2016). The cost of electricity pertaining to the Indian standards was found to be 10.4 Million USD per MW (Sharma and Thakur, 2016). Necessary calculations with 4.09% inflation rate were carried out to convert the amount reported in the literature to the present value (Plecher, 2019). And the availed conversion rates were 72 and 80 Indian rupees for every one U. S. dollar ($) and Euro (€), respectively. Five different unit operations are included in the present closed-loop biorefinery approach on lignin and sugar production from the carob pod biomass. The carob pods, with or without any primary cleaning, are soaked in methanol overnight to recover lignin-containing methanol solution (Arul Manikandan et al., 2019). Following lignin extraction, the lignin-containing methanol solution and the carob pod biomass are separated by a screen. The lignin-containing methanol solution is then distilled to recover methanol from the distillate and reused in the next batch of separation, whereas the lignin is recovered from the bottom layer in the distillation column. The capital cost for the distillation column is found out to be 11.12 million USD, and an annual operating cost of 243.38 million USD is estimated owing to its 225 MW energy consumption (Table 6.3).

The carob pods after delignification are taken to various size-reduction steps, involving roll crusher and ball mill to reduce the size of the biomass and to facilitate the sugar extraction process. The capital cost and annual operating cost for roll crusher and the

ball mill are found to be 33.13 and 22.92 million USD, respectively. Roll crusher being used in an initial reducing step, consumed 0.05 MW of energy consumption per annum, whereas the ball mill does the actual crushing and grinding operation with an annual energy consumption of 22 MW. The powdered carob pods are mixed with water in a ratio of 1:10 (w/v) using a stirrer at 200 rpm speed for 1 h under an ambient temperature of 28 ^{o}C. Capital cost for the stirrer is less in comparison with the soaking vessel, and this can be attributed to the difference in the amount of solids handled in these two processes. However, due to the annual requirement of 0.08 MW of energy, the annual operating cost is found to be 0.08 million USD. Thereafter, the sugar extracted biomass is screened from the carob pod extract. Although only the carob pod extract is considered for PHB production, future studies can be done on utilizing the water extracted carob pod biomass for further sugar extraction by acid or enzymatic digestion. Such studies on acid and/or enzymatic digestion of fibrous feedstock like spent carob pods for the production of bioethanol (Das et al., 2016), succinic acid (Kim and Dale, 2004), polylactic acid (Balakrishnan et al., 2018) and even for polyhydroxybutyrate (Saratale et al., 2019) can be found in the literature. The carob pod obtained from the screens contained 40 g/L of a sugar source, which is highly suitable to be fed directly as a carbon source into the bioreactor. Therefore, no concentration or evaporation step is required for the same. However, it needs to be supplemented with minimal salts, as mentioned in a previous section, to serve as PHB production medium.

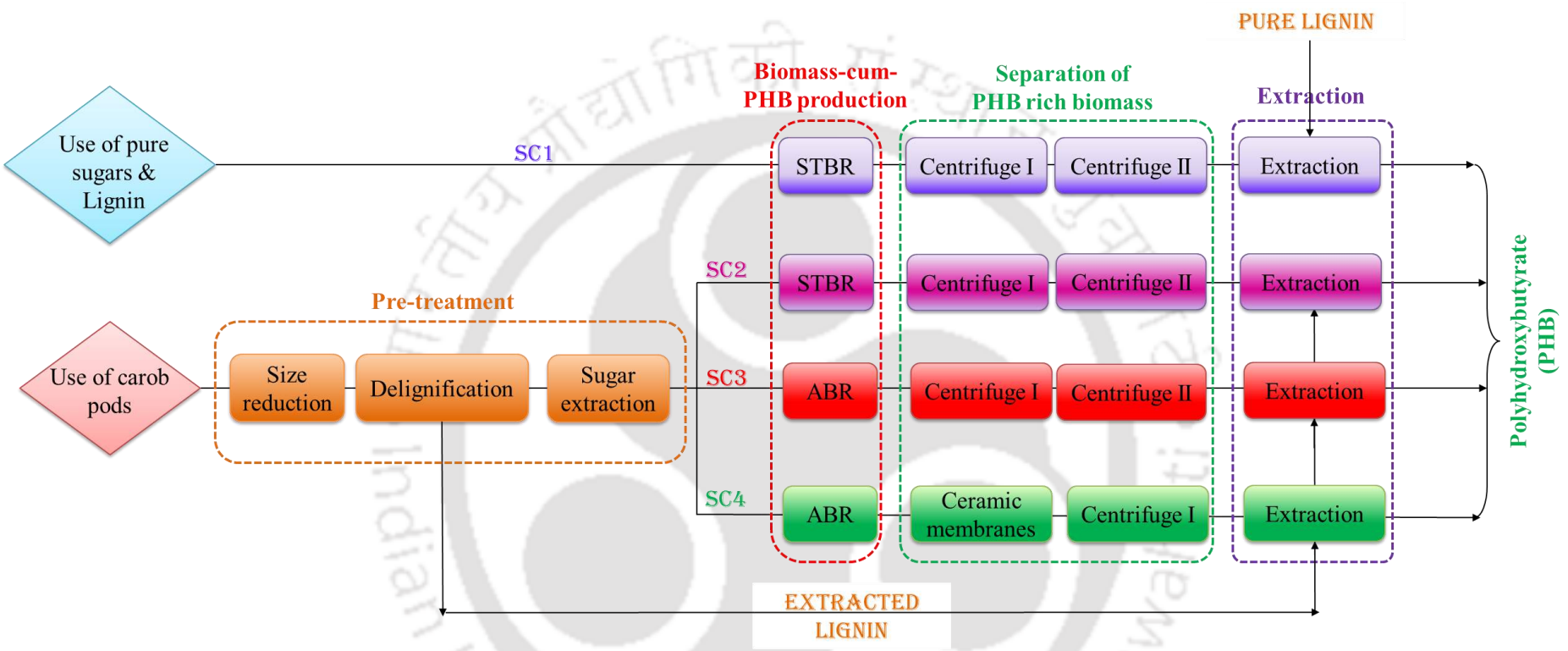

Fig. 6.4. Schematic showing the variation in the key components in the PHB plant considering different scenarios

Table 6.3. Capital cost and annual operating cost involved in the proposed PHB plant

S. No.	Unit operations/processes	Capital Cost (USD in millions)	Annual power consumption (MW)	Annual Operating Cost (USD in millions)
	Upstream processing			
Feedstock preparation (F_P)				
1	**Soaking Vessel** for lignin extraction	10.06	-	-
2	**Distillation** for lignin concentration	11.12	225	243.38
3	**Roll crusher** for dehulling	24.85	0.05	0.05
4	**Ball mill** for size reduction	33.13	22	22.92
5	**Stirrer** for sugar extraction	3.67	0.08	0.08
Biomass-cum-PHB production (B_P)				
6	**Bioreactor** Stirred tank bioreactor (STBR)	44.96	220	229.17
	Annual bioreactor (ABR)	49.69	320	458.33
7	**Air compressor**	100.57	0.02	0.21
	Downstream processing			
Separation				
8	**Membrane separation**	0.15	0.007	0.68
9	**Centrifugation** for complete dewatering	26.03	0.03	2.72
10	**Rotary drum dryers** for biomass drying	44.96	2.7	2.81
Solvent extraction				

11	**Stirrer vessel** for separation of PHB from biomass	26.4	0.08	0.6
12	**Decantation** for separation PHB rich phase	0.96	0	0
13	**Precipitation vessel** for precipitation of PHB	2.96	0.095	0.1
14	**Distillation column** to enhance the purity	11.12	225	234.38
	Finishing			
Product finishing				
14	**Filters** to separate the precipitated PHB	7.81	1.1	1.15
15	**Dryers** to dry PHB	7.45	5.7	5.94
16	**Distillation column** to enhance the purity	11.12	225	234.38
Other requirements				
17	**Screens (3 nos.)**	0.04		
18	**Mixer (2 nos.)**	0.1	0.013	0.01

6.2.5.2. Key elements involved in biomass-cum-PHB production

To compare the cost-effectiveness of the present ABR with that of the STBR, bioreactors were considered for this estimation. The volumetric capacity of both the bioreactors was fixed at 5000 m^3 per batch and operated for about 96 batches. The capital cost of ABR is quite high in comparison to that of the STBR, which is due to the large volume needed for ABR for the given working volume of 5000 m^3. The bigger size requirement in ABR is because of the space occupied by the inner rotating cylinder. As mentioned earlier, though the annular gap used in the present study is wider than the conventional Taylor and Couette bioreactor, the volumetric capacity is still less as compared to that of a STBR. Furthermore,

the annual operating cost for ABR is found to be double in comparison with that for STBR, due to the high energy requirement to drive the inner cylinder at a higher agitation rate. For instance, in the case of STBR, many stages of impellers were used and rotated at an agitation rate of 250 rpm. Whereas in the case of ABR, a single-cylinder from top to bottom is rotated at an agitation rate of 500 rpm for optimum performance. Based on the PHB titre value of 70.8 and 44.2 g/L for ABR and STBR, respectively, the annual PHB production capacity for STBR and ABR is scaled up and estimated to be 18895.5 and 30267 tonnes/annum, respectively. For 5000 m^3 bioreactor volume, a compressor with a large air delivery is necessary to ensure uniform air distribution. The cost and capacity of the bioreactor selected for the current investigation are in agreement with the literature report by Levett et al. (2016). Out of the 96 batches of PHB production, one is dedicated for inoculum preparation, and thereafter at the end of each fed-batch operation, 10% of the bioreactor volume i.e., 500 m^3 out of the total 5000 m^3 bioreactor volume is retained as inoculum for the next batch of PHB production.

6.2.5.3. Key elements involved in the separation of PHB rich biomass

The upstream process in PHB production ends up with the generation of PHB rich biomass in the bioreactor. Thereafter, the first step in downstream processing is the separation of PHB rich biomass from the spent broth (Arul Manikandan et al., 2019). For biomass separation, the conventional approach, as reported by Levett et al. (2016), involves a two-stage centrifugation step. In which the first centrifuge is used for dewatering, whereas the second one is for the caking of biomass. In the present case, a novel ceramic based membrane separation is used primarily for dewatering, followed by centrifugation for the formation of biomass cake. Both the capital cost and operating cost of the membrane separation is substantially low due to the use of cheap ceramic membranes and only 1/4th of the power consumption by the membrane separation process in comparison with that for

the centrifugation process (Biswas et al., 2016). For instance, the capital cost of the membranes is found to be 0.15 million USD, whereas for the centrifuge, it is estimated to be 26.03 million USD. The capital cost of the ceramic membranes is calculated based on the optimized flux. Based on the optimal flux value, i.e., 52 $L/m^2/h$ (Arul Manikandan et al., 2019), the area of the membrane calculated to process 5000 m^3 of bioreactor solution within 90 h is found to be 1068.4 m^2. Considering the inherent limitation of performing backwashing during the membrane separation process and in order to keep the process uninterrupted, double the surface area of the membrane, i.e., 2136.8 m^2 has opted for the techno-economic assessment. While the first membrane stack can be involved in the filtration process, the second membrane stack is taken for backwashing to regain the original flux, thus alternating the membranes for continuous operation. The cost of the present ceramic membrane, as reported by Kumar (2016), is estimated to be 69 USD/m^2. A 0.1 horsepower (HP) pump of about 13.9 USD is sufficient for the proposed plant, this was calculated based on the pumping requirement, which can deliver up to 4 m^3/h to a maximum head of 30 m. The annual power consumption for the membrane separation process is estimated to be 0.65 MW. For the centrifugation process, it was previously reported by Biswas et al. (2016) that it consumes four times more power from that required for the membrane separation process. The power consumption of the centrifugation process is thus calculated to be 2.6 MW. Hence, the annual operating cost for the membrane separation process is estimated to be 0.68 million USD, whereas for the centrifugation process, it is calculated to be 2.72 million USD (Table 6.2). Following the biomass separation step, secondary centrifugation is carried out to form biomass cake, which is then dried using a rotary drier for further PHB extraction.

For the extraction of PHB, as described in Arul Manikandan et al. (2020), the PHB rich biomass is stirred with chloroform containing lignin to rupture the bacterial cell wall

and recover PHB out of it. The PHB gets dissolved in the chloroform and settles at the bottom; the cell debris and others remain at the top. Therefore, a decanter is placed to separate the PHB containing layer, which is then treated with cold ethanol to precipitate PHB. The spent biomass from the extraction vessel and spent broth from the membrane separation process are considered the two main waste streams, and the spent broth can be treated in the wastewater treatment facility mentioned earlier. Promising strategies to convert the PHB/lipid-free bacterial biomass to bio-oil via pyrolysis (Wei et al., 2015b) and hydrothermal liquefaction (Wei et al., 2015a) techniques are reported in the literature (Paul et al., 2019). Thus, one can consider recovering value out of the waste bacterial biomass generated in the present PHB production process, as outlined in a later section of this article. In order to recover the ethanol and reuse it back for precipitation, a distillation column is useful, and a fresh ethanol feed is mixed in the mixer. PHB screened from the down product of the precipitation vessel is filtered using a rotary drum filter and, after that, it is dried using a rotary drier for final bagging.

6.2.6. Miscellaneous requirements for PHB production

As reported in the literature by Levett et al. (2016), 10% of the capital cost is allotted for maintaining the plant, which includes corrective, preventive, risk and condition-based maintenance carried out usually in any chemical process plant. As the workforce in any industry is inevitable, a budget of 20% of the total operating cost is allotted for labour and supervision. For instance, TianAn Biopolymer, a China-based PHBV producing company operated under the trademark of ENMAT^{TM} has an annual production capacity of 2000 metric tons, and it involves 70 employees, out of which 30% are technical staff having experience in the PHBV production process. In addition, 20% of the total operating cost is allotted for laboratory, which accounts mostly for installing analytical facility to routinely check the product purity, inoculum preparation and other product-related activities. As

suggested by Shahzad et al. (2017), for large capacity plants, 50% of the total capital cost is laid for piping and other control systems or instrumentation techniques used in PHB plant. A significant amount (50% of the total operating cost) is laid on the overall administration of the production plant, which is as per the report in the literature (Levett et al., 2016). Insurance coverage with 0.2% of the overall capital cost is drawn to account for any accidents in the production plant. The miscellaneous cost incurred the different scenarios is portrayed in Fig. 6.5.

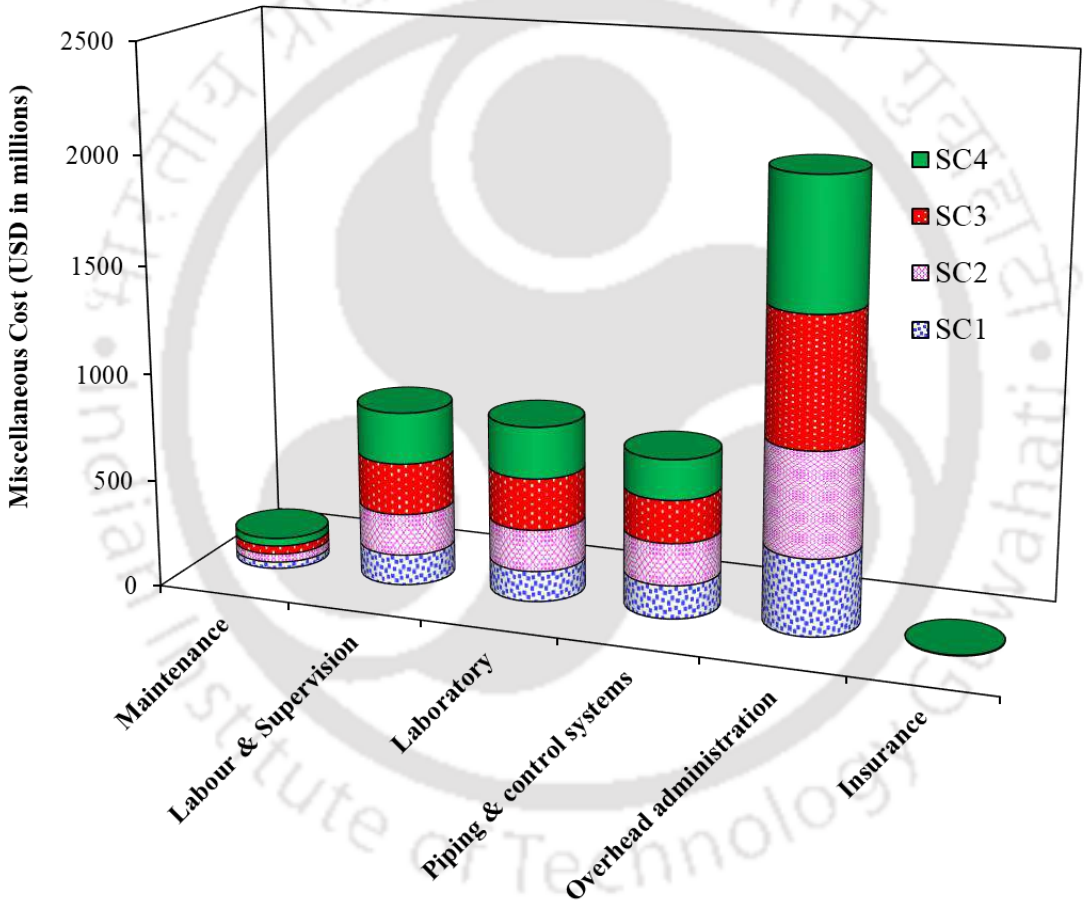

Fig. 6.5. Miscellaneous requirements in the PHB production plant considering different scenarios

6.3. Results and discussion

6.3.1. Gross revenue generated by PHB production investigated considering different scenarios

This section portrays the investment cost and annual revenue generated, considering the different scenarios in the PHB production plant. Investment laid on different aspects, base cost, miscellaneous cost, key component cost and feedstock cost under each scenario shown in Fig. 6.6. Since the sugars required for PHB production in SC1 is purchased from a supplier, the share of feedstock cost is found to be the highest (67%). In all the other scenarios from SC2 to SC4, the sugars are obtained from carob pods through various unit operations, and due to which the share of the key component cost is found to be highest (> 46%) in these scenarios. Miscellaneous cost in SC1 is 14%, whereas in SC2 to SC4, the miscellaneous cost is found to be around 38%. This is indeed a favourable outcome as it creates job opportunities and increases the economy of a country (Acs, 2006).

In order to make the present PHB cost more competitive than the PHB available in the market, an optimal selling price of 6.94 USD/Kg of PHB is chosen. This price is comparable with that of the PHB sold by Monsanto^{TM}, USA (Shahzad et al., 2017). PHB production is found to be 18895.5¸18895.5, 30267 and 30267 tonnes/annum considering SC1, SC2, SC3 and SC4, respectively. The variation in the PHB production between SC1 and SC2 from that of the SC3-SC4 can be attributed to the change in the bioreactor configuration from STBR to ABR. However, the same PHB production found in SC1 and SC2 is due to the similarity of the process, but the raw material source is different. In the case of SC1, pure sugars obtained from the market are directly used for PHB production, whereas, in SC2, the source of these sugars is from carob pods.

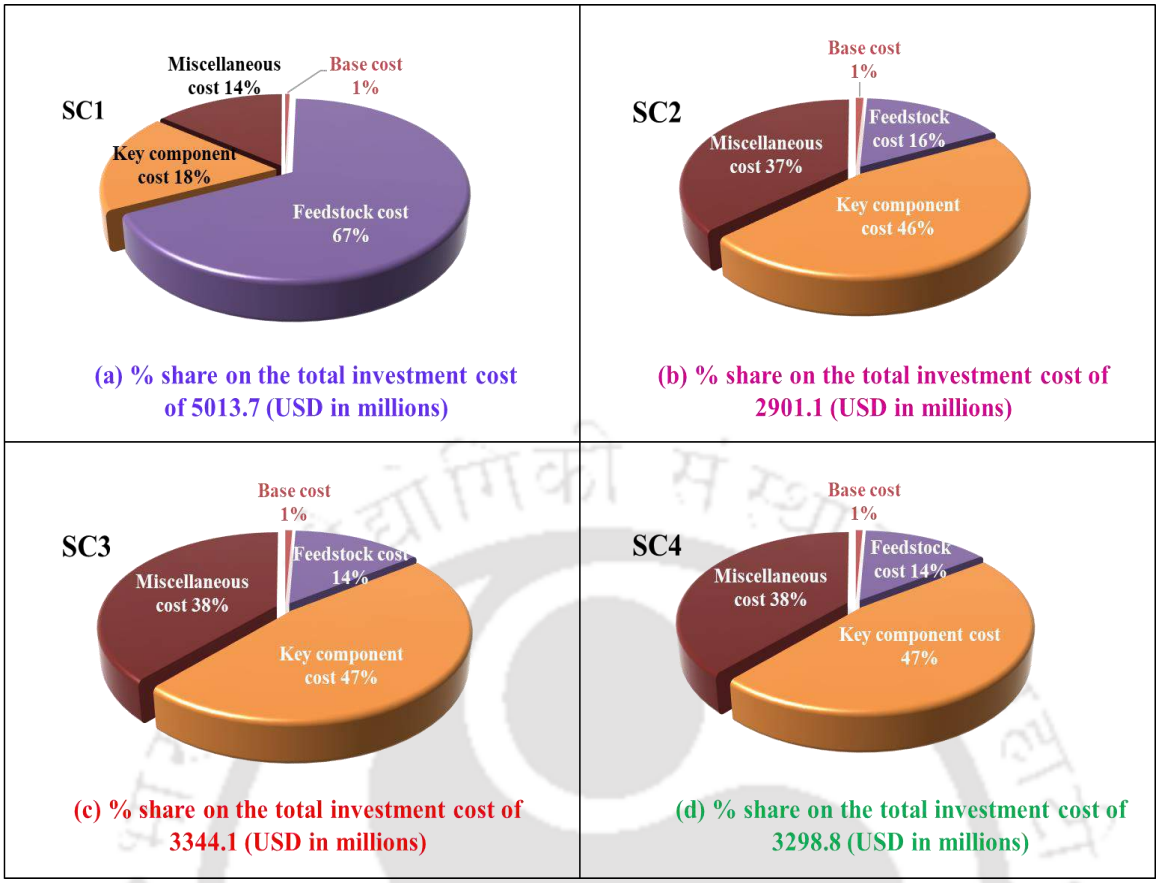

Fig. 6.6. Total investment cost on the PHB plant considering different scenarios: (a) SC1, (b) SC2, (c) SC3 and (d) SC4.

Similarly, the same PHB titre observed in SC3 and SC4 can be attributed to the similarity of the process, but with a change in the biomass separation method from centrifugation in SC3 to membrane separation in SC4. Thus the annual revenue generated through PHB from SC1, SC2, SC3 and SC4 is 446.14, 446.14, 714.64 and 714.64 million USD, respectively. However, as described previously in Section 3.4, the spent *R. eutropha* biomass is known for its use as a feedstock for bio-oil production through pyrolysis, and therefore, the spent *R. eutropha* biomass can be sold at a nominal cost of 0.014 USD/Kg, which thus accounts for annual revenue of 0.1, 0.1, 0.14 and 0.14 million USD in SC1, SC2, SC3 and SC4, respectively. Other than the sugars and lignin extracted from the carob pods, the fibrous content leftover in the carob pods can be sold at 20% of the buying cost of the carob pods i.e. 0.002 USD/Kg. Thus, further revenue created through carob pods for

the various scenarios: SC2, SC3 and SC4 is 12.9 million USD each. The absence of income through spent carob pod in SC1 is due to the fact that the sugars are purchased and not derived from the carob pods in SC1. The gross revenue generated under various scenarios are by selling spent carob, spent *R. eutropha* biomass and polyhydroxybutyrate (PHB). Majority of the revenue is generated through polyhydroxybutyrate, whereas the least revenue is created by selling the spent carob pods and through spent *R. eutropha* biomass.

6.3.2. Net revenue generated by the PHB plant considering the different scenarios

The aforementioned revenue generated by the PHB plant considering the different scenarios is the gross revenue. The net revenue generated under each scenario can be derived only after paying the due taxes. In many countries, particularly in some industrial estates of India, the government offers 100% excise duty-free for the first ten years of the start of a production plant and 100% corporate income tax exemption for first five years and thereafter 25 to 30% is to be paid as the tax (Chaurey, 2017). In general, 30% of the gross revenue generated by a PHB plant is returned back to the country in the form of taxes as per the report by Levett et al. (2016). Hence, in this study, 30% of gross revenue can be considered as paid towards taxes (USD in millions): 446.24 in SC1, 459.15 in SC2, 727.68 in SC3 and 727.68 in SC4. Thus the annual net revenue generated by the PHB product considering SC1, SC2, SC3 and SC4 is 312.37, 321.4, 509.37 and 509.37 million USD, respectively (Fig. 6.7).

The cash flow of the proposed PHB plant considering under various scenarios is shown in Fig. 6.8 and it is calculated by using the following equation (1) (Shahzad et al., 2017):

$$\text{Cash flow} = \text{Net revenue} - (\text{Operating \& maintenance cost} + \text{Capital cost}) \quad (1)$$

It can be observed from Fig. 6.8 that the pay-out period or the break-even point for SC1, SC2, SC3 and SC4 is 12.6, 6.8, 4.8 and 4.8 years, respectively. The delayed pay-out time

observed in SC1 is attributed to the high feedstock cost for purchasing sugars, i.e. the net revenue generated every year is mostly consumed for the purchase of sugars in the next calendar year.

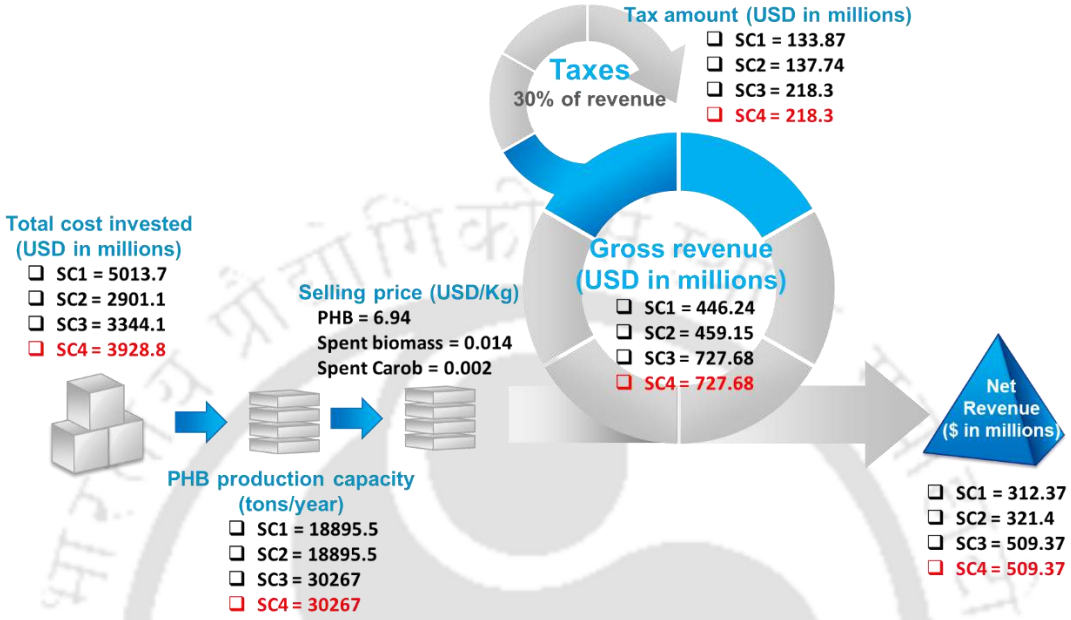

Fig. 6.7. Split-up of costs in the PHB plant considering different scenarios.

Secondly, the 6.8 years pay-out period taken in SC2 can be attributed to the less PHB production observed with STBR in comparison with that using ABR. This can be further confirmed by the drastic reduction of the pay-out period from 6.8 to 4.8 years, with a change in the bioreactor configuration from STBR to ABR. However, no change in the pay-out period was observed between SC3 and SC4, which reveals that unlike the bioreactor, the separation process seems to play a less significant role in the economics of the process. Thus, replacing centrifugation with the membrane separation process did not result in a significant reduction in the pay-out period. However, the replacement of the membrane separation process with centrifugation is still recommended in view of the turnover generated by the plant considering SC4.

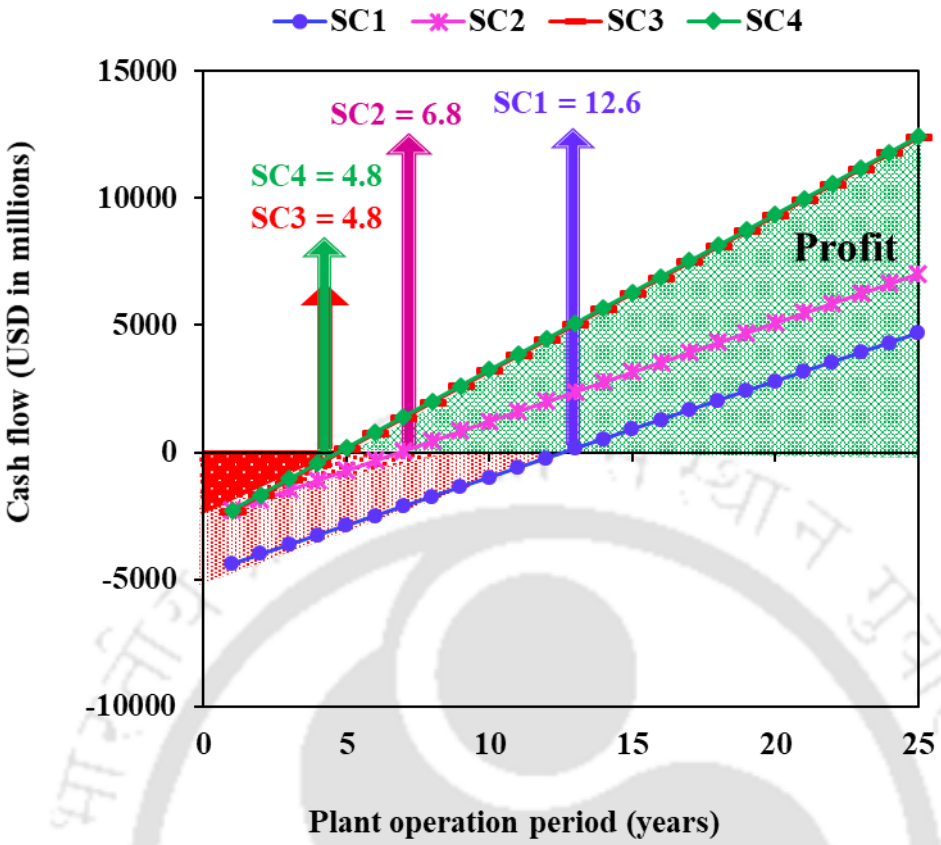

Fig. 6.8. Cash flow of the PHB plant considering different scenarios

For instance, from Fig. 6.9, it can be observed that the replacement of centrifugation with membrane separation increased the turnover from 1.35 to 1.4 billion USD. This pay-out period found in the present study is comparable with techno-economic assessment carried out for the production of biopolymer and also with other bioproducts such as biohydrogen and algal biodiesel (Galera and Gutiérrez Ortiz, 2015; Taylor et al., 2013). For instance, the biopolymer produced using slaughterhouse wastewater (SHWW) resulted in a pay-out period of 3.5 years. But when the authors tried supplementing this SHWW with amino acids, the pay-out period extended from 3.5 to 5 years. Likewise, Taylor et al. (2013) reported a pay-out period of 6 years for the production of algal biodiesel. Finally, Galera and Gutiérrez Ortiz, (2015) reported a pay-out period of 15.5 years for the assessment carried out for hydrogen and power production from supercritical water reforming of glycerol.

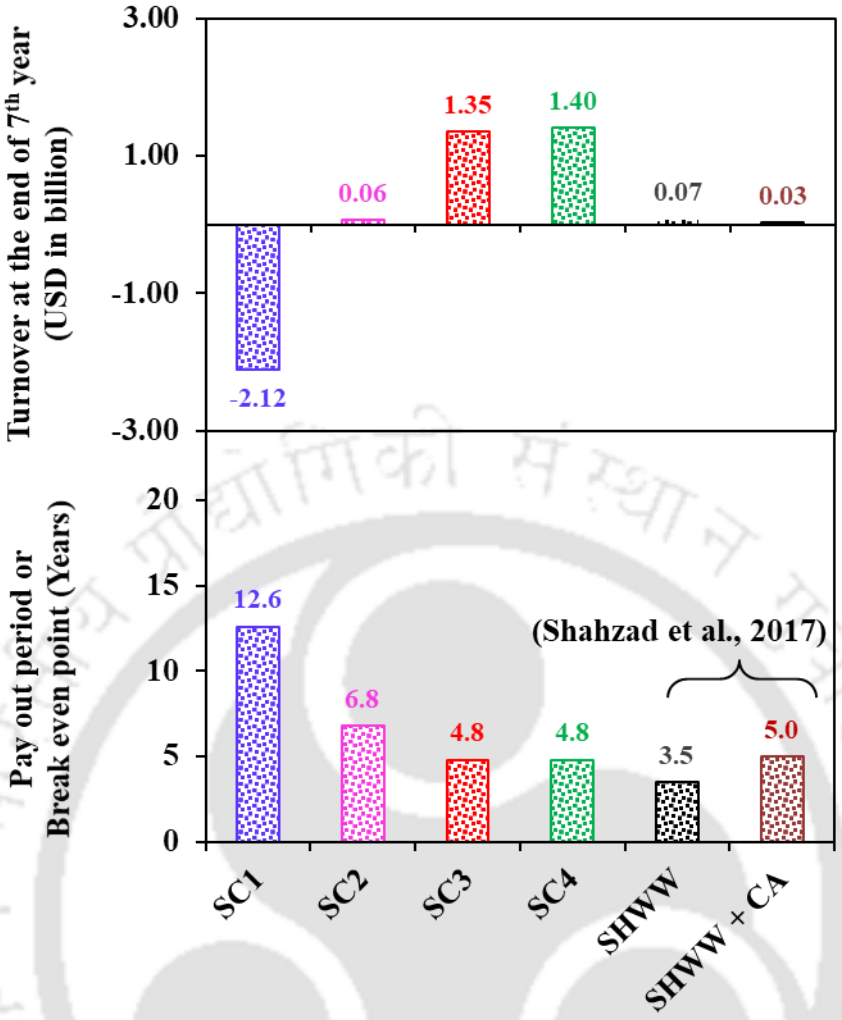

Fig. 6.9: (a) Turnover accumulated at the end of 7th year and (b) Pay out period of the proposed PHB plant considering different scenarios (SHWW - Slaughter house wastewater and CA - Casamino acid)

Thus, the application of various novel strategies along with an improved PHB production in ABR and incorporation of low-cost ceramic membrane technology for separation processes resulted in a highly profitable and cost-effective PHB production approach. However, the selling price of the PHB (6.94 USD/Kg) is higher than that of the petroleum-based products such as polyethylene terephthalate (2.2 USD/Kg) and acrylonitrile butadiene styrene (2.9 USD/Kg) (Rodríguez Toscano et al., 2019). Therefore, further research on optimization and time tuning of the production process is warranted to

make the cost of the PHB production process comparable to that of the conventional petroleum-based polymer production process.

6.4. Summary

The techno-economic assessment performed in the present study based on closed-loop biorefinery approach, including novel process alternatives for polyhydroxybutyrate production, established the cost-effectiveness of the process due to the replacement of pure sugars with crude carob pod extract and the application of annular bioreactor and membrane separation method. A complete flowsheet for the PHB production using carob pods as feedstock was successfully developed. Base price for the PHB plant along with the cost requirements for water, electricity, etc. and tax system laid on the gross revenue generated from the PHB plant were analysed in detail. Cash flow analysis revealed a drastic reduction in the pay-out period from 12.6 to 6.8 years by replacing pure sugars with carob pod extract as the feedstock. A further reduction of up to 4.8 years was seen by replacing STBR with ABR. Though the replacement of centrifugation with the membrane separation process did not significantly reduce the pay-out period, the use of the membrane separation process is still suggested in the light of the annual turnover obtained by shifting to this method. A very nominal cost can be generated by selling the spent bacterial biomass and carob pod biomass, but by integrating the spent residue with bio-oil generation system can lead to further revenue generation.

Chapter 7

Conclusions and Future perspectives

7.1. Conclusions

Polyhydroxybutyrate is found to be the best performing biopolymer currently available in the market, and its commercialization would greatly reduce the pressure on the depleting fossil petroleum sources. However, the significant cost associated with the PHB production keeps the PHB manufacturing process from actual commercialization. Therefore, the present study on PHB production directed towards efficient utilization of carob pods as the feedstock, alongside the incorporation of annular bioreactor system with alternative mechanical frameworks and integration of the upcoming membrane separation process to achieve sustainable and economical production of PHB.

Firstly, a novel bioprocess based on closed-loop biorefinery approach was developed for PHB production by using carob pods as a self-sufficient feedstock for upstream to downstream processing. Taguchi experimental design demonstrated that *R. eutropha* outperformed the *B. megaterium* with maximum PHB concentration. The prepared PHB established showed excellent characteristics as a packaging material in food packaging applications. Secondly, an innovative annular bioreactor for biomass-cum-PHB production is reported for the first time. A superior hydrodynamic was demonstrated in the ABR due to the Taylor and Couette flow prevailing in the bioreactor. Furthermore, no shear damage to the cells was observed using the ABR. Biomass and PHB production using the bioreactor was found to be 1.4 and 1.6 times better in comparison with the STBR operated under batch and fed-batch modes, respectively.

A low-cost ceramic-based membrane was prepared and evaluated for an efficient separation of PHB rich bacterial biomass. Membrane assembly with four number of membranes operated at 49 kPa was found to be effective. PHB recovery of 99.2% with a final broth flux of 35.7 $L/m^2 \cdot h$ is achieved. An inverse relationship between broth flux and PHB recovery due to applied pressure is observed in the single membrane assembly. This

relationship was overcome using the four membrane assembly. Further, increase in the number of membranes reduced the filtration resistance.

Finally, PHB/Gr-NPs nanocomposite with excellent barrier and mechanical properties was prepared by simple solution casting method. The prepared nanocomposite was found to be less cytotoxic and highly biodegradable by soil biomes, thus demonstrating its suitability for food-packaging applications. Techno-economic assessment of the PHB production process with carob pods as the feedstock was performed which revealed a drastic reduction in the pay-out period from 12.6 to 6.8 years by replacing pure sugars with carob pod extract as the feedstock. A further decrease of up to 4.8 years was seen by replacing STBR with ABR. Though the replacement of centrifugation with the membrane separation process did not significantly reduce the pay-out period, the use of the membrane-based biomass separation is recommended in the light of the high annual turnover obtained by shifting to this method. This study establishes the economics, sustainability and industrial application of the closed-loop biorefinery model involving (a) carob waste as the feedstock for PHB production and extraction, (b) annular bioreactor for improved hydrodynamics and PHB production, (c) ceramic membrane for PHB-rich biomass separation and (d) utility of PHB-nanocomposite for food packaging.

7.2. Scope for future study

In addition to the above, the following are some more suggestions for future work based on this thesis:

1. The strategy of using *Ceratonia Siliqua* pods as the feedstock for upstream to downstream processing in PHB production under a closed-loop biorefinery system is demonstrated as a benchmark in the present study. A holistic view of the present strategy on closed-loop biorefinery can be developed by extending the current approach to other lignocellulosic biomass.

2. No advanced control systems were installed in the annular bioreactor used in the present study. Therefore, development of kinetic models for continuous monitoring and control of ABR promises reduction in process perturbation, thereby resulting in an enhanced biomass-cum-PHB production.
3. Instead of placing the present tubular ceramic membrane assembly as a standalone system, the ceramic membrane assembly can be submerged into the bioreactor. By this arrangement the bioreactor can be operated in continuous mode along with the retention of PHB rich bacterial biomass. Such a system is envisaged to overcome the demerit of biomass loss and metabolite accumulation in the bioreactor, which are often observed with the bioreactor operated under continuous and fed-batch mode, respectively.
4. In the present study, a simple solution casting technique was handled to prepare the packaging material, so as to test its effectiveness in food packaging applications. However, in order to realize the commercial potential of the present PHB/Gr-NPs nanocomposite, polymeric nanocomposite films need to be produced using extrusion - cum - blow moulding technique.

Bibliography

1. Abd-El-haleem, D., Amara, A., Zaki, S., Abulhamd, A., Abulreesh, G., 2007. Biosynthesis of biodegradable polyhydroxyalkanotes biopolymers in genetically modified yeasts. Int. J. Environ. Sci. Technol. 4, 513–520. https://doi.org/10.1007/BF03325988
2. Acevedo, F., Villegas, P., Urtuvia, V., Hermosilla, J., Navia, R., Seeger, M., 2018. Bacterial polyhydroxybutyrate for electrospun fiber production. Int. J. Biol. Macromol. 106, 692–697. https://doi.org/10.1016/j.ijbiomac.2017.08.066
3. Acs, Z., 2006. INNOV0101FINAL.qxd. Innov. Technol. governance, Glob. 1, 97–107.
4. Al-Battashi, H.S., Annamalai, N., Sivakumar, N., Al-Bahry, S., Tripathi, B.N., Nguyen, Q.D., Gupta, V.K., 2019. Lignocellulosic biomass (LCB): a potential alternative biorefinery feedstock for polyhydroxyalkanoates production. Rev. Environ. Sci. Biotechnol. 18, 183–205. https://doi.org/10.1007/s11157-018-09488-4
5. Andersson H, K. and L., 2006. Kinetic Studies of Oxygen Dependence During Initial Lipid Oxidation in Rapeseed Oil. J. Food Sci. 64, 262–266.
6. Anjum, A., Zuber, M., Zia, K.M., Noreen, A., Anjum, M.N., Tabasum, S., 2016. Microbial production of polyhydroxyalkanoates (PHAs) and its copolymers: A review of recent advancements. Int. J. Biol. Macromol. 89, 161–174. https://doi.org/10.1016/j.ijbiomac.2016.04.069
7. Annamalai, N., Sivakumar, N., 2016. Production of polyhydroxybutyrate from wheat bran hydrolysate using Ralstonia eutropha through microbial fermentation. J. Biotechnol. 237, 13–17. https://doi.org/10.1016/j.jbiotec.2016.09.001
8. Anusha, S.M., Leelaram, S., Surianarayanan, M., 2016. Production of Poly (3-Hydroxybutyric Acid) by Ralstonia eutropha in a Biocalorimeter and its Thermokinetic Studies. Appl. Biochem. Biotechnol. 179, 1041–1059. https://doi.org/10.1007/s12010-016-2049-0

9. Aramvash, A., Akbari Shahabi, Z., Dashti Aghjeh, S., Ghafari, M.D., 2015. Statistical physical and nutrient optimization of bioplastic polyhydroxybutyrate production by Cupriavidus necator. Int. J. Environ. Sci. Technol. 12, 2307–2316. https://doi.org/10.1007/s13762-015-0768-3
10. Arkusz, J., Stępnik, M., Trzaska, D., Dastych, J., Rydzyński, K., 2006. Assessment of usefulness of J774A.1 macrophages for the assay of IL-1β promoter activity. Toxicol. Vitr. 20, 109–116. https://doi.org/10.1016/j.tiv.2005.06.044
11. Arrieta, M.P., Fortunati, E., Dominici, F., López, J., Kenny, J.M., 2015. Bionanocomposite films based on plasticized PLA-PHB/cellulose nanocrystal blends. Carbohydr. Polym. 121, 265–275. https://doi.org/10.1016/j.carbpol.2014.12.056
12. Arrieta, M.P., López, J., Hernández, A., Rayón, E., 2014. Ternary PLA-PHB-Limonene blends intended for biodegradable food packaging applications. Eur. Polym. J. 50, 255–270. https://doi.org/10.1016/j.eurpolymj.2013.11.009
13. Arul Manikadan, N., Pakshirajan, K., Pugazhenthi, G., 2019. Green production of polyhydroxybutyrate (PHB) using lignocellulosic biomass (Ceratonia siliqua pods) as a self-sufficient feedstock for upstream to donstream processing, in: Sathrugnan, K. (Ed.), AMRC 2019–Abstract Book: Advanced Materials Research Conference. Singapore Laboratoty Professional Society, Singapore, p. 27.
14. Arul Manikandan, N., Pakshirajan, K., Pugazhenthi, G., 2018. Taylor and Couette bioreactor - a novel bioreactor system for polyhydroxybutyrate production from Ralstonia eutropha, in: Jegatheesan, J. V (Ed.), CESE 2018–Abstract Book: The Eleventh Annual Conference on the Challenges in Environmental Science and Engineering. LJS Environment, Highton, Australia.
15. Arul Manikandan, N., Pakshirajan, K., Pugazhenthi, G., 2019a. A novel ceramic membrane assembly for the separation of polyhydroxybutyrate (PHB) rich Ralstonia

eutropha biomass from culture broth. Process Saf. Environ. Prot. 126, 106–118. https://doi.org/10.1016/j.psep.2019.04.001

16. Arza, C.R., Jannasch, P., Maurer, F.H.J., 2014. Network formation of graphene oxide in poly(3-hydroxybutyrate) nanocomposites. Eur. Polym. J. 59, 262–269. https://doi.org/10.1016/j.eurpolymj.2014.07.035
17. Baawuah, E., Christopher, K., Addai-Mensah, J., & Skinner, W., 2019. Process challenges and recent developments in magnetite beneficiation technologies. Chemeca 2019: Chemical Engineering Megatrends and Elements.
18. Babatabar, S., Zamir, S.M., Shojaosadati, S.A., Yakhchali, B., Zarch, A.B., 2019. Cometabolic degradation of bisphenol A by pure culture of Ralstonia eutropha and metabolic pathway analysis. J. Biosci. Bioeng. 127, 732–737. https://doi.org/10.1016/j.jbiosc.2018.12.001
19. Babel, S., Takizawa, S., 2010. Microfiltration membrane fouling and cake behavior during algal filtration. Desalination 261, 46–51. https://doi.org/10.1016/j.desal.2010.05.038
20. Bagheri, M., Akbari, A., Mirbagheri, S.A., 2019. Advanced control of membrane fouling in filtration systems using artificial intelligence and machine learning techniques: A critical review. Process Saf. Environ. Prot. 123, 229–252. https://doi.org/10.1016/j.psep.2019.01.013
21. Bahry, H., Pons, A., Abdallah, R., Pierre, G., Delattre, C., Fayad, N., Taha, S., Vial, C., 2017. Valorization of carob waste: Definition of a second-generation bioethanol production process. Bioresour. Technol. 235, 25–34. https://doi.org/10.1016/j.biortech.2017.03.056
22. Balakrishna Pillai, A., Jaya Kumar, A., Kumarapillai, H., 2018. Enhanced production of poly(3-hydroxybutyrate) in recombinant Escherichia coli and EDTA–microwave-

assisted cell lysis for polymer recovery. AMB Express 8. https://doi.org/10.1186/s13568-018-0672-6

23. Balakrishnan, R., Reddy Tadi, S.R., Sivaprakasam, S., Rajaram, S., 2018. Optimization of acid and enzymatic hydrolysis of kodo millet (Paspalum scrobiculatum) bran residue to obtain fermentable sugars for the production of optically pure D (−) lactic acid. Ind. Crops Prod. 111, 731–742. https://doi.org/10.1016/j.indcrop.2017.11.041
24. Barrett, J.S.F., Abdala, A.A., Srienc, F., 2014. Poly(hydroxyalkanoate) elastomers and their graphene nanocomposites. Macromolecules 47, 3926–3941. https://doi.org/10.1021/ma500022x
25. Barros, A.I., Gonçalves, A.L., Simões, M., Pires, J.C.M., 2015. Harvesting techniques applied to microalgae: A review. Renew. Sustain. Energy Rev. 41, 1489–1500. https://doi.org/10.1016/j.rser.2014.09.037
26. Beć, K.B., Morisawa, Y., Kobashi, K., Grabska, J., Tanabe, I., Tanimura, E., Sato, H., Wójcik, M.J., Ozaki, Y., 2018. Rydberg transitions as a probe for structural changes and phase transition at polymer surfaces: An ATR-FUV-DUV and quantum chemical study of poly(3-hydroxybutyrate) and its nanocomposite with graphene. Phys. Chem. Chem. Phys. 20, 8859–8873. https://doi.org/10.1039/c7cp07271f
27. Behera, R.K., Hassan, M.I., 2019. Regulatory interventions and industrial accidents: A case from India for 'Vision Zero' goals. Saf. Sci. 113, 415–424. https://doi.org/10.1016/j.ssci.2018.12.013
28. Bera, M., Maji, P.K., 2017. Effect of structural disparity of graphene-based materials on thermo-mechanical and surface properties of thermoplastic polyurethane nanocomposites. Polymer (Guildf). 119, 118–133. https://doi.org/10.1016/j.polymer.2017.05.019
29. Biocon Limited, 2019. Fortitude - Fourty years of Biocon, 28.

30. Biswas, P.P., Mondal, M., de, S., 2016. Comparison between Centrifugation and Microfiltration As Primary Clarification of Bottle Gourd (Lagenaria siceraria) Juice. J. Food Process. Preserv. 40, 226–238. https://doi.org/10.1111/jfpp.12599
31. Borowitzka, M.A., 2013. High-value products from microalgae-their development and commercialisation. J. Appl. Phycol. 25, 743–756. https://doi.org/10.1007/s10811-013-9983-9
32. Bowers, T., Vaidya, A., Smith, D.A., Lloyd-Jones, G., 2014. Softwood hydrolysate as a carbon source for polyhydroxyalkanoate production. J. Chem. Technol. Biotechnol. 89, 1030–1037. https://doi.org/10.1002/jctb.4196
33. Brar, S.K., Sarma, S.J., Pakshirajan, K., 2017. Petroleum Versus Biorefinery-Based Platform Chemicals, Platform Chemical Biorefinery. https://doi.org/10.1016/B978-0-12-802980-0.00006-7
34. Bromley, A.J., Holdich, R.G., Cumming, I.W., 2002. Particulate fouling of surface microfilters with slotted and circular pore geometry. J. Memb. Sci. 196, 27–37. https://doi.org/10.1016/S0376-7388(01)00573-7
35. Buchmann, L., Brändle, I., Haberkorn, I., Hiestand, M., Mathys, A., 2019. Pulsed electric field based cyclic protein extraction of microalgae towards closed-loop biorefinery concepts. Bioresour. Technol. 291, 121870.
36. Bugnicourt, E., Cinelli, P., Lazzeri, A., Alvarez, V., 2014. Polyhydroxyalkanoate (PHA): Review of synthesis, characteristics, processing and potential applications in packaging. Express Polym. Lett. 8, 791–808. https://doi.org/10.3144/expresspolymlett.2014.82
37. Bugnicourt, E., Cinelli, P., Lazzeri, A., Alvarez, V., 2014. Polyhydroxyalkanoate (PHA): Review of synthesis, characteristics, processing and potential applications in

packaging. Express Polym. Lett. 8, 791–808. https://doi.org/10.3144/expresspolymlett.2014.82

38. Carvalho, M., Roca, C., Reis, M.A.M., 2014. Carob pod water extracts as feedstock for succinic acid production by Actinobacillus succinogenes 130Z. Bioresour. Technol. 170, 491–498. https://doi.org/10.1016/j.biortech.2014.07.117
39. Carvalho, M., Roca, C., Reis, M.A.M., 2014. Carob pod water extracts as feedstock for succinic acid production by Actinobacillus succinogenes 130Z. Bioresour. Technol. 170, 491–498. https://doi.org/10.1016/j.biortech.2014.07.117
40. Carvalho, M., Roca, C., Reis, M.A.M., 2016. Improving succinic acid production by Actinobacillus succinogenes from raw industrial carob pods. Bioresour. Technol. 218, 491–497. https://doi.org/10.1016/j.biortech.2016.06.140
41. Carvalho, M., Roca, C., Reis, M.A.M., 2016. Improving succinic acid production by Actinobacillus succinogenes from raw industrial carob pods. Bioresour. Technol. 218, 491–497. https://doi.org/10.1016/j.biortech.2016.06.140
42. Castillo, T., Flores, C., Segura, D., Espín, G., Sanguino, J., Cabrera, E., Barreto, J., Díaz-Barrera, A., Peña, C., 2017. Production of polyhydroxybutyrate (PHB) of high and ultra-high molecular weight by Azotobacter vinelandii in batch and fed-batch cultures. J. Chem. Technol. Biotechnol. 92, 1809–1816. https://doi.org/10.1002/jctb.5182
43. Castro-Mayorga, J.L., Freitas, F., Reis, M.A.M., Prieto, M.A., Lagaron, J.M., 2018. Biosynthesis of silver nanoparticles and polyhydroxybutyrate nanocomposites of interest in antimicrobial applications. Int. J. Biol. Macromol. 108, 426–435. https://doi.org/10.1016/j.ijbiomac.2017.12.007
44. Castro-Mayorga, J.L., Martínez-Abad, A., Fabra, M.J., Olivera, C., Reis, M., Lagarón, J.M., 2014. Stabilization of antimicrobial silver nanoparticles by a

polyhydroxyalkanoate obtained from mixed bacterial culture. Int. J. Biol. Macromol. 71, 103–110. https://doi.org/10.1016/j.ijbiomac.2014.06.059

45. Cavalheiro, J.M.B.T., de Almeida, M.C.M.D., Grandfils, C., da Fonseca, M.M.R., 2009. Poly(3-hydroxybutyrate) production by Cupriavidus necator using waste glycerol. Process Biochem. 44, 509–515. https://doi.org/10.1016/j.procbio.2009.01.008
46. Cesário, M.T., Raposo, R.S., de Almeida, M.C.M.D., van Keulen, F., Ferreira, B.S., da Fonseca, M.M.R., 2014. Enhanced bioproduction of poly-3-hydroxybutyrate from wheat straw lignocellulosic hydrolysates. N. Biotechnol. 31, 104–113. https://doi.org/10.1016/j.nbt.2013.10.004
47. Chaurey, R., 2017. Location-based tax incentives: Evidence from India. J. Public Econ. 156, 101–120. https://doi.org/10.1016/j.jpubeco.2016.08.013
48. Cherubini, F., 2010. The biorefinery concept: Using biomass instead of oil for producing energy and chemicals. Energy Convers. Manag. 51, 1412–1421. https://doi.org/10.1016/j.enconman.2010.01.015
49. Costa, M.M.E., Cabral-Albuquerque, E.C.M., Alves, T.L.M., Pinto, J.C., Fialho, R.L., 2013. Use of polyhydroxybutyrate and ethyl cellulose for coating of urea granules. J. Agric. Food Chem. 61, 9984–9991. https://doi.org/10.1021/jf401185y
50. Cruz, M. V., Paiva, A., Lisboa, P., Freitas, F., Alves, V.D., Simões, P., Barreiros, S., Reis, M.A.M., 2014. Production of polyhydroxyalkanoates from spent coffee grounds oil obtained by supercritical fluid extraction technology. Bioresour. Technol. 157, 360–363. https://doi.org/10.1016/j.biortech.2014.02.013
51. Curran, S.J., Black, R.A., 2005. Oxygen transport and cell viability in an annular flow bioreactor: Comparison of laminar couette and Taylor-vortex flow regimes. Biotechnol. Bioeng. 89, 766–774. https://doi.org/10.1002/bit.20361

52. Das, S.P., Gupta, A., Das, D., Goyal, A., 2016. Enhanced bioethanol production from water hyacinth (Eichhornia crassipes) by statistical optimization of fermentation process parameters using Taguchi orthogonal array design. Int. Biodeterior. Biodegrad. 109, 174–184. https://doi.org/10.1016/j.ibiod.2016.01.008

53. Davis, R., Kataria, R., Cerrone, F., Woods, T., Kenny, S., O'Donovan, A., Guzik, M., Shaikh, H., Duane, G., Gupta, V.K., Tuohy, M.G., Padamatti, R.B., Casey, E., O'Connor, K.E., 2013. Conversion of grass biomass into fermentable sugars and its utilization for medium chain length polyhydroxyalkanoate (mcl-PHA) production by Pseudomonas strains. Bioresour. Technol. 150, 202–209. https://doi.org/10.1016/j.biortech.2013.10.001

54. Deepthi, S., Nivedhitha Sundaram, M., Vijayan, P., Nair, S. V., Jayakumar, R., 2018. Engineering poly(hydroxy butyrate-co-hydroxy valerate) based vascular scaffolds to mimic native artery. Int. J. Biol. Macromol. 109, 85–98. https://doi.org/10.1016/j.ijbiomac.2017.12.077

55. Deshmukh, R., Trivedi, V., 2013. Methemoglobin exposure produces toxicological effects in macrophages due to multiple ROS spike induced apoptosis. Toxicol. Vitr. 27, 16–23. https://doi.org/10.1016/j.tiv.2012.09.016

56. Dhar, P., Gaur, S.S., Soundararajan, N., Gupta, A., Bhasney, S.M., Milli, M., Kumar, A., Katiyar, V., 2017. Reactive Extrusion of Polylactic Acid/Cellulose Nanocrystal Films for Food Packaging Applications: Influence of Filler Type on Thermomechanical, Rheological, and Barrier Properties. Ind. Eng. Chem. Res. 56, 4718–4735. https://doi.org/10.1021/acs.iecr.6b04699

57. Dharmalingam, K., Padmavathi, G., Kunnumakkara, A.B., Anandalakshmi, R., 2019. Microwave-assisted synthesis of cellulose/zinc-sulfate‑calcium-phosphate (ZSCAP)

nanocomposites for biomedical applications. Mater. Sci. Eng. C 100, 535–543. https://doi.org/10.1016/j.msec.2019.02.109

58. Díaz-Barrera, A., Andler, R., Martínez, I., Peña, C., 2016. Poly-3-hydroxybutyrate production by Azotobacter vinelandii strains in batch cultures at different oxygen transfer rates. J. Chem. Technol. Biotechnol. 91, 1063–1071. https://doi.org/10.1002/jctb.4684
59. Dietrich, K., Dumont, M.J., Del Rio, L.F., Orsat, V., 2017. Producing PHAs in the bioeconomy — Towards a sustainable bioplastic. Sustain. Prod. Consum. 9, 58–70. https://doi.org/10.1016/j.spc.2016.09.001
60. Díez-Pascual, A.M., Díez-Vicente, A.L., 2014. Poly(3-hydroxybutyrate)/ZnO bionanocomposites with improved mechanical, barrier and antibacterial properties. Int. J. Mol. Sci. 15, 10950–10973. https://doi.org/10.3390/ijms150610950
61. Dizge, N., Soydemir, G., Karagunduz, A., Keskinler, B., 2011. Influence of type and pore size of membranes on cross flow microfiltration of biological suspension. J. Memb. Sci. 366, 278–285. https://doi.org/10.1016/j.memsci.2010.10.010
62. Du, G., Chen, L.X.L., Yu, J., 2004. High-efficiency production of bioplastics from biodegradable organic solids. J. Polym. Environ. 12, 89–94. https://doi.org/10.1023/B:JOOE.0000010054.58019.21
63. Elcik, H., Cakmakci, M., Ozkaya, B., 2016. The fouling effects of microalgal cells on crossflow membrane filtration. J. Memb. Sci. 499, 116–125. https://doi.org/10.1016/j.memsci.2015.10.043
64. Emani, S., Uppaluri, R., Purkait, M.K., 2014. Cross flow microfiltration of oil-water emulsions using kaolin based low cost ceramic membranes. Desalination 341, 61–71. https://doi.org/10.1016/j.desal.2014.02.030

65. Engineering, E., 2010. Hydrodynamics and batch biodegradation of phenol in an Internal Loop Airlift Reactor Pichiah Saravanan Kannan Pakshirajan Prabirkumar Saha * 2, 303–315.
66. Engtrakul, C., Hu, M.Z., Bischoff, B.L., Jang, G.G., 2016. Surface-Enhanced Separation of Water from Hydrocarbons: Potential Dewatering Membranes for the Catalytic Fast Pyrolysis of Pine Biomass. Energy and Fuels 30, 8343–8348. https://doi.org/10.1021/acs.energyfuels.6b01851
67. Fei, T., Cazeneuve, S., Wen, Z., Wu, L., Wang, T., 2016. Effective recovery of poly-β-hydroxybutyrate (PHB) biopolymer from Cupriavidus necator using a novel and environmentally friendly solvent system. Biotechnol. Prog. 32, 678–685. https://doi.org/10.1002/btpr.2247
68. Fiorese, M.L., Freitas, F., Pais, J., Ramos, A.M., De Aragão, G.M.F., Reis, M.A.M., 2009. Recovery of polyhydroxybutyrate (PHB) from Cupriavidus necator biomass by solvent extraction with 1,2-propylene carbonate. Eng. Life Sci. https://doi.org/10.1002/elsc.200900034
69. Fischer, G., Prieler, S., van Velthuizen, H., Lensink, S.M., Londo, M., de Wit, M., 2010. Biofuel production potentials in Europe: Sustainable use of cultivated land and pastures. Part I: Land productivity potentials. Biomass and Bioenergy 34, 159–172. https://doi.org/10.1016/j.biombioe.2009.07.008
70. Fraga, M.C., Sanches, S., Crespo, J.G., Pereira, V.J., 2017. Assessment of a new silicon carbide tubular honeycomb membrane for treatment of olive mill wastewaters. Membranes (Basel). 7. https://doi.org/10.3390/membranes7010012
71. Gahlawat, G., Sengupta, B., Srivastava, A.K., 2012. Enhanced production of poly(3-hydroxybutyrate) in a novel airlift reactor with in situ cell retention using

Azohydromonas australica. J. Ind. Microbiol. Biotechnol. 39, 1377–1384. https://doi.org/10.1007/s10295-012-1138-5

72. Galera, S., Gutiérrez Ortiz, F.J., 2015. Techno-economic assessment of hydrogen and power production from supercritical water reforming of glycerol. Fuel 144, 307–316. https://doi.org/10.1016/j.fuel.2014.12.033
73. Ganapathy, K., Ramasamy, R., Dhinakarasamy, I., 2018. Polyhydroxybutyrate production from marine source and its application. Int. J. Biol. Macromol. 111, 102–108. https://doi.org/10.1016/j.ijbiomac.2017.12.155
74. García-Pérez, T., López, J.C., Passos, F., Lebrero, R., Revah, S., Muñoz, R., 2018. Simultaneous methane abatement and PHB production by Methylocystis hirsuta in a novel gas-recycling bubble column bioreactor. Chem. Eng. J. 334, 691–697. https://doi.org/10.1016/j.cej.2017.10.106
75. Gaveau, A., Coetsier, C., Roques, C., Bacchin, P., Dague, E., Causserand, C., 2017. Bacteria transfer by deformation through microfiltration membrane. J. Memb. Sci. 523, 446–455. https://doi.org/10.1016/j.memsci.2016.10.023
76. Geim, A.K., 2011. Nobel Lecture: Random walk to graphene. Rev. Mod. Phys. 83, 851–862. https://doi.org/10.1103/RevModPhys.83.851
77. Ghoddosi, F., Golzar, H., Yazdian, F., Khosravi-Darani, K., Vasheghani-Farahani, E., 2019. Effect of carbon sources for PHB production in bubble column bioreactor: Emphasis on improvement of methane uptake. J. Environ. Chem. Eng. 7, 102978. https://doi.org/10.1016/j.jece.2019.102978
78. Goh, K., Heising, J.K., Yuan, Y., Karahan, H.E., Wei, L., Zhai, S., Koh, J.X., Htin, N.M., Zhang, F., Wang, R., Fane, A.G., Dekker, M., Dehghani, F., Chen, Y., 2016. Sandwich-Architectured Poly(lactic acid)-Graphene Composite Food Packaging Films. ACS Appl. Mater. Interfaces 8, 9994–10004. https://doi.org/10.1021/acsami.6b02498

79. Goswami, L., Vinoth Kumar, R., Borah, S.N., Arul Manikandan, N., Pakshirajan, K., Pugazhenthi, G., 2018. Membrane bioreactor and integrated membrane bioreactor systems for micropollutant removal from wastewater: A review. J. Water Process Eng. 26, 314–328. https://doi.org/10.1016/j.jwpe.2018.10.024
80. Gowda, V., Shivakumar, S., 2014. Agrowaste-based Polyhydroxyalkanoate (PHA) production using hydrolytic potential of Bacillus thuringiensis IAM 12077. Brazilian Arch. Biol. Technol. 57, 55–61. https://doi.org/10.1590/S1516-89132014000100009
81. Gupta, P., Vardhan, S., Al Haque, M.S., 2015. Study of success factors of TPM implementation in Indian industry towards operational excellence: An overview. IEOM 2015 - 5th Int. Conf. Ind. Eng. Oper. Manag. Proceeding 1–6. https://doi.org/10.1109/IEOM.2015.7093740
82. Guzman Lagunes, F., Winterburn, J.B., 2016. Effect of limonene on the heterotrophic growth and polyhydroxybutyrate production by Cupriavidus necator H16. Bioresour. Technol. 221, 336–343. https://doi.org/10.1016/j.biortech.2016.09.045
83. Haas, C., El-Najjar, T., Virgolini, N., Smerilli, M., Neureiter, M., 2017. High cell-density production of poly(3-hydroxybutyrate) in a membrane bioreactor. N. Biotechnol. 37, 117–122. https://doi.org/10.1016/j.nbt.2016.06.1461
84. Han, J.H., 2005. Innovations in food packaging. Elsevier.
85. Hazarika, J., Pakshirajan, K., Sinharoy, A., Syiem, M.B., 2015. Bioremoval of Cu(II), Zn(II), Pb(II) and Cd(II) by Nostoc muscorum isolated from a coal mining site. J. Appl. Phycol. 27, 1525–1534. https://doi.org/10.1007/s10811-014-0475-3
86. He, W., Xue, L., Gorczyca, B., Nan, J., Shi, Z., 2018. Comparative analysis on flocculation performance in unbaffled square stirred tanks with different height-to-width ratios: Experimental and CFD investigations. Chem. Eng. Res. Des. 132, 518–535. https://doi.org/10.1016/j.cherd.2018.01.055

87. Heidari, H., Sedighi, M., Zamir, S.M., Shojaosadati, S.A., 2017. Bisphenol A degradation by Ralstonia eutropha in the absence and presence of phenol. Int. Biodeterior. Biodegrad. 119, 37–42. https://doi.org/10.1016/j.ibiod.2016.10.052

88. Helling, A., Kubicka, A., Schaap, I.A.T., Polakovic, M., Hansmann, B., Thiess, H., Strube, J., Thom, V., 2017. Passage of soft pathogens through microfiltration membranes scales with transmembrane pressure. J. Memb. Sci. 522, 292–302. https://doi.org/10.1016/j.memsci.2016.08.016

89. Hu, M.Z., Engtrakul, C., Bischoff, B.L., Lu, M., Alemseghed, M., 2018. Surface-engineered inorganic nanoporous membranes for vapor and pervaporative separations of water–ethanol mixtures. Membranes (Basel). 8. https://doi.org/10.3390/membranes8040095

90. Hu, S., McDonald, A.G., Coats, E.R., 2013. Characterization of polyhydroxybutyrate biosynthesized from crude glycerol waste using mixed microbial consortia. J. Appl. Polym. Sci. 129, 1314–1321. https://doi.org/10.1002/app.38820

91. Hubacz, R., Wroński, S., 2004. Horizontal Couette-Taylor flow in a two-phase gas-liquid system: Flow patterns. Exp. Therm. Fluid Sci. 28, 457–466. https://doi.org/10.1016/j.expthermflusci.2003.07.004

92. Huschner, F., Grousseau, E., Brigham, C.J., Plassmeier, J., Popovic, M., Rha, C., Sinskey, A.J., 2015. Development of a feeding strategy for high cell and PHA density fed-batch fermentation of Ralstonia eutropha H16 from organic acids and their salts. Process Biochem. 50, 165–172. https://doi.org/10.1016/j.procbio.2014.12.004

93. Hwang, K.J., Hsueh, C.L., 2003. Dynamic analysis of cake properties in microfiltration of soft colloids. J. Memb. Sci. 214, 259–273. https://doi.org/10.1016/S0376-7388(02)00556-2

94. Inan, K., Sal, F.A., Rahman, A., Putman, R.J., Agblevor, F.A., Miller, C.D., 2016. Microbubble assisted polyhydroxybutyrate production in Escherichia coli. BMC Res. Notes 9, 1–7. https://doi.org/10.1186/s13104-016-2145-9

95. Issaoui, M., Limousy, L., Lebeau, B., Bouaziz, J., Fourati, M., 2017. Manufacture and optimization of low-cost tubular ceramic supports for membrane filtration: application to algal solution concentration. Environ. Sci. Pollut. Res. 24, 9914–9926. https://doi.org/10.1007/s11356-016-8285-6

96. Jamshidi, A.M., Sohrabi, M., Vahabzadeh, F., Bonakdarpour, B., 2001. Hydrodynamic and mass transfer characterization of a down flow jet loop bioreactor. Biochem. Eng. J. 8, 241–250. https://doi.org/10.1016/S1369-703X(01)00115-2

97. Jayakumar, A., Prabhu, K., Shah, L., Radha, P., 2019. Biologically and environmentally benign approach for PHB-silver nanocomposite synthesis and its characterization. Polym. Test. 81, 106197. https://doi.org/10.1016/j.polymertesting.2019.106197

98. Jha, P., Dharmalingam, K., Nishizu, T., Katsuno, N., Anandalakshmi, R., 2019. Effect of Amylose–Amylopectin Ratios on Physical, Mechanical, and Thermal Properties of Starch-Based Bionanocomposite Films Incorporated with CMC and Nanoclay. Starch/Staerke 1900121, 1–9. https://doi.org/10.1002/star.201900121

99. Jia, X., Qi, L., Zhang, Y., Yang, X., Wang, H., Zhao, F., Lu, W., 2017. Computational fluid dynamics simulation of a novel bioreactor for sophorolipid production. Chinese J. Chem. Eng. 25, 732–740. https://doi.org/10.1016/j.cjche.2016.09.014

100. Jiang, L., Shen, X. P., Wu, J. L., & Shen, K.C., 2010. Preparation and characterization of graphene/poly (vinyl alcohol) nanocomposites. J. Appl. Polym. Sci. 118, 275–279.

101. Jing, X., Qiu, Z., 2012. Effect of low thermally reduced graphene loadings on the crystallization kinetics and morphology of biodegradable poly(3-hydroxybutyrate). Ind. Eng. Chem. Res. 51, 13686–13691. https://doi.org/10.1021/ie3018466

102.Joyyi, L., Ahmad Thirmizir, M.Z., Salim, M.S., Han, L., Murugan, P., Kasuya, K. ichi, Maurer, F.H.J., Zainal Arifin, M.I., Sudesh, K., 2017. Composite properties and biodegradation of biologically recovered P(3HB-co-3HHx) reinforced with short kenaf fibers. Polym. Degrad. Stab. 137, 100–108. https://doi.org/10.1016/j.polymdegradstab.2017.01.004

103.Kai, D., Chong, H.M., Chow, L.P., Jiang, L., Lin, Q., Zhang, K., Zhang, H., Zhang, Z., Loh, X.J., 2018. Strong and biocompatible lignin /poly (3-hydroxybutyrate) composite nanofibers. Compos. Sci. Technol. 158, 26–33. https://doi.org/10.1016/j.compscitech.2018.01.046

104.Kai, D., Zhang, K., Liow, S.S., Loh, X.J., 2019. New Dual Functional PHB-Grafted Lignin Copolymer: Synthesis, Mechanical Properties, and Biocompatibility Studies. ACS Appl. Bio Mater. 2, 127–134. https://doi.org/10.1021/acsabm.8b00445

105.Kajaste, R., 2014. Chemicals from biomass - Managing greenhouse gas emissions in biorefinery production chains - A review. J. Clean. Prod. 75, 1–10. https://doi.org/10.1016/j.jclepro.2014.03.070

106.Kalaiyezhini, D., Ramachandran, K.B., 2015. Biosynthesis of poly-3-hydroxybutyrate (PHB) from glycerol by paracoccus denitrificans in a batch bioreactor: Effect of process variables. Prep. Biochem. Biotechnol. 45, 69–83. https://doi.org/10.1080/10826068.2014.887582

107.Khanna, S., Srivastava, A.K., 2005. Statistical media optimization studies for growth and PHB production by Ralstonia eutropha. Process Biochem. 40, 2173–2182. https://doi.org/10.1016/j.procbio.2004.08.011

108.Kim, J., Shi, W., Yuan, Y., Benjamin, M.M., 2007. A serial filtration investigation of membrane fouling by natural organic matter. J. Memb. Sci. 294, 115–126. https://doi.org/10.1016/j.memsci.2007.02.020

109.Kim, S., Dale, B.E., 2004. Global potential bioethanol production from wasted crops and crop residues. Biomass and Bioenergy 26, 361–375. https://doi.org/10.1016/j.biombioe.2003.08.002

110.Kim, S., Dale, B.E., 2004. Global potential bioethanol production from wasted crops and crop residues. Biomass and Bioenergy 26, 361–375. https://doi.org/10.1016/j.biombioe.2003.08.002

111.Koller, M., Niebelschütz, H., Braunegg, G., 2013. Strategies for recovery and purification of poly[(R)-3-hydroxyalkanoates] (PHA) biopolyesters from surrounding biomass. Eng. Life Sci. 13, 549–562. https://doi.org/10.1002/elsc.201300021

112.Kong, B., Shanks, J. V., Vigil, R.D., 2013. Enhanced algal growth rate in a Taylor vortex reactor. Biotechnol. Bioeng. 110, 2140–2149. https://doi.org/10.1002/bit.24886

113.Kumar, S., Gupta, N., Pakshirajan, K., 2015. Simultaneous lipid production and dairy wastewater treatment using Rhodococcus opacus in a batch bioreactor for potential biodiesel application. J. Environ. Chem. Eng. 3, 1630–1636. https://doi.org/10.1016/j.jece.2015.05.030

114.Kumar, S., Mandal, A., Guria, C., 2016. Synthesis, characterization and performance studies of polysulfone and polysulfone/polymer-grafted bentonite based ultrafiltration membranes for the efficient separation of oil field oily wastewater. Process Saf. Environ. Prot. 102, 214–228. https://doi.org/10.1016/j.psep.2016.03.011

115.Kumar, S., Singh, S.P., Mishra, I.M., Adhikari, D.K., 2009. Recent advances in production of bioethanol from lignocellulosic biomass. Chem. Eng. Technol. 32, 517–526. https://doi.org/10.1002/ceat.200800442

116.Kumar, V.R., 2016. Novel low cost ceramic and zeolite-ceramic composite tubular membranes for liquid phase separation applications. Doctoral thesis, Indian Institute of Technology Guwahati.

117.Kuntzler, S.G., Almeida, A.C.A. de, Costa, J.A.V., Morais, M.G. de, 2018. Polyhydroxybutyrate and phenolic compounds microalgae electrospun nanofibers: A novel nanomaterial with antibacterial activity. Int. J. Biol. Macromol. 113, 1008–1014. https://doi.org/10.1016/j.ijbiomac.2018.03.002

118.Lan, Y., Liu, H., Cao, X., Zhao, S., Dai, K., Yan, X., Zheng, G., Liu, C., Shen, C., Guo, Z., 2016. Electrically conductive thermoplastic polyurethane/polypropylene nanocomposites with selectively distributed graphene. Polymer (Guildf). 97, 11–19. https://doi.org/10.1016/j.polymer.2016.05.017

119.Levett, I., Birkett, G., Davies, N., Bell, A., Langford, A., Laycock, B., Lant, P., Pratt, S., 2016. Techno-economic assessment of poly-3-hydroxybutyrate (PHB) production from methane - The case for thermophilic bioprocessing. J. Environ. Chem. Eng. 4, 3724–3733. https://doi.org/10.1016/j.jece.2016.07.033

120.Li, F., Yu, H.-Y., Wang, Y.-Y., Zhou, Y., Zhang, H., Yao, J.-M., Abdalkarim, S.Y.H., Tam, K.C., 2019. Natural Biodegradable Poly(3-hydroxybutyrate- co -3-hydroxyvalerate) Nanocomposites with Multifunctional Cellulose Nanocrystals/Graphene Oxide Hybrids for High-Performance Food Packaging . J. Agric. Food Chem. 67, 10954–10967. https://doi.org/10.1021/acs.jafc.9b03110

121.Li, G., Li, H., Wei, G., He, X., Xu, S., Chen, K., Ouyang, P., Ji, X., 2018. Hydrodynamics, mass transfer and cell growth characteristics in a novel microbubble stirred bioreactor employing sintered porous metal plate impeller as gas sparger. Chem. Eng. Sci. 192, 665–677. https://doi.org/10.1016/j.ces.2018.08.025

122.Liguori, R., Faraco, V., 2016. Biological processes for advancing lignocellulosic waste biorefinery by advocating circular economy. Bioresour. Technol. 215, 13–20. https://doi.org/10.1016/j.biortech.2016.04.054

123.Lizarraga-Valderrama, L. R., Panchal, B., Thomas, C., Boccaccini, A. R., & Roy, I., 2016. Biomedical applications of polyhydroxyalkanoates, in: Biomaterials From Nature for Advanced Devices and Therapies. Wiley, pp. 339–383.

124.Lopes, M.S.G., Gosset, G., Rocha, R.C.S., Gomez, J.G.C., Ferreira Da Silva, L., 2011. PHB biosynthesis in catabolite repression mutant of Burkholderia sacchari. Curr. Microbiol. 63, 319–326. https://doi.org/10.1007/s00284-011-9981-6

125.Luengo, J.M., García, B., Sandoval, A., Naharro, G., Olivera, E.R., 2003. Bioplastics from microorganisms. Curr. Opin. Microbiol. 6, 251–260. https://doi.org/10.1016/S1369-5274(03)00040-7

126.medjemem, N., Harabi, A., Bouzerara, F., Foughali, L., Boudaira, B., Guechi, A., Brihi, N., 2016. Elaboration and characterization of low cost ceramics microfiltration membranes applied to the sterilization of plant tissue culture media. J. Taiwan Inst. Chem. Eng. 59, 79–85. https://doi.org/10.1016/j.jtice.2015.07.032

127.Mirbagheri, S.A., Bagheri, M., Bagheri, Z., Kamarkhani, A.M., 2015. Evaluation and prediction of membrane fouling in a submerged membrane bioreactor with simultaneous upward and downward aeration using artificial neural network-genetic algorithm. Process Saf. Environ. Prot. 96, 111–124. https://doi.org/10.1016/j.psep.2015.03.015

128.Morineau-Thomas, O., Jaouen, P., Legentilhomme, P., 2002. The role of exopolysaccharides in fouling phenomenon during ultrafiltration of microalgae (Chlorella sp. and Porphyridium purpureum): Advantage of a swirling decaying flow. Bioprocess Biosyst. Eng. 25, 35–42. https://doi.org/10.1007/s00449-001-0278-1

129.Mukherjee, D., Bhattacharya, P., Jana, A., Bhattacharya, S., Sarkar, S., Ghosh, S., Majumdar, S., Swarnakar, S., 2018. Synthesis of ceramic ultrafiltration membrane and

application in membrane bioreactor process for pesticide remediation from wastewater. Process Saf. Environ. Prot. 116, 22–33. https://doi.org/10.1016/j.psep.2018.01.010

130.Munoz, L.E.A., Riley, M.R., 2008. Utilization of cellulosic waste from tequila bagasse and production of polyhydroxyalkanoate (pha) bioplastics by Saccharophagus degradans. Biotechnol. Bioeng. 100, 882–888. https://doi.org/10.1002/bit.21854

131.Naranjo, J.M., Cardona, C.A., Higuita, J.C., 2014. Use of residual banana for polyhydroxybutyrate (PHB) production: Case of study in an integrated biorefinery. Waste Manag. 34, 2634–2640. https://doi.org/10.1016/j.wasman.2014.09.007

132.Naseem, U., Awan, M.B., Saeed, B., Abbas, N., Nawaz, S., Hussain, M., 2019. Experimental investigation of flow instabilities in a wide gap turbulent rotating Taylor-Couette flow. Case Stud. Therm. Eng. 14, 100449. https://doi.org/10.1016/j.csite.2019.100449

133.Nath, K., 2017. Membrane separation processes. PHI Learning Pvt. Ltd.

134.Nonato, R. V., Mantelatto, P.E., Rossell, C.E.V., 2001. Integrated production of biodegradable plastic, sugar and ethanol. Appl. Microbiol. Biotechnol. 57, 1–5. https://doi.org/10.1007/s002530100732

135.Obruca, S., Benesova, P., Petrik, S., Oborna, J., Prikryl, R., Marova, I., 2014. Production of polyhydroxyalkanoates using hydrolysate of spent coffee grounds. Process Biochem. 49, 1409–1414. https://doi.org/10.1016/j.procbio.2014.05.013

136.Pan, W., Perrotta, J.A., Stipanovic, A.J., Nomura, C.T., Nakas, J.P., 2012. Production of polyhydroxyalkanoates by Burkholderia cepacia ATCC 17759 using a detoxified sugar maple hemicellulosic hydrolysate. J. Ind. Microbiol. Biotechnol. 39, 459–469. https://doi.org/10.1007/s10295-011-1040-6

137.Patnaik, P.R., 2006. Dispersion optimization to enhance PHB production in fed-batch cultures of Ralstonia eutropha. Bioresour. Technol. 97, 1994–2001. https://doi.org/10.1016/j.biortech.2005.09.027

138.Paul, T., Baskaran, D., Pakshirajan, K., Pugazhenthi, G., 2019. Continuous bioreactor with cell recycle using tubular ceramic membrane for simultaneous wastewater treatment and bio-oil production by oleaginous Rhodococcus opacus. Chem. Eng. J. 367, 76–85. https://doi.org/10.1016/j.cej.2019.02.050

139.Paule, A., Lauga, B., Ten-Hage, L., Morchain, J., Duran, R., Paul, E., Rols, J.L., 2011. A photosynthetic rotating annular bioreactor (Taylor-Couette type flow) for phototrophic biofilm cultures. Water Res. 45, 6107–6118. https://doi.org/10.1016/j.watres.2011.09.007

140.Pham, V.T.H., Truong, V.K., Quinn, M.D.J., Notley, S.M., Guo, Y., Baulin, V.A., Al Kobaisi, M., Crawford, R.J., Ivanova, E.P., 2015. Graphene Induces Formation of Pores That Kill Spherical and Rod-Shaped Bacteria. ACS Nano 9, 8458–8467. https://doi.org/10.1021/acsnano.5b03368

141.Piry, A., Heino, A., Kühnl, W., Grein, T., Ripperger, S., Kulozik, U., 2012. Effect of membrane length, membrane resistance, and filtration conditions on the fractionation of milk proteins by microfiltration. J. Dairy Sci. 95, 1590–1602. https://doi.org/10.3168/jds.2011-4292

142.Piry, A., Kühnl, W., Grein, T., Tolkach, A., Ripperger, S., Kulozik, U., 2008. Length dependency of flux and protein permeation in crossflow microfiltration of skimmed milk. J. Memb. Sci. 325, 887–894. https://doi.org/10.1016/j.memsci.2008.09.025

143.Plecher, H., 2019. Inflation rate in India 2024. Statistica.

144.Pradella, J.G. da C., Taciro, M.K., Mateus, A.Y.P., 2010. High-cell-density poly (3-hydroxybutyrate) production from sucrose using Burkholderia sacchari culture in airlift

bioreactor. Bioresour. Technol. 101, 8355–8360. https://doi.org/10.1016/j.biortech.2010.05.046

145.Pradhan, S., Borah, A.J., Poddar, M.K., Dikshit, P.K., Rohidas, L., Moholkar, V.S., 2017. Microbial production, ultrasound-assisted extraction and characterization of biopolymer polyhydroxybutyrate (PHB) from terrestrial (P. hysterophorus) and aquatic (E. crassipes) invasive weeds. Bioresour. Technol. 242, 304–310. https://doi.org/10.1016/j.biortech.2017.03.117

146.Pragya, N., Pandey, K.K., Sahoo, P.K., 2013. A review on harvesting, oil extraction and biofuels production technologies from microalgae. Renew. Sustain. Energy Rev. 24, 159–171. https://doi.org/10.1016/j.rser.2013.03.034

147.Qiao, J., Lew, C.M.J., Karthikeyan, A., Wang, C.H., 2014. Production of PEX protein from QM7 cells cultured in polymer scaffolds in a Taylor-Couette bioreactor. Biochem. Eng. J. 88, 179–187. https://doi.org/10.1016/j.bej.2014.04.012

148.Qiao, J., Yan, W.C., Teoh, J.H., Tong, Y.W., Wang, C.H., 2018. Experimental and computational studies of oxygen transport in a Taylor-Couette bioreactor. Chem. Eng. J. 334, 1954–1964. https://doi.org/10.1016/j.cej.2017.11.137

149.QUAST, D.G., KAREL, M., RAND, W.M., 1972. Development of a Mathematical Model for Oxidation of Potato Chips As a Function of Oxygen Pressure, Extent of Oxidation and Equilibrium Relative Humidity. J. Food Sci. 37, 673–678. https://doi.org/10.1111/j.1365-2621.1972.tb02723.x

150.Radhika, D., Murugesan, A.G., 2012. Bioproduction, statistical optimization and characterization of microbial plastic (poly 3-hydroxy butyrate) employing various hydrolysates of water hyacinth (Eichhornia crassipes) as sole carbon source. Bioresour. Technol. 121, 83–92. https://doi.org/10.1016/j.biortech.2012.06.107

151.Rahnama, F., Vasheghani-Farahani, E., Yazdian, F., Shojaosadati, S.A., 2012. PHB production by Methylocystis hirsuta from natural gas in a bubble column and a vertical loop bioreactor. Biochem. Eng. J. 65, 51–56. https://doi.org/10.1016/j.bej.2012.03.014

152.Ramezani, M., Kong, B., Gao, X., Olsen, M.G., Vigil, R.D., 2015. Experimental measurement of oxygen mass transfer and bubble size distribution in an air-water multiphase Taylor-Couette vortex bioreactor. Chem. Eng. J. 279, 286–296. https://doi.org/10.1016/j.cej.2015.05.007

153.Ramezani, M., Legg, M.J., Haghighat, A., Li, Z., Vigil, R.D., Olsen, M.G., 2017. Experimental investigation of the effect of ethyl alcohol surfactant on oxygen mass transfer and bubble size distribution in an air-water multiphase Taylor-Couette vortex bioreactor. Chem. Eng. J. 319, 288–296. https://doi.org/10.1016/j.cej.2017.03.005

154.Ray, S., Kalia, V.C., 2017. Biomedical Applications of Polyhydroxyalkanoates. Indian J. Microbiol. 57, 261–269. https://doi.org/10.1007/s12088-017-0651-7

155.Raza, Z.A., Abid, S., Banat, I.M., 2018. Polyhydroxyalkanoates: Characteristics, production, recent developments and applications. Int. Biodeterior. Biodegrad. 126, 45–56. https://doi.org/10.1016/j.ibiod.2017.10.001

156.Rodríguez Toscano, A., Mojica Herazo, J.C., Millán, R.R., Hernández Palma, H.G., Saucedo Martinez, J.A., 2019. Approach methodology for the sustainable design of packaging through computational tools: Case study: Water bottles. Case Stud. Therm. Eng. 16, 1–11. https://doi.org/10.1016/j.csite.2019.100561

157.Rodríguez-Contreras, A., Marqués-Calvo, M.S., Gil, F.J., Manero, J.M., 2016. Modification of titanium surfaces by adding antibiotic-loaded PHB spheres and PEG for biomedical applications. J. Mater. Sci. Mater. Med. 27. https://doi.org/10.1007/s10856-016-5723-4

158.Roshanida, A.R., Ahmadun, F.R., Barghash, H.F.A., Hassim, M.H., 2018. Liquid state bioconversion continuous bioreactor of sewage sludge treatment: Determination and evaluation of mixed fungi growth kinetics. Process Saf. Environ. Prot. 120, 128–135. https://doi.org/10.1016/j.psep.2018.08.030

159.Saratale, G.D., Oh, M.K., 2015. Characterization of poly-3-hydroxybutyrate (PHB) produced from Ralstonia eutropha using an alkali-pretreated biomass feedstock. Int. J. Biol. Macromol. 80, 627–635. https://doi.org/10.1016/j.ijbiomac.2015.07.034

160.Saratale, R.G., Saratale, G.D., Cho, S.K., Kim, D.S., Ghodake, G.S., Kadam, A., Kumar, G., Bharagava, R.N., Banu, R., Shin, H.S., 2019. Pretreatment of kenaf (Hibiscus cannabinus L.) biomass feedstock for polyhydroxybutyrate (PHB) production and characterization. Bioresour. Technol. 282, 75–80. https://doi.org/10.1016/j.biortech.2019.02.083

161.Saratale, R.G., Saratale, G.D., Cho, S.K., Kim, D.S., Ghodake, G.S., Kadam, A., Kumar, G., Bharagava, R.N., Banu, R., Shin, H.S., 2019. Pretreatment of kenaf (Hibiscus cannabinus L.) biomass feedstock for polyhydroxybutyrate (PHB) production and characterization. Bioresour. Technol. 282, 75–80. https://doi.org/10.1016/j.biortech.2019.02.083

162.Satagopan, S., Tabita, F.R., 2016. RubisCO selection using the vigorously aerobic and metabolically versatile bacterium Ralstonia eutropha. FEBS J. 283, 2869–2880. https://doi.org/10.1111/febs.13774

163.Sathesh Prabu, C., Murugesan, A.G., 2010. Effective utilization and management of coir industrial waste for the production of poly- β- hydroxybutyrate (phb) using the bacterium azotobacter beijerinickii. Int. J. Environ. Res. 4, 519–524. https://doi.org/10.22059/ijer.2010.238

164. Savenkova, L., Gercberga, Z., Nikolaeva, V., Dzene, A., Bibers, I., Kalnin, M., 2000. Mechanical properties and biodegradation characteristics of PHB-based films. Process Biochem. 35, 573–579. https://doi.org/10.1016/S0032-9592(99)00107-7

165. Serafim, L.S., Lemos, P.C., Oliveira, R., Reis, M.A.M., 2004. Optimization of polyhydroxybutyrate production by mixed cultures submitted to aerobic dynamic feeding conditions. Biotechnol. Bioeng. 87, 145–160. https://doi.org/10.1002/bit.20085

166. Shah, R., 2010. Gujarat to double water charges for industry. Times of India.

167. Shahbazi, M., Ahmadi, S.J., Seif, A., Rajabzadeh, G., 2016. Carboxymethyl cellulose film modification through surface photo-crosslinking and chemical crosslinking for food packaging applications. Food Hydrocoll. 61, 378–389. https://doi.org/10.1016/j.foodhyd.2016.04.021

168. Shahzad, K., Narodoslawsky, M., Sagir, M., Ali, N., Ali, S., Rashid, M.I., Ismail, I.M.I., Koller, M., 2017. Techno-economic feasibility of waste biorefinery: Using slaughtering waste streams as starting material for biopolyester production. Waste Manag. 67, 73–85. https://doi.org/10.1016/j.wasman.2017.05.047

169. Sharma, A.K., Thakur, N.S., 2016. Analyze the factors effecting the development of hydro power projects in hydro rich regions of India. Perspect. Sci. 8, 406–408. https://doi.org/10.1016/j.pisc.2016.04.090

170. Shogren, R., Wood, D., Orts, W., Glenn, G., 2019. Plant-based materials and transitioning to a circular economy. Sustain. Prod. Consum. 19, 194–215. https://doi.org/10.1016/j.spc.2019.04.007

171. Silva, L.F., Taciro, M.K., Michelin Ramos, M.E., Carter, J.M., Pradella, J.G.C., Gomez, J.G.C., 2004. Poly-3-hydroxybutyrate (P3HB) production by bacteria from xylose, glucose and sugarcane bagasse hydrolysate. J. Ind. Microbiol. Biotechnol. 31, 245–254. https://doi.org/10.1007/s10295-004-0136-7

172.Sindhu, R., Silviya, N., Binod, P., Pandey, A., 2013. Pentose-rich hydrolysate from acid pretreated rice straw as a carbon source for the production of poly-3-hydroxybutyrate. Biochem. Eng. J. 78, 67–72. https://doi.org/10.1016/j.bej.2012.12.015

173.Snell, K.D. and O.P.P., 2009. PHA bioplastic: A value-added coproduct for biomass biorefineries. Biofuels Bioprod. Biorefining-Biofpr 3, 46–467.

174.Socha, A.M., Parthasarathi, R., Shi, J., Pattathil, S., Whyte, D., Bergeron, M., George, A., Tran, K., Stavila, V., Venkatachalam, S., Hahn, M.G., Simmons, B.A., Singh, S., 2014. Efficient biomass pretreatment using ionic liquids derived from lignin and hemicellulose. Proc. Natl. Acad. Sci. U. S. A. 111.

175.Tavares, L.Z., Da Silva, E.S., Da Cruz Pradella, J.G., 2004. Production of poly(3-hydroxybutyrate) in an airlift bioreactor by Ralstonia eutropha. Biochem. Eng. J. 18, 21–31. https://doi.org/10.1016/S1369-703X(03)00117-7

176.Taylor, B., Xiao, N., Sikorski, J., Yong, M., Harris, T., Helme, T., Smallbone, A., Bhave, A., Kraft, M., 2013. Techno-economic assessment of carbon-negative algal biodiesel for transport solutions. Appl. Energy 106, 262–274. https://doi.org/10.1016/j.apenergy.2013.01.065

177.Tiwari, K.K., Singh, N.K., Patel, M.P., Tiwari, M.R., Rai, U.N., 2011. Metal contamination of soil and translocation in vegetables growing under industrial wastewater irrigated agricultural field of Vadodara, Gujarat, India. Ecotoxicol. Environ. Saf. 74, 1670–1677. https://doi.org/10.1016/j.ecoenv.2011.04.029

178.Tripathi, A.D., Raj Joshi, T., Kumar Srivastava, S., Darani, K.K., Khade, S., Srivastava, J., 2019. Effect of nutritional supplements on bio-plastics (PHB) production utilizing sugar refinery waste with potential application in food packaging. Prep. Biochem. Biotechnol. 49, 567–577. https://doi.org/10.1080/10826068.2019.1591982

179. Vaidya, A.A., Collet, C., Gaugler, M., Lloyd-Jones, G., 2019. Integrating softwood biorefinery lignin into polyhydroxybutyrate composites and application in 3D printing. Mater. Today Commun. 19, 286–296. https://doi.org/10.1016/j.mtcomm.2019.02.008

180. Valapa, R.B., Pugazhenthi, G., Katiyar, V., 2015. Effect of graphene content on the properties of poly(lactic acid) nanocomposites. RSC Adv. 5, 28410–28423. https://doi.org/10.1039/c4ra15669b

181. Valentino, F., Karabegovic, L., Majone, M., Morgan-Sagastume, F., Werker, A., 2015. Polyhydroxyalkanoate (PHA) storage within a mixed-culture biomass with simultaneous growth as a function of accumulation substrate nitrogen and phosphorus levels. Water Res. 77, 49–63. https://doi.org/10.1016/j.watres.2015.03.016

182. Van-Thuoc, D., Quillaguamán, J., Mamo, G., Mattiasson, B., 2008. Utilization of agricultural residues for poly(3-hydroxybutyrate) production by Halomonas boliviensis LC1. J. Appl. Microbiol. 104, 420–428. https://doi.org/10.1111/j.1365-2672.2007.03553.x

183. Vasanth, D., Pugazhenthi, G., Uppaluri, R., 2011. Fabrication and properties of low cost ceramic microfiltration membranes for separation of oil and bacteria from its solution. J. Memb. Sci. 379, 154–163. https://doi.org/10.1016/j.memsci.2011.05.050

184. Vasanth, D., Pugazhenthi, G., Uppaluri, R., 2013. Cross-flow microfiltration of oil-in-water emulsions using low cost ceramic membranes. Desalination 320, 86–95. https://doi.org/10.1016/j.desal.2013.04.018

185. Venkata Mohan, S., Hemalatha, M., Chakraborty, D., Chatterjee, S., Ranadheer, P., Kona, R., 2020. Algal biorefinery models with self-sustainable closed loop approach: Trends and prospective for blue-bioeconomy. Bioresour. Technol. 295, 122128.

186. Vidal-Mas, J., Resina-Pelfort, O., Haba, E., Comas, J., Manresa, A., Vives-Rego, J., 2001. Rapid flow cytometry - Nile red assessment of PHA cellular content and

heterogeneity in cultures of Pseudomonas aeruginosa 47T2 (NCIB 40044) grown in waste frying oil. Antonie van Leeuwenhoek, Int. J. Gen. Mol. Microbiol. 80, 57–63. https://doi.org/10.1023/A:1012208225286

187. Vinoth Kumar, R., Kumar Ghoshal, A., Pugazhenthi, G., 2015. Elaboration of novel tubular ceramic membrane from inexpensive raw materials by extrusion method and its performance in microfiltration of synthetic oily wastewater treatment. J. Memb. Sci. 490, 92–102. https://doi.org/10.1016/j.memsci.2015.04.066

188. Wang, J., Yu, H.Q., 2007. Biosynthesis of polyhydroxybutyrate (PHB) and extracellular polymeric substances (EPS) by Ralstonia eutropha ATCC 17699 in batch cultures. Appl. Microbiol. Biotechnol. 75, 871–878. https://doi.org/10.1007/s00253-007-0870-7

189. Waszak, M., Gryta, M., 2016. The ultrafiltration ceramic membrane used for broth separation in membrane bioreactor. Chem. Eng. J. 305, 129–135. https://doi.org/10.1016/j.cej.2015.11.058

190. Wei, L., Liang, S., Coats, E.R., McDonald, A.G., 2015a. Valorization of residual bacterial biomass waste after polyhydroxyalkanoate isolation by hydrothermal treatment. Bioresour. Technol. 198, 739–745. https://doi.org/10.1016/j.biortech.2015.09.086

191. Wei, L., Liang, S., Guho, N.M., Hanson, A.J., Smith, M.W., Garcia-Perez, M., McDonald, A.G., 2015b. Production and characterization of bio-oil and biochar from the pyrolysis of residual bacterial biomass from a polyhydroxyalkanoate production process. J. Anal. Appl. Pyrolysis 115, 268–278. https://doi.org/10.1016/j.jaap.2015.08.005

192. Wen, H.Q., Du, J., Xing, D.F., Ding, J., Ren, N.Q., Liu, B.F., 2017. Enhanced photo-fermentative hydrogen production of Rhodopseudomonas sp. nov. strain A7 by biofilm

reactor. Int. J. Hydrogen Energy 42, 18288–18294. https://doi.org/10.1016/j.ijhydene.2017.04.150

193.Wu, Y.W., Yang, S.H., Hwangbo, M., Chu, K.H., 2019. Analysis of Zobellella denitrificans ZD1 draft genome: Genes and gene clusters responsible for high polyhydroxybutyrate (PHB) production from glycerol under saline conditions and its CRISPR-Cas system. PLoS One 14, 1–20. https://doi.org/10.1371/journal.pone.0222143

194.Xu, J.Z., Zhang, Z.J., Xu, H., Chen, J. Bin, Ran, R., Li, Z.M., 2015. Highly Enhanced Crystallization Kinetics of Poly(l -lactic acid) by Poly(ethylene glycol) Grafted Graphene Oxide Simultaneously as Heterogeneous Nucleation Agent and Chain Mobility Promoter. Macromolecules 48, 4891–4900. https://doi.org/10.1021/acs.macromol.5b00462

195.Xu, P., Yang, W., Niu, D., Yu, M., Du, M., Dong, W., Chen, M., Jan Lemstra, P., Ma, P., 2020. Multifunctional and robust polyhydroxyalkanoate nanocomposites with superior gas barrier, heat resistant and inherent antibacterial performances. Chem. Eng. J. 382, 122864. https://doi.org/10.1016/j.cej.2019.122864

196.Yadav, B., Pandey, A., Kumar, L.R., Tyagi, R.D., 2019. Bioconversion of waste (water)/ residues to bioplastics- A circular bioeconomy approach. Bioresour. Technol. 122584. https://doi.org/10.1016/j.biortech.2019.122584

197.Yoganand, K.N., Muralidharan, M., Nimkar, S., Anand, B., 2019. Fidelity of prespacer capture and processing is governed by the PAM mediated interactions of Cas1-2 adaptation complex in CRISPR-Cas type I-E system. J. Biol. Chem. jbc.RA119.009438. https://doi.org/10.1074/jbc.RA119.009438

198.Yousuf, R.G., Winterburn, J.B., 2016. Date seed characterisation, substrate extraction and process modelling for the production of polyhydroxybutyrate by Cupriavidus

necator. Bioresour. Technol. 222, 242–251. https://doi.org/10.1016/j.biortech.2016.09.107

199. Yu, J., Stahl, H., 2008. Microbial utilization and biopolyester synthesis of bagasse hydrolysates. Bioresour. Technol. 99, 8042–8048. https://doi.org/10.1016/j.biortech.2008.03.071

200. Zare, M., Namratha, K., Ilyas, S., Hezam, A., Mathur, S., Byrappa, K., 2019. Applications of Polymer , Composite , and Coating Materials Smart Fortified PHB-CS Biopolymer with ZnO-Ag Nanocomposites for Enhanced Shelf Life of Food Packaging Smart Fortified PHB-CS Biopolymer with ZnO-Ag Nanocomposites for. https://doi.org/10.1021/acsami.9b15724

201. Zhang, Y., Sun, W., Wang, H., Geng, A., 2013. Polyhydroxybutyrate production from oil palm empty fruit bunch using bacillus megaterium R11. Bioresour. Technol. 147, 307–314. https://doi.org/10.1016/j.biortech.2013.08.029

202. Zhao, F., Chu, H., Yu, Z., Jiang, S., Zhao, X., Zhou, X., Zhang, Y., 2017. The filtration and fouling performance of membranes with different pore sizes in algae harvesting. Sci. Total Environ. 587–588, 87–93. https://doi.org/10.1016/j.scitotenv.2017.02.035

203. Zúñiga, C., Morales, M., Le Borgne, S., Revah, S., 2011. Production of poly-β-hydroxybutyrate (PHB) by Methylobacterium organophilum isolated from a methanotrophic consortium in a two-phase partition bioreactor. J. Hazard. Mater. 190, 876–882. https://doi.org/10.1016/j.jhazmat.2011.04.011

List of publications

❖ **Book chapter**

1. N. Arul Manikandan, Kannan Pakshirajan and G. Pugazhenthi, Value addition of waste lignocellulosic biomass through polyhydroxybutyrate production, *Waste Biorefinery: Integrating Biorefineries for Waste Valorisation*, Elsevier, March 2020 (eBook ISBN: 9780128182291; Hardcover ISBN: 9780128182284).

❖ **Publications in international journals**

1. Arul Manikandan, Kannan Pakshirajan and G. Pugazhenthi, A closed-loop biorefinery approach for polyhydroxybutyrate (PHB) production using sugars from carob pods as the sole raw material and downstream processing using the co-product lignin, *Bioresource Technology*, 307 (2020) 123247.
2. Arul Manikandan, Kannan Pakshirajan and G. Pugazhenthi, Preparation and characterization of environmentally safe and highly biodegradable microbial polyhydroxybutyrate (PHB) based graphene nanocomposites for potential food packaging applications, *International Journal of Biological Macromolecules*, 154 (2020) 866-877.
3. Arul Manikandan, Kannan Pakshirajan and G. Pugazhenthi, A novel ceramic membrane assembly for the separation of polyhydroxybutyrate (PHB) rich *Ralstonia eutropha* biomass from culture broth, *Process Safety and Environmental Protection*, 126 (2019) 106-118.
4. Arul Manikandan, Kannan Pakshirajan and G. Pugazhenthi, Taylor and Couette flow mediated improved hydrodynamics in an annular bioreactor for shear stress-free biomass growth and PHB production by *Ralstonia eutropha*, *Process Biochemistry*. To be submitted.
5. Arul Manikandan, Kannan Pakshirajan and G. Pugazhenthi, Techno-economic assessment of large scale polyhydroxybutyrate (PHB) production from waste carob pods in a closed-loop biorefinery based setup with novel bioprocessing strategies, *Chemosphere*. To be submitted.

❖ **Presentation in international/national conferences**

1. N. Arul Manikandan, Kannan Pakshirajan, and G. Pugazhenthi, *Siliquapods* as a novel feedstock for sustainable polyhydroxybutyrate (PHB) production, *Industrial Pollution and Control Technology-2019 (IPACT 2019)*, 13-14 March 2019, Annamalai University, Tamil Nadu, India.

2. N. Arul Manikandan, Kannan Pakshirajan, and G. Pugazhenthi, Effect of graphene on the thermal properties of polyhydroxybutyrate (PHB) nanocomposites, *Composite Materials for General Engineering, Armour and Aerospace Applications,* 28-29 September 2018, PSG College of Technology, Coimbatore, India.
3. N. Arul Manikandan, Kannan Pakshirajan and G. Pugazhenthi, A novel ceramic membrane assembly for the separation of polyhydroxybutyrate rich *Ralstonia eutropha* biomass from culture broth, *11th International Conference on the Challenges in Environmental Science and Engineering (CESE-2018),* 04-08 November 2018, Bangkok, Thailand.
4. N. Arul Manikandan, Kannan Pakshirajan and G. Pugazhenthi, Taylor-Couette bioreactor - a novel bioreactor system for polyhydroxybutyrate production from *Ralstonia eutropha*, *11th International Conference on the Challenges in Environmental Science and Engineering (CESE-2018),* 04-08 November 2018, Bangkok, Thailand.
5. N. Arul Manikandan, Kannan Pakshirajan and G. Pugazhenthi, Green production of polyhydroxybutyrate (PHB) using lignocellulosic biomass (*Ceratonia siliqua* pods) as a self-sufficient feedstock for upstream to downstream processing, *International Conference on Advanced Materials Research (AMRC 2019),* 26-27 September 2019, National University of Singapore (NUS), Singapore.
6. N. Arul Manikandan, Kannan Pakshirajan, and G. Pugazhenthi, Preparation and characterization of polyhydroxybutyrate (PHB) nanocomposites with graphene Nano platelets, *2nd International Conference on Nanoscience and Nanotechnology (ICNAN-2019),* 29 November – 01 December 2019, Vellore Institute of Technology (VIT), Vellore, Tamil Nadu, India.
7. N. Arul Manikandan, Kannan Pakshirajan and G. Pugazhenthi, Closed loop biorefinery for polyhydroxybutyrate (PHB) production, *24th Biological Sciences Graduate Congress (BSGC 2019),* 19-21 December 2019, University of Malaya, Kuala Lumpur, Malaysia [Second runner up award for oral presentation].